

GEOLOGY OF THE CRYSTALLINE BASEMENT COMPLEX,
EASTERN TRANSVERSE RANGES, SOUTHERN CALIFORNIA:
CONSTRAINTS ON REGIONAL TECTONIC INTERPRETATION

Thesis by
Robert Edward Powell

In Partial Fulfillment of the Requirements
for the Degree of
Doctor of Philosophy

California Institute of Technology
Pasadena, California

1981
(Submitted January 7, 1981)

'Tis the gift to be simple

'Tis the gift to be free...

Shaker Hymn

ACKNOWLEDGEMENTS

Over the past several years, I have become indebted to many people who have contributed materially and intellectually toward the completion of this study. Leon T. Silver, my thesis advisor, initially helped select the area of study and provided insight and advice along the way as well as financial support. Robert V. Sharp, of the U.S. Geological Survey at Menlo Park, sponsored my support as a U.S.G.S. geological field assistant, provided color aerial photographic coverage for most of the Eastern Transverse Ranges, and invited me to accompany him on an overflight along the left-lateral faults of the Eastern Transverse Ranges. Keith A. Howard, also of the U.S. Geological Survey at Menlo Park, provided additional color aerial photographs in the northern Pinto Mountains, a base map for the compilation of Plate I, and one and a half days of helicopter support. I am particularly indebted to his active interest in my work and to his many efforts on my behalf. Gary S. Fuis, of Caltech and the U.S. Geological Survey at Caltech and Menlo Park, was generously supportive at several critical junctures during the course of the study.

Field work was supported by my Veterans Administration educational benefits, funds earned as a U.S. Geological Survey geological field assistant, personal savings and loans, and NSF Grant Nos. EAR 76-23153 and EAR 74-00155 awarded to L. T. Silver. Petrographic thin-sections were financed by NSF Grant Nos. EAR 76-23153 and EAR 74-00155. Thesis preparation and reproduction was supported by NSF Grant EAR 76-23153 and by personal loans.

Numerous discussions with colleagues at Caltech, including Ted Labotka, Tom H. Anderson, Bob Gregory, Jim Quick, Bruce Carter, Stein

Jacobsen, Bob Criss, Henry Shaw, Cleve Solomon, Alan Gillespie, Ray Weldon, and Elizabeth Thomas, proved especially fruitful. Carl Johnson, Peter German, and Vic Lamanuzzi, of the U.S. Geological Survey at Caltech, helped me with the hypocenter computer plot in Chapter VI. I would also like to thank several people who accompanied me at various stages on working excursions into my field area, including Lynn Tennyson, Gary Fuis, Toni Callaway, Joel Everson, Lee Silver, Bob V. Sharp, Keith Howard, Paul Stone, Scott Cameron, and Chuck Douthitt.

Leon Silver critically read the entire thesis, and Clarence Allen reviewed Chapter VI. Barclay Kamb and Kerry Sieh offered constructive critical comments. I am grateful for their thoughtful efforts which yielded improvements in the manuscript.

Finally, I deeply appreciate the patience and understanding of my family and friends who often received less attention than was their due during this rite of passage. As always, my parents, Edward G. and Marion S. Powell, followed this endeavor with unflagging interest and enthusiasm, including a trip into the desert. Manya Maas kindly helped me in the preparation of the thesis, and gently kept me sane.

ABSTRACT

About 3000 km² within the crystalline basement complex of the Eastern Transverse Ranges in the Chuckwalla, Orocopia, Eagle, Cottonwood, Hexie, Little San Bernardino, and Pinto Mountains of Riverside County, California were mapped at scales of 1:36,000 and 1:62,500 and compiled at 1:125,000 (Plate I). Pre-Jurassic(?) (i.e., older than the Mesozoic batholiths) rocks of the crystalline complex comprise two lithologically distinct terranes. These terranes are called the Joshua Tree and San Gabriel terranes for regions of southern California in which their lithologies were initially characterized. The two terranes are superposed along a previously unrecognized low-angle fault system of regional extent, the Red Cloud thrust.

During the course of this study, the structurally lower Joshua Tree terrane has been defined as a stratigraphically coherent group of crystalline rocks that consists of Precambrian granite capped by a paleo-weathered zone and overlain nonconformably by orthoquartzite that interfingers westward with pelitic and feldspathic granofelses. The quartzite contains near-basal quartz/quartzite clast conglomerates, and has well-preserved cross-bedding that appears upright wherever it has been observed. Pelitic and feldspathic granofelses crop out to the west of the quartzite exposures in four lithologically different belts that trend northnorthwest throughout the area mapped. These lithologic belts are interpreted to have been derived from stratigraphically interfingering sedimentary protoliths deposited in a basin offshore from a quartzose beach-sand protolith. In proximity to the early Red Cloud thrust, this whole stratigraphic package was pervasively deformed to granite gneiss, stretched pebble conglomerate, lineated quartzite, and schist.

A northeast-trending pattern of metamorphic isograds was orthogonally superimposed on the northnorthwest-trending protoliths of the Pinto gneiss. A central andalusite zone, located in the southern Little San Bernardino and Hexie, and northern Eagle Mountains, is flanked to the northwest and southeast by sillimanite zones. Coincident with this symmetrical distribution of aluminosilicates is an asymmetrical distribution of other pelitic mineral zones, with prograde cordierite-aluminosilicate-biotite- and K-feldspar-aluminosilicate-bearing assemblages to the northwest in the northern Little San Bernardino and Pinto Mountains, staurolite-bearing assemblages in a narrow zone in the southern Little San Bernardino-Hexie and northern Eagle Mountains, and retrograde chlorite-muscovite-bearing assemblages in the southernmost Little San Bernardino, Cottonwood, southern Eagle, Orocopia, and Chuckwalla Mountains. One occurrence of chloritoid-sillimanite in the central Eagle Mountains is apparently also retrograde. The crossing isograds are interpreted to result from a temporal increase in P_{H_2O} relative to P_T from south to north through the field area. Comparison of the pelitic assemblages with experimental studies suggests peak conditions of $P_T \approx 3.5$ to 4 kb, $T \approx 525$ to 625°C . The early prograde metamorphism pre-dated the thrusting event; the retrograde stage may have overlapped in time with the emplacement of the San Gabriel terrane allochthon. Cordierite-orthoamphibole-bearing assemblages are present in one stratigraphic zone of the Pinto gneiss.

In this study, the Precambrian lithologies of the San Gabriel terrane are viewed as a three-part deep crustal section, with uppermost amphibolite grade pelitic (Hexie) gneiss intruded by granodioritic (Soledad) augen gneiss at the highest level, retrograded granulite (Augustine) gneiss at an intermediate level, and syenite-mangerite-jotunite at the lowest level ex-

posed in the Eastern Transverse Ranges. The Hexie gneiss, characterized by sillimanite-garnet-biotite-bearing assemblages, is thrust over andalusite-bearing granulites of the Pinto gneiss.

The Red Cloud thrust system is inferred to have developed in three or four sequential structural events: 1) early thrusting that probably moved parallel to the ENE mineral lineations recorded in both plates; 2) regional folding of the initial thrust surface around NNE-trending axes; 3) later thrusting that broke with some component of westward movement across a fold in the older thrust surface to produce a stacking of crystalline thrust plates of the two terranes; 4) continued or renewed folding of both thrust faults with eventual overturning toward the SW. It is consistent with all observations to date to link these structural events into a single regional tectonic episode that resulted in westward-vergent allochthonous emplacement of the San Gabriel terrane over Joshua Tree terrane. The thrust timing can only be loosely bracketed in time between 1195 m.y. and 165 m.y. ago.

The pre-batholithic terranes and the westward-vergent Red Cloud thrust are considered to be exotic with respect to the pre-batholithic rocks and structures exposed to the north and east of the field area. The bounding discontinuity has been obliterated by intrusion of both suites of Mesozoic batholithic rocks.

The Mesozoic plutonic rocks comprise two batholithic suites, both of which intrude the Joshua Tree and San Gabriel terranes and the Red Cloud thrust system. NW-SE trending belts of plutonic lithologies have been mapped within each suite: the oldest lithology of the younger suite intrudes the youngest lithology of the older suite. The older suite, Jurassic(?), lying to the NE, appears to have an alkalic character; the

younger suite, Cretaceous(?), appears calc-alkaline. The older suite consists of biotite- and K-feldspar-bearing gabbro-diorites intruded by low-quartz monzogranites. The younger suite includes hornblende-biotite-sphene granodiorite intruded by porphyritic monzogranites, intruded in turn by nonporphyritic monzogranite.

The Eastern Transverse Ranges south of the Pinto Mountain fault are defined by several Cenozoic E-W left-lateral strike-slip faults that have a cumulative westward displacement from S to N of about 50 km. The left-lateral faults are interpreted to form part of a conjugate fault set with complementary right-lateral faults in the Mojave and Colorado Deserts. Along the western boundary of the Eastern Transverse Ranges in the Little San Bernardino Mountains, the crystalline rocks have been pervasively cataclased by an event that post-dates intrusion of the Cretaceous(?) plutonic rocks. The cataclasis is attributed to the Vincent-Orocopia-Chocolate Mountain thrust that is thought to superpose the diverse pre-batholithic and batholithic rocks of the Eastern Transverse Ranges above Pelona-type schist. The cataclastic foliation is folded along the length of the Little San Bernardino Mountains in an antiform that is inferred to be cored with Pelona-type schist. This fold may have formed a single antiformal feature comprising all the crystalline-rock antiforms now recognized along the San Andreas fault that are cored by Pelona-type schist. Displacements of the piercing points formed by the antiformal axis apparently indicate 220 km of right-lateral offset on the present San Andreas strand and about 80 km of right-lateral offset along a fragmented older San Andreas strand that consisted of the San Francisquito, Fenner, and Clemens Well faults and a buried extension of this fault beneath the alluvial fill of the valley between the Chocolate and Chuckwalla Mountains.

PLEASE NOTE:

Plate I was not microfilmed
due to extremely dark back-
ground. Available for con-
sultation at the California
Institute of Technology.

UNIVERSITY MICROFILMS INTERNATIONAL

TABLE OF CONTENTS

	(page)
I. INTRODUCTION	1
OVERTURE	2
EASTERN TRANSVERSE RANGES	4
PREVIOUS WORK	9
PRESENT STUDY	14
II. JOSHUA TREE TERRANE	20
INTRODUCTION	21
JOSHUA TREE GRANITE GNEISS	26
PALEO-WEATHERED ZONE	38
PINTO GNEISS	43
Introduction	43
Pinto Mountain Quartzite	46
<u>Introduction</u>	46
<u>Cross-bedded Quartzite Lithosome</u>	47
<u>Vitreous White Quartzite Lithosome</u>	52
Lost Horse Granofels	54
Baumonk Mill Granofels	61
Music Valley Gneiss	68
Black Eagle Granofels-Schist	71
STRATIGRAPHIC FACIES MODEL	80
METAMORPHISM	91
Introduction	91
Pelitic Assemblages	94
<u>Andalusite/sillimanite-bearing assemblages</u>	97

<u>Biotite/Cordierite/Garnet/Staurolite/Chloritoid/ Chlorite-Bearing Assemblages</u>	105
<u>Pelitic Gneiss Synthesis</u>	114
<u>Plagioclase + Quartz + Biotite Gneiss</u>	130
Ferromagnesian Assemblages	136
<u>Talc/Orthoamphibole + Chlorite ± Cordierite ± Clinoamphibole-Bearing Assemblages</u>	136
<u>Ferromagnesian Hornfels/Schist Historical Review</u>	143
<u>Ferromagnesian Granofels/Schist Synthesis</u>	148
<u>Aluminous enclaves</u>	156
Age of Metamorphism	167
Geothermal Gradient	168
DEFORMATION	169
III. SAN GABRIEL TERRANE	171
INTRODUCTION	172
HEXIE GNEISS	175
SOLEDAD GRANODIORITE-AUGEN GNEISS	182
AUGUSTINE GNEISS	189
SYENITE-MANGERITE-JOTUNITE	205
REGIONAL CORRELATION	211
IV. PRE-BATHOLITHIC DEFORMATION	212
RED CLOUD THRUST SYSTEM	213
Introduction	213
Early Thrusting Stage	218
<u>Big Wash Area, Eagle Mountains</u>	218
<u>Hayfield Area, Eagle Mountains</u>	218
<u>Red Cloud Canyon Area, Chuckwalla Mountains</u>	218
<u>Cottonwood Pass Window</u>	223

<u>Synthesis of Early Thrust Segments</u>	224
Late Thrusting Stage	239
<u>Chuckwalla Mountains</u>	239
<u>Central Pinto Mountains</u>	240
<u>Northern Eagle Mountains</u>	244
<u>Cottonwood Pass</u>	244
<u>Synthesis of Late Thrust segments</u>	244
Combined Early and Late Thrusting Stages	246
Folding Phase	251
Tectonic Synthesis	260
Age of the Red Cloud Thrust System	262
An Analogy in Tectonic Style	263
REGIONAL TECTONIC SETTING (PRE-BATHOLITHIC)	265
V. MESOZOIC BATHOLITHIC TERRANE	273
INTRODUCTION	274
JURASSIC(?) BATHOLITHIC SUITE	277
Gabbro-Diorites	277
<u>Field Relations</u>	277
<u>Petrography</u>	280
Monzogranites (Quartz Monzonites)	284
<u>Field Relations</u>	284
<u>Petrography</u>	287
Summary	288
CRETACEOUS(?) BATHOLITHIC SUITE	289
Hornblende-Biotite Granodiorite	289
<u>Field Relations</u>	289
<u>Petrography</u>	290

Porphyritic Monzogranite (Quartz Monzonite)	293
<u>Field Relations and Petrography</u>	293
Monzogranite (Quartz Monzonite)	298
<u>Field Relations and Petrography</u>	298
Summary	299
DIKES	301
Introduction	301
Quartz Latite Dikes	301
Trachyte Dikes	303
Dacite Dike	303
Other Dikes	305
VI. POST-BATHOLITHIC TECTONICS	307
INTRODUCTION: PRELIMINARY STATEMENT OF CONCLUSIONS	308
LEFT-LATERAL FAULTS OF THE EASTERN TRANSVERSE RANGES	315
Introduction	315
Pinto Mountain Fault	316
Blue Cut Fault	317
Porcupine Wash and Substation Faults (Hexie and Eagle Mountains)	319
Smoke Tree Wash and Victory Pass Faults (Cottonwood-Hexie and Eagle Mountains)	321
Chiriaco Fault	322
Corn Springs Wash Fault (Chuckwalla Mountains)	325
Ship Creek Fault (Chuckwalla Mountains)	326
Salton Wash and Aztec Mines Wash Faults	327
Summary	328
RIGHT-LATERAL FAULTS IN THE MOJAVE DESERT	334
Introduction	334

Northwestern Mojave Desert	334
Southeastern Mojave Desert	336
Summary of Right- and Left-lateral Strike-slip Fault Pattern	338
ZONE OF CATACLASIS AND BRECCIATION IN THE LITTLE SAN BERNARDINO MOUNTAINS	340
REVIEW OF PELONA-TYPE SCHIST AND THE VINCENT-CHOCOLATE MOUNTAIN THRUST	349
Introduction	349
Lithology	350
Tectonic Setting	352
TECTONIC SYNTHESIS	361
Eastern Transverse Ranges	361
San Andreas Fault	365
Mojave Desert-Transverse Ranges	368
Southern California	371
VII. CONCLUSIONS	394
REFERENCES	403
APPENDIX	430

PLATES

- I. Geologic map of the crystalline basement complex in the southern Eastern Transverse Ranges, southern California (in pocket).
- II. Legend for the geologic map (Plate I) and structure sections (Plate III) (Appendix, p. 430).
- III. Structure sections, crystalline basement complex, Eastern Transverse Ranges, southern California (in pocket).
- IV. Stratigraphic columns -- Pinto Mountain Quartzite (in pocket).
- V. Lithosomes, mineral assemblages, and isograds within the Pinto gneiss of the Joshua Tree terrane (in pocket).
- VI. Palinspastic reconstruction of the San Andreas fault system in southern California (in pocket).
Explanation (Appendix, p. 438).
- VII. Evolution of the San Andreas fault system in southern California (in pocket).
Explanation (Appendix, p. 440).

FIGURES	(page)
1-1. Overview of the principal physiographic, geographic, and late Cenozoic structural features in southern California and northwestern Mexico.	6, 7
1-2. Geologic map and cross-sections of the crystalline basement complex of the southern Eastern Transverse Ranges. . .	16, 17
2-1. Panoramic photo-mosaic looking north in the central Pinto Mountains.	23
2-2. Outcrop photographs of lithologies within the Joshua Tree terrane.	28
2-3. Photomicrographs of samples from the Joshua Tree granite-granite gneiss, paleo-weathered zone, and Pinto Mountain quartzite of the Joshua Tree terrane.	31
2-4. Modes of the Joshua Tree granite-granite gneiss plotted on quartz-potassium feldspar-plagioclase (QKP) and quartz-feldspar-mafics (QFM) ternary diagrams.	35
2-5. Outcrop and hand sample photographs of Pinto Mountain quartzite, Lost Horse granofels, and Iron Chief dolomite of the Pinto gneiss.	49
2-6. Hand sample photographs of the Black Eagle, Baumonk Mill, Music Valley, and Lost Horse granofels of the Pinto gneiss.	56
2-7. Photomicrographs of samples from the pelitic Lost Horse granofels of the Pinto gneiss.	60
2-8. Photomicrographs of samples from the ferromagnesian Lost Horse granofels of the Pinto gneiss.	63
2-9. Photomicrographs of samples from the Black Eagle granofels-schist, Iron Chief dolomite, Baumonk Mill granofels, and Music Valley gneiss of the Pinto gneiss.	66
2-10. Photomicrographs of samples from the Black Eagle granofels of the Pinto gneiss and the paleo-weathered zone.	74
2-11. Stratigraphic model for the Pinto gneiss.	83
2-12. Schematic representation of a possible Pinto gneiss trajectory through a petrogenetic grid for pelitic compositions.	96
2-13. Experimental curves in the $Al_2O_3-SiO_2-H_2O$ system.	101
2-14. Experimental and calculated curves in the system $K_2O-Al_2O_3-SiO_2-H_2O$	104

2-15.	Experimental curves in the system $K_2O-MgO/FeO-Al_2O_3-SiO_2-H_2O$	113
2-16.	Combined experimental curves for the system $K_2O-MgO/FeO-Al_2O_3-SiO_2-H_2O$ (chlorite + muscovite + quartz) pertinent to the metamorphism of the pelitic rocks of the Pinto gneiss.	117
2-17.	Hypothetical P_T -T trajectories not completely consistent with the distribution and sequence of prograde and retrograde mineral assemblages in the pelitic rocks of the Pinto gneiss.	119
2-18.	Isotherms inclined relative to isobars that are parallel to the earth's surface.	122
2-19.	Model for the metamorphic evolution of the Pinto gneiss.	126, 127
2-20.	Selected experimental curves in the system $Na_2O/CaO-Al_2O_3-SiO_2-H_2O$	132
2-21.	Experimentally determined curves for the beginning of melting for rocks of granitic composition.	135
2-22.	Photomicrograph of aluminous enclave.	138
2-23.	Experimental curves in the systems $MgO-SiO_2-H_2O$ and $MgO/FeO-Al_2O_3-SiO_2-H_2O$	142
2-24.	Combined experimental curves for the system $MgO/FeO-Al_2O_3-SiO_2-H_2O$ (chlorite + quartz) pertinent to the metamorphism of the ferromagnesian rocks of the Pinto gneiss.	152
2-25.	Schematic topologies for $MgO-SiO_2-Al_2O_3$ and $FeO-SiO_2-Al_2O_3$ ternary faces (represented on parallel planes) of the $MgO-FeO-SiO_2-Al_2O_3$ tetrahedron.	159-162
3-1.	Photographs of Hexie and Soledad gneisses in outcrop.	177
3-2.	Photomicrographs of Hexie and Soledad gneisses from the San Gabriel terrane.	179
3-3.	Modal compositions of samples of Soledad granodiorite and augen gneiss from the San Gabriel terrane, plotted on quartz-K-feldspar-plagioclase (QKP) and quartz-feldspar-mafics (QFM) diagrams.	187
3-4.	Photographs of Hexie and Augustine gneisses in outcrop.	191
3-5.	Modal compositions of samples of Augustine gneiss from the San Gabriel terrane, plotted on quartz-K-feldspar-plagioclase (QKP) and quartz-feldspar-mafics (QFM) diagrams.	195
3-6.	Photomicrographs of samples of Augustine gneiss from the San Gabriel terrane.	198

3-7.	Photomicrographs of samples of Augustine gneiss and mangerite from the San Gabriel terrane.	202
3-8.	Modal compositions of samples of mangerite-jotunite plotted on quartz-K-feldspar-plagioclase (QKP) and quartz-feldspar-mafics (QFM) diagrams.	208
4-1.	Photographs of the Red Cloud thrust system.	216
4-2.	Photographs of mylonites in the Red Cloud thrust system.	220
4-3.	Photomicrographs of mylonite samples from the Red Cloud thrust system.	222
4-4.	Schematic down-structure views of the Red Cloud thrust system, viewed from south of the Chuckwalla Mountains.	226
4-5.	Mineral and pebble lineations within the deformational fabric related to the emplacement of the San Gabriel allochthon, plotted on lower hemisphere equal area stereographic projections.	228
4-6.	Minor fold axes and mineral lineations within the deformational fabric related to emplacement of the San Gabriel allochthon, plotted on a lower hemisphere equal area stereographic projections.	231
4-7.	Minor fold axes within the deformational fabric related to emplacement of the San Gabriel allochthon, plotted on lower hemisphere equal area stereographic projections.	233
4-8.	Directions of inferred movement along the Red Cloud thrust system.	238
4-9.	Schematic cross-section diagramming the disruption of the stratigraphy of the Joshua Tree terrane by the later Red Cloud thrust.	243
4-10.	Alternative cross-sectional interpretations for the relationship between the early and late strands of the Red Cloud thrust system.	248
4-11.	Tectonic evolution of the Red Cloud thrust system.	254-259
4-12.	Discontinuity in the basement rocks of the Eastern Transverse Ranges and Mojave Desert.	267
5-1.	Outcrop photographs of textures and intrusive relationships of plutonic rocks of the Mesozoic batholithic suites.	279
5-2.	Modes of older batholithic suite plotted on quartz-K-feldspar-plagioclase (QKP) and quartz-feldspar-mafics (QFM) ternary diagrams.	283

5-3.	Photomicrographs of samples from the older batholithic suite.	286
5-4.	Photomicrographs of undeformed and cataclasized samples from the younger batholithic suite.	292
5-5.	Modes of younger batholithic suite plotted on quartz-K-feldspar-plagioclase (QKP) and quartz-feldspar-mafics (QFM) ternary diagrams.	296
6-1.	Index map of southern California showing the distribution of crystalline basement exposures, Cenozoic strike-slip faults, Cenozoic cataclastic zones (C), Cenozoic Vincent-Orocopia-Chocolate Mountain thrust (V, O, CM), and Provinces I (extensive Tertiary terrestrial sedimentary and volcanic cover) and II (devoid of Tertiary cover).	310
6-2.	Earthquake hypocenter profiles in the Eastern Transverse Ranges, showing abrupt shallow lower limits of seismicity.	331
6-3.	Model for the early Cenozoic generation of Transverse Ranges-Mojave Desert crustal block as a tectonic block distinct from the Sierra Nevada and Peninsular Ranges blocks.	377
6-4.	Restoration of magnetic anomaly and fracture zone patterns of the northeastern Pacific Ocean floor relative to North America that is proposed to align the Sedna and Surveyor fracture zones with the Garlock fault and Gila River lineament, respectively.	381-385

TABLES	(page)
2-I. Modal compositions of samples from the Joshua Tree granite-granite gneiss.	33
2-II. Parageneses and modes of samples from the Joshua Tree paleo-weathered zone.	39
2-III. Parageneses and modes of samples from the Pinto Mountain quartzite.	51
2-IV. Parageneses of samples from the Lost Horse lithosome of the Pinto gneiss.	58
2-V. Parageneses of samples from the Baumok Mill lithosome of the Pinto gneiss.	67
2-VI. Parageneses of samples from the Music Valley lithosome of the Pinto gneiss.	77
2-VII. Parageneses of samples from the Black Eagle lithofacies of the Pinto gneiss.	78
3-I. Parageneses for samples of Hexie gneiss.	181
3-II. Modal compositions for samples of Soledad granodiorite and augen gneiss.	185
3-III. Modal compositions for samples of Augustine gneiss.	193
3-IV. Modal compositions of samples of syenite-mangerite-jotunite. .	206
5-I. Modes of samples from the older batholithic suite.	281
5-II. Modes of samples from the younger batholithic suite.	294
5-III. Modes of samples from the quartz latite dike swarm.	304

I. INTRODUCTION

OVERTURE

Southern California has been part of a tectonically active continental margin throughout the Mesozoic and Cenozoic eras. In a complex pattern of structurally juxtaposed and superposed lithologic assemblages, its geology has recorded translational and convergent interactions between the North American continent and various Pacific oceanic plates. In contrast to the passively imprinted magnetic signature on the ocean floor, California's intensely deformed continental record, formed as part of a broad marginal zone of tectonic response, graphically attests to the immense disruptive power of great crustal plates crushing against one another through time. In the detailed unravelling of this zone of deformation, much remains to be learned about the evolution of continental margin processes.

In southern California, a complicated Mesozoic-Cenozoic history of recurrent strike-slip faulting and thrusting, with intermittent coeval continental margin sedimentary and volcanic accumulation, and batholithic emplacement, has yielded an evolvingly chaotic tectonic mosaic in which widely diverse basement terranes are compounded along a baffling array of structures. The overprint of these continental margin tectonic processes has severely disrupted pre-Mesozoic paleo-geologic patterns, leaving disjointed remnants as clues toward palinspastic reconstruction of their pre-Mesozoic configuration. Although there is a growing understanding of many of the pieces, this geological jigsaw puzzle has yet to be reconstructed.

In southern California, specific contributions can still be made in range-by-range regional synthesis within crystalline complexes. Rigorous stepwise palinspastic reconstruction of the geologic evolution of southern California requires the recognition and characterization of each distinct lithologic terrane together with its boundary and sequencing relationships

to adjacent terranes.

This thesis was conceived to implement such a characterization for the crystalline rocks of part of the Eastern Transverse Ranges. From a regional evolutionary perspective, the crystalline complex of these ranges has been a poorly understood nexus of markedly disparate geologic terranes. The objective of the thesis has been to piece together a tectonic framework that is at once amenable to further observational and analytical tests within the area studied, and also has some predictive and interpretative value in understanding the geologic evolution of broader regions.

EASTERN TRANSVERSE RANGES

The Eastern Transverse Ranges are situated immediately east of the San Andreas fault in San Bernardino and Riverside counties in central southern California (Figure 1-1A,B). Collectively, they define a 50 kilometer wide physiographic belt that trends southeast from the San Bernardino Mountains to the Orocopia and Little Chuckwalla Mountains. Individually, the Eastern Transverse Ranges are an echelon east-west trending mountain ranges that lie athwart the northwest trend of their collective provincial belt. Thus, although the individual ranges are indeed transverse to the predominant northwest-southeast structural and physiographic grain of California, the eastern subprovince as a whole is part of that regional grain. These ranges correspond roughly to the eastern third of the Transverse Range physiographic province as defined by Jahns (1954, fig. 4, p. 11). The eastern ranges included by Jahns in his Transverse Range province consist of the San Bernardino, Little San Bernardino, Pinto, Hexie, Cottonwood, and Eagle Mountains. In the present study, however, the southern limit of this eastern structural and physiographic subprovince is drawn somewhat farther south than the boundary shown by Jahns to incorporate the Orocopia, Chuckwalla, and Little Chuckwalla Mountains.

The Eastern Transverse Ranges physiographic subprovince is a structural block bounded by active and inactive Cenozoic faults. The southwestern boundary lies along the San Andreas fault system. The northern and northeastern boundary is located along the northern frontal thrust system of the San Bernardino Mountains and at the Pinto Mountain fault along the north flank of the Pinto Mountains. The eastern boundary occurs at the Sheephole fault east of the Pinto and northern Eagle Mountains, and along Chuckwalla Valley east of the southern Eagle and Chuckwalla Mountains.

Figure 1-1. Overview of the principal physiographic, geographic, and late Cenozoic structural features in southern California and northwestern Mexico.

A. Photomosaic constructed from Skylab 4 (SL4) hand-held photographs (after Silver et al., 1977b).

B. Location map for physiographic, geographic, and structural features seen in the photomosaic:

SB	San Bernardino Mountains	C	Cucamonga fault
SG	San Gabriel Mountains	RH	Raymond Hill fault
SP	Sierra Pelona	SM	Santa Monica fault
SM	Santa Monica Mountains	MC	Malibu Canyon fault
F	Frazier Mountain		
P	Mt. Pinos		

6



A

The southern boundary lies along a largely combination of structures immediately south of the Orocopia, Chuckwalla, and Little Chuckwalla Mountains.

The distinctive physiography of the Eastern Transverse Ranges is structurally controlled by several east-west trending, near-vertical left-lateral fault zones. From north to south the major fault zones include the Pinto Mountain, Blue Cut, Chiriaco, and Salton Creek-Aztec Mines Wash faults. Several smaller left-lateral fault zones exist between these major breaks.

In a regional context, these faults exhibit a conjugate geometric relationship to the range-bounding faults of the western Mojave and Colorado Deserts which trend northnorthwest-southsoutheast and have right-lateral displacements. In the western half of the San Bernardino Mountains this conjugate strike-slip pattern gives way to a pattern of the range-bounding thrust faults seen along the north flank of the range and in Banning Pass. Similar range-bounding thrust faults with a component of left-lateral slip characterize the Transverse Ranges province west of the San Andreas fault.

The present physiographic Eastern Transverse Ranges formed structurally in response to Cenozoic deformational events that were superimposed on older geologic trends parallel to the continental margin. These older northwest to northnorthwest trends include the Mesozoic batholithic belts, as well as a distinctive belt of pre-batholithic rocks with its own northnorthwest-trending lithologic and structural grain. No evidence has been found during the course of this study for any pre-Cenozoic expression of an east-west transverse structural or physiographic province. The pre-Cenozoic crystalline complex of the Eastern Transverse Ranges has been the principal focus of this study, but the bedrock patterns established may be used to constrain palinspastic reconstructions of Cenozoic faulting in southern California.

PREVIOUS WORK

This section presents a general overview of previous geologic studies that have been conducted in the Eastern Transverse Ranges. More detailed discussion of pertinent studies will be presented in later chapters devoted to the lithologic terranes distinguished during the course of this study. Although previous work within the Eastern Transverse Ranges had indicated that a variety of crystalline terranes were present, the stratigraphic and structural relationships among these terranes were not understood. Pre-batholithic rocks variously described in the San Bernardino, Eagle, and Orocochia to Chuckwalla Mountains were lithologically, and to the extent known, geochronologically different, such that some combination of stratigraphic transitions and/or structural discontinuities was needed to accommodate the incongruities. An understanding of the nature of these pre-batholithic stratigraphic and structural relationships is one of the objectives of this study.

In the San Bernardino Mountains, pre-Mesozoic rocks in the Baldwin Lake-Big Bear Lake area include Precambrian basement gneisses nonconformably overlain by Eocambrian(?) through Paleozoic shelf quartzites and carbonates (Vaughan, 1922; Woodford and Harriss, 1928; Guillou, 1953; Richmond, 1960; Dibblee, 1964a,d, 1967f,g; Silver, 1971; Stewart and Poole, 1975; S. Cameron, personal comm.). The basement gneisses include a section of layered psammitic and/or metavolcanic quartzo-feldspathic gneiss interlayered (by intrusive and/or tectonic processes) with intrusive quartz dioritic to quartz monzonitic augen gneiss (Silver, 1971; R. Powell, unpub. map). No pelitic gneiss has been recognized in the country rock. U-Pb isotopic systematics in zircons from the intrusive orthogneiss yield an age of about 1720 m.y. (Silver, 1971).

Late Paleozoic fossils occur in limestones in the higher parts of a sedimentary section that has undergone generally low-grade contact metamorphism (Woodford and Harriss, 1928; Richmond, 1960). The section has been fragmented by a combination of thrust faults and high-angle faults (Guillou, 1953; Richmond, 1960; Dibblee, 1964a,d, 1967f,g; R. Powell, unpub. map; S. Cameron, personal comm.). One regional northwest-trending overturned fold occurs east of Baldwin Lake (Dibblee, 1964a,d, 1967f,g; R. Powell, unpub. map). The core of the fold involves Precambrian basement and its eastern flank has broken along a thrust fault. The direction of overturning and thrusting indicate a northeastward direction of tectonic transport during a pre-batholithic deformational episode.

Both the Precambrian basement and the overlying metasedimentary rocks are provincially correlative with rocks of the southern Great Basin in southern California and Nevada. The basement gneisses of the Baldwin Lake area are geochronologically part of a Precambrian age province that includes the basement rocks of the southern Great Basin (Silver, 1971; Silver et al., 1962). The overlying Eocambrian through Paleozoic stratigraphic section has been lithologically correlated with the miogeoclinal-shelf sedimentary rocks of the southern Great Basin (Stewart and Poole, 1975).

Pre-Mesozoic rocks in the southernmost Eastern Transverse Ranges are distinct from those of the San Bernardino Mountains. In the western Oro-copia Mountains, they had been shown to be part of a kindred suite comprising retrograded granulite gneiss, anorthosite-gabbro, and syenite-mangerite that were correlative with more extensive exposure of the same suite in the San Gabriel Mountains and Soledad Basin (Crowell and Walker, 1962; Crowell, 1962; Silver, 1971). In addition, Silver (1971) had identified exposures of the syenite-mangerite suite farther east in the Little Chuckwalla Moun-

tains. U-Pb isotopic systematics in zircons indicate that granulite-grade metamorphism occurred about 1400 m.y., followed by anorthosite-gabbro emplacement which culminated in the intrusion of syenite-mangerite at 1200 m.y. (Silver, 1971). Silver (1971) had also established the presence of a pre-granulite 1655 m.y. old porphyritic granodioritic to granitic augen gneiss, originally intrusive into layered gneisses in the Soledad Basin and in the Orocopia and Chuckwalla Mountains. At no place in the Transverse Ranges are the rocks of this Precambrian terrane known to be overlain by quartzites or any other pre-Cenozoic sedimentary cover.

In the central Eastern Transverse Ranges, a variety of lithologies had been recognized, but few pre-batholithic (pre-Mesozoic ?) structural or stratigraphic relationships had been established. Pre-mid-Mesozoic metasedimentary quartzites and carbonates of unknown affinity had been mapped and described in the Eagle and Pinto Mountains (Harder, 1912; Hadley, 1945; Dubois and Brummett, 1968; Hope, 1966). No fossils have been found in these rocks. Undifferentiated gneisses were described by W. J. Miller as Pinto Gneiss in the Pinto Mountains (Miller, 1938) and as the Chuckwalla Complex in a strip map along the southern flanks of the Little San Bernardino, Cottonwood, and Eagle Mountains and the northern flanks of the Orocopia and Chuckwalla Mountains (Miller, 1944). Miller (1946) later incorporated the Pinto Gneiss within the Chuckwalla Complex, a viewpoint adopted by Hope (1966) in producing a geologic map along the Blue Cut fault for which he combined a variety of lithologies into an undifferentiated gneiss terrane. Hope did, however, distinguish an intrusive quartz monzonite gneiss within his layered gneiss terrane.

Mesozoic plutonic rocks of batholithic dimension in the ranges south and east of the San Bernardino Mountains had been noted by several geologists.

A variety of plutonic rocks assigned to the Mesozoic have been described in the Little San Bernardino Mountains (MacLellan, 1936; Miller, 1944, 1946; Proctor, 1968), in the Pinto Mountains (Miller, 1938, 1946; Rogers, 1961), in the Little San Bernardino and Pinto Mountains (Dibblee, 1964d, 1967d,f), in the Little San Bernardino, Pinto, Hexie, and northern Eagle Mountains (Hope, 1966, 1969), in the northern Eagle Mountains (Harder, 1912; Hadley, 1945; Dubois and Brummett, 1968), and peripherally in the southern Cottonwood and Eagle Mountains and northern Orocochia and Chuckwalla Mountains (Miller, 1944, 1946). In the early studies, a Mesozoic age assignment was based loosely on lithologic correlation with plutonic rocks that intruded Paleozoic rocks such as those in the San Bernardino Mountains. In general, undeformed plutonic rocks were thought to be Mesozoic and highly deformed intrusive rocks were categorized as Precambrian, a criterion that has not proved reliable. More recently, scattered age determinations based on K-Ar (Bishop, 1964; Armstrong and Suppe, 1973) and U-Pb (L. Silver, personal comm.) have yielded Jurassic and Cretaceous apparent ages for batholithic rocks in the area studied. In light of the extensive area of anomalously young K-Ar ages in the San Bernardino Mountains and southern Mojave Desert (Miller and Morton, 1980), K-Ar ages in the southern Eastern Transverse Ranges cannot be trusted as emplacement ages without corroboration.

Cenozoic geologic features previously recognized within the Eastern Transverse Ranges include post-batholithic dike swarms and the east-west left-lateral faults that structurally control the transverse physiography. Dike rocks were discussed by Hope (1966) and Powell (1975). By analogy with the Transverse Ranges west of the San Andreas fault, east-west faults within the Eastern Transverse Ranges had long been thought to have left-lateral displacement (Hill, 1928; Hill and Dibblee, 1953; Hill, 1954; Allen, 1957),

but it has only been recently that such displacements have been documented for the Pinto Mountain fault (Dibblee, 1967d,f, 1968c), the Blue Cut fault (Hope, 1966, 1969), and the Chiriaco fault (Powell, 1975).

Cenozoic and probable Cenozoic features that had been recognized around the margins of the Eastern Transverse Ranges include the Orocochia thrust (Crowell, 1962, 1974; Crowell and Walker, 1962; Ehlig, 1968), the Sheep Hole fault (Hope, 1966, 1969; Rotstein et al., 1976), and faults of the San Andreas system (Allen, 1957; Crowell, 1962, 1975). The only known occurrence of Eocene marine beds east of the San Andreas fault in southern California had been identified in the central Orocochia Mountains (Crowell and Susuki, 1959). Mid-Cenozoic continental basin deposits of Oligo-Miocene volcanic rocks, terrestrial conglomerates, and lacustrine deposits had been demonstrated to nonconformably overlap the Eocene marine rocks and crystalline basement in the southcentral Orocochia Mountains (Crowell and Susuki, 1959), and crystalline basement in the southernmost Chuckwalla and Little Chuckwalla Mountains (Jennings, 1967; Crowe, 1973). This volcanic and sedimentary basin was known to extend southeastward through the Chocolate, Little Mule, and Palo Verde Mountains into southwestern Arizona (Jennings, 1967; Crowe, 1973; Dillon, 1975; Haxel, 1977).

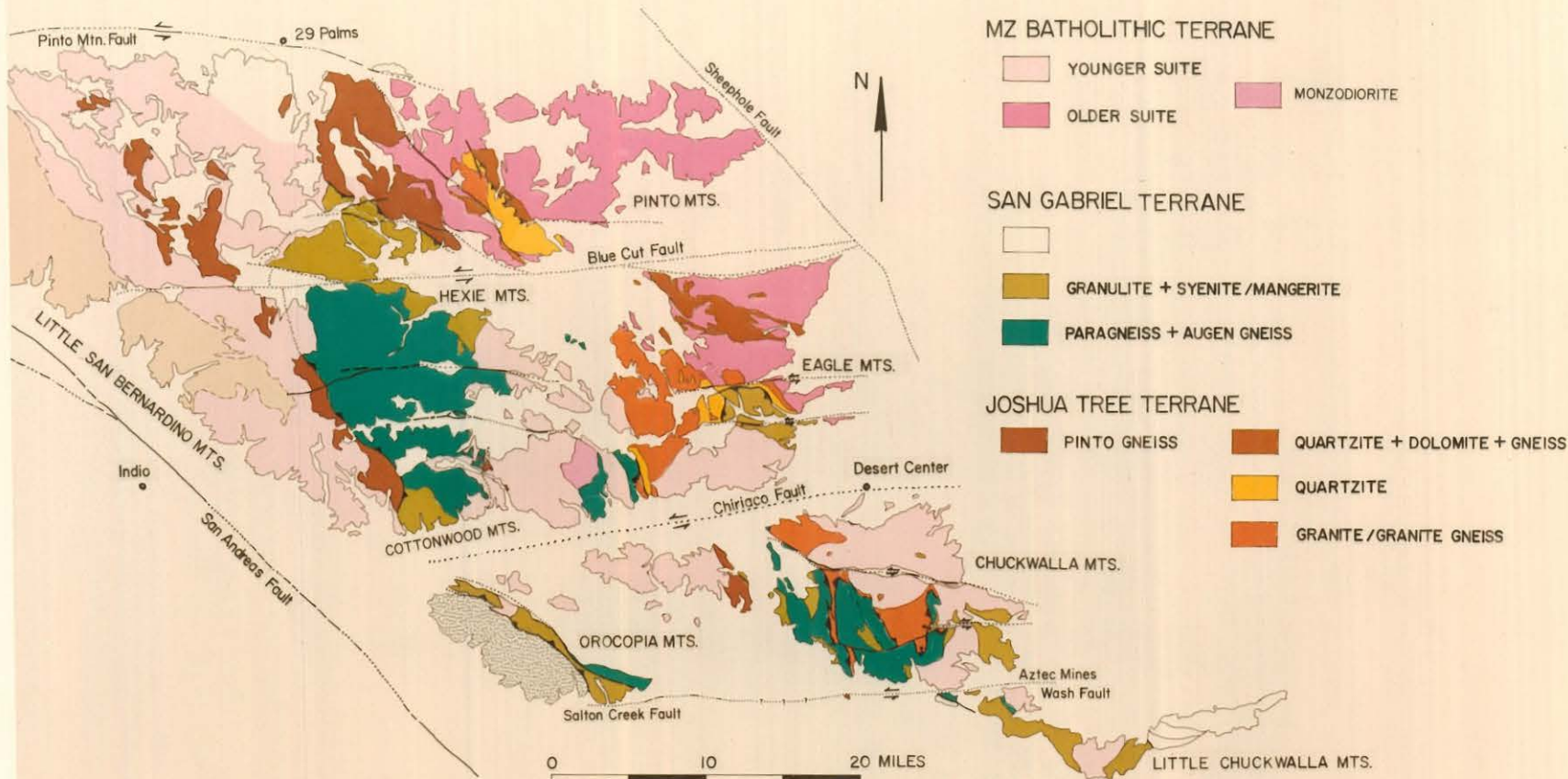
PRESENT STUDY

This thesis is a synthesis of my field and petrographic studies in the crystalline rocks of the Eastern Transverse Ranges, combined with an attempt to integrate what I have learned with the results of previous and concurrent investigators. In the course of this study, I have mapped the crystalline rocks of approximately half of the Eastern Transverse Ranges at scales of 1:36,000 and 1:62,500. The area mapped includes about 3,000 square kilometers in the Chuckwalla, Eagle, Cottonwood, Hexie, and parts of the Orocochia, Little tle San Bernardino, and Pinto Mountains (Figure 1-2A,B). The thesis was designed and carried out as a study in regional tectonics, as part of Prof. Silver's ongoing geochronologic and tectonic research program.

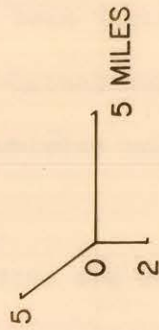
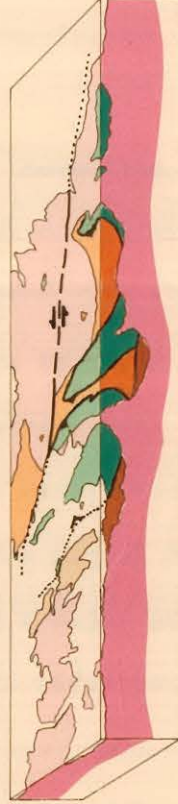
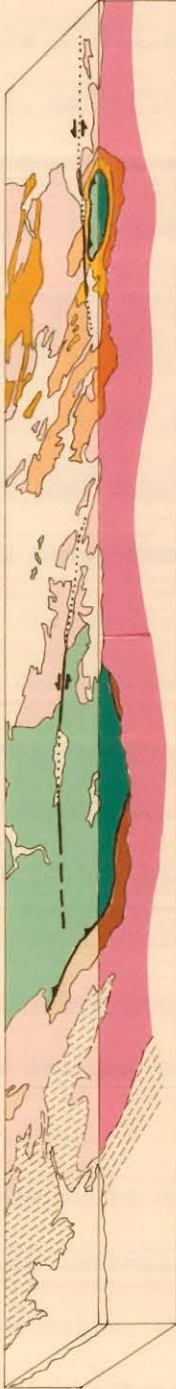
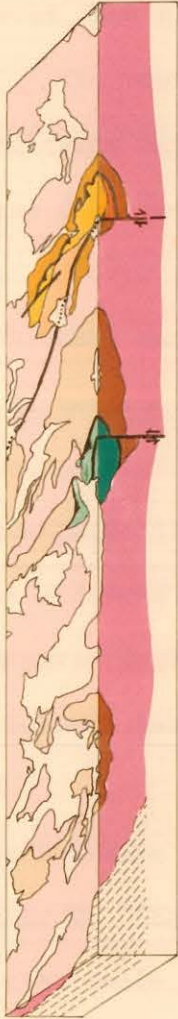
A broader areal perspective, encompassing the work within my field area, has been acquired through detailed mapping exercises conducted either as student or teaching assistant in the advanced field course at Caltech. Parts of Transverse Ranges Cenozoic continental basins were mapped in the Cuyama Badlands (under the direction of R.P. Sharp), Soledad Basin and Orocochia Mountains (L.T. Silver), the Mecca Hills and Cajon Creek at the San Andreas fault (C.R. Allen). Peninsular Ranges batholithic and pre-batholithic rocks were mapped in the Jurupa Mountains (H.P. Taylor), along the San Jacinto fault (C.R. Allen), and in Baja California (L.T. Silver). In the Mojave Desert, pre-batholithic and batholithic rocks were studied in the Marble and Ship Mountains (A.L. Albee) and in the Kilbeck Hills (L.T. Silver). Crystalline rocks in the Eastern Transverse Ranges south of the field area were mapped with L.T. Silver in the Little Chuckwalla Moutains. In preparation for my candidacy examination, I prepared a detailed map for part of the Precambrian crystalline basement nonconformably overlain by quartzites in the Baldwin Lake area of the San Bernardino Mountains. I

Figure 1-2. Geologic map and cross-sections of the crystalline basement complex of the southern Eastern Transverse Ranges:

- A. Geologic map (preliminary version) compiled from field sheets and the Salton Sea (Jennings, 1967), Santa Ana (Rogers, 1966), San Bernardino (Rogers, 1969), and Needles (Bishop, 1964) sheets of the Geologic Map of California (1:250,000). The gray wavy pattern in the Orocochia Mountains represents Orocochia schist. The tan color represents a post-batholithic deformational terrane. For details, refer to Plate I.
- B. Block-diagram cross-sections constructed along east-west lines of section through the Orocochia-Chuckwalla Mountains, Cottonwood-Eagle Mountains, Hexie-Eagle Mountains, and Pinto Mountains, respectively, from south to north. The block diagrams are constructed from the geologic map using a single point perspective (see, e.g., Raisz, 1962) from the southeast, such that the cross-sectional face is true scale. The position of the lines of cross-section on the map are apparent from the geologic map patterns on the surfaces of block diagrams. The dash pattern represents the post-batholithic deformational terrane shown in tan on the map.



MZ BATHOLITHIC TERRANE
SAN GABRIEL TERRANE
JOSHUA TREE TERRANE



have also mapped in the Paleozoic carbonate rocks along the central northern flank of the San Bernardino Mountains. Field trips led by those who have worked in geologic terranes surrounding my field area have contributed greatly to my appreciation of the diversity and complexity of southern California geology.

The principal arguments I will develop lend themselves to organization in terms of pre-batholithic, batholithic, and post-batholithic tectonic relationships. The thesis has been organized around this three-part framework. The term "batholithic" is used loosely here to refer to several episodes of Mesozoic batholithic emplacement, probably both Jurassic and Cretaceous, but possibly with (Permo)Triassic and early Cenozoic plutons as well. The pre-batholithic rocks within the area mapped comprise two lithologically distinct terranes superposed along a major pre-intrusive low-angle fault system (Red Cloud thrust). I will refer to these tectonic terranes informally as the Joshua Tree terrane (autochthonous? and para-autochthonous) and the San Gabriel terrane (allochthonous). These terranes and their tectonic superposition are dealt with in Chapters II, III, and IV. Because both of the terranes are lithologically distinct from all known pre-batholithic rocks to the east and to the north of my field area, they are inferred to be exotic terranes that have been juxtaposed along a pre-intrusive fault (or faults) against their pre-batholithic counterparts in the Baldwin Lake area of the San Bernardino Mountains and in the Mojave Desert.

The Mesozoic batholithic rocks of the field area are discussed briefly in Chapter V. They represent several episodes of magmatic emplacement on a batholithic scale. Geographically, these episodes fall into two overlapping northwest-southeast belts: a northeastern belt that consists of a gabbroic

to dioritic suite intruded by younger granite and porphyritic monzogranite (quartz monzonite); a southwestern belt that includes successively intrusive sub-belts of granodiorite, porphyritic monzogranite, coarse- to very coarse-grained equigranular monzogranite. The oldest rock type of the southwestern belt intrudes the youngest rock-type of the northeastern belt. The northeastern belt has yielded Jurassic ages, the southwestern belt Cretaceous ages (Bishop, 1964; Armstrong and Suppe, 1973; L. Silver, personal comm.)

The physiography and boundaries of the Eastern Transverse Ranges are controlled by post-batholithic structures, such that they define a structural as well as a geomorphic province. The eastern, southern, and western boundaries served to limit the extent of the area mapped for this thesis. The regional bedrock patterns and their abrupt termination at each of these boundaries provide potential constraints for palinspastic reconstructions along the bounding structures. These structures and plausible reconstructions are discussed in Chapter VI.

II. JOSHUA TREE TERRANE

INTRODUCTION

The term Joshua Tree terrane informally designates a regionally distinctive stratigraphic grouping of crystalline lithologies in the Eastern Transverse Ranges. The name has been chosen because each of the lithologies of the terrane, as well as their contact and sequencing relationships, can be observed within or immediately adjacent to Joshua Tree National Monument. For convenience, lithologic units within the terrane are also given informal names. General relationships within the Joshua Tree terrane, identified in this investigation, are summarized below, then discussed in greater detail in following sections.

The Joshua Tree terrane consists of a basement of Precambrian granite and granite gneiss that is nonconformably overlain (Figure 2-1) by a stratigraphic sequence that consists of two quartzite units, a heterogeneous unit of pelitic and ferriferous granofels and schist with subordinate carbonate rocks, and three homogeneous units that are successively pelitic granofels, quartz-plagioclase-biotite-muscovite gneiss and aluminosilicate-bearing pelitic granofels. The metasedimentary lithosomes are inferred to have accumulated in synchronous but laterally distinct depositional environments ranging offshore (westward) from a shoreline beach environment. The stratigraphic sequence is thought to have been diachronously generated as these depositional regimes migrated alternately shoreward and basinward through time. An ancient weathering zone caps the granite-granite gneiss beneath the overlying quartzites.

These stratigraphic units of the Joshua Tree terrane now occur in two structural packages exposed in northnorthwest-trending lithologic belts through the Eastern Transverse Ranges. Granite basement successively overlain by generally westward dipping lithosomes of quartzite, pelitic and

Figure 2-1. Panoramic photo-mosaic looking north in the central Pinto Mountains: light-colored Pinto Mountain quartzite rests nonconformably on darker Joshua Tree granite.



ferriferous pelitic granofels and schist, and minor carbonate rocks crop out in an eastern belt that extends through the Chuckwalla, Eagle, and central Pinto Mountains. Compositionally distinct lithosomes of pelitic and feldspathic granofels and gneiss are distributed in subparallel belts to the west in the Orocopia, Cottonwood, Hexie, Little San Bernardino, western Pinto, and southwestern San Bernardino Mountains. The easternmost of these western lithosomes is inferred to have interfingered with the pelitic lithosome of the eastern belt that interfingers in turn with the quartzite. These two lithologic belts have been telescoped by translation westward along a pre-batholithic thrust fault (part of the Red Cloud thrust system discussed in Chapter IV) that structurally superposes rocks of a more easterly (shoreward) stratigraphic setting over those of a more westerly (basinward) setting.

The entire Joshua Tree terrane has been regionally metamorphosed apparently in a single episode during which pressure-temperature conditions advanced along an andalusite-sillimanite facies series trajectory. The zonal distribution of metamorphic mineral assemblages linked by north-northeast- to northeast-trending isograds is combined with experimental results from the literature to suggest peak conditions within the field area at least as high as $P_T \approx 3.5$ to 3.8 kb and $T \approx 500$ to 550°C accompanied by a temporal and spatial northward increase in $P_{\text{H}_2\text{O}}/P_T$. The metamorphism is not related to intrusion of the Mesozoic batholiths, but rather at least partially predates, and is perhaps partially coeval with, the structural emplacement of the San Gabriel terrane allochthon along the Red Cloud thrust system. The metamorphic isograds are truncated by the early Red Cloud thrust and appear to show a slight westward to north-westward component of displacement across the later Red Cloud thrust

fault that has also telescoped the stratigraphic lithosomes. The orthogonal trends of the stratigraphic lithosomes and their metamorphic overprint produce a grid-like bedrock pattern that potentially constrains palinspastic reconstructions involving the Joshua Tree terrane.

JOSHUA TREE GRANITE-GRANITE GNEISS

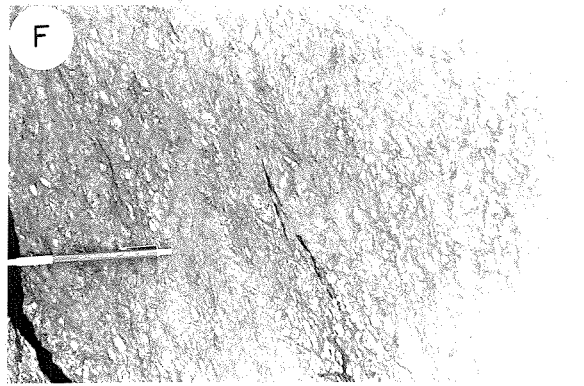
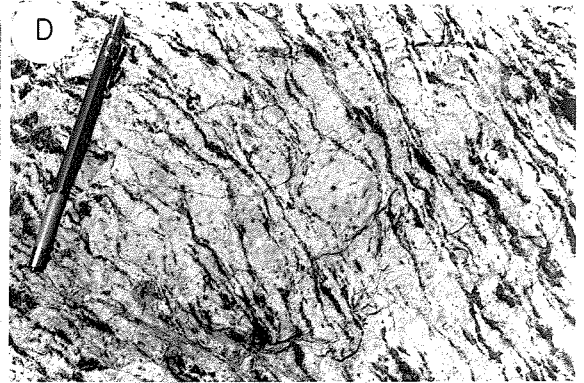
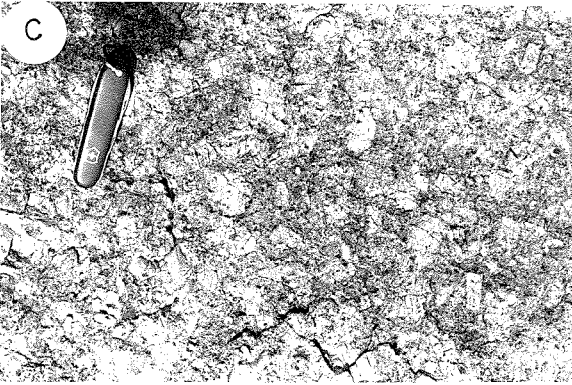
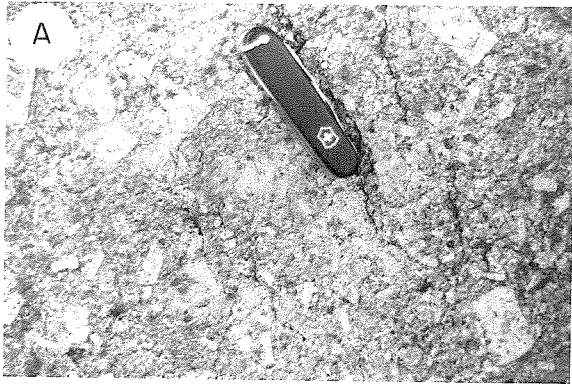
The Joshua Tree granite-granite gneiss is an informal name for the oldest unit yet found within the Joshua Tree terrane. It is a previously undifferentiated part of the Chuckwalla Complex (Miller, 1946), although its deformed lithology was accurately reported by Hope (1966, p. 8-9) as part of the gneiss complex he mapped in the northwestern Eagle Mountains. Hope correlated his gneiss complex with Miller's Chuckwalla Complex.

The Joshua Tree granite-granite gneiss crops out in a discontinuous band of batholithic proportions that stretches 80 kilometers from the Chuckwalla Mountains northnorthwestward through the Eagle and central Pinto Mountains (Plate I). Undeformed porphyritic granite and granite porphyry in the Pinto Mountains gives way southward to flasered granite gneiss that is strikingly uniform in its lithologic characteristics over 200 square kilometers of disconnected exposures. The unit is preserved in a structural slice within a folded thrust system (see Chapter IV). It is the sole lithology represented beneath the nonconformity of the Joshua Tree terrane: the country rock into which the granite must have intruded has not been found in the map area.

In the Chuckwalla and Eagle Mountains, the unit is intensely deformed granite gneiss (Figure 2-2B,D), with rare occurrences of relict granite porphyry to porphyritic granite textures. Northwestward into the Pinto Mountains, the deformational fabric disappears. At the northernmost limit of its exposure, the unit is undeformed granite porphyry (Figure 2-2A,C), nonconformably overlain by quartzite. Previous maps (Bishop, 1964; Hope, 1966, 1969; Jennings, 1967) have erroneously shown this undeformed granite as part of a Mesozoic batholithic unit intrusive into quartzite.

Figure 2-2. Outcrop photographs of lithologies within the Joshua Tree terrane.

- A. Joshua Tree granite, Pinto Mountains.
- B. Joshua Tree granite gneiss, Chuckwalla Mountains.
- C. Joshua Tree granite, Pinto Mountains.
- D. Joshua Tree granite gneiss, Chuckwalla Mountains.
- E. Paleo-weathered zone beneath nonconformity, little deformed, Pinto Mountains.
- F. Paleo-weathered zone, deformed, Eagle Mountains.
- G. Quartz/quartzite pebble conglomerate, Pinto Mountain quartzite, little deformed, Pinto Mountains. Tabular black siltite clast appears to be draped over white quartz/quartzite clasts.
- H. Quartz/quartzite pebble conglomerate, Pinto Mountain quartzite, intensely deformed, Eagle Mountains.



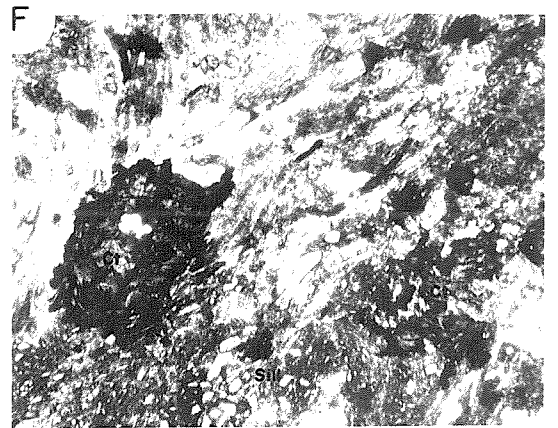
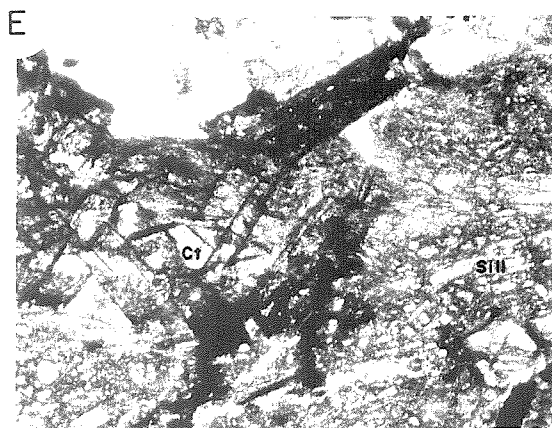
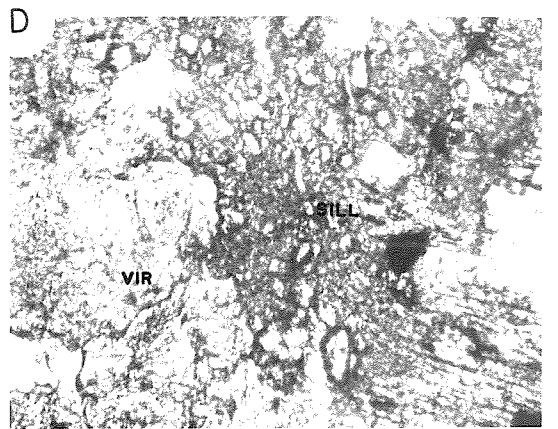
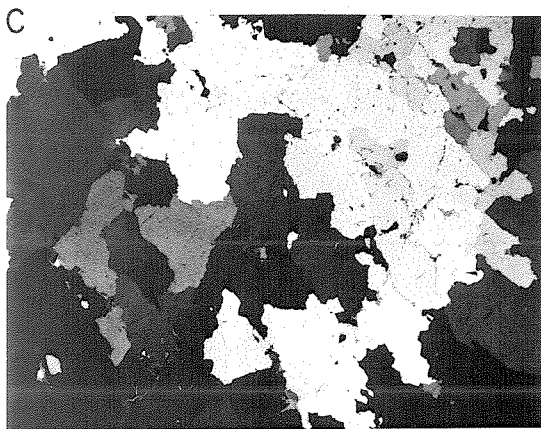
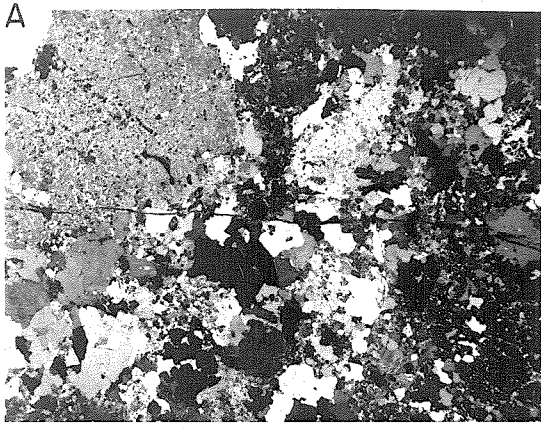
On weathered outcrops, both the granite and the granite gneiss are characterized by a distinctive light to moderate rusty brown patina of desert varnish. In fresh exposures, the porphyritic granite and granite porphyry are gray to light gray, and the granite gneiss is light gray to white. Relative to the overlying quartzite, both the granite and granite gneiss are less resistant to erosion; relative to the Mesozoic intrusive rocks, the granite gneiss is erosionally more resistant. The porphyritic granite characteristically weathers to spheroidal boulders, whereas the granite gneiss weathers to tabular boulders that reflect its fabric.

In hand-specimen, the leucocratic undeformed porphyritic granite (Figure 2-2A,C) exhibits large to very large (1 to 6 cm) euhedral gray phenocrysts of potassium feldspar (5 to 25%) and spheroidal phenocrysts (0.5 to 2 cm) of gray to blue quartz (3 to 10%) set in a fine-grained matrix (0.5 to 1.5 mm) of quartz and feldspar (50 to 75%). Plagioclase phenocrysts (0.5 to 2 cm), with a greenish or aquamarine tint, occur in varying abundance (0 to 5%). Mafic minerals generally constitute less than 5% of the rock, but may make up as much as 10%, and occur as clots (0.25 to 2 cm) of biotite and chlorite. Figure 2-3A shows the undeformed porphyritic granite in thin-section.

The granite gneiss is characteristically a leucocratic flaser augen gneiss, in which the augen are predominantly spindle-shaped aggregates of feldspar and quartz (Figure 2-2B,D). Potassium feldspar porphyroblasts with "pressure-shadow" aggregates of quartz and feldspar also are present. In thin-section, broken feldspar megacrysts are ubiquitous, as are strained and recrystallized "megacrystic" aggregates of quartz (Figure 2-3B). Large broken allanite crystals are common. Gneissic foliation is defined by quartzo-feldspathic layers 1-2 cm thick separated by wispy, discontinuous

Figure 2-3. Photomicrographs of samples from the Joshua Tree granite-granite gneiss, paleo-weathered zone, and Pinto Mountain quartzite of the Joshua Tree terrane:

- A. Joshua Tree granite: undeformed porphyritic granite. Sample Pinto-40P: crossed nicols, horizontal field of 2.6 cm.
- B. Joshua Tree granite gneiss: foliated granite augen gneiss. Sample Chkwal-45P: crossed nicols, horizontal field of 1.9 cm.
- C. Pinto Mountain quartzite: vitreous white quartzite lithology with sutured boundaries between recrystallized quartz grains. Sample Pinto-88P: crossed nicols, horizontal field of 1.6 cm.
- D. Pinto Mountain quartzite: intergrown viridine (VIR)(andalusite) and sillimanite (SILL) from the cross-bedded quartzite lithosome. Sample Eagle 31P: uncrossed nicols, horizontal field of 0.5 mm.
- E. Metamorphosed paleo-weathered zone: coexisting chloritoid (Ct), sillimanite (Sill), muscovite, and quartz. Sample Eagle 72-P: uncrossed nicols, horizontal field of 1 mm.
- F. Metamorphosed paleo-weathered zone: coexisting chloritoid (Ct), sillimanite (Sill), muscovite, and quartz. Sample Eagle 72-P: uncrossed nicols, horizontal field of 2 mm.



stringers of biotite. Modally, biotite forms less than 10% of the rock. Modes for the Joshua Tree granite-granite gneiss are listed in Table 2-I and plotted on ternary diagrams in Figure 2-4.

An incompletely preserved deformational gradient between granite and granite gneiss is seen in the Pinto Mountains, in which the foliation represents a cataclastic fabric superimposed on the porphyritic granite. Feldspar phenocrysts have resisted disintegration to remain as relics in the form of augen. Quartz phenocrysts have been flattened, smeared, and recrystallized during deformation. Similarly, the mafic clots of the porphyritic granite have been stretched and recrystallized into the biotite wisps of the granite gneiss. The textural features indicate that the physical conditions, including temperature, total and water pressure, and shear stress, at which the granite was deformed must have created an environment that permitted brittle fracture of feldspar, annealing of quartz, and recrystallization of biotite. Fine-grained, equigranular granitic gneiss occurs in the flaser augen gneiss in planar zones one to two meters thick. These layers may derive from nonporphyritic parts of the original granite, or they may represent zones that have been more thoroughly cataclastic with finer-grained recrystallization than the surrounding flasered gneiss.

The areas of intense deformation in the massive granite gneiss are coincident with areas of intense deformation in the overlying paleo-weathered zone and stretched quartzite/quartz-pebble conglomerates. The implication of this coincidence is that granite, weathered zone, and quartzite were all involved in a single, younger deformational event. If this interpretation is valid, fabric analysis within the three units should yield systematic relationships, even if the specific deformational

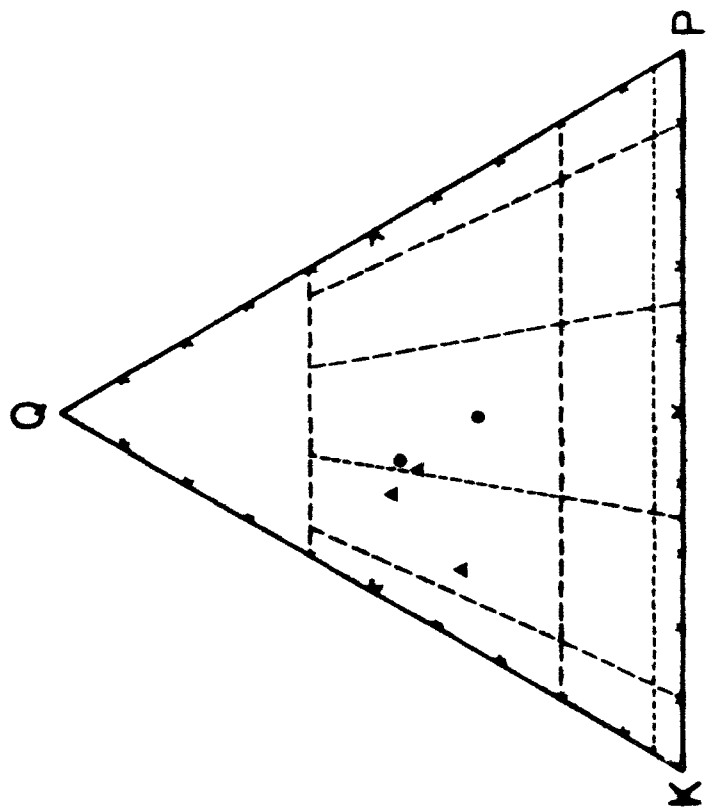
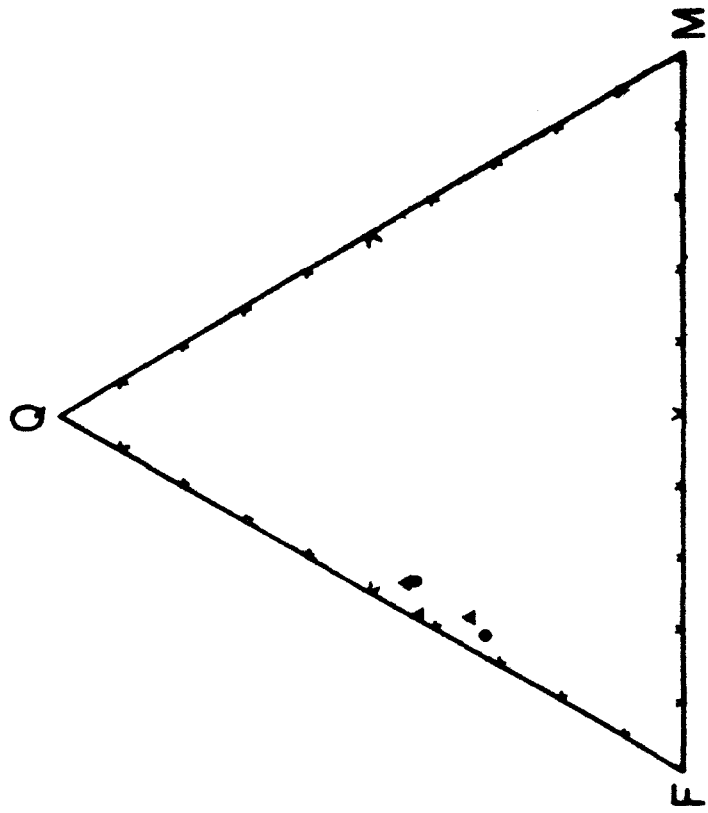
Table 2-I. Modal compositions of samples from the Joshua Tree granite-granite gneiss:

Sample: (Points)	Chuckwalla Mts.	Eagle Mts.		Pinto Mts.	
	<u>Chk-39*</u> (1012)	<u>E-35*</u> (1511)	<u>E-42*</u> (1045)	<u>P-24†</u> (2899)	<u>P-40†</u> (1953)
Quartz	43.9	39.4	34.1	42.1	30.8
Microcline	36.3	33.6	50.7	31.3	31.8
Plagioclase (Oligoclase)	14.3	18.9	9.4	18.7	30.6
Biotite	4.5	1.0	5.3	5.2	3.3
Muscovite	tr	6.9	0.5	--	2.0
Allanite	--	0.1	--	1.0	tr
Epidote	tr	--	tr	--	0.05
Apatite	tr	tr	tr	--	tr
Zircon	tr	0.1	tr	--	0.05
Opaques	1.0	tr	--	0.8	1.4

*granite gneiss

†granite

Figure 2-4. Modes of the Joshua Tree granite-granite gneiss plotted on quartz-potassium feldspar-plagioclase (QKP) and quartz-feldspar-mafics (QFM) ternary diagrams. Subdivisions of the QKP triangle represent Streckeisen's (1967) classification. Solid circles represent granite; triangles represent granite gneiss.



response is different for each lithology. The nature and timing of the deformational event is discussed further in Chapter IV. Suffice it to say at this point that, although the deformational fabric within the granite gneiss is complex, there is a suggestion of pattern and sequence to elements of fabric that recur throughout the area mapped, although orientations of the elements vary. Locally, in the highly deformed areas, the granite gneiss has apparently been remobilized. Flasered granite gneiss is cross-cut by little-deformed or undeformed stringers and irregular segregations of porphyritic granite. These mobilizates are especially well-exposed in the washes of the northern Eagle Mountains. Although sequentially they post-date the deformation that has affected the granite and superjacent paleo-weathered zone and quartzite, the significance of these mobilizates is not well-understood. Their development is consistent with the proposed high-temperature rehydration event of the Joshua Tree terrane metamorphic episode--but only if the rehydration was related to the allochthon emplacement, inasmuch as the mobilizates cross-cut the deformational fabric. This topic is discussed below in the section devoted to the metamorphism of the Pinto gneiss. Apparently rootless quartz-muscovite veins that cross-cut both the quartzite and paleo-weathered zone in the central Eagle Mountains may have a similar origin.

The isotopic geochronology of the Joshua Tree granite-granite gneiss is currently being investigated by Prof. Silver. Cogenetic suites of zircons from samples of deformed porphyritic granite from the Chuckwalla and Eagle Mountains, and undeformed granite from the Pinto Mountains yield three distinct patterns of isotopic disturbance (L. Silver, personal comm.). Although all of these suites demonstrate the Precambrian age of the granite-granite gneiss basement, complex patterns of discordance

preclude a positive demonstration of synchronicity for the three samples. A minimum basement age of about 1650 m.y. is inferred from this preliminary stage of the isotopic investigation (L. Silver, personal comm.).

PALEO-WEATHERED ZONE

In the Pinto, Eagle, and Chuckwalla Mountains, the porphyritic granite-granite gneiss is capped by a metamorphosed aluminous zone three to five meters thick that is inferred to have originated as an ancient weathering zone. The zone is characterized by abundant quartz, muscovite/potassium feldspar, and aluminosilicates, with rare chloritoid (Table 2-II, Figure 2-3E,F). In thin-section, the rock contains up to 40% aluminosilicate, although 10-12%, or less, is more typical (Figure 2-10D). The aluminosilicate is commonly about a third to fully replaced by fine- to coarse-grained white mica. Quartz is generally 50-55% of the the rock, with muscovite making up the remainder. Potassium feldspar, where present, is more or less replaced by muscovite. Zircon and iron oxides are present as accessories. The base of this zone is a sharply defined transition from the the underlying granite, marked by the abrupt disappearance of feldspar. Although the feldspar phenocrysts of the granite disappear at the contact, in the Pinto Mountains, where the granite is undeformed and the schist relatively little-deformed, the spheroidal quartz phenocrysts locally persist into the inferred weathered zone with the same spatial distribution and size variation that they exhibit in the porphyritic granite (Figure 2-2E).

Feldspar in the granite beneath the aluminous zone becomes progressively more altered up toward the contact. At the present grade of metamorphism, this alteration is represented by increasingly abundant muscovite. The muscovite was probably transformed from incipient alteration products such as illite and kaolinite. At least one relic of incompletely altered muscovitic granite occurs up within the lower part of the schist zone at a locality in the Eagle Mountains (T4S, R13E, Sec. 36, NW 1/4).

Table 2-II. Parageneses and modes of samples from the Joshua Tree
paleo-weathered zone:

Sample: (Points)	<u>E-30</u>	<u>E-34</u>	<u>E-72</u>	<u>P-33</u> (1925)	<u>P-34</u> (2485)	<u>P-42</u> (1747)	<u>Chk-245</u>
Quartz	x	x	x	54.5	53.9	52.0	x
Muscovite	x	x	x	33.0	33.8	19.5	x
K-feldspar							x
Al ₂ SiO ₅			sil	and 10.8	and 11.2	and 25.5	sil
Chloritoid			x				
Opaques*	m,h	m,h	h	m 1.6	m 1.1	m 2.9	m
Zircon	x	x	x	tr	tr	0.1	

* m magnetite
h hematite

If the metamorphic assemblage of muscovite, aluminosilicate, and quartz within the schist is inferred to derive from a protolith of illite, kaolinite, and quartz, then the protolith is mineralogically equivalent to modern weathering zones that have developed on granites in humid climates, where chemical weathering processes are vigorous (cf. Ruxton and Berry, 1957 (Hong Kong); Bjørlykke, K., 1975 (Uganda); Harrison, 1933 (British Guiana), fide Keller, 1955). Ruxton and Berry (1957, p. 1272-1273) describe a developmental sequence in one such weathering profile on a granite in Hong Kong. In the earliest phases of weathering, alteration of massive granite is followed by isolation of relict blocks (corestones) of massive granite surrounded by gruss. The third phase is marked by gradual destruction of the corestones and breakdown of feldspar into clay and silica, commonly, but not always, preserving the granitic texture. Each of these phases yields a zone of weathering that is vertically superposed on that of the preceding phase. In time, these zones encroach downward until a lower limit of weathering is reached, after which the later zones continue to develop at the expense of the earlier (deeper) zones. Thus, in this model, an old-age weathering profile is characterized by thick zones of clay and quartz, and compressed zones of relict corestones and gruss.

If the aluminous zone above the Joshua Tree granite is derived from a weathering profile, the abrupt transition from altered massive granite to muscovite-aluminosilicate-quartz schist suggests that the parent profile was an old-age form in the above sequence, marked by advanced third-phase and fourth-phase weathering zones. The granite block described within the schist in the Eagle Mountains may represent a rare relict corestone. Any relict granitic texture and residual feldspar

that may have remained near the base of the weathering zone above massive granite have been obliterated during subsequent metamorphism. Potassium feldspar now found in the schist zone was probably all produced metamorphically from the breakdown of muscovite, followed by subsequent retrograde reconversion to muscovite. Similarly, if any sedimentary reworking of weathering products occurred prior to deposition of the overlying quartzite, the metamorphic overprint has masked the evidence. It is distinctly possible that some upper part of the original profile was removed during transgression of the Pinto Mountain quartzite beach environment. Kaolinite incorporated from the aluminous zone could have provided a source for Al_2O_3 now forming aluminosilicates in the cross-bedded lithosome of the Pinto Mountain quartzite.

In the Pinto Mountains, the metamorphosed paleo-weathered zone is relatively little-deformed, with slight to moderate foliation and some kink-folding. To the south, in the Eagle and Chuckwalla Mountains, the zone has been more intensely deformed concomitantly with the underlying granite, and is represented by a strongly foliated and kink-banded schist with quartz augen (Figure 2-2F). The augen are commonly spindle-shaped in the third dimension, with their direction of elongation parallel to that of the overlying stretched quartzite/quartz pebbles. It is inferred that during the deformational event the quartz phenocrysts of the granite were destroyed by smearing and recrystallization in the granite gneiss, whereas in the weathered zone, the micas absorbed much of the deformation, so that the relict quartz phenocrysts, although recrystallized, have been preserved as augen. Quartz veins are common and are typically deformed by intra-formational chevron folds.

In both the little-deformed and deformed terranes, the weathering zone is commonly poorly exposed beneath quartzite rubble, because it is less resistant than both the underlying granite and the overlying quartzite (Figure 2-1).

PINTO GNEISS

Introduction

The Pinto gneiss was named and first described by Miller (1938, p. 418-419, p. 424 ff.) in the Pinto Mountains, five to ten miles south to southeast of Twentynine Palms. Exposures of the gneiss in the area Miller mapped lie mostly east of the Pinto Basin Road. Miller described scattered narrow bands of light- to dark-gray quartzites and of dark amphibolite included as discontinuous lenses in extensive biotite gneiss that is commonly migmatitic. As described by Miller, the Pinto gneiss is actually a crystalline complex incorporating orthogneisses as well as metasedimentary rocks. In the present study, a major pre-batholithic thrust fault has also been recognized within this gneiss complex (see Chapter IV).

In 1944, Miller mapped in reconnaissance a strip from Palm Springs to Blythe in which he assigned all pre-batholithic gneisses and foliated batholithic rocks of the Little San Bernardino, Cottonwood, Orocopia, Eagle, and Chuckwalla Mountains into the undifferentiated Chuckwalla complex (Miller, 1944). Later, he included the pre-batholithic Pinto gneiss in the Chuckwalla complex on the basis of similarity in lithologic character, degree of deformation and migmatization (Miller, 1946). In view of this correlation, it is proposed here that the name Pinto gneiss be redefined as described below. Miller concluded that the quartzites and marbles of the Eagle Mountains mining district were younger rocks faulted into the Chuckwalla complex.

Hope (1966, 1969), in a map of the geology along the Blue Cut fault, subdivided the pre-batholithic rocks into three groups. The older two groups consist of an undifferentiated complex of granite gneiss, layered

gneiss, migmatite, and minor quartzite intruded by quartz monzonite gneiss. Together they are equivalent to Miller's Chuckwalla complex. The youngest group comprises metamorphosed quartzite, schist, and marble that are equivalent to the metasedimentary rocks of the Eagle Mountain Mine area (Harder, 1912; Hadley, 1945). Hope inferred that the Eagle Mountain Mine section rests on a Chuckwalla complex basement.

In this study, the name Pinto gneiss is informally redefined to designate a stratigraphically related group of metasedimentary and questionably metasedimentary units within the pre-batholithic Chuckwalla complex of the Eastern Transverse Ranges. Quartzite, pelitic gneiss, minor limestone and dolomite, and hematite-quartz and hematitic pelitic schist are certainly derived from sedimentary protoliths. Quartz-plagioclase-biotite-muscovite gneiss and ferromagnesian cordierite-orthoamphibole-chlorite gneiss intercalated with the pelitic gneisses are possibly metametasedimentary. Pinto gneiss is an appropriate name for this package of rocks because each of the constituent lithologies crops out in the central and western Pinto Mountains.

The subdivisions of the Pinto gneiss are distributed in five principal northnorthwest-trending, generally westward-dipping lithologic belts. Each belt exhibits distinctive mineralogical and textural characteristics that are remarkably uniform throughout the field area (see Plate V). These belts of uniform lithology are interpreted to have been derived from distinct volumes of rock, or lithosomes, within the sedimentary protolith. The two easternmost lithosomes comprise the Pinto Mountain quartzite, which constitutes a shoreline facies nonconformably deposited on Joshua Tree granite. Westward or basinward from the quartzites, the Pinto gneiss consists of the heterogeneous pelitic, feldspathic, and

ferriferous Black Eagle granofels/schist with minor carbonate rocks, the pelitic Baumonk Mill granofels, the feldspathic Music Valley gneiss, and the pelitic Lost Horse granofels with minor ferromagnesian layers.

In view of the sedimentary origin and stratigraphic interfingering, both demonstrable and inferred, for the protoliths of the Pinto gneiss subdivisions, it may become expedient to classify the gneiss as the Pinto group, and its principal subdivisions as formations with members. However, because only remnants of the Pinto gneiss are preserved, and because interpolation between these isolated exposures is highly interpretive, this step has been deferred pending further study.

Persistent gneissic foliation consists of segregations of biotite and muscovite versus granular minerals. Where phyllosilicates predominate, the gneiss is schistose; where granular minerals predominate, it has a laminated granofelsic texture. Foliated segregations are a few millimeters to a few centimeters thick and parallel thicker compositional layering that is probably bedding. It seems likely that the gneissic segregations in part reflect protolithic compositional laminae. Where quartz, biotite, plagioclase, and some muscovite and potassium feldspar occur as metamorphic assemblages approximating minimum melt composition (Music Valley gneiss), the gneiss is migmatitic with locally mobilized segregations clearly discordant to foliation. These migmatitic gneisses are complexly folded with no systematic fold axis orientation, which locally imparts an intensely deformed appearance in outcrop.

Foliated granitic rocks and amphibolites of uncertain affinities locally intrude Pinto gneiss in the Pinto and Little San Bernardino-Hexie Mountains. It has not been ascertained whether these intrusives are related to the Mesozoic batholiths or represent older plutonic activity.

Pinto Mountain Quartzite

Introduction. Quartzite in the Eagle Mountain Mine area was first described by Harder (1912), who discussed quartzite occurrences in three stratigraphic intervals: a lower schist and quartzite series, a middle vitreous quartzite series, and an upper dolomite and quartzite series. More recent studies (Hadley, 1945; Hope, 1966; Dubois and Brummett, 1968) recapitulate and elaborate upon Harder's stratigraphic section. Hope and Dubois and Brummett circumstantially advocate a Paleozoic age for the Eagle Mountain Mine metasedimentary rocks. Dubois and Brummett (1968, p. 1597) also refer briefly to a "Precambrian sequence comprising gneisses and schists with local quartzites" found in the southern Eagle Mountains and in adjoining ranges to the west and north of the Eagle Mountains mining district. In the Pinto Mountains, quartzite was mapped by Hope (1966, 1969) as correlative with the vitreous quartzite unit in the Eagle Mountains. Early in the course of his study, Hope abandoned attempts to subdivide the quartzite unit.

In this study, a stratigraphic and structural context has been established which permits correlation of these and other quartzite occurrences in the region. The quartzite occurs as a generally westward-dipping tabular stratigraphic unit sandwiched between the Joshua Tree granite-granite gneiss and the Black Eagle granofels/schist. The lower and eastern boundary of the quartzite is marked by the paleo-weathered zone that caps the Joshua Tree granite; the upper and western boundary interfingers with Black Eagle granofels/schist. Lithosomes of the quartzite and granofels/schist appear to have been concurrently generated as time-transgressive accumulations in differing depositional environments.

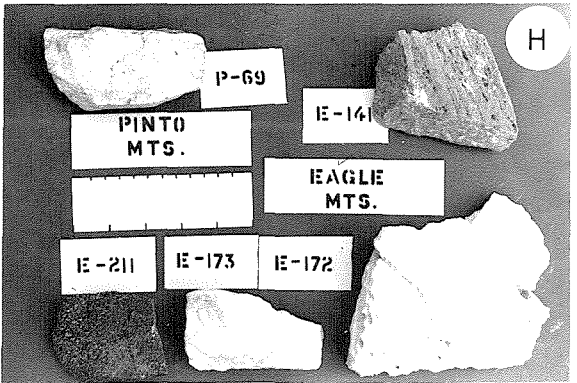
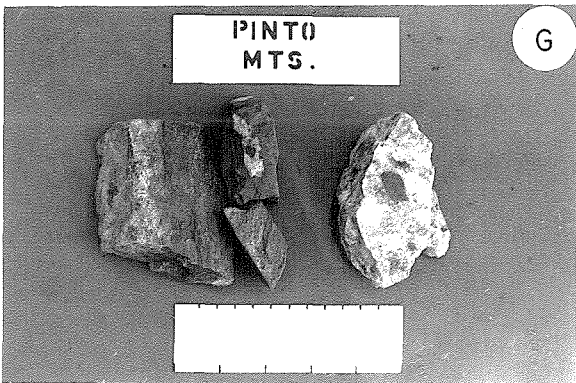
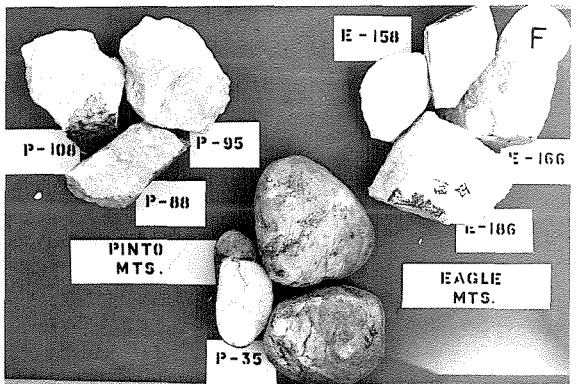
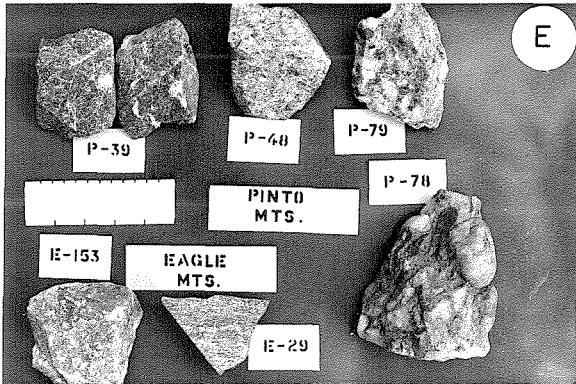
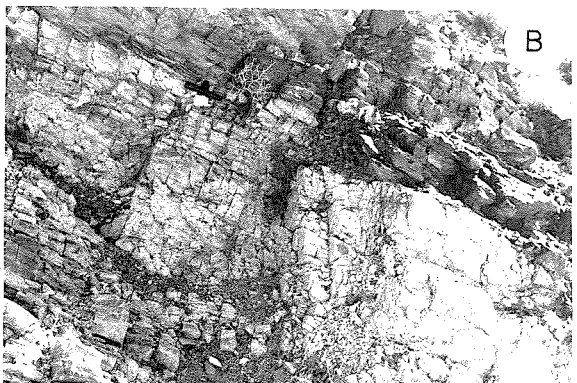
The quartzite lithofacies is extensively exposed on Pinto Mountain in the central Pinto Mountains (Figure 2-1, Plate I). Because these exposures are the least deformed of any in the region, the unit is informally referred to as Pinto Mountain quartzite. The Pinto Mountain quartzite also crops out extensively in the Eagle Mountain Mine area of the northern Eagle Mountains, along the upper reaches of Big Wash in the central Eagle Mountains, and in the southern Eagle Mountains north of the Hayfield pumping station on the Colorado River aqueduct. Thin remnants of basal quartzite preserved on a basement of Joshua Tree granite gneiss in the southwesternmost Chuckwalla Mountains are structurally truncated by the Red Cloud thrust (see Chapter IV).

Lithologically, the Pinto quartzite comprises two interfingering diachronous subfacies that constitute the easternmost lithosomes of the Pinto gneiss. The more easterly and stratigraphically lower of the two lithosomes consists of cross-bedded quartzite with interbedded quartzite/quartz-pebble conglomerates. The more westerly lithosome is very pure, coarse-grained vitreous white quartzite described by earlier workers in the Eagle Mountain mining district (Harder, 1912; Hadley, 1945; Dubois and Brummett, 1968). Measured stratigraphic columns including the quartzite are shown in Plate IV.

Cross-bedded Quartzite Lithosome. The cross-bedded quartzite is coarse- to very coarse-grained, light- to dark-gray to bluish-gray, vitreous, and compositionally mature. It is generally medium-bedded to massive and characterized by low-angle sets of tangential planar cross-laminations a few millimeters to a centimeter thick (Figure 2-5A). The cross-bedded unit typically displays a vitreous coarse mottling effect produced by

Figure 2-5. Outcrop and hand sample photographs of Pinto Mountain quartzite, Lost Horse granofels, and Iron Chief dolomite of the Pinto gneiss:

- A. Pinto Mountain quartzite: cross-bedded lithosome, Pinto Mountains.
- B. Pinto Mountain quartzite: vitreous white lithosome, Eagle Mountains.
- C. Lost Horse granofels: andalusite schist, Little San Bernardino-Hexie Mountains.
- D. Lost Horse granofels, Little San Bernardino-Hexie Mountains.
- E. Pinto Mountain quartzite: hand samples of cross-bedded lithosome and conglomerate. Scale shows centimeters and inches.
- F. Pinto Mountain quartzite: hand samples of vitreous white lithosome and cobbles of white quartz/quartzite (P-35) from the conglomerate.
- G. Pinto Mountain quartzite: hand samples of hematite-aluminosilicate-quartz layers from vitreous lithosome and jasper clast in the conglomerate. Scale shows centimeters and inches.
- H. Iron Chief dolomite: hand samples. Scale shows centimeters and inches.



light gray to white recrystallized quartz grains intermingled with darker gray quartz grains (Figure 2-5E). Laminations and cross-laminations are commonly delineated by slight variations in the relative abundances of the lighter and darker gray quartz grains. Thin black laminae (<1 mm) of opaque minerals occur sporadically. In thin-section, the quartzite of this lithosome is >90% quartz, with the remainder andalusite and/or sillimanite, muscovite, hematite and/or magnetite-ilmenite. Andalusite is typically partly or entirely viridine with colorless to greenish-yellow or greenish-yellow to bluish-green pleochroism (Figure 2-3D). In some grains, the color is sufficiently intense to give anomalous interference colors of green to blue-green. Opaque minerals include magnetite-ilmenite and hematite. Modes are listed in Table 2-III.

Quartzite/quartz-clast conglomerates interfinger with the cross-bedded quartzite in 0.5 to 3 meter beds that are more abundant in the lower half of any given vertical section through the unit. In the Pinto Mountains, undeformed conglomerates contain well-rounded pebbles and cobbles of coarsegrained pure white quartzite or vein quartz, fine-grained flinty black quartzite, and fine-grained flinty red jasper (Figures 2-2G, 2-5E,F,G). White quartzite or vein quartz clasts constitute an estimated 85-90% of the clast population, black quartzite 5-15%, and jasper <1%. In the Pinto Mountains, undeformed white quartzite or vein quartz clasts have well-rounded, roughly equant to slightly flattened or elongate solid forms, whereas the black quartzite clasts are commonly tabular or ellipsoidal. Rare red jasper pebbles are ellipsoidal and seem to be found in clusters. Clasts make up 75-85% of the rock with a matrix of coarse-grained light gray to bluish-gray quartzite. Texturally, the conglomerates can be either clast-supported or matrix-supported, with tabular

Table 2-III. Parageneses and modes of samples from the Pinto Mountain quartzite:

Sample: (Points)	white					x-bedded		cgl.
	<u>P-63</u> (1563)	<u>P-88</u> (1370)	<u>E-166</u> (1747)	<u>P-70</u>	<u>P-105</u>	<u>E-29</u>	<u>E-79</u>	<u>E-31</u>
Quartz	96.6	97.9	99.0	x	x	x	x	x
Plagioclase (oligoclase)	2.6			x				
Al ₂ SiO ₅ *						v,s		v,s
Muscovite	0.8	2.1	1.0		x	x	x	x
Biotite				x			x	
Accessories*	z,o	z,o		o	z,o	a,o		z,o

- * v viridine
s sillimanite
z zircon
a apatite
o opaques

black siltite clasts commonly draped over white quartzite or vein quartz clasts (Figure 2-2G). The matrix quartzite is identical to the cross-bedded quartzites of the surrounding section. In the Eagle Mountains, these rocks are deformed into stretched pebble conglomerates with pebble aspect ratios as high as 10:2:1 (Figure 2-2H). On weathered surfaces of the conglomerate, hematite imparts a rusty brown stain on the varicolored clasts and matrix resulting in a distinctive mottled-pudding effect.

In thin-section, the white quartzite or vein quartz clasts are extremely pure quartz (>99%) with coarse interlocking quartz grains. The fine-grained black quartzites contain recrystallized quartz with abundant very fine-grained specular hematite that is arranged in laminar and circular to elliptical trains which may represent, respectively, relict bedding and grain or granule boundaries.

The cross-bedded quartzite unit forms cliffs that have a tan to brownish-gray color in contrast to the overlying vitreous white quartzite. Thicknesses for the unit are shown on Plate IV.

Vitreous White Quartzite Lithosome. The very coarse-grained, vitreous white quartzite lithosome of the Pinto Mountain quartzite is compositionally supermature. Point counts on three thin-sections yield estimates of 96 to >99% quartz, with trace amounts of sodic oligoclase, white mica, hematite, zircon, and rutile. From a distance, the unit invariably forms white, blocky ledges (Figure 2-5B). At the outcrop scale, the quartzite is white to yellowish, brownish, or reddish white, the coloration a result of iron-oxide staining. On fresh surfaces, the rock is white to light gray. Bedding is generally obscure or obliterated by recrystallization, giving the rock a massive appearance. Rare thin (~1mm)

dark laminations of opaque minerals locally suggest bedding. Very well-developed jointing leads to the blocky-weathered outcrops.

In thin-section, slightly undulose, very coarse (up to 1 cm) inequigranular quartz grains exhibit a distinctive interpenetrating or lobate sutured texture with small inclusions of white mica and plagioclase (Figure 2-3C). There is no petrographic evidence for relict detrital quartz grains with silica overgrowths. This texture is sufficiently arresting in both hand specimen and thin-section to instill curiosity as to whether it is geologically non-unique, or whether it may indicate some particular combination of sedimentary and subsequent metamorphic processes, possibly including processes of accumulation and diagenesis, the role of water, deformational history, and temperature-pressure history. The quartz invariably contains a dusting of extremely fine opaques (iron-oxide?) that are commonly concentrated in linear trains within a grain. Twinned sodic oligoclase is present in varying amounts up to 2 or 3 percent and is commonly partially or completely altered to fine-grained white mica. Coarse-grained muscovite also occurs. Both zircon and rutile occur in rounded and idiomorphic grains, but zircon is more commonly rounded and rutile idiomorphic.

The development of this type of texture elsewhere has been interpreted to involve thermal recrystallization with slight deformation. For instance, very coarse-grained, light-colored, glassy-looking clean quartzites with interlocking grains occur within the inner contact aureole beneath the Bushveld complex of South Africa. Hall and du Toit (1923, p. 74-77) attribute the texture to thermal recrystallization of a very pure quartz protolith. The quartzites generally show no trace of an original detrital nature, although at one locality they report an equigranular,

medium-grained quartzite with scattered centers of recrystallization that coalesce toward the Bushveld contact. Grain size in these South African quartzites also reaches or surpasses 1 cm. The Pinto Mountain quartzite has been subjected to a high temperature, low pressure metamorphism (see below) that may not be unlike that beneath the Bushveld ultramafic complex.

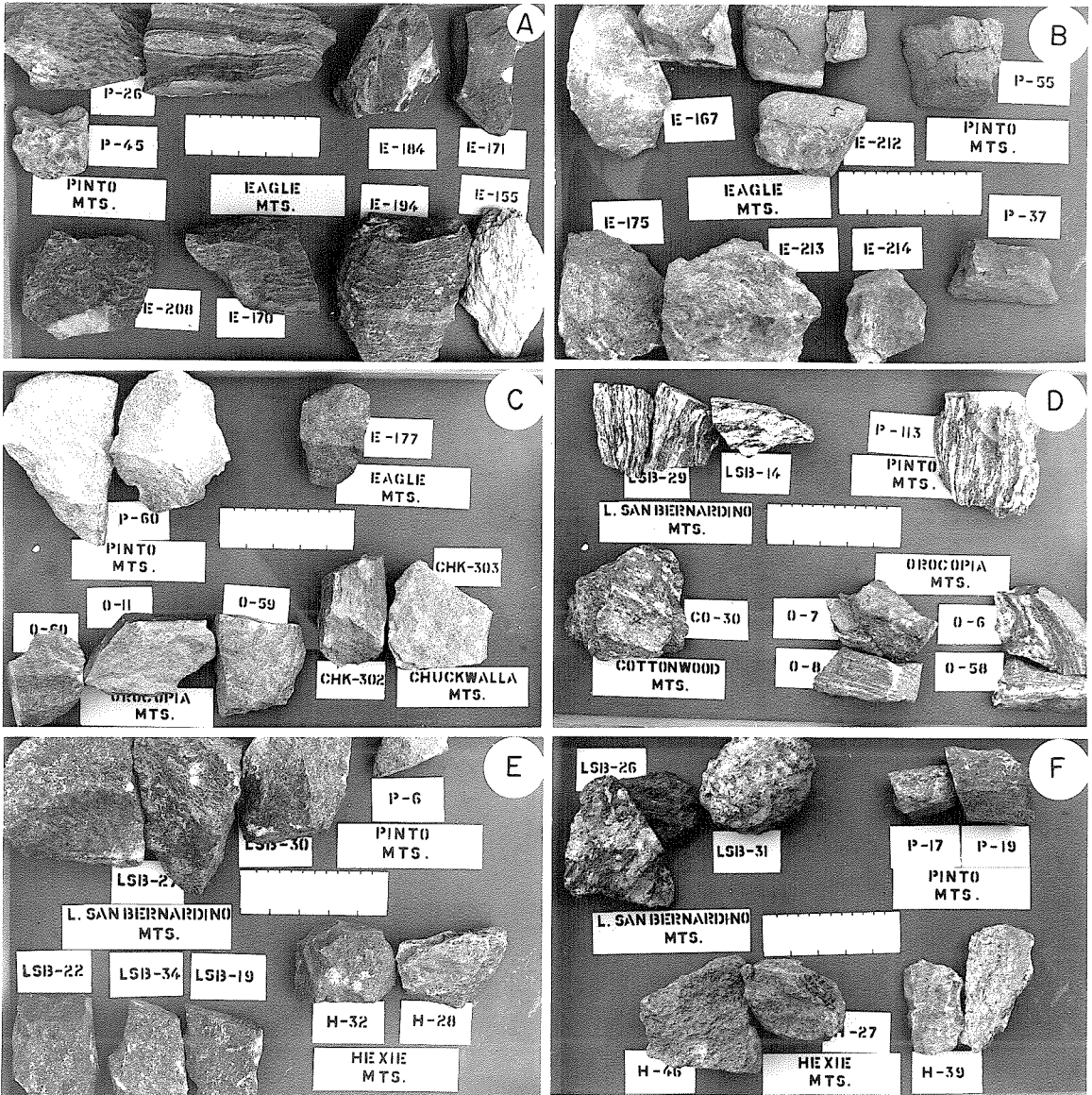
Lost Horse Granofels

The westernmost (Lost Horse) lithosome of the Pinto gneiss crops out in the Cottonwood, Hexie, western Pinto, and Little San Bernardino Mountains (Plate V). The name Lost Horse is derived from Lost Horse Mountain in the Little San Bernardino Mountains where the granofels occurs in a large pendant within Cretaceous batholithic rocks. It is predominantly pelitic gneiss characterized by the presence of quartz, biotite, andalusite and/or sillimanite, and cordierite. Muscovite is usually present; potassium feldspar, plagioclase, staurolite, and/or garnet may be present. Granofelsic and subordinate schistose units of pelitic gneiss make up compositionally and texturally distinct layers with thicknesses up to a few meters. The granofelsic gneiss commonly weathers to form dark brownish-gray, vitreous ledges (Figure 2-5D). Subordinate ferromagnesian layers are characterized by the presence of chlorite plus orthoamphibole (anthophyllite or gedrite) and cordierite, or talc and clinoamphibole.

The granofelsic pelitic gneiss is massive to laminated, dark bluish-gray, vitreous, and extremely tough when fresh (Figure 2-5D). The rock is generally medium-grained (1-2 mm), equigranular, composed predominantly of quartz and cordierite (Figure 2-6E). Staurolite, sillimanite (where present as separate grains), and andalusite are roughly equidimensional in the same size range. Garnet is usually slightly smaller (~1 mm).

Figure 2-6. Hand sample photographs of the Black Eagle, Baumonk Mill, Music Valley, and Lost Horse granofelses of the Pinto gneiss:

- A. Black Eagle granofels-schist: pelitic. Scale shows centimeters and inches.
- B. Black Eagle granofels: ferriferous pelitic. Scale shows centimeters and inches.
- C. Baumonk Mill granofels: pelitic. Scale shows centimeters and inches.
- D. Music Valley gneiss: feldspathic. Scale shows centimeters and inches.
- E. Lost Horse granofels: pelitic. Scale shows centimeters and inches. Sample P-6 is misplaced Baumonk Mill granofels.
- F. Lost Horse granofels: ferromagnesian. Scale shows centimeters and inches.



Biotite and muscovite are subordinate to and disseminated through the granular minerals.

In thin-section, the granofelsic gneiss has a granoblastic texture (Figure 2-7A to E). Quartz occurs as interpenetrating, sutured grains with undulating extinction. Cordierite is found as idioblastic (against quartz) equant grains, with grain boundaries and fractures commonly altered pseudomorphously to an isotropic, commonly pleochroic mustard-yellow mineral. Sillimanite occurs as idioblastic crystals and clusters of crystals, commonly intergrown with cordierite. Andalusite occurs as equant, idioblastic grains. Staurolite also occurs as equant grains, usually as relict grains armored in overgrowths of intergrown cordierite and sillimanite. Biotite is characteristically green to greenish-brown which suggests a high Fe^{+3} content relative to Ti (Deer, Howie, and Zussman, 1966, p. 213). Observed assemblages for the granofelsic gneiss are tabulated in Table IV. The schistose pelitic gneiss is characterized by a higher percentage of biotite and muscovite than occurs in the granofelsic gneiss. Abundant large porphyroblasts of andalusite up to 5 cm long can be found at some localities (Figures 2-5C, 2-7B).

The distinctive suite of assemblages that characterize the ferromagnesian layers (1 to 30 cm thick) are conformably interlayered within the pelitic gneiss of the Lost Horse lithosome. There is no evidence for intrusive or structural emplacement of these layers. Furthermore, their apparent occurrence in a single stratigraphic zone near the base of the Lost Horse lithosome indicates that the ferromagnesian lithology may be a constituent stratiform accumulation unit of the diachronous facies package, although volumetrically the lithology represents less than 1% of the section (Figure 2-6F).

Table 2-IV. Parageneses of samples from the Lost Horse lithosome of the Pinto gneiss:

<u>PELITIC</u>													
	Little San Bernardino Mts.						Hexie Mts.						
Sample:	<u>LSB-19</u>	<u>LSB-22</u>	<u>LSB-24</u>	<u>LSB-27</u>	<u>LSB-34</u>	<u>LSB-35</u>	<u>H-16</u>	<u>H-17</u>	<u>H-20</u>	<u>H-25</u>	<u>H-29</u>	<u>H-31</u>	<u>H-32</u>
Quartz	x	x	x	x	x	x	x	x	x	x	x	x	x
Muscovite	x	x	x	x	x		x	x	x		x	x	x
Andalusite			x				x	x	x	x	x	x	x
Sillimanite	x	x	x	x	x	x							
Biotite	x	x	x	x	x	x	x	x	x	x	x	x	x
Chlorite†	(a)	(a)	(a)	(a)	(a)	(a)	(a)	(a)	(a)	(a)	(a)	(a)	(a)
Staurolite†		(x)	(x)	(x)									
Cordierite	x	x	x	x	x	x				x			x
Garnet		x		x		x					x	x	
Plagioclase	x		x			x	x			x	x		
Accessories*	z,o	z,o	z,o	z,o	z,o	z,o,a	z,o,a	z,o,a	z	z,a	z,o	z,o	z

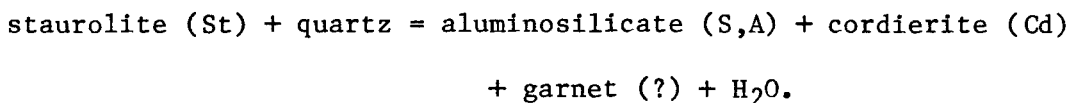
<u>FERROMAGNESIAN</u>							
	Pinto Mts.		L. San Berdo. Mts.		Hexie Mts.		
Sample:	<u>P-17</u>	<u>P-19</u>	<u>LSB-26</u>	<u>H-27</u>	<u>H-39a</u>	<u>H-39b</u>	<u>H-46</u>
Quartz	x	x		x			x
Biotite	x	x	x	x			x
Chlorite	x	x	x	x	x	x	x
Corundum†			(x)				
Spinel†			(x)				
(hercynite)							
Staurolite†			(x)				
Cordierite	x	x	x	x			
Garnet	x	x					x
Plagioclase		x					
Orthoamphibole	x	x	x	x			
Clinoamphibole	x				x	x	
Talc					x	x	
Accessories*	z	z,o,a		z,o	z,o,a	z,o,a	z,o

* z zircon
o opaques
a apatite

† (a) retrograde alteration
(x) relict mineral

Figure 2-7. Photomicrographs of samples from the pelitic Lost Horse granofels of the Pinto gneiss:

A. Textural evidence for the reaction



Garnet may disappear and biotite (B) appear by the reaction



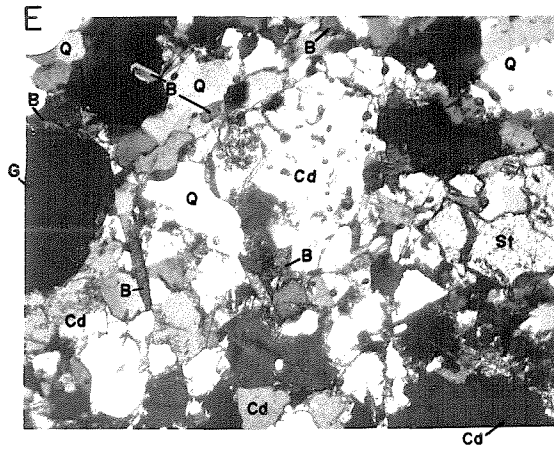
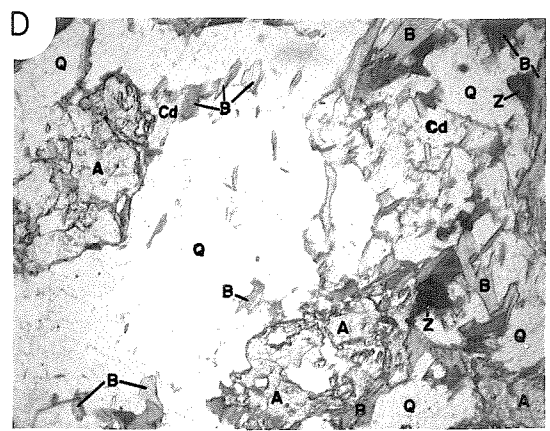
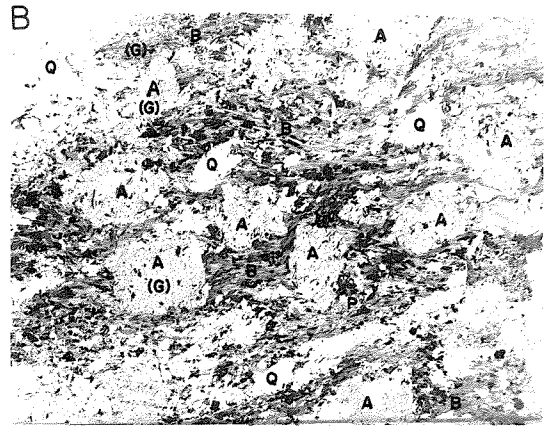
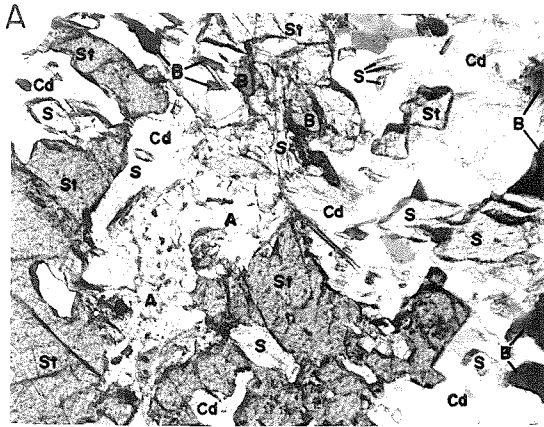
Sample L. San Berdo-24P: partially crossed nicols, horizontal field of 1 mm.

B. Andalusite (A) + garnet ((G): small grains not visible on the photograph) + biotite (B) + quartz (Q) + plagioclase (P) + opaques (black, not labeled). Sample Hexie-31P: uncrossed nicols, horizontal field of 2.4 cm.

C. Textural evidence for the reaction cited in Fig. 2-6A. Sample L. San Berdo-24P: uncrossed nicols, horizontal field of 2 mm.

D. Andalusite (A) + cordierite (Cd) + biotite (B) + quartz (Q) + zircon (Z). Sample Hexie-32P: uncrossed nicols, horizontal field of 2 mm.

E. Garnet (G) + cordierite (Cd) + biotite + quartz + relict staurolite (St). Sillimanite (not shown) is also present. Sample L. San Berdo-22P: crossed nicols, horizontal field of 2 mm.



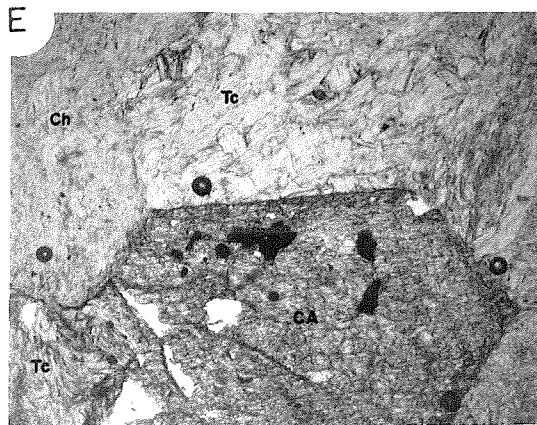
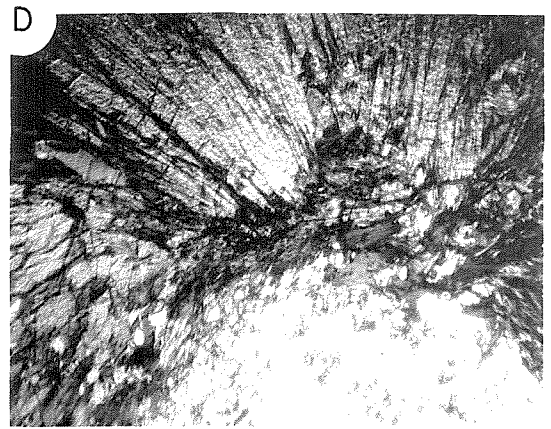
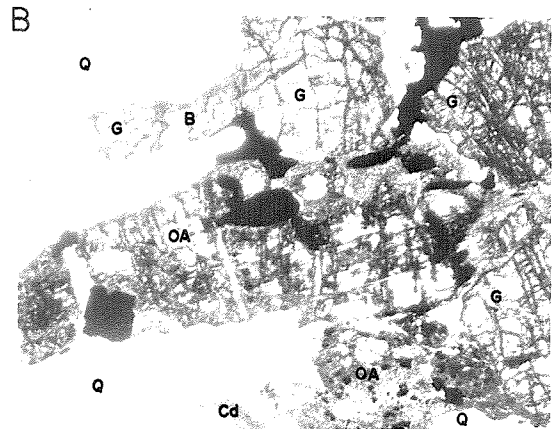
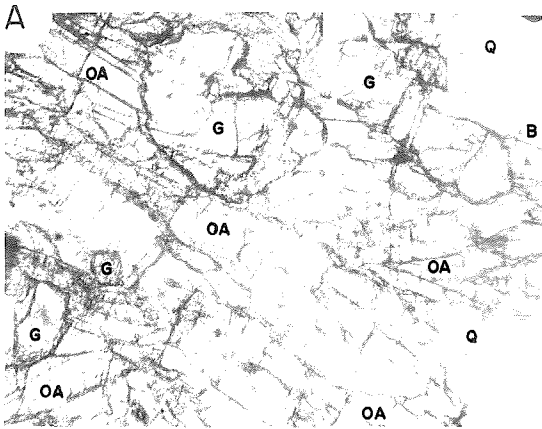
Chlorite is present in all of the ferromagnesian samples collected. More northerly samples in the Little San Bernardino and Pinto Mountains contain orthoamphibole (anthophyllite-gedrite), cordierite, and biotite (Figure 2-8A,B). At one locality in the Pinto Mountains, cummingtonite and garnet occur with orthoamphibole (Figure 2-8A,B). Talc and clinoamphibole occur at one locality in the southern Hexie Mountains (Figure 2-8E). The texture of the ferromagnesian layers is both foliated and nonfoliated. Where present, the foliation is defined by compositionally distinct microlaminae with amphiboles and sheet silicates lying within the plane of foliation. Where the rock is not foliated, it is characterized by radiating clusters of amphibole up to 2 cm in diameter that typically coalesce (Figure 2-8C,D). Cordierite and chlorite usually fill the interstices; quartz is present in a few samples. In one sample, corundum rimmed by spinel and staurolite occurs as inclusions within cordierite grains (Figure 2-22). These inclusions represent ferro-aluminous enclaves within the ferromagnesian units similar to those described in cordieriteanthophyllite rocks in New Hampshire and Finland (Robinson and Jaffe, 1969; Eskola, 1914). The enclaves are about 2 mm in diameter. These lithologies and their textures will be discussed further in a later section devoted to the metamorphism of the Pinto gneiss.

Baumonk Mill Granofels

The central (Baumonk Mill) lithologic belt in the Pinto gneiss also consists of granofelsic pelitic gneiss that crops out in the central Pinto Mountains, as roof pendants in Cretaceous quartz monzonite in Cottonwood Pass between the Eagle and Cottonwood Mountains, in the easternmost

Figure 2-8. Photomicrographs of samples from the ferromagnesian Lost Horse granofels of the Pinto gneiss:

- A. Orthoamphibole (OA) + garnet (G) + quartz (Q) in association with cordierite (not shown) and biotite (not shown). Sample Pinto-17P: uncrossed nicols, horizontal field of 2 mm.
- B. Orthoamphibole (OA) + garnet (G) + cordierite (Cd) + biotite (not shown) + chlorite (retrograde) + quartz (Q). Sample Pinto-19P: uncrossed nicols, horizontal field of 2 mm.
- C. Orthoamphibole in radiating suns, cordierite in coarse xenoblastic grains, and quartz in fine-grained interstitial mosaics; chlorite is also present in the rock. Sample Hexie-27P: crossed nicols, horizontal field of 1.8 cm.
- D. Orthoamphibole radiating from central light-colored cordierite grain. Sample L. San Bernardino-26P: partially crossed nicols, horizontal field of 3.2 mm.
- E. Chlorite (Ch) + talc (Tc) + clinoamphibole (CA). Sample Hexie-39BP: uncrossed nicols, horizontal field of 2 mm.



Orocopia Mountains, and as an island in the alluvium at the old Baumonk Mill site on Bradshaw Road 2 km southwest of the Chuckwalla Mountains (Plate V).

The high quartz content of the rock gives it a bluish-gray vitreous luster on fresh surfaces that is rather similar to the granofelsic rocks of the Lost Horse lithosome (Figure 2-6C). In contrast to that gneiss in thin-section, however, the Baumonk Mill granofels is characterized by abundant quartz plus amoeboid sericitic aggregates and subordinate red brown biotite (Figure 2-9E). The abundance of sericitic aggregates imparts a light bluish-gray color and a friable nature to weathered exposures of the gneiss. On weathered surfaces, biotite is typically visible as black to reddish-black or gray to bleached euhedral flakes.

Mineral assemblages for the granofelsic gneiss of the Baumonk Mill lithosome are tabulated in Table 2-V. Quartz makes up 50-60% of the rock. It is generally coarse- to very coarse-grained and occurs both in equant grains and clusters of grains and as elongate lenses or ribbons. It is slightly to moderately undulose. Amoeboid aggregates of very fine-grained sericite, quartz, and opaques form 25-30% of the gneiss. Within the aggregates, chlorite commonly occurs in addition to white mica, and biotite is rarely present. Qualitative scans with the electron microprobe indicate the presence of muscovite, quartz, iron-oxide, and chlorite within the aggregates. Texturally, in view of the much coarser grain size of the quartz and biotite as well as commonly pseudomorphic outlines, these aggregates seem to represent fine-grained replacements of a coarse-grained mineral. Although feldspar, cordierite, andalusite (viridine?), or an early-formed phengite must all be considered as possible precursors to the aggregates, only cordierite has been found

Figure 2-9. Photomicrographs of samples from the Black Eagle granofels-schist, Iron Chief dolomite, Baumonk Mill granofels, and Music Valley gneiss of the Pinto gneiss:

- A. Black Eagle granofels: andalusite porphyroblasts with interstitial quartz. Sample Pinto-51P: crossed nicols, horizontal field of 2.7 cm.
- B. Black Eagle schist: textural evidence for the reaction
 muscovite + quartz (Q) = K-feldspar (K) + andalusite (A) +
 sillimanite (S) + H₂O.
 Biotite (B) is also present. Sample Eagle-77P: uncrossed nicols, horizontal field of 2 mm.
- C. Iron Chief dolomite. Sample Eagle-173P: crossed nicols, horizontal field of 2.3 cm.
- D. Iron Chief dolomite: dolomite is light-colored; hematite is dark-colored. Sample Eagle-211P: uncrossed nicols, horizontal field of 1.5 cm.
- E. Baumonk Mill granofels: quartz (Q) + biotite (B) + aggregates of sericite, chlorite, and opaques (Ser) pseudomorphous after cordierite(?). Sample Chkwal-304P: partially crossed nicols, horizontal field of 2 mm.
- F. Music Valley gneiss: quartz (Q) + plagioclase (P) + biotite (B) + chlorite (not shown). Sample Orocop-7P: partially crossed nicols, horizontal field of 2 mm.

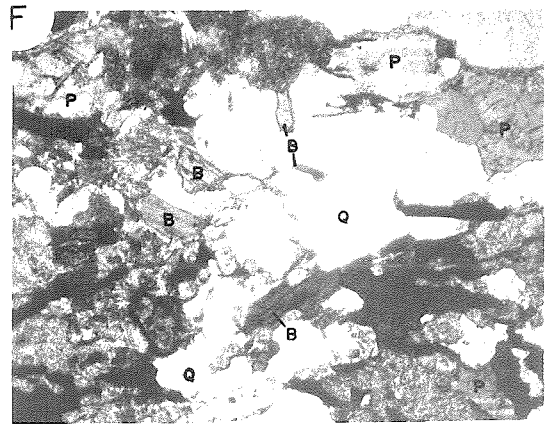
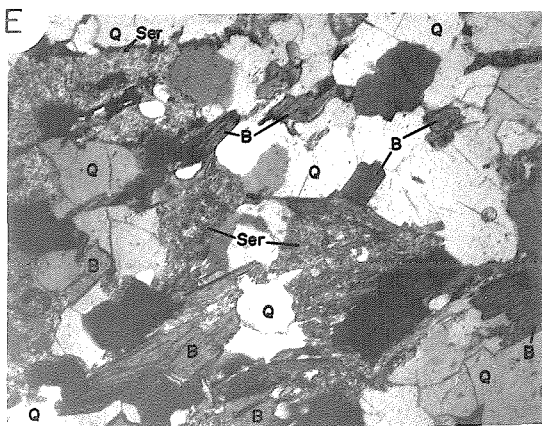
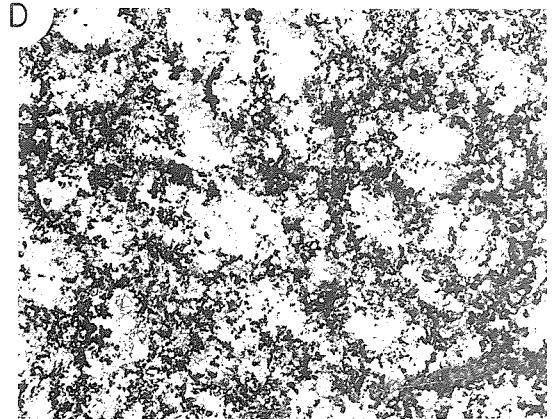
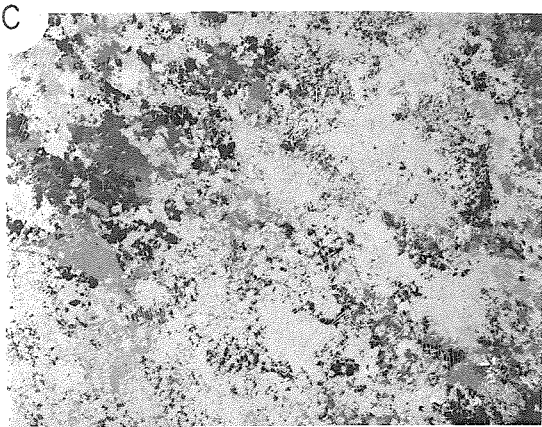
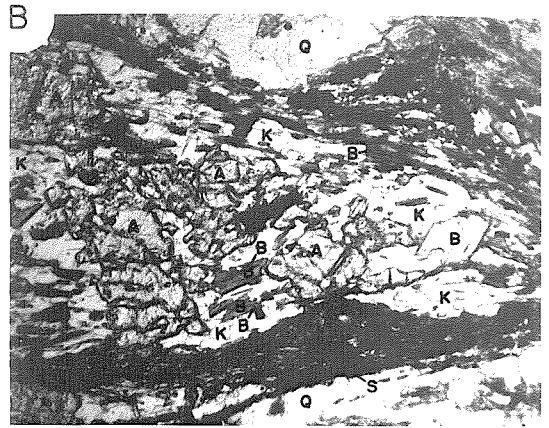
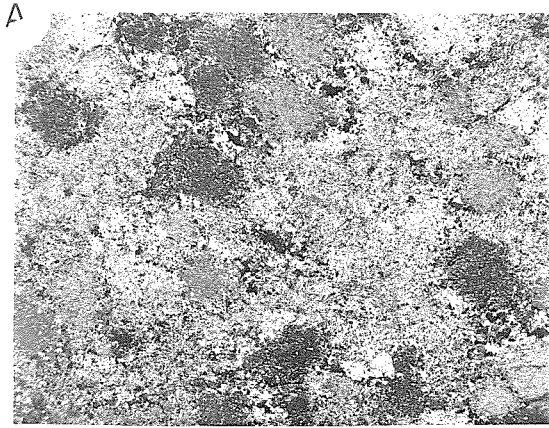


Table 2-V. Parageneses of samples from the Baumonk Mill lithosome of the Pinto gneiss:

Sample:	Orocopia Mts.			Chuckwalla Mts.		Eagle Mts.		Pinto Mts.	
	<u>0-11</u>	<u>0-61</u>	<u>0-62</u>	<u>Chk-303</u>	<u>Chk-304</u>	<u>E-177</u>	<u>E-202</u>	<u>P-6</u>	<u>P-60</u>
Quartz	x	x	x	x	x	x	x	x	x
Muscovite	x	x	x	x	x	x	x	x	x
Biotite [†]	x	x	x	x	x	x	(p)	x	x
Chlorite [†]	(a)	(a)	(a)	(a)	(a)	(a)	(a)	(a)	(a)
Cordierite [†]	(p)	(p)	(p)	(p)	(p)	(p)	(p)	(x)/(p)	(p)
Accessories*	z,o,e	z,o,e	z,o,e	z,o,e	z,h,e	z,o,e	z,o	z,o	z,o,e

* z zircon
o opaques
h hematite
e epidote

† (a) retrograde alteration
(x) relict mineral
(p) pseudomorphously replaced

as a relic surrounded by partially developed identical aggregates of sericite, chlorite, and quartz. This relic occurs in the south-central Pinto Mountains. Three general observations are consistent with the interpretation of cordierite as the pseudomorphed mineral: 1) in units in which they occur, the aluminosilicates have survived throughout the field area; 2) in the adjacent Music Valley gneiss, plagioclase is never completely altered, and in a few thin-sections of rock thought to be transitional between the two lithosomes, plagioclase and the pseudomorphous aggregates coexist as texturally distinct entities; 3) to the north, where cordierite is fresh in the Lost Horse and Black Eagle lithosomes, it can be found as relics in the intervening Baumonk Mill lithosome, whereas to the south where cordierite is not found or else is extensively retrograded in flanking lithosomes, it is completely pseudomorphed in the Baumonk Mill granofels. These observations will be referred to in a later section on metamorphism in the Pinto gneiss.

Red-brown biotite is ubiquitous, commonly occurring as euhedral hexagonal plates. Especially to the south, the biotite is usually chloritized. It constitutes 15-20% of the gneiss. The red to red-brown color suggests a high proportion of Ti relative to Fe^{+3} (Deer, Howie, Zussman, 1966, p. 213).

Music Valley Gneiss

Geographically, the Music Valley gneiss is located between the Lost Horse and Baumonk Mill lithosomes. Rocks assigned to the Music Valley facies belt are exposed in the eastern Orocopia, Cottonwood, Hexie, Little San Bernardino, central and western Pinto Mountains (Plate V, Figure 2-6D). The name is taken from a valley in the central Pinto Mountains

which transects the gneiss in its upper reach.

Mineralogically, the Music Valley gneiss is composed of quartz, oligoclase, biotite, and small amounts of muscovite (Figure 2-9F). Potassium feldspar, sericitic aggregates, garnet, and/or chlorite may be present. Garnet occurs as relics within masses of sericite and chlorite, or as clustered small grains enclosed within and apparently intergrown with larger plagioclase grains. Chlorite is seen replacing biotite as well. The gneiss is characterized by the presence of abundant, large zircons, both rounded and idioblastic. An unidentified uniaxial positive radioactive mineral with lower birefringence and lower relief than zircon also occurs. Minerals consistent with these optical properties include thorite and xenotime. The xenotime mineralization described by Evans (1964) in Music Valley of the central Pinto Mountains occurs in the Music Valley lithosome. Mineral assemblages are listed in Table 2-VI. Compositionally, the Music Valley gneiss could have been derived from either an igneous or a sedimentary protolith. Intrusive or extrusive quartz keratophyre is a possible igneous precursor. A sedimentary protolith would require either a depositional environment that favored a clastic concentration of sodium minerals (for instance, plagioclase or paragonite) or concentration through diagenetic processes such as the growth of authigenic minerals (for example, analcite, sodium-rich zeolites, or paragonite). No convincing relict textures, either igneous or sedimentary, have been recognized through the subsequent metamorphic overprint.

Any stratigraphic interpretation concerning the protolith for the Music Valley gneiss must be consistent with several observations. First, the Music Valley lithology is an intrinsic subunit of the Pinto gneiss: there is no evidence for structural contacts, nor any striking discordance

or interruption in the outcrop character of the Pinto gneiss in crossing from Music Valley gneiss into either Baumonk Mill or Lost Horse granofels. Along the eastern limit of its exposure, Music Valley gneiss is intercalated with Baumonk Mill granofels in layers that range in thickness approximately from tenths of a meter to one or two meters. The interlayered lithologies are exposed in the easternmost Orocopia Mountains, in pendants within the Cretaceous batholithic rocks in the vicinity of Cottonwood Pass between the Eagle and Cottonwood Mountains, and in the central Pinto Mountains. Similarly, along the western limit of its exposure in the Hexie and Little San Bernardino Mountains, Music Valley gneiss is intercalated with Lost Horse granofels. Thin-sections of samples from both transitions show interlaminated mineralogical compositions intermediate between each pair of lithologies. Thus sillimanite can be found with abundant oligoclase in the Music Valley gneiss-Lost Horse granofels transition. Finally, the observed distribution of Music Valley gneiss is confined between the flanking metasedimentary granofels units.

With these observations in mind, the protolith for the Music Valley gneiss is tentatively interpreted to have been a sedimentary lithosome time-transgressively accumulated between the Baumonk Mill and Lost Horse lithosomes. Within this framework, the marginal intercalations are seen as a sedimentary intertonguing of lithosomes. It must be pointed out that the fragmentary preservation of Pinto gneiss remnants permits more complicated stratigraphic interpretations in which the intercalations might be viewed as volcanic-sediment interfingering. However, these alternatives require postulation of additional stratigraphic relationships that have not yet been observed. Although an intercalated intrus-

ive injection into the sedimentary protolith can be hypothesized as a precursor of the Music Valley gneiss, that intrusion would have had to occur at a relatively shallow level (see section on metamorphism) at which unequivocal cross-cutting relationships should have developed. No such relationship has yet been observed.

The schistose feldspathic gneiss of the Music Valley lithosome is commonly migmatitic with quartzo-feldspathic segregations that range from concordant laminae to discordant masses (Figure 2-6D). This ultrametamorphism is confined to the Music Valley gneiss which mineralogically approximates a composition that would melt at a lower temperature than the flanking lithosomes. In anatexis experiments beginning with quartz-biotite-plagioclase rocks with model compositions approximately equivalent to that of the Music Valley gneiss, melting begins at 660-690°C and $P_{H_2O} = 2$ kb, yielding quartz, plagioclase, and K-feldspar (Winkler, 1976, p. 312-313; cf. Merrill et al., 1970; Tuttle and Bowen, 1958). At slightly higher pressure than for these experiments, the temperatures reached during metamorphism of the Pinto gneiss, as indicated by the pelitic assemblages, may be as high as 600-650°C (see below).

Black Eagle Granofels-Schist

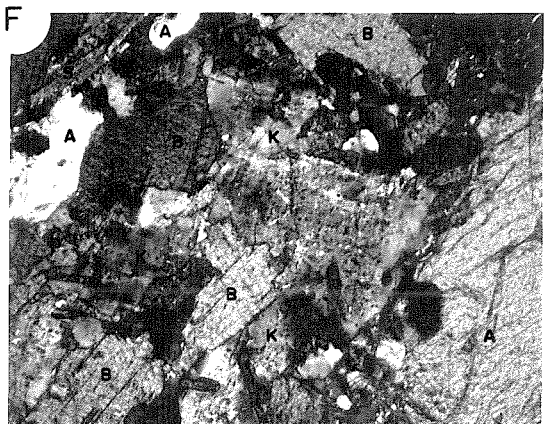
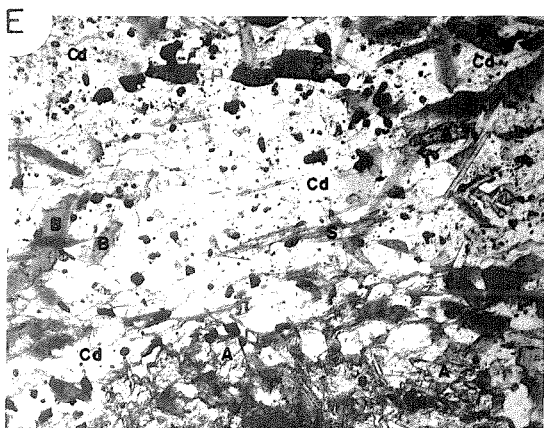
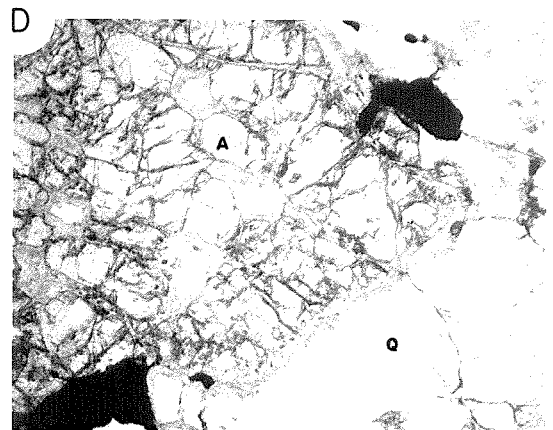
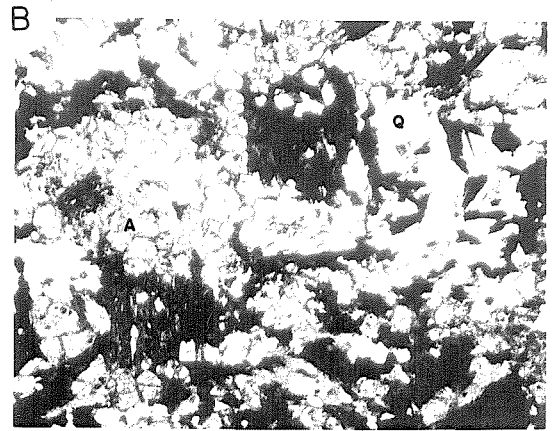
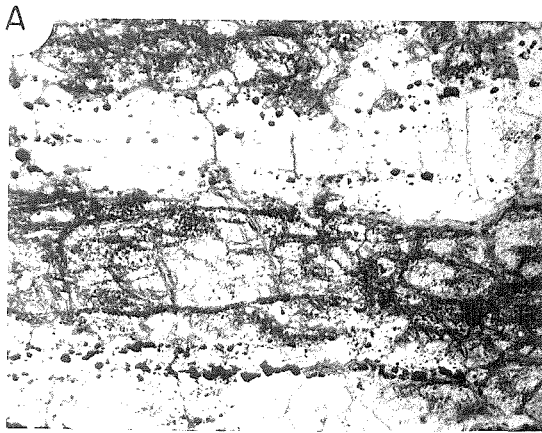
The Black Eagle lithosome of the Pinto gneiss consists of a heterogeneous assortment of subfacies that is situated stratigraphically and geographically between the Baumonk Mill granofels to the west and Pinto Mountain quartzite to the east (Plate V). Various subfacies of the lithosome crop out in the Eagle and central Pinto Mountains, both above and below the thrust fault (later Red Cloud thrust: see Chapter IV) that has telescoped the stratigraphic section. The principal lithologies

include pelitic and ferriferous pelitic granofels and schist (Figure 2-6A,B), dolomite marble (Figure 2-5H), and calcite marble. Occurrences of each of these subfacies appear to be laterally and diachronously discontinuous, so that reconstruction of exact stratigraphic settings and relationships is difficult within the area mapped.

In the upper plate of the later Red Cloud thrust fault in the Eagle and Pinto Mountains, pelitic granofels and ferriferous pelitic granofels and schist interfinger eastward with the Pinto Mountain quartzite. These lithologies occur sandwiched between white quartzite of the outer Pinto Mountain quartzite lithosome in a pattern of cyclical mirrored repetitions shown in stratigraphic columns (Plate IV) from both ranges. The pelitic rocks contain assemblages of quartz + muscovite/K-feldspar + andalusite/sillimanite + biotite (Figure 2-9B). K-feldspar occurs with the breakdown of muscovite + quartz. Ferromagnesian minerals generally form a small percentage of the rock. Andalusite characteristically occurs in spongiform poikiloblastic porphyroblasts with inclusions of quartz and opaque minerals (Figures 2-9A, 2-10A). Texturally, the pelitic unit is granofels in the Pinto Mountains, and granofels and schist in the Eagle Mountains, exhibiting the same deformational gradient shown by the Joshua Joshua Tree granite and Pinto Mountain quartzite. Ferriferous rock in the upper plate contains quartz, pseudomorphic aggregates of fine-grained sericite that are probably replacements of K-feldspar or sodic plagioclase, and specular hematite intergrown with corundum(?) (Figure 2-10C). The corundum(?) is twinned, uniaxial negative to biaxial negative with $2V \approx 20^\circ$. The unit occurs stratigraphically basinward from, and above, the pelitic schist. As with pelitic rock, it is granofelsic in the Pinto Mountains and schistose in the Eagle Mountains.

Figure 2-10. Photomicrographs of samples from the Black Eagle granofels of the Pinto gneiss and the paleo-weathered zone:

- A. Black Eagle granofels: andalusite with trains of included opaques. Sample Pinto-45P: uncrossed nicols, horizontal field of 2 mm.
- B. Black Eagle granofels: biotite + hematite (black), andalusite neutral with high relief), and quartz (white). Sample Pinto-55P: uncrossed nicols, horizontal field of 2 mm.
- C. Laminated Black Eagle granofels: quartz + sericitic aggregates (white) and hematite (black); tourmaline and zircon are also present. Sample Pinto-37P: uncrossed nicols, horizontal field of 2.5 cm.
- D. Granofels from paleo-weathered zone: andalusite (A), quartz (Q), and magnetite (black). The andalusite is partially altered to sericite along fractures. Sample Pinto-42P: uncrossed nicols, horizontal field of 2 mm.
- E. Black Eagle granofels: cordierite (Cd) + andalusite (A) + sillimanite (S) + biotite (B) + K-feldspar (not shown). Sample Pinto-104P: uncrossed nicols, horizontal field of 2 mm.
- F. Black Eagle granofels: K-feldspar (K) + andalusite (A) + sillimanite (S) + biotite (B). Sample Pinto-83P: crossed nicols, horizontal field of 2 mm.



In the lower plate of the later Red Cloud thrust in the Pinto Mountains, the pelitic granofels in the Black Eagle lithosome generally has a higher ferromagnesian content than the schist of the upper plate in both the Pinto and Eagle Mountains (Figure 2-10B,E,F). Abundant biotite is brown to red-brown in color. Cordierite, occurring to the north, is poikiloblastic and xenoblastic (Figure 2-10E). In the northern Eagle Mountains, ferriferous pelitic rock occurs in the lower plate stratigraphically between the vitreous white quartzite and biotitic pelitic granofels. The unit corresponds to the "schistose meta-arkose" mapped in the Eagle Mountain Mine area (Harder, 1912; Hadley, 1945; Dubois and Brummett, 1968). It pinches out immediately west of the location of the Cactus Mine measured section (T35, R13E, S27). The nonresistant ferriferous unit erodes between ridges of more resistant quartzite and granofels plus dolomite to form topographic lows marked by gently rounded, smooth hummocks and saddles. From a distance, these subdued exposures have a distinctive lavender cast. The surface of the the hummocks is generally weathered debris which gives rise to their smooth topography. Outcrops occur mostly in stream bottoms. The unit varies in thickness from 0 to about 65 meters. In outcrop, the ferriferous unit has a varicolored, mottled appearance including red, purple, lavender, blue, gray, and white. Much of the mottling appears to be the result of hydrothermal bleaching and staining at the outcrop scale. The rock has a foliation with a phyllitic sheen common on its surfaces (Figure 2-6B).

The ferriferous unit contains at least two lithologies, both of which are iron-rich. The more abundant of the two lithologies contains some combination of andalusite, staurolite, cordierite(?), plagioclase,

potassium feldspar, tourmaline, and pseudomorphic aggregates of fine-grained muscovite, quartz and iron oxide in addition to quartz and hematite. The other lithology is a finely laminated (~ 1 mm) quartz-hematite rock. Some of the silica in this unit occurs in transversely crystallized laminae that are brown in transmitted light and white in reflected light and that may be relict chalcedony. Mineral assemblages for the pelitic and ferriferous units of the Black Eagle lithofacies are tabulated in Table 2-VII.

Thin beds of calcite marble (<1 m thick) occur at one locality in the Pinto Mountains in the upper plate of the thrust and at one locality in the Eagle Mountains in the lower plate. In both instances, the marble occurs in pelitic granofels within about ten meters of the contact with the vitreous white quartzite lithosome. In addition to calcite, the units contain calc-silicate minerals including clinopyroxene and forsterite.

In the northern Eagle Mountains, a coarsely recrystallized tan-weathering, white dolomite (Figure 2-5H) is found stratigraphically above the ferriferous and pelitic units in the Cactus Mine section. The upper contact of this unit, informally called the Iron Chief dolomite, is truncated by Mesozoic intrusive rocks. The dolomite forms bold, buff-colored ridges that stand out in stark contrast to both the underlying dark pelitic granofels and the cross-cutting Jurassic intrusives. The Iron Chief dolomite is for the most part pure, very coarse-grained dolomite with interlocking recrystallized grains up to 1 cm across (Figure 2-9C). Although generally massive, bedding is shown by scattered layers that are rich in dark-brown weathering chert nodules. In addition thin layers of white calcite marble (Figure 2-5H), quartzite, and fer-

Table 2-VI. Parageneses of samples from the Music Valley lithosome of the Pinto gneiss:

Sample:	Orocopia Mts.				Eagle Mts.				Cottonwood Mts.
	<u>0-5</u>	<u>0-7</u>	<u>0-8</u>	<u>0-58</u>	<u>E-192</u>	<u>E-194</u>	<u>E-196</u>	<u>E-204a,b</u>	<u>Co-3</u>
Quartz	x	x	x	x	x	x	x	x	x
Muscovite	x	x	x	x	x	x	x	x	x
K-feldspar								x	
Biotite	x	x	x	x	x	x	x	x	x
Chlorite	x	x	x	x	x	x	x	x	x
Garnet			x						
Plagioclase	x	x	x	x	x	x	x	x	x
Accessories*	z,o	z,o,a	z,o,a	z,o,a	z,o	z,o	z,o	z,o,a	z,o,a

Sample:	Hexie Mts.	Little San Bernardino Mts.				Pinto Mts.	
	<u>H-11</u>	<u>LSB-14</u>	<u>LSB-21</u>	<u>LSB-28</u>	<u>LSB-32</u>	<u>P-113</u>	<u>P-115</u>
Quartz	x	x	x	x	x	x	x
Muscovite	x	x		x	x	x	
K-feldspar	x				x		x
Biotite	x	x	x	x	x	x	x
Chlorite	x					x	x
Garnet							
Plagioclase	x	x	x	x	x	x	x
Accessories*	z,o	z,o,a	z,o,a	z,o,a	z,o,a	z,o	z,o,a

* z zircon
o opaques
a apatite

Table 2-VII. Parageneses of samples from the Black Eagle lithofacies of the Pinto gneiss:

<u>PELITIC</u>											
<u>Eagle Mts.</u>											
Upper Plate of Later Red Cloud Thrust										Lower Plate	
Sample:	<u>E-23</u>	<u>E-28</u>	<u>E-71</u>	<u>E-73</u>	<u>E-77</u>	<u>E-78</u>	<u>E-79</u>	<u>E-80</u>	<u>E-109</u>	<u>E-188</u>	<u>E-191</u>
Quartz	x	x	x	x	x	x	x	x	x	x	x
Muscovite	x	x	x	x	x	x	x	x	x	x	(a)
K-feldspar [†]			(x)	(p?)	(x)				(x)		
Andalusite [†]		(x)		(x)	(x)					(x)	(x)
Sillimanite [†]	(x)			(x)	(x)	(x)	(p?)	x	(x)		
Biotite [†]	x	x	x	x	x	x	x	x	x	(x)	(x)
Chlorite [†]	(a)			(a)			(a)			(a)	(a)
Staurolite [†]										(x)	
Cordierite [†]										(p?)	(p?)
Garnet [†]			x							(p?)	
Plagioclase									x	x	
Accessories*	z,o,a	z,o,a	z	z,o	z,o	z,o	z,o,a	z,o	z,o,a	z,o	z,h

<u>Pinto Mts.</u>											
Upper Plate						Lower Plate					
Sample:	<u>P-82</u>	<u>P-83</u>	<u>P-84</u>	<u>P-86</u>	<u>P-103</u>	<u>P-104</u>	<u>P-26a</u>	<u>P-45</u>	<u>P-46</u>	<u>P-51</u>	<u>P-55</u>
Quartz							x	x	x	x	x
Muscovite			tr	x	tr	tr	x	x	x	x	x
K-feldspar [†]	x	x	x	(p?)	x	x			(p?)	(p?)	(p?)
Andalusite	x	x	x	x	x	x	x	x	x	x	x
Sillimanite	x	x	x	x	x	x					
Biotite	x	x	x		x	x	x			x	
Chlorite [†]				(a)							
Cordierite [†]			x	(p?)	x	x					
Garnet											
Plagioclase											
Accessories*	z,o,a	z,o,a	z,o,a	z,o	z,o	z,o	z,o	z,h	h	z,h	z,h

* z zircon		† (a) retrograde alteration
o opaques		(x) relict mineral
h hematite		(p) pseudomorphous replacement
a apatite		

<u>FERRIFEROUS PELITIC</u>															
<u>Eagle Mts.</u>										<u>Pinto Mts.</u>					
Lower Plate of Later Red Cloud Thrust										Upper Plate		Lower Plate			
Sample:	<u>E-167</u>	<u>E-168</u>	<u>E-170</u>	<u>E-171</u>	<u>E-174</u>	<u>E-175</u>	<u>E-176</u>	<u>E-212</u>	<u>E-213</u>	<u>E-215</u>	<u>E-37</u>	<u>E-38</u>	<u>P-85</u>	<u>P-90</u>	<u>P-102</u>
Quartz	x	x	x	x	x	x	x	x	x	x	x	x	x	x	x
Muscovite [†]	(a)	(a)	(a)	(a)	(a)	(a)									
K-feldspar [†]		x	(x)	(p?)											
Andalusite															
Sillimanite ^{†§}	f	(p?)	(p?)	(p)	(p?)	f		f	f	f	f	f			
Biotite [†]		x	x	x		(x)	(x)/(p)								
Chlorite [†]	(a)				(a)	(a)	(a)	(a)	(a)	(a)			x	x	(p)
Staurolite	(p)				(x)/(p)			(p?)	(p)	(p)			(a)	(a)	(a)
Cordierite	(p?)				x/(p)	(p?)		(p?)	(p?)	(p)					
Garnet															
Plagioclase		x	x	x	x	x	x								
Hematite	x	x	x	x	x	x	x	x	x		x	x	x	x	x
Accessories*	z,a	z,e	z,e	z,t	z,t	z,e	z	z,e,a	z	z	z,t	z,t	z	z,a	z

* z zircon		† (a) retrograde alteration	§ f fibrolite
a apatite		(x) relict mineral	
e epidote		(p) pseudomorphous replacement	
t tourmaline			
c corundum			

riferous marbles (Figure 2-9D). are derived from protolithic interbeds of limestone, sandstone, and iron-rich layers.

The dolomite occurs extensively in the Eagle Mountain Mine area where it commonly contains lenses of iron ore. In the central Pinto Mountains only remnants of the unit are preserved. One small exposure just west of Pinto Mountain (T2S, R11E) appears to be faulted into the white quartzite lithosome; another occurs as an isolated pendant in Jurassic quartz monzonite (center of T15, R11E). Although it has been mapped as a separate unit, the Iron Chief dolomite is tentatively included within the Black Eagle lithofacies of the Pinto gneiss. It may represent a shelf carbonate bank within the stratigraphic facies model proposed above. However, since the upward and eastward contact relationships have not been established, an alternative interpretation would place the dolomite unconformably above the Pinto gneiss and quartzite.

To date, a stratigraphic linking between the Black Eagle and Baumonk Mill lithosomes of the Pinto gneiss can only be inferred. Younger structural and intrusive events have buried and obliterated the contact. The link is inferred on the basis of the mapped distribution in lithologic belts and the observed intercalation between other pairs of lithosomes. Later metamorphic isograds transect all lithosomes of the Pinto gneiss with no observable disruption between the Black Eagle and Baumonk Mill granofels, so that at least no post-metamorphic structure is concealed between them. With further mapping it may yet be possible to find a remnant of the contact preserved in the south-central Pinto Mountains.

STRATIGRAPHIC FACIES MODEL

Although the diachronous lithofacies model described above is consistent with the observed distribution of lithologic types in the Joshua Tree terrane, it must be emphasized that the model represents a framework interpretively, albeit painstakingly, reconstructed from isolated remnants of a once-continuous terrane that has been sliced and folded in a pre-batholithic thrust system, fragmented by two Mesozoic batholithic intrusions, and further disrupted by Cenozoic strike-slip faults. Indeed the understanding of both the stratigraphy and the structure has grown stepwise in reciprocating interchanges. This stratigraphic model is presented because so far it has worked in relation to the structural interpretation (and vice versa), and because it has further predictive value that allows continued testing. In the preceding sections the stratigraphic model has been used as an organizational vehicle for the presentation of field and petrographic observations for each compositional subdivision of the Pinto gneiss. The purpose of this section is to emphasize interrelationships among the differing facies, and to discuss implications for depositional environments, provenance, and regional correlation. It is also necessary to evaluate alternative interpretations for some of the observations. Many crucial avenues of investigation relevant to testing this model are as yet unprobed, but the prospects for its synthetic value are exciting enough to warrant preliminary discussion. The intent of this discussion is not to conclusively demonstrate the arguments presented, but rather to explore some of the model's ambiguities, and to anticipate some of its potential for palinspastic reconstruction.

It is unequivocal that granite basement is nonconformably overlain by

cross-bedded quartzite which in turn interfingers with and is overlain by pure, white quartzite and pelitic and ferriferous metasedimentary rocks with minor interbedded carbonate (Figure 2-11). Beginning with the shoreline quartzites this systematic sequence of lithosomes consistently occurs upward and westward from exposures of the Joshua Tree granite. Cross-bedding observed in the Pinto and Eagle Mountains is always upright. These stratigraphic relationships strongly favor, if they do not uniquely define, a predominantly eastward transgressive facies model. However, vertical stratigraphic sections measured in the quartzite show cyclical repetition of oscillating upright stratigraphic sequences which indicate episodic regressions of the sea, with concomitant prograding facies accumulation. Stratigraphic columns are shown in Plate IV. The repeating vertical cycles involving cross-bedded quartzite, vitreous white quartzite, pelitic schist, and ferriferous schist in the Pinto and Eagle Mountains provide evidence through an application of Walther's "law of correlation of facies" that all four were deposited in laterally concurrent sedimentary environments. The other compositional belts of Pinto gneiss are inferred to represent additional offshore environments.

The cross-bedded quartzite and pebble conglomerates are unquestionably clastic and were deposited in a relatively high energy environment. In this stratigraphic model, a beach environment is inferred. As a test of the model, systematic analysis of cross-bedding should yield results consistent with origin in a shoreface or foreshore setting. The observed tangential planar cross-bedding with low-angled bed-sets are consistent with a longshore bar origin (cf. Reineck and Singh, 1975, p. 302; Thompson, 1937; McKee and Sterrett, 1961). The steeply-dipping, convex

Figure 2-11. Stratigraphic model for the Pinto gneiss:

Crosses: Joshua Tree granite capped by an ancient weathering zone.

Line-dot pattern: Cross-bedded Pinto Mountain quartzite with lenses
of conglomerate.

Dots: Vitreous white Pinto Mountain quartzite.

Cross-hatch pattern: Ferriferous pelitic Black Eagle granofels.

Brick pattern: Iron Chief dolomite.

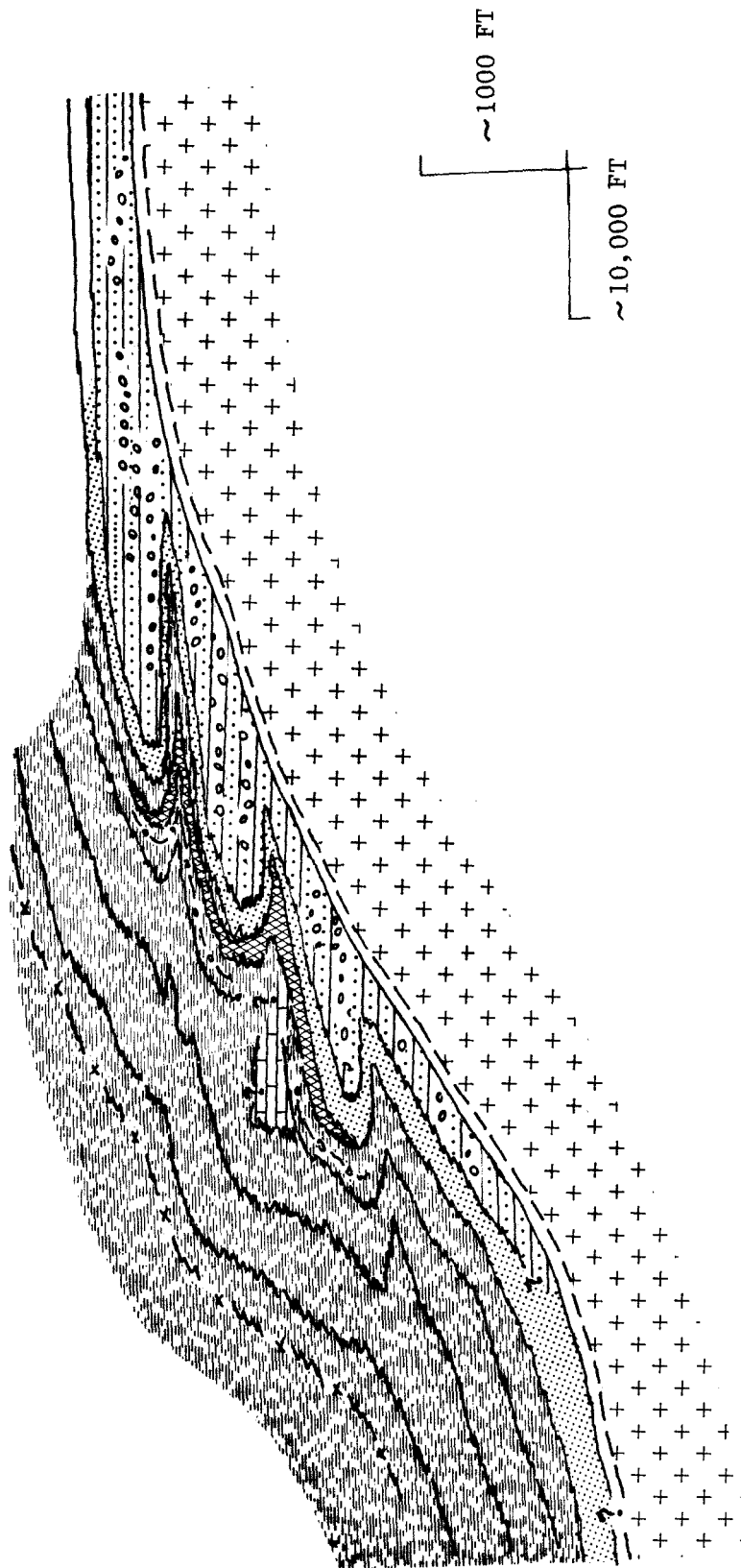
Dashes: Pelitic Black Eagle granofels,
Baumonk Mill granofels,
Music Valley gneiss,
Lost Horse granofels.

Circle-dash: Calcite marble zone in Black Eagle granofels.

X-dash: Ferromagnesian granofels zone in Lost Horse granofels.

E

W



laminae sets that might be expected in coastal dunes (Reineck and Singh, 1975, p. 289-290) have not been observed.

Two interpretations are possible for the clast provenance for the conglomerates of the Pinto Mountain quartzite. The obvious interpretation is that they are basal or near-basal orthoquartzite or vein quartz clast conglomerates deposited above an unconformity. Such compositionally mature conglomerates are common in cross-bedded beach sands (Pettijohn, 1975, p. 166). In the Pinto Mountain quartzite, the conglomerate clasts are exclusively quartzites and/or vein quartz; there are no clasts of Joshua Tree granite. The compositional maturity of the conglomerates requires a source terrane at sufficient transport distance to winnow out clasts less stable than quartzite; and/or a quartzite source terrane at sufficient distance to permit rounding of pebble- and cobble-sized clasts. No such source terrane is found within the area studied. A test of this interpretation must await palinspastic reconstruction of the tectonic fragment of Joshua Tree terrane in the Eastern Transverse Ranges with exposures elsewhere that may contain source terrane remnants.

Several observations render this interpretation somewhat troubling. First, the predominant clast type is coarse-grained vitreous white quartz that is texturally identical to the outlying, coeval vitreous white quartzite lithofacies. In addition, the clasts of fine-grained, black, specular hematitic quartzite and jasper could easily have been derived from the protolith for the iron-oxide rich subfacies of the Black Eagle lithofacies as well as from thin (1-3 cm) interbeds of such material in the vitreous white quartzite lithosome. Lastly, the relatively large tabular clasts of black hematitic siltite are unlikely to have been transported any great distance, and their apparent draped structure is more easily interpreted

as soft sediment deformation than some process of metamorphic deformation.

The alternative interpretation for the clast provenance is that they are rip-up clasts derived from the two lithofacies immediately offshore from the cross-bedded quartzite facies. Such an interpretation would favor a higher percentage of white quartzite clasts over hematite quartzite. An obvious implication of this interpretation is that at the time of clast formation the source for the clasts was not quartzite, but rather a semi-consolidated chert or partially cemented quartz arenite requiring, respectively, chemical or colloidal precipitation or rapid diagenesis in water shallow enough to be above at least storm-wave base. Then wave action operating on irregularities in the surface of the precipitate or on silica-cemented concretions(?) of quartzite could tear off semi-hardened fragments and deposit them on the beach, rounding the clasts in the process. The thoroughly recrystallized, very coarse-grained white quartzite of the Joshua Tree terrane apparently requires only that a very clean quartz protolith be subjected to temperatures high enough to promote recrystallization. This initial condition is satisfied equally well by either clean chert or silica-cemented mature quartz sandstone.

Quartz within samples of both the conglomerate clasts and the vitreous white quartzite lithosome is very coarse-grained with sutured grain boundaries and is faintly clouded with extremely fine black dust. However, in the limited number of thin-sections so far examined, samples from the quartzite lithosome invariably show less than a percent disseminated detrital zircon and rutile, whereas these accessories have not been observed in clast thin-sections. The lack of heavy minerals in the white conglomerate clasts apparently favors a vein-quartz origin for the cobbles, but the sampling is insufficient to make a strong argument.

Offshore from the depositional environment for the vitreous white quartzite lithosome, the question of clastic-vs.-chemical sedimentation can also be raised for the depositional environments for the diverse compositional belts within the Pinto gneiss protolith. The mineralogical uniformity of the Pinto gneiss lithosomes throughout the area mapped presumably reflects compositionally homogeneous protoliths. Within the context of the proposed stratigraphic model, such homogeneity would seem to require long-term tectonic and climatic stability in order to maintain the lateral array of depositional environments for sufficient time to diachronously accumulate the observed lithosomes. Tectonic and climatic quiescence would favor low-energy offshore depositional environments which would permit the development and maintenance of several lateral facies belts with chemically distinct sedimentary accumulations. The deep weathering of the Joshua Tree granite prior to deposition of the Pinto Mountain quartzite and gneiss circumstantially supports the case for tectonic and climatic stability. A number of first-order observations can be made about the chemical composition of the Pinto gneiss protolith based on its metamorphic mineralogy. These observations are meant to emphasize the persistent compositional uniformity of each of the diachronously linked lithosomes, and are no more than qualitative guidelines that may serve as a basis for quantitative chemical characterization. First, the gneiss as a whole contains very little calcium. CaO is abundant only in the carbonates of the Black Eagle lithofacies. Otherwise, small quantities are present in some of the ferriferous units of the Black Eagle lithofacies in sodic plagioclase, and in the Music Valley lithosome in plagioclase and perhaps garnet. Sodium is significant only in the plagioclase-bearing units. Iron, on the other hand, is

uncommonly abundant in the ferriferous schists of the Black Eagle lithosome. The metamorphic mineralogy of the ferromagnesian schists of the Lost Horse lithofacies predominantly includes components of MgO, FeO, Al₂O₃, SiO₂, H₂O. The proportions of these components as expressed in the mineral parageneses do not sum to any common sedimentary rock type, especially one that would fit into a time-transgressive stratigraphy. These rocks contain significantly less K₂O (all contained in biotite) than the enveloping pelitic rocks. The basinward color variation in metamorphic biotites from red-brown through yellowish green-brown to green-brown may reflect a decreasing Ti/Fe⁺³ ratio across the Pinto gneiss lithofacies from Ti > Fe⁺³ through Ti ≈ Fe⁺³ to Fe⁺³ > Ti (cf. Deer, Howie, and Zussman, 1966, p. 213). Apparent variations in the quantities of other components from one lithosome to the next seem to be reflected in changing mineralogical modal abundances.

Processes which could contribute to compositionally distinct belts parallel to shore within a sedimentary basin include

- 1) Primary or diagenetic chemical precipitation of differing authigenic minerals (or conversely, chemical leaching) in response to changes in aqueous solution chemistry, and/or

- 2) Deposition of differing clay minerals due to differing rates of flocculation or settling, perhaps combined with transformation (for example, cation exchange) during settling or after deposition. Clearly, no conclusions can be drawn about protolithic mineralogy based on the foregoing observations and discussion. Quantitative chemical analyses of each lithosome, however, would provide a test for the inferred homogeneity and should reflect protolithic chemical compositions if the metamorphism has

been isochemical. Systematic analyses would also provide another fingerprint for correlation of the Joshua Tree terrane in tectonic reconstructions.

The stratigraphic model presented for the Pinto gneiss protolith is characterized by compositionally uniform lithosomes that accumulated in stable and quiescent environments. Transitions between adjacent environments within the basin of accumulation were abrupt and apparently time-transgressive. In the geologic record there are some intriguing similarities between the stratigraphic model proposed for the Pinto gneiss and those for the Superior-type iron-formations, that, in North America, occur in the Laborador Trough, the Lake Superior region in Michigan, Minnesota, and Ontario, the Black Hills of South Dakota, and the northern Rocky Mountains in Wyoming and Montana (Bayley and James, 1973). Commonly, the iron-formation occurs in a stratigraphic package comprised of vitreous quartzite with interbedded schist overlain by iron-formation in turn overlain by pelitic argillites and/or graywackes (see, e.g., White, 1954; Bayley and James, 1973).

In particular, in the Mesabi Range of Minnesota, the Animikie group consists of Pokegama Quartzite overlain by Biwabik Iron-Formation overlain in turn by Virginia Argillite. (The sequence is Pokegama Quartzite, Gunflint Iron-formation, Rove Formation in the Gunflint Lake region of Ontario and Minnesota). White (1954) interprets the Pokegama and Biwabik Formations to be interfingering diachronous units with vertically mirrored lithologic sequences indicative of transgressive and regressive cycles. The cross-bedded clastic Pokegama quartzite (10 to 115 m thick) is interpreted to have developed in a retrograding shoreline beach environment as it migrated across a low-lying pre-Animikie erosion surface.

Basinward from this high-energy beach environment, Biwabik Formation conditions progressively favored chemical precipitation of chert, hematitic chert and jasper, minor chert-siderite, chert-magnetite, and iron silicates with some siderite. Thin quartz-mica (pelitic) argillites occur locally between the Pokegama and Biwabik Formations. Intraformational conglomerates occur throughout the Biwabik formation. A basal conglomerate with scattered siliceous algal structures is locally present. All clasts are derived from Biwabik cherts and taconites, which Grout and Broderick (1919, p. 7) interpret to be derived from the breaking up of newly formed Biwabik sediments. White (1954) concludes that the pelitic Virginia Argillite conformably overlies the Biwabik Iron-Formation, but that its deposition may have been brought on by an episode of tectonic activity which produced abundant fine clastic materials that swamped chemical processes. This interpretation contrasts with the lateral facies interpretation for the offshore pelitic gneisses of the Joshua Tree terrane.

There are enough similarities in lithologic content, stratigraphic cross-section (see White, 1954, figs. 8, 10, p. 42, 45), and inferred depositional environment (see White, 1954, fig. 11, p. 46) between this three-part stratigraphic package that includes the iron-formation, and the Pinto gneiss stratigraphic sequence of quartzite, ferriferous/pelitic/carbonate rocks, and pelitic gneiss (Figure 2-11), that some understanding of the Pinto gneiss may accrue from pursuing the analogy. Additionally, if the Pinto stratigraphic suite originally had an along-strike length comparable to that of the Animikie Group (~ 200 miles), then there is some hope for matching the exotic Joshua Tree rocks with other remnants of an initially more extensive terrane.

The iron-formation analogy offers an alternative interpretation for the source of the iron mined by Kaiser Steel Corporation at Eagle Mountain. Earlier investigators have attributed the iron concentration to hydrothermal replacement of carbonate with iron emanating from the Jurassic quartz monzonite, dismissing the possibility of a sedimentary iron source. The location of the ores at Eagle Mountain, however, are confined to two stratigraphic zones: one between the Pinto ferriferous schist and dolomite (see Plate IV), and one above the dolomite beneath an upper vitreous quartzite (Harder, 1912; Hadley, 1945; Dubois and Brummett, 1968). Within the stratigraphic model presented above, these two zones may be time-transgressively equivalent in a stratigraphic position where iron-oxide might be expected (cf. White, 1954). Later modification during the batholithic emplacement in the mine area has certainly obscured the stratigraphic relationships if they exist, and because of the mining operation, I have not yet attempted to gain access to the area to pursue this line of reasoning.

METAMORPHISM

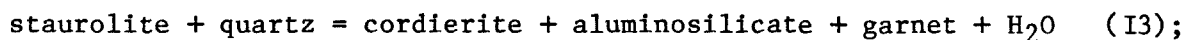
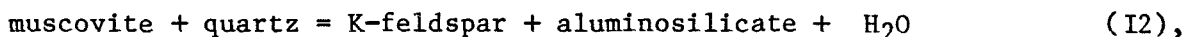
Introduction

The Joshua Tree terrane has been regionally metamorphosed under conditions of relatively low pressure and high temperature (andalusite-sillimanite facies series), and probably under changing conditions of P_{H_2O} , to produce metamorphic mineral assemblages characteristic of the hornblende-hornfels facies and low-pressure amphibolite facies. Metamorphic mineral assemblages in the pelitic lithologies of the Pinto gneiss occur in clear-cut zones delineated by observed and inferred isograds (Plate V). From northnorthwest to southsoutheast through the field area, the principal zonal distinctions in the pelitic lithosomes comprise a symmetrical distribution of sillimanite-andalusite-sillimanite, coincident with an asymmetrical distribution of cordierite-aluminosilicate, staurolite, and chlorite-muscovite or chloritoid-aluminosilicate. Garnet occurs sporadically in the northern zones; biotite is ubiquitous. Relict mineral assemblages indicate that the more hydrous assemblages to the south are at least in part retrograded from previously stable cordierite-bearing assemblages equivalent to those occurring now to the north. There is some suggestion that the rehydration reaction boundaries migrated progressively northward through time. The superimposition of the symmetrical distribution of the aluminosilicates and the asymmetrical distribution of Fe-Mg-Al silicates can be interpreted to indicate intersecting isograds, apparently produced during a single metamorphic episode. The isograd pattern and the sequencing relationships indicated by the relict and retrograde assemblages are consistent with northnorthwestward spatial and temporal increase in P_{H_2O} relative to P_T along a given P_T -T gradient.

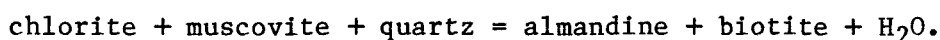
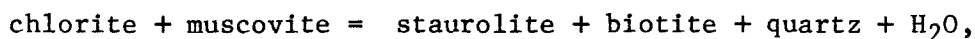
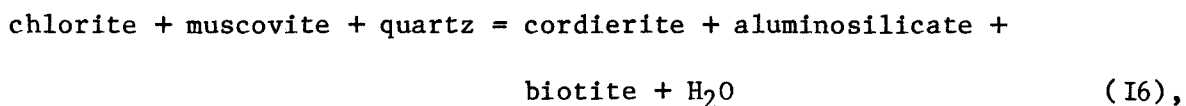
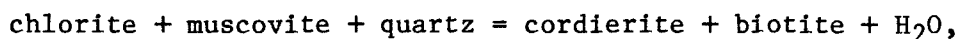
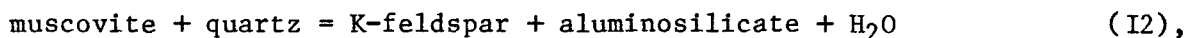
Isograds between the zones of mineral assemblages can be represented

by reactions inferred from textural evidence and/or the mineral assemblages themselves. Texturally and mineralogically recorded equilibrium reactions consist of prograde and retrograde sets of discontinuous and continuous reactions:

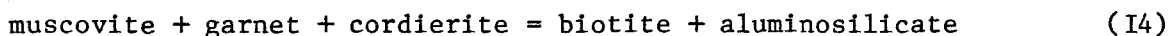
Prograde:



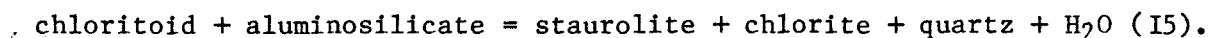
Retrograde:



Mineralogically inferred equilibrium reactions may include the prograde discontinuous reaction



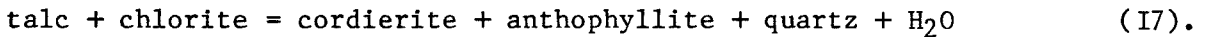
and the retrograde discontinuous reaction involving



The surface traces of these reaction planes or zones (isograds) trend roughly eastnortheast-west southwest, an orientation that is orthogonal both to the protolithic sedimentary trends and to the lithologic and age trends of

the Mesozoic batholithic belts.

Phase-assemblages within limited occurrences of ferromagnesian-rich, lime- and potash-poor units in the Pinto gneiss suggest a zonal distribution that mimics that of the muscovite-quartz-rich pelitic assemblages. In this case the major zonal distinctions are cordierite-orthoamphibole-chlorite versus talc-chlorite. Biotite, garnet, quartz, and clinoamphibole may be present. In one sample cummingtonite is present in addition to anthophyllite-gedrite. Corundum, spinel, and staurolite are found in ferro-aluminous enclaves in one sample from the Little San Bernardino Mountains in the cordierite-orthoamphibole zone. The inferred equilibrium reaction across the zonal boundary is



This isograd is drawn parallel to those of the pelitic assemblages.

The zonal distributions of mineral assemblages are interpreted to record a single metamorphic episode comprising early prograde dehydration within the Pinto gneiss as it advanced along an appropriate P_T - T trajectory, later rehydration as $P_{\text{H}_2\text{O}}$, initially less than P_T , approached equality with P_T , and perhaps renewed dehydration after increasing $P_{\text{H}_2\text{O}}/P_T$ stabilized at unity or even at some $P_{\text{H}_2\text{O}} < P_T$. When compared with experimental results, the observed phase assemblages and texturally preserved equilibrium reactions are consistent with formation at $P_T \approx 3.5$ to 3.8 kb, $T \approx 500$ to 525°C (for Holdaway's aluminosilicate triple point), with $P_{\text{H}_2\text{O}}$ varying from $< 0.3P_T$ to $\sim P_T$ from north to south within the field area, and through time in the southern part of the area.

Neither the prograde nor the retrograde stages of the metamorphism of the Pinto gneiss can be related to the intrusion of the Mesozoic batholiths.

The prograde metamorphic minerals predate and are overprinted by the thrust-related deformational fabric; in part, growth of the retrograde minerals may be coincident with development of that fabric.

Pelitic Assemblages

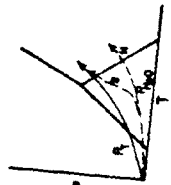
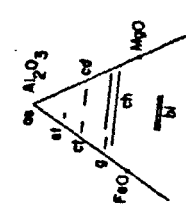
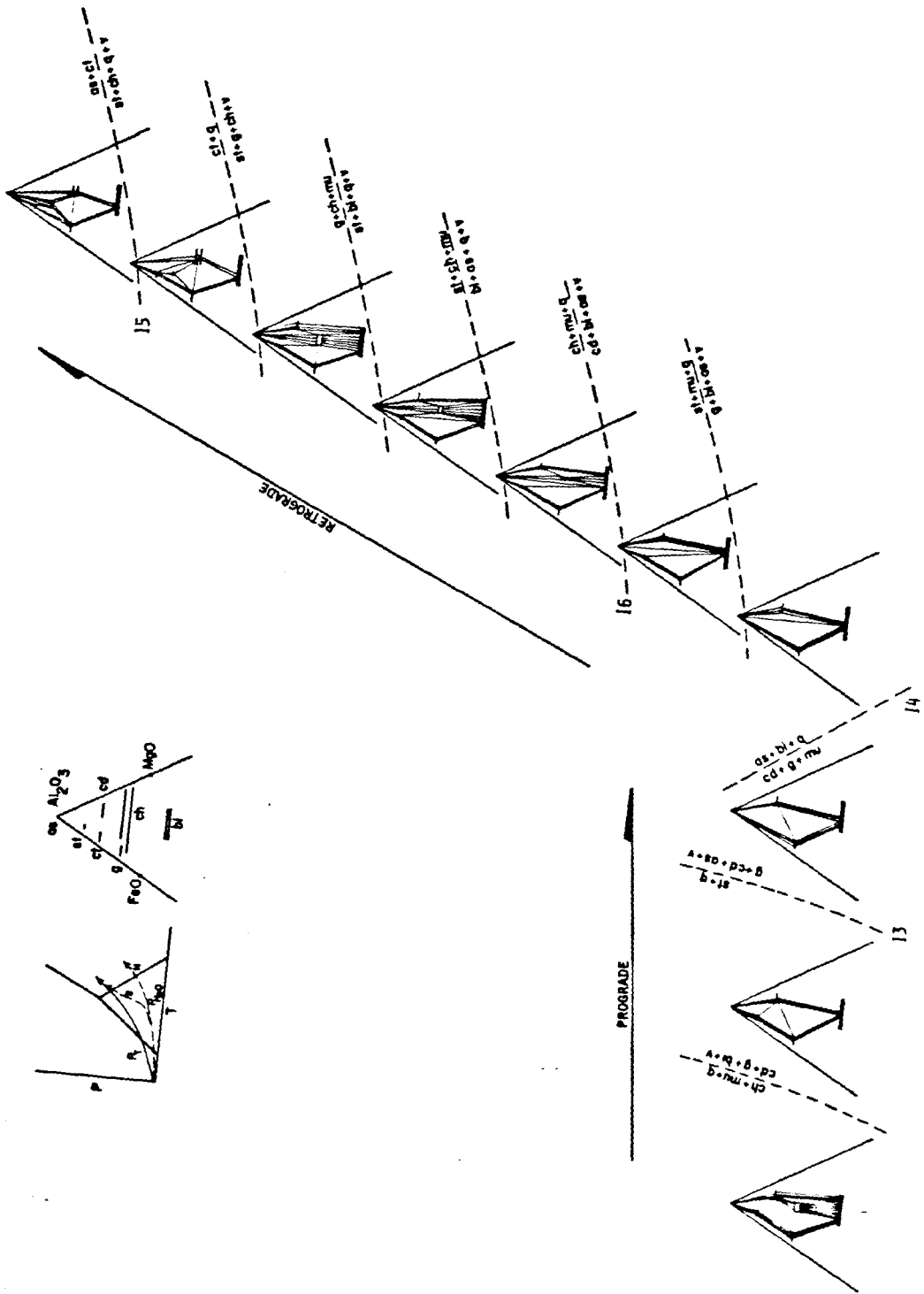
The pelitic assemblages tabulated above in the sections devoted to descriptions of the Pinto gneiss lithosomes are qualitatively represented in Thompson's AKFM projection in Figure 2M2. Placed on a map, the diagrams indicate an increase in metamorphic grade northnorthwestward through the field area. Metamorphic reactions are discussed on the basis of textural evidence where observed; otherwise, probable reactions are hypothesized on the basis of topology of the AKFM projections and by analogy with reactions recognized in other metamorphic terranes. The AKFM topologies are constrained by the generally observed mineralogical array of $Mg/(Fe + Mg)$ values in which garnet < staurolite < chloritoid < biotite < chlorite < cordierite (Hess, 1969; Albee, 1972; Thompson, 1976; Labotka, 1978), and by the theoretical $Mg/(Fe + Mg)$ shifts of continuous reactions with increasing temperature as predicted by Thompson (1976).

Two sequences of AKFM diagrams are shown in Figure 2M2: a prograde sequence inferred to have developed along some P_T -T trajectory at $P_{H_2O} < P_T$, and a retrograde sequence inferred to have developed as $P_{H_2O} \rightarrow P_T$ at about the time the trajectory intersected the andalusite = sillimanite phase boundary. The reactions are consistent with the petrogenetic grid shown by Labotka (1978) (cf. Albee, 1965; Hess, 1969; Thompson, 1976), although the grid must be located differently in P_T -T space to permit the coexistence of chloritoid + sillimanite.

Figure 2-12. Schematic representation of a possible Pinto gneiss trajectory through a petrogenetic grid for pelitic compositions (see Hess, 1969; Albee, 1972; Thompson, 1976; Labotka, 1978). The path is consistent with the observed assemblages and texturally inferred reactions (I3 to I6: see text) for the pelitic lithologies of the Pinto gneiss. Not all three-phase fields shown in the AKFM diagrams have been found. For the prograde sequence, $P_{H_2O} < P_T$; for the retrograde sequence $P_{H_2O} \rightarrow P_T$. Mineral compositions in the AKFM diagram are shown in the right inset. In the left inset, possible P-T trajectories for the prograde sequence (N) that was formed in both the north and south but was retrograded in the south along trajectory (S).

Phase symbols:

as	aluminosilicate
st	staurolite
ct	chloritoid
cd	cordierite
g	garnet
ch	chlorite
bi	biotite
q	quartz
mu	muscovite
v	water vapor



Andalusite/sillimanite-bearing assemblages. Pelitic assemblages that contain andalusite and/or sillimanite occur in the Lost Horse and Black Eagle granofelses as well as in the paleo-weathered zone developed on the Joshua Tree granite. Aluminosilicates, including viridine, are also found dispersed in the cross-bedded lithosome of the Pinto Mountain quartzite, and in thin (1 to 3 cm), red layers consisting of hematite, quartz, and andalusite within the vitreous white quartzite lithosome. Textural characteristics of those minerals in each lithosome have been described in previous sections. No aluminosilicates have been found in either the Baumonk Mill granofels or the Music Valley gneiss.

Within the field area, the distribution of andalusite and sillimanite occurrences at the earth's surface delineate two traces of the andalusite = sillimanite (I1) reaction surface (Plate V). The southern reaction boundary, with sillimanite to the southeast and andalusite to the northwest, runs northeast through the Eagle Mountains. It is offset left-laterally along the Cenozoic Victory Pass fault. At two localities near the trace, but displaced somewhat into the sillimanite field, textural evidence is seen for the reaction

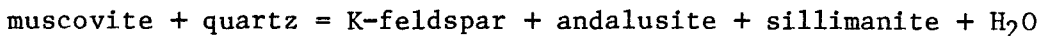
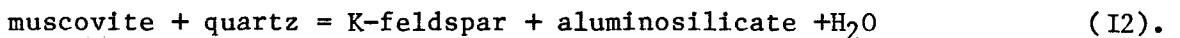
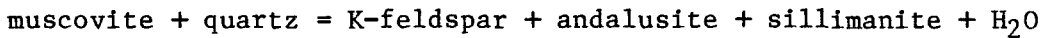


(Figure 2-9B), which is a special case of the reaction



For some kinetic or compositional reason, in this reaction andalusite is able to form or persist metastably in the sillimanite field. The prograde assemblage in these occurrences has subsequently been partially retrograded to muscovite and quartz.

The northern trace of the equilibrium reaction boundary, with andalusite to the southeast and sillimanite to the northwest, runs northeast through the Little San Bernardino, Hexie, and Pinto Mountains. In the Pinto Mountains, the younger break of the Red Cloud thrust system has apparently displaced a segment of this reaction boundary northwestward to superpose andalusite-bearing rocks above sillimanite-bearing rocks. Textural evidence for the reaction



is again observed in the central Pinto Mountains north of the trace of the phase transition boundary (Figure 2-10F). Once again the occurrence is somewhat displaced into the sillimanite stability field, but here is not significantly retrograded.

The two traces are on opposite limbs of a synformally folded or formed andalusite = sillimanite reaction surface. This surface may represent either an isograd at a specific temperature and pressure consistent with a given point on the experimental univariant curve, or it may represent a reaction boundary that defines a surface of mutually changing temperature and pressure consistent with some segment of the experimental univariant curve. In the former case, the occurrence of potassium feldspar-andalusite-sillimanite assemblages near the transition boundary fixes a $P_{\text{H}_2\text{O}}$ compatible with the specific $P_{\text{T}}-T$ conditions; in the latter case, $P_{\text{H}_2\text{O}}$ must vary in space and/or time in a manner that permits reaction (I2) to form both sillimanite and andalusite under changing $P_{\text{T}}-T$ conditions. In the latter case, reaction boundaries (I1) and (I2) would be intersecting. In the former case, if $P_{\text{H}_2\text{O}}/P_{\text{T}}$ was constant, isograds (I1) and (I2) would be parallel, whereas if $P_{\text{H}_2\text{O}}/P_{\text{T}}$ was changing, the isograds would cross.

An assemblage of K-feldspar + sillimanite + biotite + quartz in the paleo-weathered zone of the southwesternmost Chuckwalla Mountains has been partially retrograded to muscovite + chlorite + quartz. A couple of samples of muscovite-quartz schist in the Big Wash area of the Eagle Mountains contain relics and possible pseudomorphs of andalusite and K-feldspar. These occurrences are evidence in support of the cases involving intersecting isogradic surfaces. This discussion will be pursued below in a section devoted to the synthesis of observations on the metamorphism of the pelitic gneisses.

Experimental aluminosilicate phase relationships have been studied by a number of investigators with surprisingly little agreement in the resulting stability fields (Newton, 1966a,b; Weill, 1966; Althaus, 1967; Richardson et al., 1969; Holdaway, 1971; Brown and Fyfe, 1971; cf. Zen, 1969). The phase transition boundaries for some of these recent experimental studies are compiled in Figure 2-13. Each has been cited in various petrologic studies, but those of Richardson, Gilbert, and Bell (1969) and Holdaway (1971) have been most widely accepted. The discrepancies arise from the experimental difficulty in locating the andalusite = sillimanite transition. Of the various triple points, that of Holdaway yields a slope for the andalusite = sillimanite transition that most closely agrees with calorimetric experiments involving disordering enthalpies (Navrotsky et al., 1973), enthalpies of formation and reaction for andalusite and sillimanite (Anderson and Kleppa, 1969; Anderson et al., 1977), and cryolite solubility studies of andalusite and sillimanite at one atmosphere (Weill, 1966).

Holdaway's experiments offer two possible explanations for the anomalous occurrence of andalusite within the sillimanite field as discussed above in the context of reaction (I2) where it has produced both andalusite

Figure 2-13. Experimental curves in the $\text{Al}_2\text{O}_3\text{-SiO}_2\text{-H}_2\text{O}$ system:

kyanite-andalusite-sillimanite invariant point and univariant curves:

- A Althaus, 1967
- RGB Richardson, Gilbert, & Bell, 1969
- N Newton, 1966a
- H Holdaway, 1971
- W Weill, 1966
- BF Brown & Fyfe, 1971

kaolinite + 2 quartz = pyrophyllite + H_2O

- 1 Thompson, 1970a (cf. Hemley & Jones, 1964, p. 563; Reed & Hemley, 1966, p. C164; Velde & Kornprobst)

pyrophyllite + 6 diaspore = 4 aluminosilicate + 4 H_2O

- 2 Haas & Holdaway, 1973

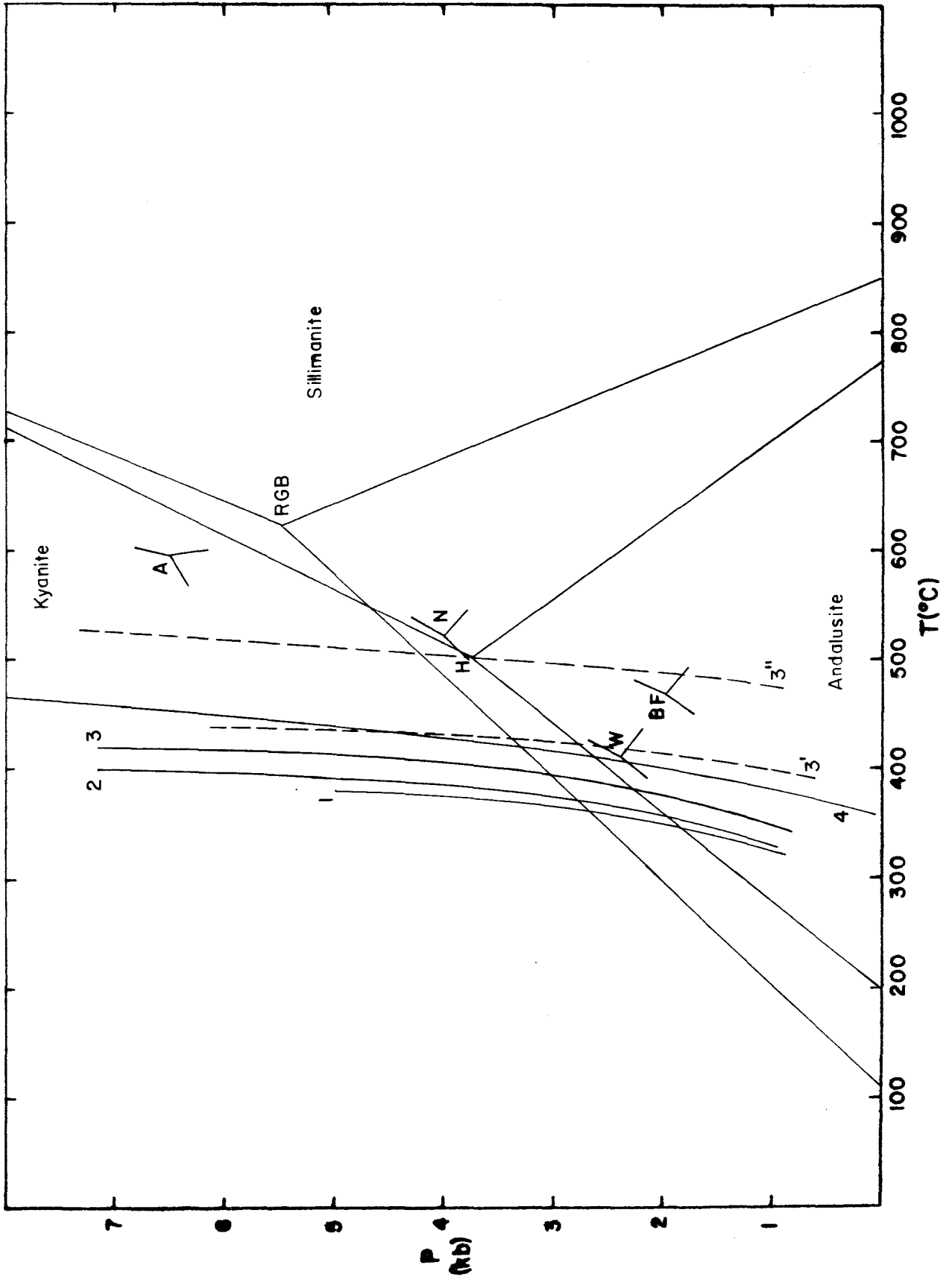
pyrophyllite = aluminosilicate + 3 quartz + H_2O

- 3 Haas & Holdaway, 1973
- 3' Kerrick, 1968
- 3" Althaus, 1969 (cf. Hemley, 1967; Velde & Kornprobst, 1969)

2 diaspore = corundum + H_2O

- 4 Haas, 1972
Fyfe & Hollander, 1964

(For further discussion of the $\text{Al}_2\text{O}_3\text{-SiO}_2\text{-H}_2\text{O}$ system, see Day, 1976 and Perkins et al., 1979.)



and sillimanite. If the reaction produced fibrolite, it could react to form andalusite metastably up to 200°C above the stable andalusite-sillimanite boundary, followed by very sluggish conversion to coarse-grained sillimanite (cf. Holdaway, 1971). Alternatively, if Al-Si disordered sillimanite were produced by the reaction, it could, at temperatures slightly higher than the stable boundary, react to form stable sillimanite plus andalusite, followed again by sluggish conversion of andalusite to stable sillimanite. Still another possible interpretation requires that the reaction introduce compositional impurities (Fe^{+3} and/or Mn) into the aluminum silicates in sufficient quantity to slightly increase the stability field of andalusite at the andalusite = sillimanite boundary (Strens, 1968, p. 846; Albee and Chodos, 1969, p. 315; Chinner et al., 1969, p. 111; Okrusch and Evans, 1970, p. 267).

Andalusite may have formed in part from the dehydration of pyrophyllite, a reaction experimentally produced with reversals by Althaus (1966), Hemley (1967), Kerrick (1968), and Haas and Holdaway (1973). The different experimental results (Figure 2-13) show a rather large temperature range, but all curves occur at temperatures lower than the probable peak temperatures for the Pinto gneiss metamorphism.

Experimental results for the breakdown of muscovite + quartz at $P_{\text{H}_2\text{O}} = P_T$ are shown in Figure 2-14 (Evans, 1965; Althaus et al., 1970; Chatterjee and Johannes, 1974). The combined dehydration curves from these studies define a narrow band that will be considered the stability limit of muscovite + quartz in the discussion that follows. In addition to experimental uncertainty, the width of the band is in part due to different Al-Si structural ordering states of feldspars in the experiments (Helgeson et al., 1978, p. 142-144). If $P_{\text{H}_2\text{O}} < P_T$, the dehydration curve occurs at lower temperatures

Figure 2-14. Experimental and calculated curves in the system $K_2O-Al_2O_3-SiO_2-H_2O$:

muscovite + quartz = aluminosilicate + K-feldspar + H_2O

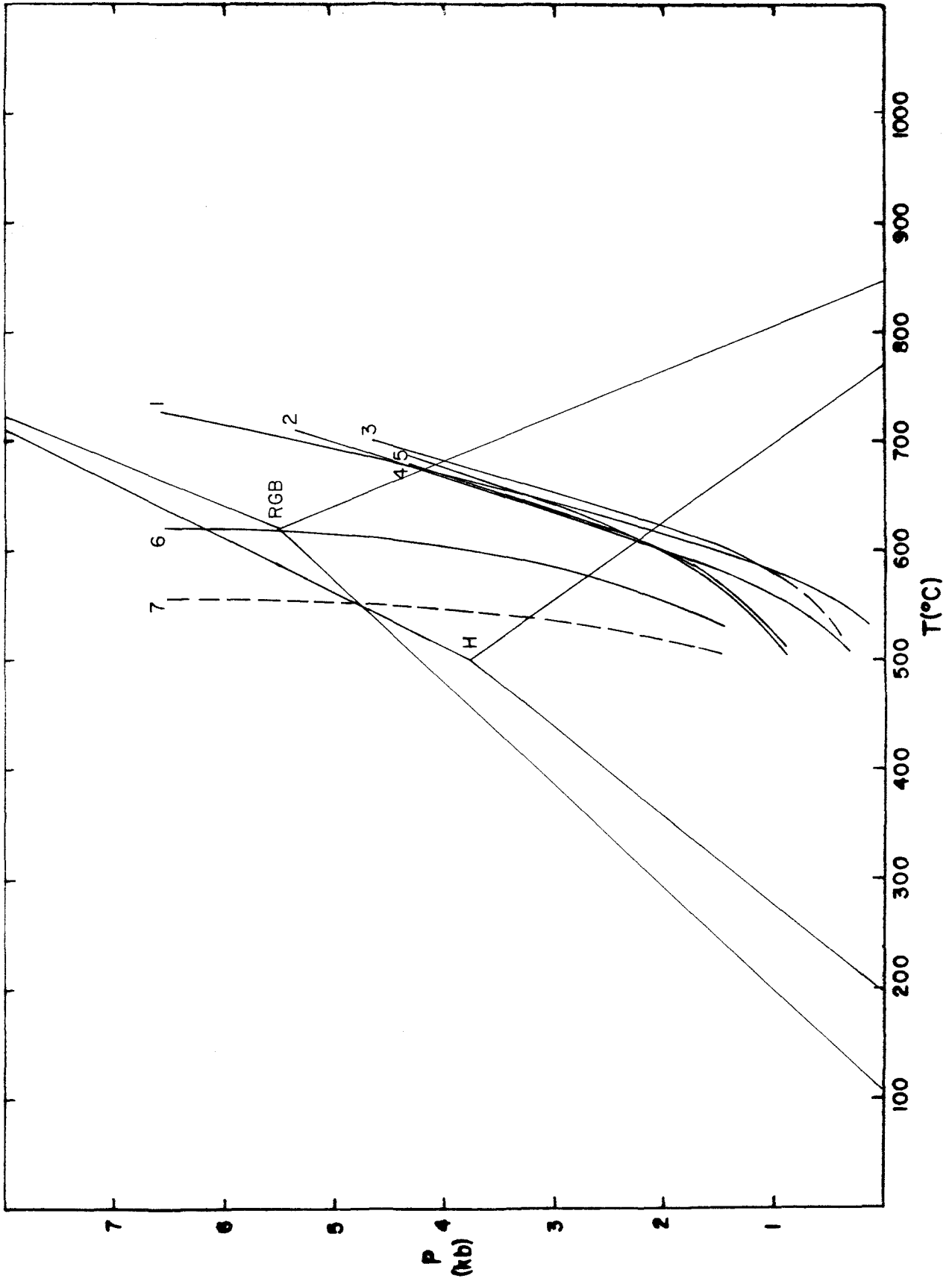
$$P_{H_2O} = P_T$$

- 1 andalusite (Chatterjee & Johannes, 1974)
- 2 sillimanite (Chatterjee & Johannes, 1974)
- 3 andalusite (Althaus et al., 1970)
- 4 sillimanite (Evans, 1965)
- 5 andalusite (Evans, 1965)

$$P_{H_2O} < P_T$$

- 6 andalusite, $P_{fluid} = P_{CO_2} + P_{H_2O}$, $X_{H_2O} = 0.5$ (Kerrick, 1972)
- 7 calculated for $P_{H_2O} = 0.1 P_T$ (Hoschek, 1969)

Aluminosilicate invariant point (H, RGB) and univariant curves from Figure 2-12.



(Thompson, 1955; Greenwood, 1961). For the muscovite + quartz reaction, Hoschek (1969) and Kerrick (1972) have calculated dehydration curves for $P_{H_2O} < P_T$, and Kerrick (1972) has experimentally determined the curve at $P_{H_2O} = 0.5P_T$. Kerrick's curve for $P_{H_2O} = 0.5P_T$ and Hoschek's curve for $P_{H_2O} = 0.1P_T$ are shown in Figure 2-14.

Biotite/Cordierite/Garnet/Staurolite/Chloritoid/Chlorite-Bearing Assemblages.

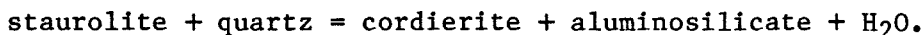
The distribution of occurrences of metamorphic Fe-Mg-Al silicates define northeast- to eastnortheast-trending zones that transect the various lithosomes of Pinto gneiss within the field area (Plate V). Cordierite is found over a broad area to the north in the Pinto and northern Little San Bernardino Mountains. Staurolite occurs in narrow colinear zones across the south-central Little San Bernardino and northern Eagle Mountains. Garnet is found in both zones. Chlorite occurs in the southern Little San Bernardino and Hexie, Cottonwood, Eagle, and Orocopia Mountains in the association chlorite + muscovite quartz as retrograde replacement of all of the above minerals. Chloritoid is found at a single locality in the central Eagle Mountains. Several isograds are inferred from changing mineral parageneses at the boundaries of these zones, in some cases with supporting textural evidence.

Cordierite (Figures 2-7, 2-10E) occurs throughout the Lost Horse granofels in the Hexie, Little San Bernardino, and Pinto Mountains, and at a couple of localities in the Black Eagle facies of the central Pinto Mountains, beneath the younger Red Cloud thrust. Exposures of both the Black Eagle granofels in the Pinto Mountains and the Lost Horse granofels in the Pinto and northern Little San Bernardino Mountains are characterized by little-altered assemblages of cordierite + sillimanite/andalusite + biotite ± quartz

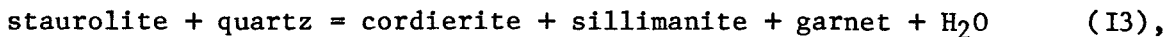
± muscovite ± K-feldspar. To the south, in the southern Little San Bernardino, southwestern Hexie, and northern Eagle Mountains, occurrences of these assemblages in the Lost Horse and Black Eagle granofelses have been extensively retrograded, as discussed below. Cordierite also occurs at one locality in the Baumonk Mill granofels in the south-central Pinto Mountains, where it is partially pseudomorphed by chlorite + muscovite + quartz. The unretrograded assemblage in the Baumonk Mill granofels is cordierite + biotite + quartz + muscovite.

Relics and pseudomorphs of staurolite are found at a few localities in both the Lost Horse granofels in the south-central Little San Bernardino and central Hexie Mountains, and in the Black Eagle granofels in the northernmost Eagle Mountains. These occurrences are confined to narrow zones immediately south of the little-altered cordierite-aluminosilicate-bearing assemblages in both lithosomes. The zonal boundaries in the two lithosomes are interpreted as colinear segments of a single isogradic surface with an east-northeast surface trace, although the bulk compositions of the intervening Baumonk Mill and Music Valley lithosomes did not yield the diagnostic assemblages. In the Lost Horse lithosome, staurolite is observed as relics armored in grains of cordierite intergrown with crystalline sillimanite (Figure 2-7A,C,E, 2-10E). At one locality slightly farther south in the Little San Bernardino Mountains, relict staurolite is rimmed by chlorite and muscovite. In the Black Eagle lithosome the mineral also occurs as relics surrounded by chlorite and muscovite, and as pseudomorphs replaced by cordierite(?) and fibrolitic sillimanite(?).

The textural evidence provided by staurolite armored within overgrowths of cordierite and sillimanite indicates a reaction such as



However, since cordierite generally has a much higher Mg/(Fe + Mg) ratio than staurolite (Thompson, 1957; Albee, 1968), a more likely reaction involving chlorite is



a discontinuous terminal reaction. Reaction (I3) is suggested by a few samples from both the Lost Horse and Black Eagle lithosomes that contain all of the phases involved in the reaction. This reaction represents the prograde disappearance of staurolite from the AKFM diagram (Figure 2-12).

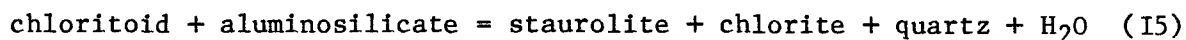
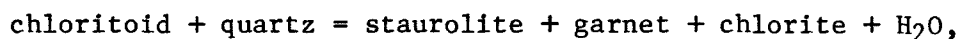
Garnet has been observed in the Lost Horse granofels in the northern and central Little San Bernardino Mountains with cordierite-biotite-sillimanite \pm staurolite and biotite-andalusite. In the northern Little San Bernardino Mountains, it is rimmed by cordierite in cordierite-biotite-sillimanite-bearing assemblages, whereas in the south-central part of the range it occurs in some of the staurolite-bearing assemblages. Slightly farther south, it occurs with biotite and andalusite in an assemblage somewhat retrograded to chlorite and muscovite. Relict garnet also occurs at one locality in a pelitic schist of the Black Eagle lithosome in the Big Wash area of the Eagle Mountains. The absence of garnet in some of the staurolite-bearing rocks of the Lost Horse granofels where staurolite is breaking down by reaction (I3) suggests that the discontinuous reaction



closely follows reaction (I3) (see Thompson, 1976, fig. 7).

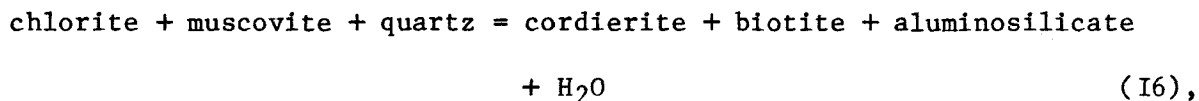
The assemblage of chloritoid + sillimanite + muscovite + quartz from

the paleo-weathered zone in the upper plate of the younger Red Cloud thrust occurs in the Big Wash area of the central Eagle Mountains. Although this lone occurrence does not define a zone, its position near the southern trace of the aluminosilicate isograd lies south of the staurolite zone. A transition from chloritoid- to staurolite-bearing assemblages is not observed, but one may be inferred to involve a reaction of chloritoid with aluminosilicate or and quartz:

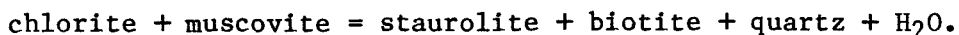


(cf. Tilley, 1925; Hoschek, 1967; Thompson and Norton, 1968; Richardson, 1968). The apparently stable coexistence of chloritoid and sillimanite is consistent with Holdaway's determination of the aluminosilicate triple point (see Figures 2-13, 2-16).

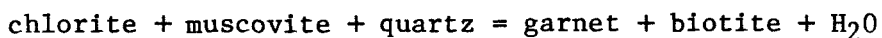
In the Lost Horse granofels, cordierite-andalusite-biotite-quartz \pm muscovite assemblages occur south of the narrow staurolite zone, but cordierite, aluminosilicate, and biotite are extensively retrograded to chlorite and muscovite. One relict staurolite-bearing assemblage found in the southern Little San Bernardino Mountains is also extensively retrograded to chlorite and muscovite. Retrogradation of staurolite and possibly cordierite to chlorite and muscovite also occurs in the Black Eagle lithosome of the northern Eagle Mountains. These relationships are interpreted as retrograde crossings of dehydration boundaries represented by the discontinuous reaction



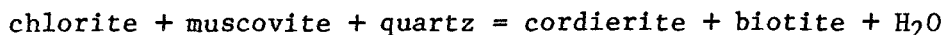
and the continuous reaction



The relict garnet-biotite-andalusite assemblage in the Lost Horse granofels in the Hexie Mountains is retrograded to chlorite and muscovite. Garnet(?) pseudomorphs completely replaced by chlorite and muscovite also occur in the Black Eagle lithosome of the northernmost Eagle Mountains indicating retrogression of the continuous reaction



(cf. Thompson and Norton, 1968). In the Baumonk Mill granofels, the partially retrograded cordierite-biotite-quartz-muscovite assemblage in the south-central Pinto Mountains gives way southward in the Cottonwood-Eagle and Orocopia Mountains, and at the Old Baumonk Mill site south of the western Chuckwalla Mountains, to muscovite-chlorite-quartz pseudomorphs of cordierite with chloritized biotite, indicating retrograde crossing of a reaction zone defined by a continuous reaction such as



(cf. Turner, 1968, p. 128). These complete pseudomorphs are texturally and mineralogically identical to those that partially replace cordierite in the Baumonk Mill granofels of the Pinto Mountains. The absence of aluminosilicate suggests a relatively Al_2O_3 -poor, MgO-rich bulk chemistry. From these retrograde reactions of the prograde assemblages, it is inferred that the prograde minerals were initially formed from chlorite-muscovite-quartz assemblages.

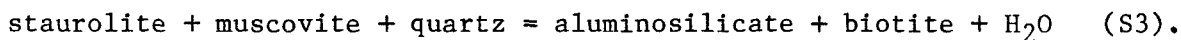
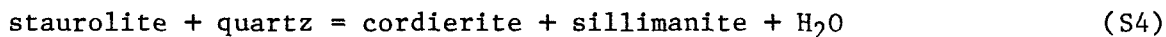
The areal distributions of biotite, cordierite, garnet, staurolite,

chloritoid, and chlorite are combined with published petrogenetic grids and experimental results to hypothesize that the various ferromagnesian-aluminum silicates formed in zones of differing P_T - T - P_{H_2O} northnorthwest to southsoutheast across a metamorphic gradient. Although some bulk compositional variation is evident within a given lithosome (especially the Black Eagle lithosome), in general each lithosome is inferred to be rather uniform.

Pertinent petrogenetic grids include those of Albee (1965), Hess (1969), Thompson (1976), and Labotka (1978). Experimental results that bear on the stability of chlorite, chloritoid, staurolite, cordierite, and garnet in association with muscovite \pm quartz \pm aluminosilicate are shown in Figure 2-15. These reactions are dependent on bulk composition, $Mg/(Fe + Mg)$ ratio, and f_{O_2} , in addition to P_T , T , and P_{H_2O} . Most of the experimentally investigated reactions involving ferromagnesian-aluminum silicates are continuous reactions that shift in P_T - T space with changes in bulk compositional $Mg/(Fe + Mg)$ ratio. In addition, many discontinuous reactions that were experimentally run with only MgO or FeO become continuous reactions with the addition of the other component in a natural environment. For a given bulk composition these continuous reactions occur through a zone rather than at a surface in P_T - T space. In general, the end member curves will delineate the limits of the continuous reaction zones, although this is not true for the breakdown of chlorite + muscovite + quartz to cordierite + biotite. At best, experimental curves have been determined for a given reaction at only a few specific compositions. Because the $Mg/(Fe + Mg)$ ratios of the phase and bulk compositions of the Pinto gneiss are not known, and because additional phases are sometimes present in the natural assemblages linked by isograd reactions within the Pinto gneiss, the experi-

mental curves must be considered only as more or less crude approximations of the location of the isograds in P_T - T space. With this cautionary stipulation in mind, it is tentatively anticipated that the P_T - T spatial sequence of experimental dehydration curves and their location relative to Holdaway's aluminosilicate triple point can be used to anchor the petrogenetic grids in P_T - T - P_{H_2O} space. In order to accommodate the coexistence of cordierite and sillimanite, the grid positioning must be different than those advocated by Albee, Hess, Thompson, or Labotka.

The location in P_T - T - P_{H_2O} space of reaction (I3), linking the cordierite-aluminosilicate zone with the staurolite zone, is assumed to be approximated by two experimentally determined dehydration curves (Figure 2-15):



The experimentally determined location of the dehydration reaction

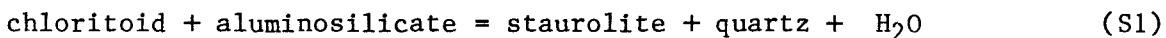


(Figure 2-15) is assumed to approximate the disappearance of chloritoid in the observed chloritoid-sillimanite-muscovite-quartz assemblage (isograd reaction I5). The reaction

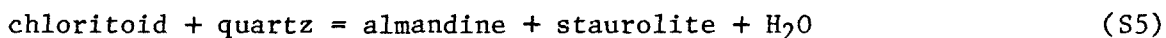


(Figure 2-15) occurs at only slightly higher temperatures than reaction (S1).

Experimental curves for reaction involving dehydration of chlorite + muscovite \pm quartz consist of two determinations of the discontinuous reaction

Figure 2-15. Experimental curves in the system K_2O - MgO / FeO - Al_2O_3 - SiO_2 - H_2O :

8 chloritoid + 10 aluminosilicate = 2 staurolite + 3 quartz + 4 H_2O

S1 Richardson, 1968: FeO , QFM buffer, $P_{H_2O} = P_T$, sillimanite
(cf. Hoschek, 1967, unbuffered);

49 chlorite + 151 muscovite = 44 staurolite + 151 biotite + 360 quartz
+ 696 H_2O

S2 Hoschek, 1969: $Mg/(Fe + Mg) = 0.4$, QFM buffer, $P_{H_2O} = P_T$;

10 staurolite + 8 muscovite + 15 quartz = 98 aluminosilicate + 8 biotite
+ 20 H_2O

S3 Hoschek, 1969: $Mg/(Fe + Mg) = 0.4$, QFM buffer, $P_{H_2O} = P_T$;

2 staurolite + 15 quartz = 4 cordierite + 10 aluminosilicate + 4 H_2O

S4 Richardson, 1968: FeO , QFM buffer, $P_{H_2O} = P_T$, sillimanite;

23 chloritoid + 8 quartz = 4 staurolite + 5 almandine + 21 H_2O

S5 Ganguly, 1969: FeO , NNO buffer (cf. Richardson, 1968);

chlorite + muscovite + 2 quartz = cordierite + phlogopite + 3.5 H_2O

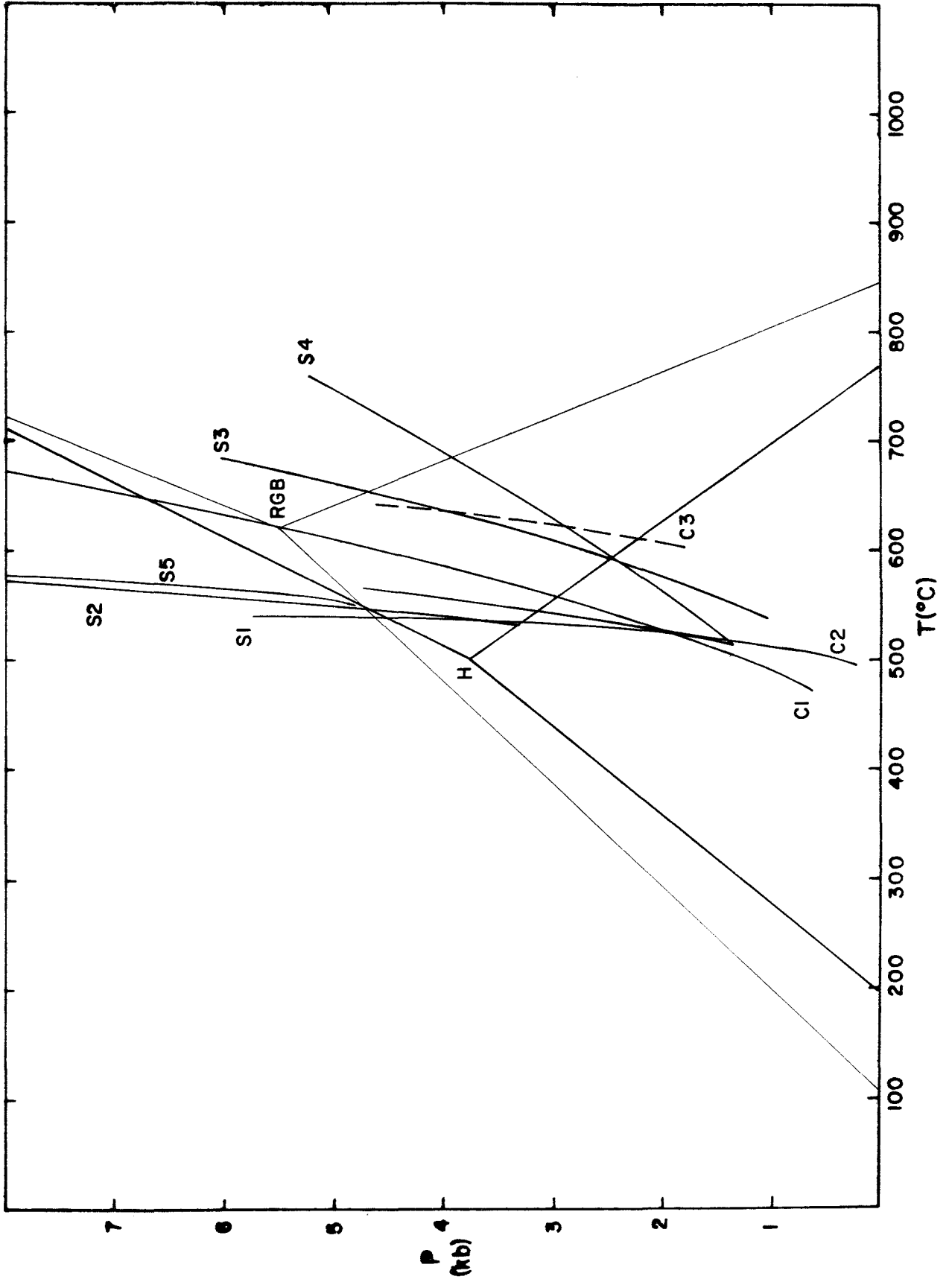
C1 Bird & Fawcett, 1973: MgO (cf. Seifert, 1970a; Schreyer & Seifert, 1970)

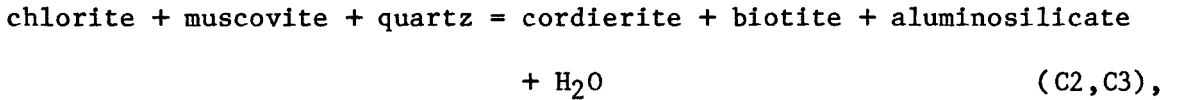
chlorite + muscovite + quartz = cordierite + biotite + aluminosilicate
+ H_2O

C2 Hirschberg & Winkler, 1968: $Mg/(Fe + Mg) = 0.2, 0.6$, NNO buffer,

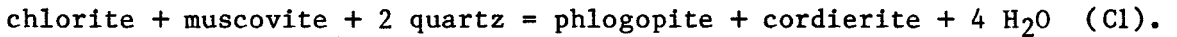
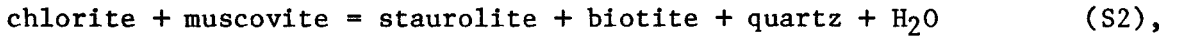
C3 Burnell & Rutherford, 1979: $Mg/(Fe + Mg) = 0.5$, QFM buffer;

Other experimental studies on the stability of staurolite include those of Ganguly (1968, 1972). Other experimental studies on the stability of chloritoid include those of Ganguly (1968), Ganguly and Newton (1968), and Grieve and Fawcett (1974).





and the continuous reactions



Reaction (C2) is used to approximate the location of isograd reaction (I6).

Pelitic Gneiss Synthesis. In the Eastern Transverse Ranges, the andalusite = sillimanite transition, strictly P_T - T controlled, defines a remnant of a gently downwarped surface with andalusite-bearing rocks occurring in an eastnortheast-trending trough. The surface may have been generated either at the specific pressure and temperature at which a single regional P_T - T gradient intersected a point on the phase boundary, or along the locus of points in P_T - T space at which a continuous range of P_T - T gradients intersected a segment of the phase boundary.

The Fe-Mg-Al silicate-bearing pelitic assemblages occur in zones that, from northnorthwest to southsoutheast, are characterized by cordierite-sillimanite-biotite or cordierite-biotite, staurolite-quartz, chlorite-muscovite-quartz, and chloritoid-sillimanite. These zones, limited by dehydration reaction boundary surfaces, are asymmetrically disposed in an array that intersects the andalusite = sillimanite transition surface. There is considerable textural evidence indicating that the cordierite-aluminosilicate-biotite, K-feldspar-aluminosilicate, and cordierite-biotite bearing assemblages once existed farther south than the present southern limit of the little-altered assemblages, but were subsequently retrograded

to more hydrous assemblages involving chlorite-muscovite-quartz and chloritoid-sillimanite. The occurrence of relics of relatively dehydrated cordierite-aluminosilicate-biotite, cordierite-K-feldspar-aluminosilicate-biotite, and K-feldspar-aluminosilicate \pm biotite bearing assemblages within the retrograded chlorite-muscovite bearing assemblages require either a decrease in temperature or an increase in P_{H_2O} , or some combination of the two.

The experimental results previously discussed have been summarized in Figure 2-16. Within the context of Figure 2-16, four P_T - T - P_{H_2O} trajectories that might generate the observed distribution of metamorphic mineral assemblages will be considered. A conventional representation of a regional metamorphism on a P - T diagram would show a single geothermal gradient (P - T trajectory) along which the metamorphism had developed. With such an approach for the metamorphism of the Pinto gneiss, the P_T - T path would intersect the andalusite = sillimanite boundary at a single point, which would represent the P_T - T conditions for that isograd surface in the Eastern Transverse Ranges. For $P_{H_2O} = P_T$, this intersection to the north would have to be at or very near the intersection of the andalusite = sillimanite boundary and the dehydration curve for muscovite + quartz = K-feldspar + aluminosilicate + H_2O : approximately 2-2.5 kb, and 600-625°C (Figure 2-17, trajectory (a)); whereas to the south, the intersection of the P_T - T trajectory and the phase boundary would have to lie between the triple point and the dehydration stability limit for the assemblage chloritoid + sillimanite + muscovite + quartz: approximately 3.5-3.6 kb and 500-525°C (Figure 2-17, trajectory (a')). The range for these two points of intersection are obviously not compatible.

One P_T - T representation which incorporates both the observed distri-

Figure 2-16. Combined experimental curves for the system $K_2O-MgO/FeO-Al_2O_3-SiO_2-H_2O$ (chlorite + muscovite + quartz) pertinent to the metamorphism of the pelitic rocks of the Pinto gneiss. Curves are referenced in Figures 2-13, 2-14, 2-15.

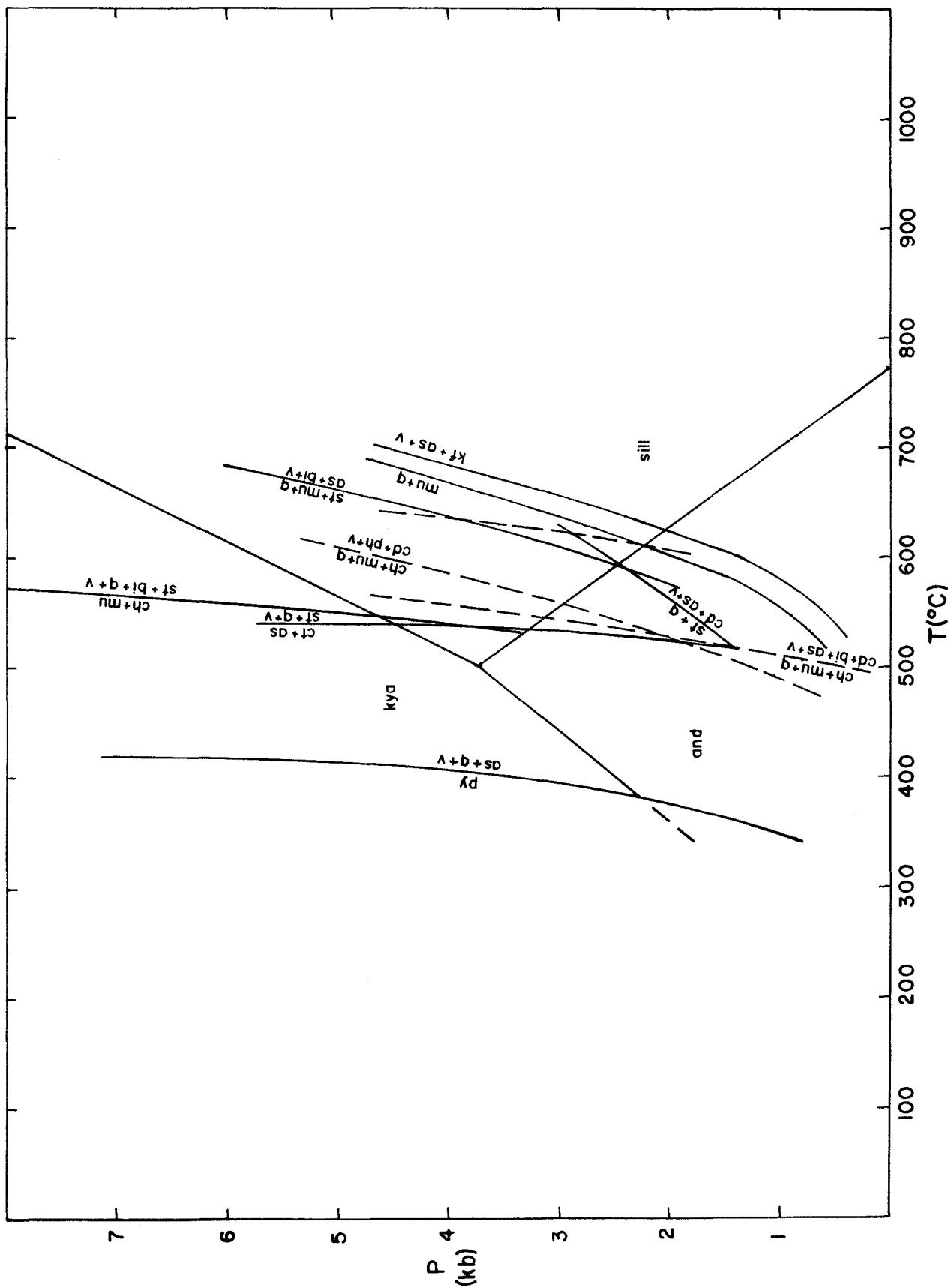
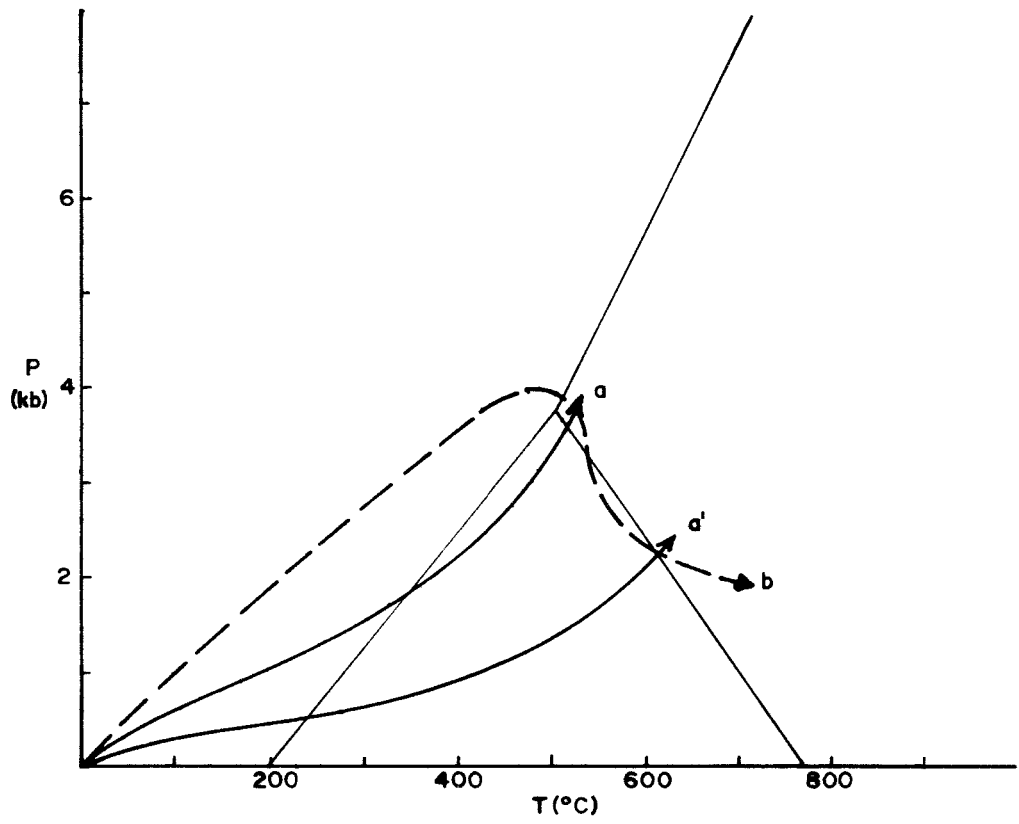


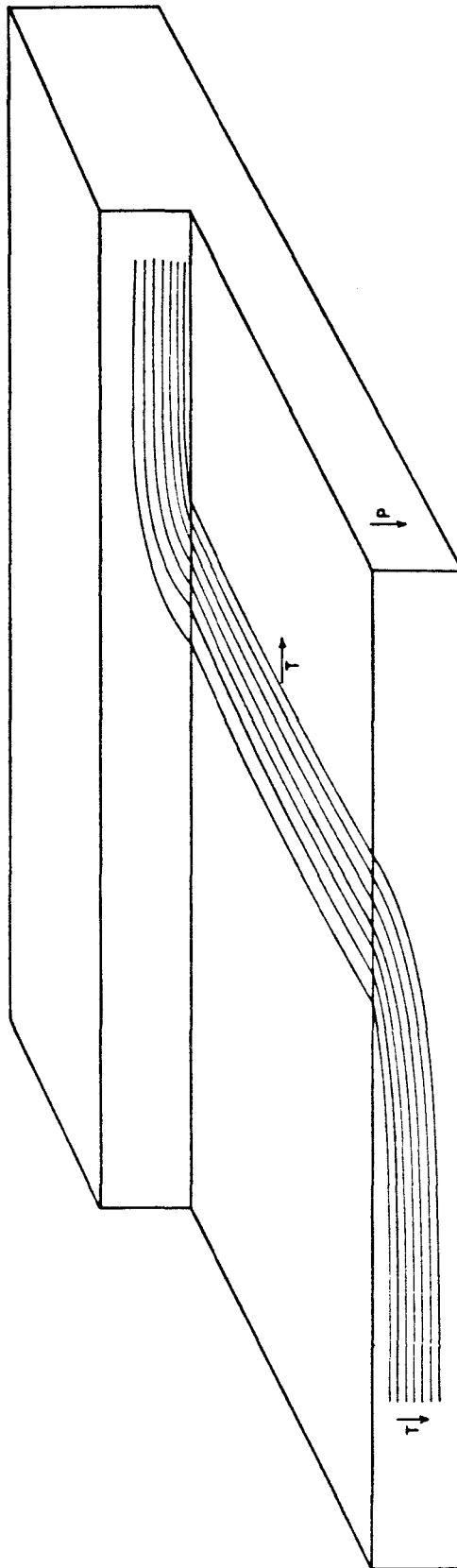
Figure 2-17. Hypothetical P - T trajectories not completely consistent with the distribution and sequence of prograde and retrograde mineral assemblages in the pelitic rocks of the Pinto gneiss. See text for explanation.



bution of pelitic mineral assemblages and reaction boundaries and the experimentally determined P-T relationships is shown in Figure 2-17 as the segment of trajectory (b) between trajectories (a) and (a'). At the culmination of the metamorphism of the Pinto gneiss, the present surface of the earth along a northnorthwest-southsoutheast line of section could be interpreted to have transected P_T -T space along that curve segment. Such an interpretation implies either that the fossil geothermal gradient was regionally inverted, i.e. that T was increasing with depth, or that the geothermal gradient was steepening from northnorthwest to southsoutheast within the 70-km span of the map area. Since there is no evidence for a superposed heat source or for an overturned nappe, the geothermal gradient would have had to have varied. The pressure gradient is strictly depth-controlled, but the temperature gradient may have been inclined to produce a configuration such as that shown in Figure 2-18, with the present surface of the earth shown by curve NW-SE. In this interpretation the conditions of metamorphism would have ranged from $T \approx 500$ to 525°C , $P_T \approx 3.5$ to 3.6 kb to accommodate chloritoid + sillimanite in the southsoutheast to at least $T \approx 600$ to 625°C , $P_T \approx 2.5$ kb to accommodate the staurolite-out reaction at about the aluminosilicate phase boundary in the northnorthwest. Although this interpretation would generate crossing isograds, it does not satisfactorily explain the relict and retrograde assemblages observed in the southern and central ranges.

A third P_T -T trajectory might develop with increasing P_T and T along path (b) in Figure 2-17, then decreasing P_T with continued increase in T, perhaps recording tectonic uplift combined with a thermal aureole related to plutonic emplacement into a terrane already undergoing regional metamorphism. Such a history has been proposed for the metamorphism of the

Figure 2-18. Isotherms inclined relative to isobars that are parallel to the earth's surface. The present surface of the earth in the Eastern Transverse Ranges is represented by the cutaway surface.



Irish Dalradian rocks in the Connemara area of western Ireland (Yardley, 1980). However, the retrogradation of the Pinto gneiss is not consistent with the prograde dehydration assemblages that might be expected along this P_T - T trajectory.

A more complicated interpretation, in which $P_{H_2O} < P_T$ in the southsoutheast but is reduced to $P_{H_2O} < P_T$ northnorthwestward while a fixed geothermal gradient is maintained, would permit the dehydration curves affecting the presence of chloritoid or chlorite versus staurolite or cordierite to shift to lower temperatures. Such a shift would produce the southsoutheast to northnorthwest array of dehydration reactions observed to intersect the andalusite = sillimanite boundary, but would not explain the southern domain of relict and retrograde assemblages. It is also necessary to temporarily increase P_{H_2O} relative to P_T from southsoutheast to northnorthwest through the field area (Figures 2-19A,B).

Within the area of study there are two obvious geologic events which could have been responsible for a regional retrograde event: intrusion of the Mesozoic batholiths and emplacement of the San Gabriel allochthon. The rehydration evidently is not related simply to intrusion of the Mesozoic batholiths inasmuch as both the northern prograde domain and southern retrograde domain have been equally intruded by two distinct batholiths that trend northwest through the region. In terms of recognized pre-batholithic features, the retrograde assemblages are spatially proximate to the trace of the early Red Cloud thrust that is extensively exposed in the retrograded domain south of the Pinto and central Little San Bernardino Mountains, whereas only remnants of the early thrust occur in the prograde domain of the Pinto and northern Little San Bernardino Mountains. Retrograde metamorphism of the Pinto gneiss associated with the emplacement of the San

Gabriel terrane allochthon would be consistent with the observation that chlorite-muscovite retrograde assemblages also occur in the pelitic gneiss of the allochthon near the basal thrust.

Although it is difficult to link the retrograde metamorphism conclusively to a specific intrusive or tectonic event, a few textural arguments can be presented that appear to link the prograde and retrograde reactions as integral parts of a single metamorphic episode. In this regard, the metamorphic history of the Pinto gneiss can be viewed as an interplay between prograde dehydration and retrograde rehydration in the following sequence (Figure 2-19A,B):

1. Prograde dehydration of the protolith along some P_T -T trajectory, with $P_{H_2O} < P_T$ in the early stages of metamorphism;
2. Retrograde rehydration caused by P_{H_2O} approaching P_T at some later stage of metamorphism such that the dehydration curves sweep forward along the P_T -T trajectory through the position of the volume of rock undergoing metamorphism;
3. At some $P_{H_2O} \leq P_T$ the dehydration curves will stabilize so that, if metamorphism continues along the P_T -T trajectory, renewed dehydration will eventually occur.

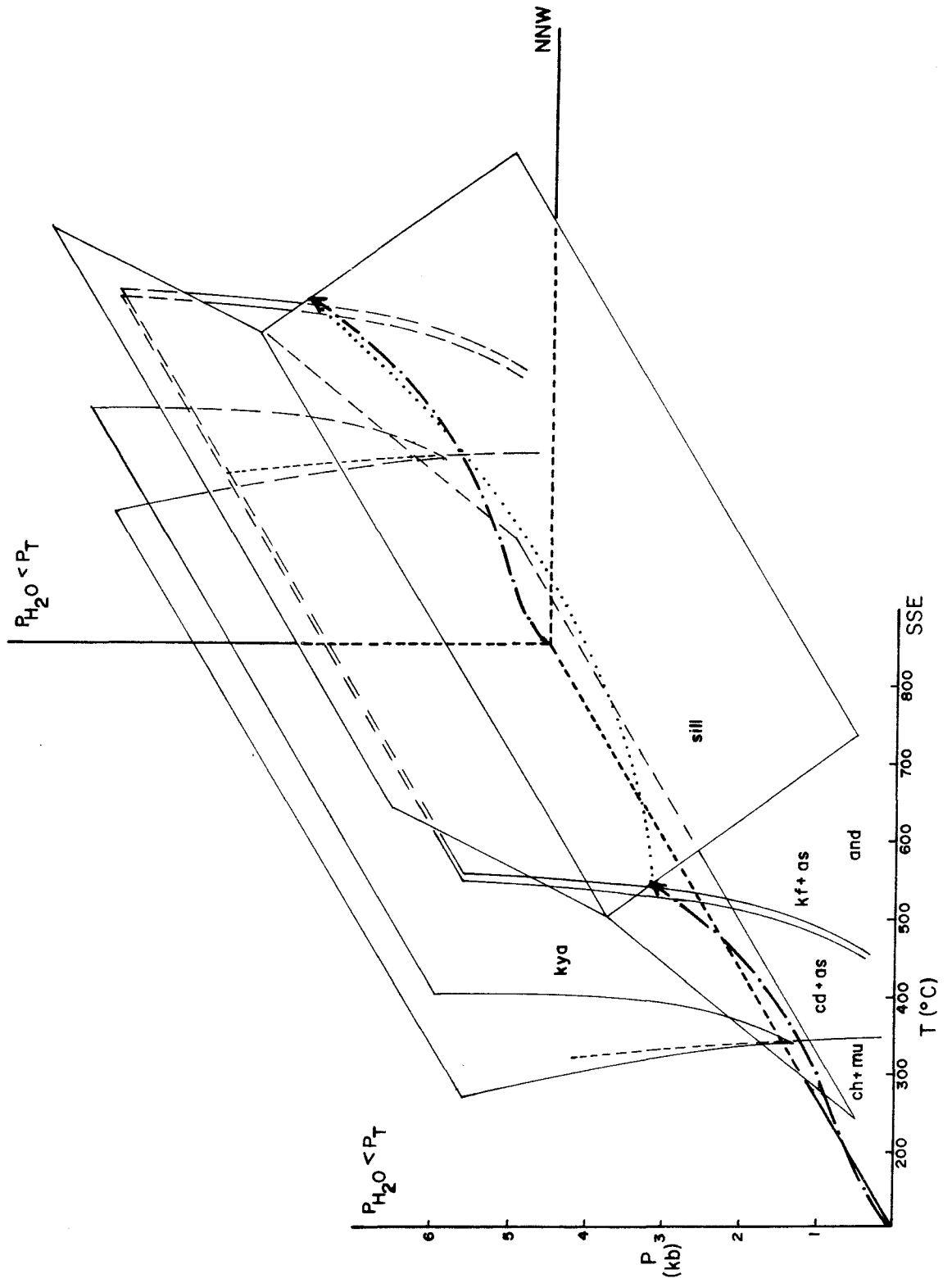
For the metamorphism of the Pinto gneiss, the P_T -T trajectory is constrained to cross the andalusite = sillimanite phase boundary at some point between its intersection with the muscovite + quartz dehydration curve at $P_{H_2O} = P_T$ and the aluminosilicate triple point.

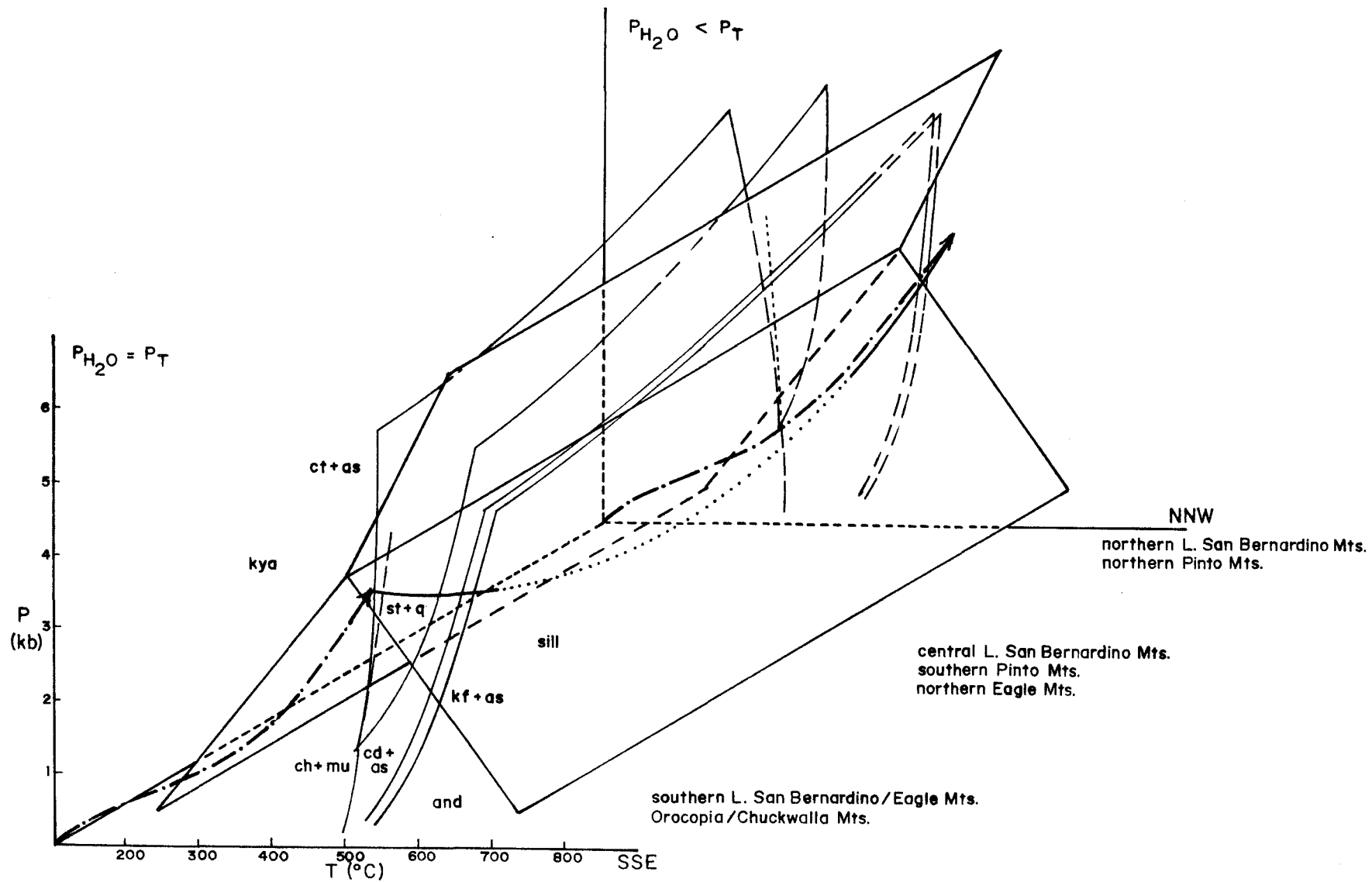
Some of the textural relationships produced in the metamorphic reactions within the Pinto gneiss can be interpreted to be consistent with the

Figure 2-19. Model for the metamorphic evolution of the Pinto gneiss. Reaction curves are taken from Figure 2-16. Heavy dash-dot arrows represent P_T -T trajectory. See text for discussion.

A. Early stage prograde metamorphism at $P_{H_2O} < P_T$.

B. Later retrograde metamorphism to the south as $P_{H_2O} \rightarrow P_T$.





hypothetical sequence of dehydration at relatively low $P_{T,T}$ where $P_{H_2O} < P_T$, followed by rehydration at higher $P_{T,T}$ as $P_{H_2O} \rightarrow P_T$, perhaps followed in turn by renewed dehydration at still higher $P_{T,T}$. For instance, reaction (I2), in producing both andalusite and sillimanite as well as K-feldspar at the expense of muscovite and quartz, may have recorded such a sequence:

1. Dehydration of muscovite + quartz in the andalusite stability field at a relatively low $P_{T,T}$ and $P_{H_2O} < P_T$;
2. Partial rehydration as $P_{H_2O} \rightarrow P_T$, and crossing of the aluminosilicate phase boundary as $P_{T,T}$ increased;
3. Metastable persistence of andalusite somewhat into the sillimanite field, and stabilization of the muscovite + quartz dehydration curve at $P_{H_2O} < P_T$;
4. Renewed dehydration of muscovite + quartz, this time in the sillimanite stability field.

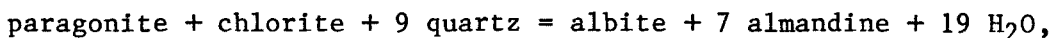
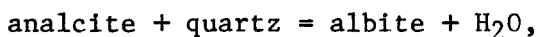
Similarly, the chlorite-muscovite-quartz pseudomorphs after cordierite in most of the Baumonk Mill granofels can be interpreted to indicate a prograde dehydration reaction followed by retrograde rehydration caused by an increase in P_{H_2O} progressively from the south.

If the retrograde metamorphism of the Pinto gneiss is integrally mixed with the prograde metamorphism, and if the retrograde metamorphism is in some way related to the emplacement of the San Gabriel allochthon, then it would follow that the tectonic event must overlap in time with the metamorphic episode. Observations about the growth of metamorphic minerals and the development of fabrics associated with the thrusting (see Chapter IV) provide some sequencing relationships. In the Eagle Mountains relict early prograde minerals such as K-feldspar, sillimanite, and andalusite are foli-

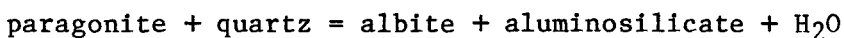
ated and microfolded in the thrust-related fabric. These same minerals in the Pinto Mountains are granoblastic and undeformed, so that the allochthon was emplaced after their formation. Foliated retrograde muscovite and chlorite are not diagnostic because they would show the foliation whether they grew syntectonically or were deformed after growth. Chloritoid, however, commonly grows across the fabric in a syntectonic environment. In the single observed occurrence in the Eagle Mountains, chloritoid grains do transect the thrust-related fabric, which would be consistent with growth in a thrust-related retrograde metamorphism, and would not be consistent with earlier growth followed by superimposition of the deformational fabric. These comments must only be considered as a plausible synthesis of a limited number of observations that can serve as a guide for further investigation.

Inasmuch as the metamorphism of pelitic shales consists of progressive dehydration of hydrous minerals, the concept of variable P_{H_2O} relative to P_T deserves some discussion. Within the context of the above interpretation, P_{H_2O} must have been externally controlled during the metamorphism of the Pinto gneiss. Because the P_T - T trajectory is rather shallow, indicative of a maximum depth of perhaps 10 km, it is possible that during the early stages of metamorphism the fluid phase was in communication with the earth's surface, such that P_{H_2O} was controlled by hydrostatic rather than lithostatic pressure. With increasing burial the closure of cracks eventually would seal off communication with the surface, and P_{H_2O} would approach P_T , possibly rather abruptly. Alternatively, the emplacement of the San Gabriel allochthon might place an impermeable superstrate above the Pinto gneiss effectively increasing P_{H_2O} relative to P_T , at the same time that P_T is increased by the tectonic overburden.

Plagioclase + Quartz + Biotite Gneiss. The Music Valley gneiss consists primarily of plagioclase (sodic oligoclase), quartz, and biotite. In addition there are scattered intergrowths of garnet and plagioclase. If, as discussed in an earlier section, the gneiss is derived from a Na-rich sedimentary protolith (or an altered volcanic rock) that contained plagioclase, or authigenic analcite or paragonite, in addition to some combination of kaolinite, illite, and montmorillonite, then the following reactions could have contributed to the present parageneses at the metamorphic grade of the flanking pelitic granofelses:



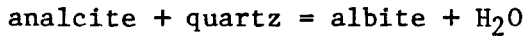
Experimentally, the first reaction (Figure 2-20, curve (1)) proceeds at about 200°C at low pressure (Thompson, 1971a). The second reaction has not been experimentally determined, although because of an additional reactant phase it probably occurs at lower temperatures than the reaction



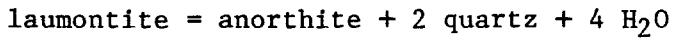
(Chatterjee, 1972) shown as curve (4) in Figure 2-20. If the second reaction is responsible for the intergrown plagioclase and garnet, it must have consumed all of the available paragonite because no aluminosilicate is found in the Music Valley gneiss even though the metamorphic grade of the pelitic rocks indicates that the dehydration curve for reaction (4) must have been crossed.

Because the plagioclase is not pure albite, the experimental curves for analogous calcium reactions are also shown in Figure 2-20. The reaction

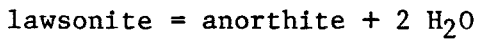
Figure 2-20. Selected experimental curves in the system $\text{Na}_2\text{O}/\text{CaO}-\text{Al}_2\text{O}_3-\text{SiO}_2-\text{H}_2\text{O}$:



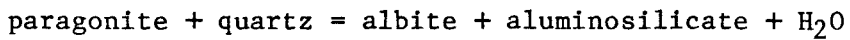
1 Thompson, 1971a;



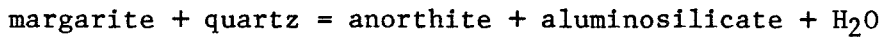
2 Thompson, 1970b;



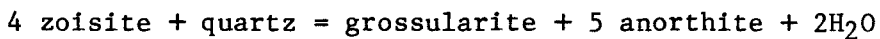
3 Thompson, 1971b;



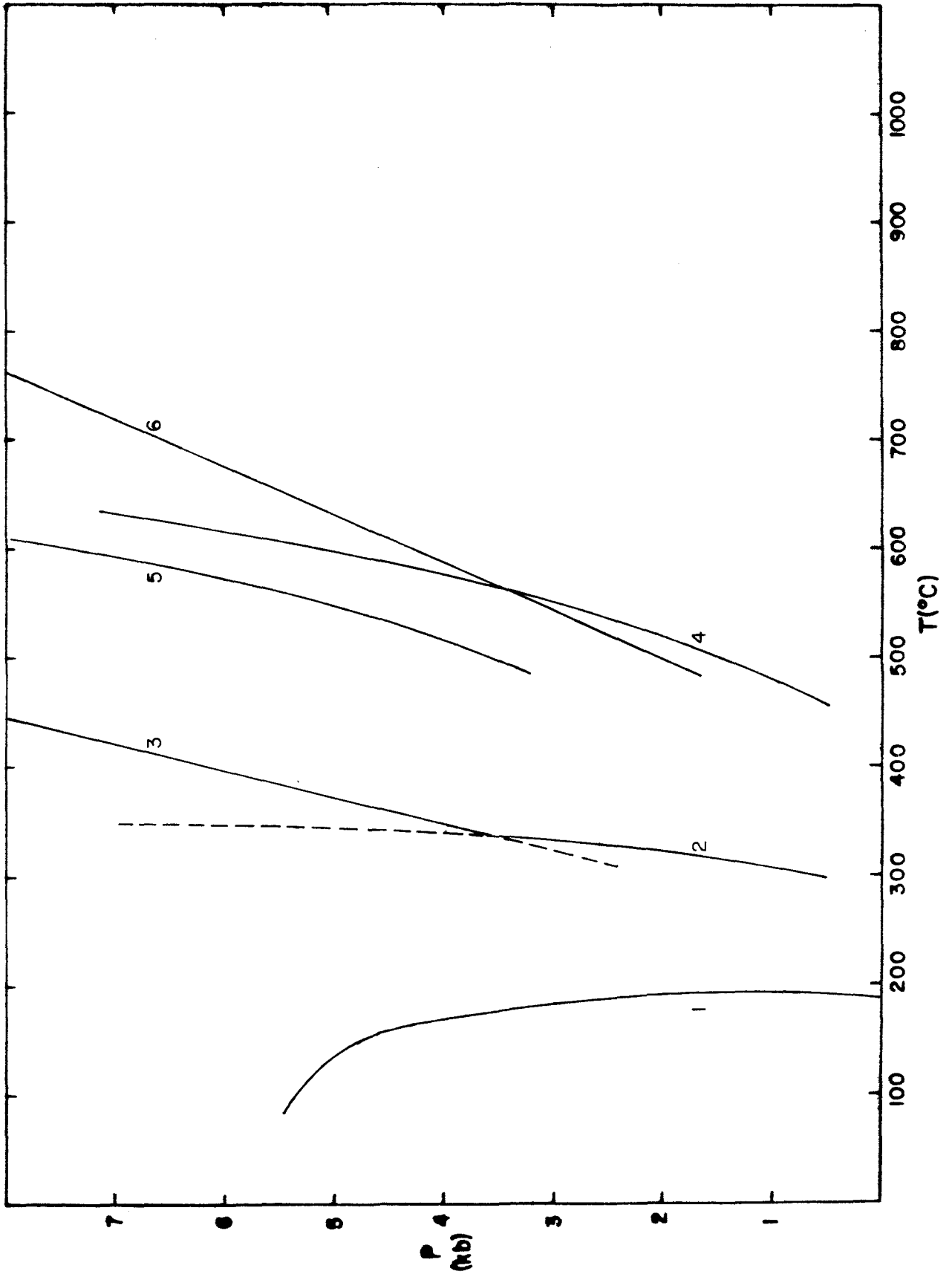
4 Chatterjee, 1972;

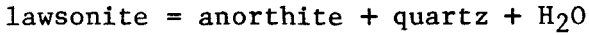


5 Storre & Nitsch, 1974;



6 Newton, 1966c.

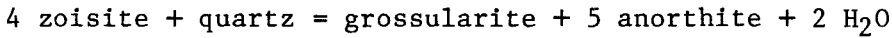




is shown as curve (2) in Figure 2-20. Waikarite also breaks down to form anorthite + quartz at slightly higher temperatures (Thompson, 1970b). The reaction



(Thompson, 1971b), followed by



(curve (6), Figure 2-20), could lead to intergrown garnet and plagioclase in the Ca-bearing system.

The extensive migmatization, both lit-par-lit and in mobilizes discordant to foliation, suggests that the peak temperature for the metamorphism of the Music Valley gneiss was sufficient to begin melting the rock. As discussed earlier, the composition of the Music Valley gneiss approximates the granitic minimum-melt composition, so that it would begin to melt at a lower temperature than the flanking pelitic lithologies. Experimentally determined curves for the beginning of melting of granite and pegmatite are shown in Figure 2-21. The lower melting temperatures of pegmatite have been attributed to the presence of fluid components, such as fluorine, in addition to water. Without the influence of such additional fluid components, the experimental melting curves indicate a slightly higher temperature for peak metamorphism than do the pelitic assemblages when matched to Holdaway's aluminosilicate triple point. As noted above, however, the use of the triple point of Richardson, Gilbert, and Bell apparently would not permit the coexistence of chloritoid and sillimanite. Slight compositional

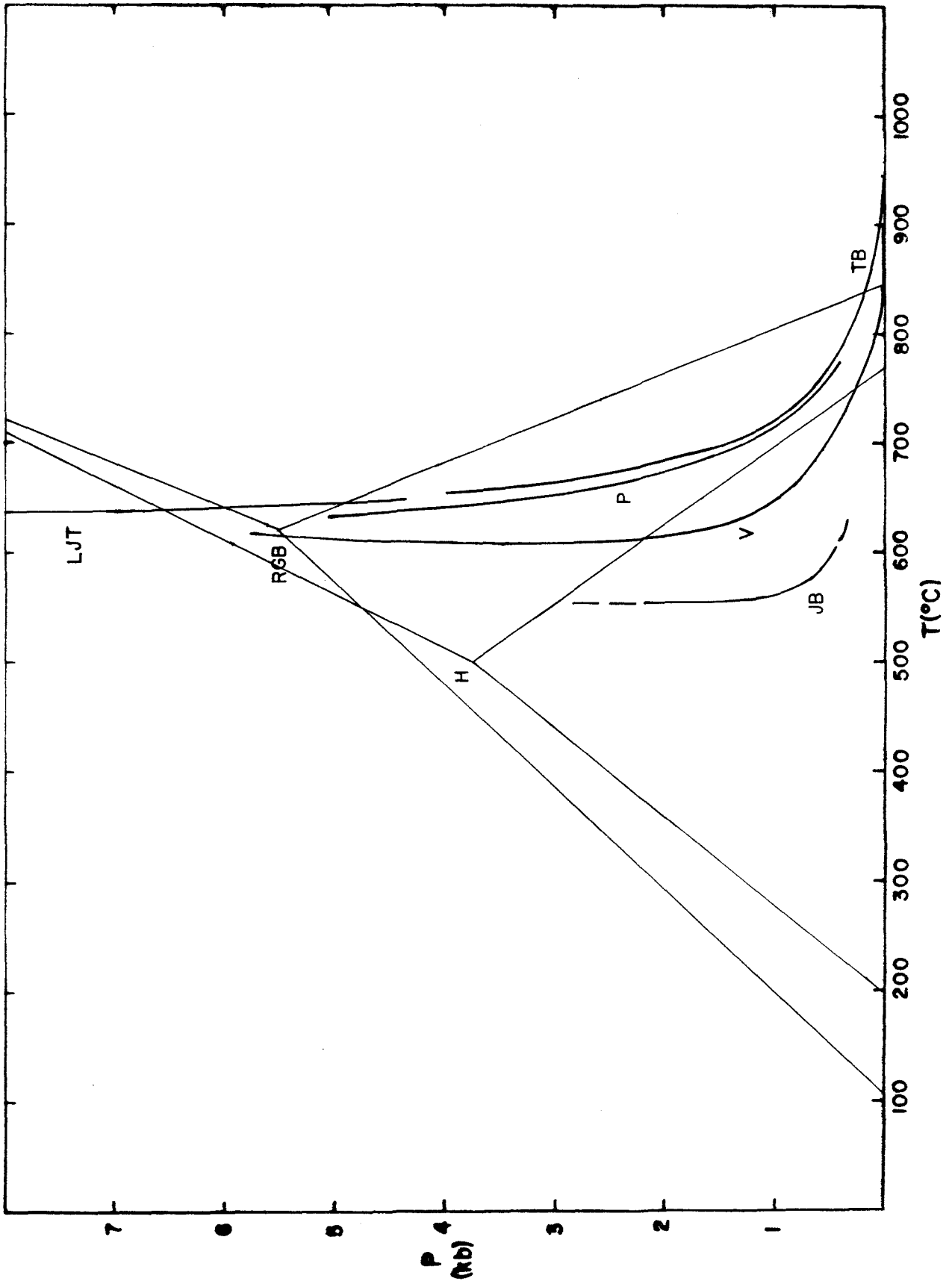
Figure 2-21. Experimentally determined curves for the beginning of melting for rocks of granitic composition:

Granite

- TB Tuttle and Bowen (1958)
- P Piwinskii (1968)
- LJT Luth, Jahns, and Tuttle (1964)

Pegmatite

- V Vaughan (1963)
- JB Jahns and Burnham (1958)



variations in either system could account for the discrepancy.

Ferromagnesian Assemblages

Talc/Orthoamphibole + Chlorite ± Cordierite ± Clinoamphibole-Bearing Assemblages. Assemblages of talc + chlorite versus orthoamphibole + cordierite are asymmetrically distributed in the Hexie, Little San Bernardino, and Pinto Mountains, with the latter occurring to the north of the former. On the basis of a very limited number of samples, this distribution has been inferred to reflect the presence of an isograd characterized by the reaction



The trace of this reaction boundary is only a point where it crosses the thin ferromagnesian unit, but it can be inferred to have a northnortheast-southsouthwest orientation parallel to those marking pelitic reactions.

The talc-orthoamphibole boundary occurs in the southwestern Hexie Mountains.

In one sample from the Little San Bernardino Mountains, cordierite is found to include ferro-aluminous enclaves of corundum + spinel + staurolite. The enclaves are armored from further reaction within the overgrowths of cordierite. In one instance, corundum is clearly rimmed by green spinel (hercynite?) + staurolite (Figure 2-22). The spinel and staurolite are intergrown to some extent; the staurolite is volumetrically more significant. The rimming sequence is not always complete, however, so that cordierite is seen in contact with each of the enclave minerals at some point in the thin section. The presence of corundum and spinel relics indicates that free silica was not available for reaction in the early stages of metamorphism. The green color of the spinel and the presence of staurolite indicate that iron was more abundant than magnesium in the enclave reactions.

Figure 2-22. Photomicrograph of aluminous enclave: corundum rimmed by spinel (hercynite) and staurolite, all of which are armored in cordierite.

A. Photomicrograph: Sample L. San Berdo-26P: partially crossed nicols;
horizontal field of 2 mm.

B. Illustration traced from photomicrograph:

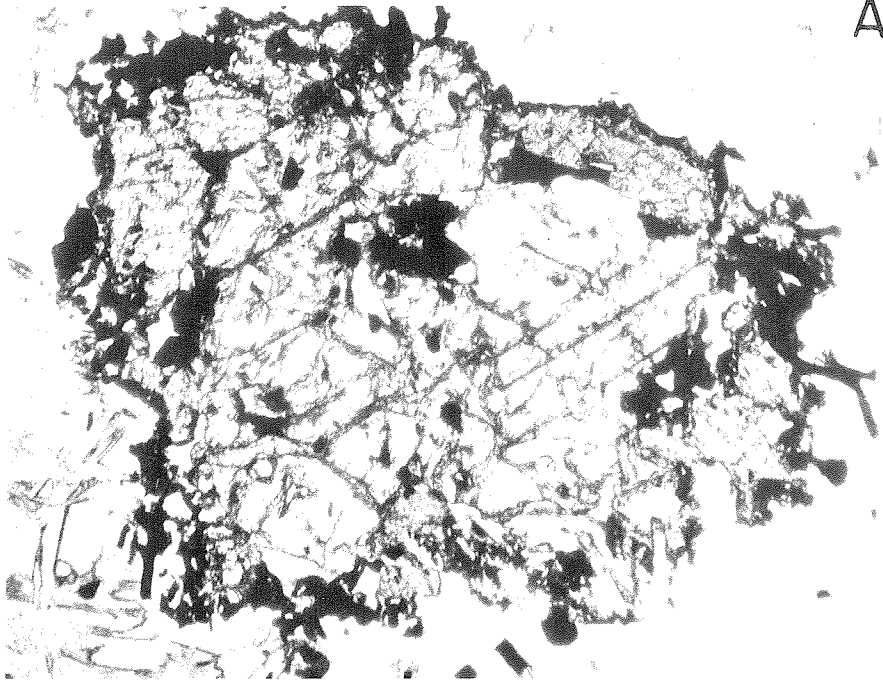
Dots: corundum

Black: hercynite

Cross-hatch pattern: staurolite

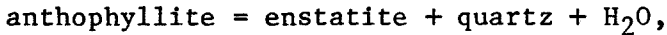
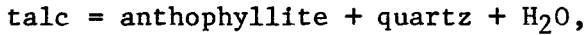
White: cordierite

Ruled pattern: chlorite

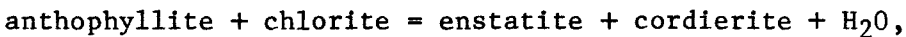
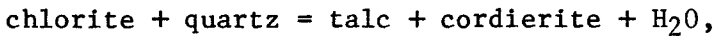


Experimental results bearing on the stability of talc, anthophyllite, and enstatite in the system $\text{MgO-SiO}_2\text{-H}_2\text{O}$ are summarized in Figure 2-23.

The reactions involved are



curves (9, 9', 9'') and (11, 11', 11'', 11'''), respectively, in Figure 2-23. The high temperatures indicated for the anthophyllite-forming reaction is incompatible with temperatures indicated by the associated pelitic assemblages as discussed above. Since chlorite is always present with talc or anthophyllite in the Pinto gneiss, experimental and estimated curves for the system $\text{MgO/FeO-Al}_2\text{O}_3\text{-SiO}_2\text{-H}_2\text{O}$ are also shown in Figure 2-23. Within this chemical system, talc, anthophyllite, and enstatite (hypersthene) are formed by the reactions



respectively curves (2, 2'), (7), and (8) in Figure 2-23. The anthophyllite-forming reaction still occurs at temperatures too high for the associated pelitic assemblages. The addition of iron into the system reduces these temperatures, but also progressively reduces the stability field of talc (Akella and Winkler, 1966). This discussion will be resumed following a summary of the literature on the occurrence of cordierite-orthoamphibole-bearing assemblages.

Figure 2-23. Experimental curves in the systems MgO-SiO₂-H₂O and MgO/FeO-Al₂O₃-SiO₂-H₂O:

2 chlorite + 4 quartz + 8 aluminosilicate = 5 cordierite + 8 H₂O

1 MgO (Seifert & Schreyer, 1970)

6 chlorite + 29 quartz = 8 talc + 3 cordierite + 16 H₂O

2 MgO (Chernosky, 1975; cf. Chernosky, 1974; cf. Fleming & Fawcett, 1976)

2' MgO (Fawcett & Yoder, 1966)

chlorite + quartz ± magnetite = garnet + H₂O

3 FeO, IQF buffer (Hsu, 1968)

3' FeO, IM-IW buffer (Hsu, 1968)

3'' FeO/MgO (X_{pyrope} = 0.1, 0.2), QFM buffer (Hsu & Burnham, 1969)

3''' FeO/MgO (X_{pyrope} = 0.3), QFM buffer (Hsu & Burnham, 1969)

3'''' FeO, QFM buffer (Hsu, 1968)

chlorite + quartz = gedrite + cordierite + H₂O

4 Mg/(Fe + Mg) = 0.56, QFM buffer (Akella & Winkler, 1966)

chlorite + aluminosilicate = cordierite + corundum + H₂O

5 MgO (Seifert, 1973; cf. Velde, 1973)

chlorite + corundum = cordierite + spinel + H₂O

6 MgO (Schreyer, 1976, after Seifert, 1970b)

6' MgO (Velde, 1973)

2 chlorite + 16 talc = 8 anthophyllite + cordierite + quartz + H₂O

7 MgO, approximated (Schreyer, 1976, fig. 9, p.304, after Seifert, 1970b)

2 chlorite + 7 anthophyllite = 57 enstatite + cordierite + 15 H₂O

8 MgO, approximated (Schreyer, 1976, fig. 9, p.304, after Seifert, 1970b)

7 talc = 3 anthophyllite + 4 quartz + 4 H₂O

9 MgO (Greenwood, 1963, 1971)

9' MgO (Chernosky & Autio, 1979)

9'' MgO (Hemley et al., 1977)

Figure 2-23 (cont.)

gedrite + quartz = hypersthene + cordierite + H₂O

10 Mg/(Fe + Mg) = 0.56, QFM buffer (Akella & Winkler, 1966)

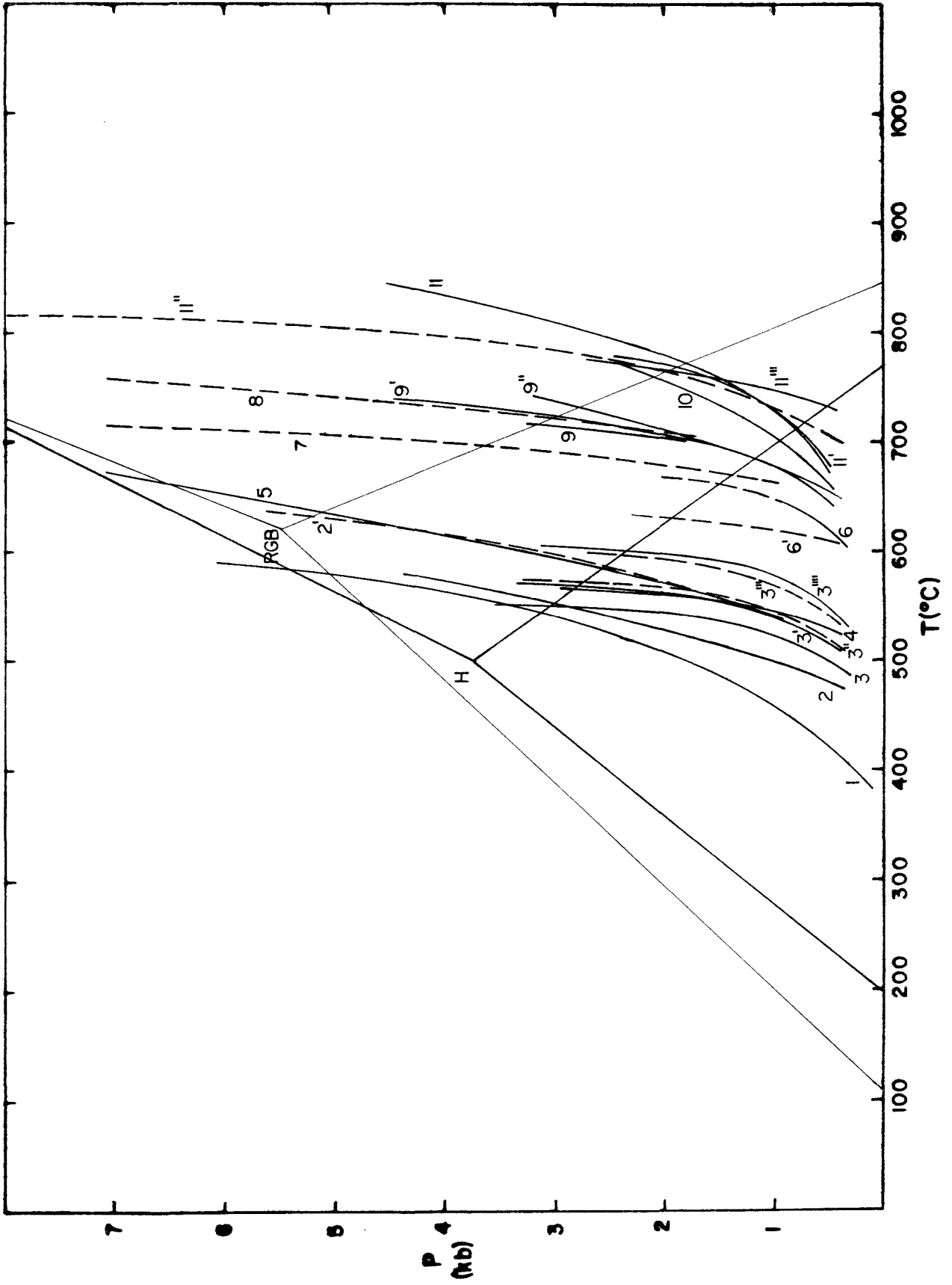
anthophyllite = 7 enstatite + quartz + H₂O

11 MgO (Hemley et al., 1977)

11' MgO (Chernosky & Autio, 1979)

11" MgO, calculated (Zen, 1971)

11''' MgO (Greenwood, 1963)



Ferromagnesian Hornfels/Schist Historical Review. Historically, cordierite-orthoamphibole bearing metamorphic assemblages have been somewhat problematical. With peculiar bulk compositions that are predominantly $\text{Mg}(\text{Fe})\text{O}-\text{SiO}_2-\text{Al}_2\text{O}_3$ with virtually no CaO , K_2O , Na_2O , they seem to require an unusual genetic explanation. Because such bulk compositions (chemically equivalent to chlorite + quartz) are not normally produced by primary sedimentary or volcanic processes, they are generally thought to develop through some secondary process or combination of processes. Explanations for the cordierite-anthophyllite mineral parageneses have incorporated a variety of both syn-metamorphic and pre-metamorphic processes, but none of the published interpretations are entirely consistent with the stratigraphic and metamorphic settings developed above for the Pinto gneiss.

Each of the proposed syn-metamorphic processes involves open-system movement of cations at some stage of metamorphism resulting in magnesium + iron enrichment of the metamorphic rock relative to the protolith:

(1) In the Orijärvi region of Finland, Eskola (1914, p. 262; 1915) attributed the formation of cordierite-anthophyllite schists within a meta-sedimentary/metavolcanic terrane to metasomatic replacement of CaO , Na_2O , and K_2O by MgO and FeO . The source for the Mg and Fe was hypothesized to have been hydrothermal fluids emanating from nearby intrusive granites. Geijer (1916, 1923) reached similar conclusions for the origin of the cordierite-anthophyllite rocks of the Falun region, Sweden. In the Pinto gneiss there is no apparent source for such emanations.

(2) Thirty-six years later, Touminen and Mikkola (1950) reinterpreted the origin of the cordierite-anthophyllite schists of the Orijärvi region. They argued for residual enrichment of Mg (Fe) due to removal of

Ca, Na, and K during deformational recrystallization in the early stages of metamorphism: during intense folding, clay-rich protoliths were penetratively deformed and recrystallized as they flowed into the fold hinges, forming phacoliths of MgO-FeO rich sheet structure minerals. Then, during a later stage of progressive regional metamorphism, chlorite + quartz reacted to form cordierite + anthophyllite. There is no evidence that the ferromagnesian rocks of the Pinto gneiss are localized in phacoliths in fold axes or along zones of intense deformation.

(3) At the base of the Stillwater Complex in Montana, Butler (1964) argues for chemical fractionation within a contact metamorphic aureole that has resulted in Si + K depletion and Mg + Fe + Al enrichment as compared to the average schist in the country rock. The aureole has been overprinted on a sedimentary protolith including quartzite, banded ironstone, and pelitic rocks and is inferred to have imposed gradational compositional changes involving major and trace elements. In the Pinto gneiss, no superjacent ultramafic intrusive body has been preserved, and the chemical variations are more readily explained in terms of pre-metamorphic variations in the sedimentary protolith.

(4) Residual enrichment in MgO, FeO, and Al₂O₃ by partial melting of an argillaceous protolith has been proposed for cordierite-anthophyllite gneisses on the Haugesund Peninsula of western Norway (Sørbye, 1964) and for cordieritegedrite gneisses in Harcourt Township, Ontario (Lal and Moorhouse, 1968). Grant (1968) proposed in general that cordierite-anthophyllite schists evolved from pelitic rocks through a process of partial melting, accompanied by filter press removal of a K-Na-Al-Si granitic melt, and followed by recrystallization of the Mg-Si-Al residuum to cordierite-anthophyllite-bearing assemblages. No remnants of mobilizate remain in or around the

ferromagnesian rocks of the Pinto gneiss to indicate such an origin. In addition, required temperatures in excess of 650–700°C at $P \approx 2\text{ kb}$ are not compatible with the temperature range indicated by the enveloping pelitic assemblages.

(5) To explain cordierite-anthophyllite rocks in the Kragerø district on the south coast of Norway, Brøgger (1934) argued for the relative enrichment of Mg, Fe, and Al by removal of lime and alkalis during metamorphism. For the same area, Bugge (1943) advocated formation during regional migmatization with Mg supplied by bordering amphibolites.

One class of pre-metamorphic processes called upon to develop the distinctive bulk composition of the cordierite-anthophyllite rocks is low-temperature hydrothermal alteration of mafic volcanics or volcanoclastic rocks which are subsequently metamorphosed. Another class of pre-metamorphic processes involves sedimentary processes which incorporate volcanogenic material, either pyroclastic or volcanoclastic:

(1) At Yalwal, New South Wales (Australia), Vallance (1967) has traced hydrothermally altered Devonian basalts and volcanic breccias into the contact aureole of a Carboniferous granite. Outside the aureole, the aphanitic and glassy basalts have been extensively chloritized with loss of Ca; amygdals are commonly filled with chlorite and/or silica. Within the aureole, the chloritized basalts and amygdals have been isochemically metamorphosed to cordierite-anthophyllite assemblages (+ quartz, biotite, andesine, hematite, almandine, hypersthene). Aluminous enclaves are not reported.

(2) At several Canadian locations cordierite-anthophyllite rocks are now thought to represent metamorphosed products of older hydrothermal pipes associated with sulfide ore emplacement in volcanic rocks. In the Rouyn-

Noranda region of Quebec, the pipes show extensive chlorite + quartz alteration in connection with the sulfides. Where these pipes lie within the contact aureole of the Dufault granodiorite, cordierite + anthophyllite assemblages have formed at the expense of chlorite + quartz (de Rosen-Spence, 1969). A similar interpretation is presented by Froese (1969) for the Coronation Mine area in Saskatchewan, although no granites are observed in association with the metamorphism. At the Coronation Mine, cordierite-anthophyllite assemblages occur in close spatial association with sulfide ores in the regionally metamorphosed Amisk Group. Since the gangue minerals of the ore zone and the surrounding rocks have undergone the same degree of metamorphism, Froese concludes that the cordierite-anthophyllite rocks represent a metamorphosed zone of pre-metamorphic chloritization associated with sulfide mineralization. The protolith for the Amisk Group is inferred to have included volcanic and sedimentary rocks. No sulfide minerals are found with the cordierite-orthoamphibole rocks of the Pinto gneiss.

(3) Cordierite-anthophyllite gneiss in The Middle Ordovician Ammonoosuc Volcanics at Richmond, New Hampshire are interpreted to be metamorphosed sediments derived from weathered or hydrothermally altered volcanic terranes, perhaps involving some reaction with sea water (Robinson and Jaffe, 1969). In the metavolcanic/metasedimentary terrane at Manitouwadge, Ontario, Canada, James, Grieve, and Pauk (1978) envisage a cordierite-anthophyllite protolith composed of either pyroclastic or volcanoclastic sediments deposited in an aqueous environment rich in Fe and Mg that resulted in replacement of alkalis and calcium. The authors cite heterogeneous compositional laminations within the gneisses as evidence for a sedimentary process.

The historical development of ideas concerning the development of

cordierite-anthophyllite rocks in the Lands End aureole of Cornwall, England has been an interplay between pre-metamorphic and syn-metamorphic models for generating rocks of the appropriate bulk composition. Most of the hornfelses in the Lands End aureole consist of compositionally laminated metamorphic rocks mineralogically characterized by a great variety of assemblages including various combinations of hornblende, cummingtonite, anthophyllite, plagioclase, cordierite, diopside, grossular, biotite, and quartz (Tilley, 1935; Floyd, 1965). These assemblages are generally thought to be derived from mafic volcanic rocks or sills with some interbedded argillaceous rocks. The thin compositional layering of the hornfelses persists through laterally gradational, chemically and mineralogically distinct zones within the aureole.

(1) On the basis of field and petrographic observations, Tilley and Flett (1929) proposed contact metamorphism of weathered basalt protoliths, from which Ca had been leached, to produce cordierite-anthophyllite hornfelses within the compositionally laminated greenstones of Kenidjack at Lands End, Cornwall.

(2) After acquiring chemical analyses of the greenstones and cordierite-anthophyllite rocks, however, Tilley (1935) concluded that the enrichment trends in Mg and Fe^{++} were incompatible with atmospheric weathering processes, and must be due to metasomatic removal of Ca and redistribution of Si, K, Na, Mg, Fe with closely associated potash-enriched biotite hornfels. These exchanges took place within hydrothermal solutions derived from the Lands End granite.

(3) In a more recent study of the Lands End aureole, Floyd (1965) agreed with a metasomatic origin for the cordierite-anthophyllite rocks and argued

for complementary exchange of Fe/Mg and Ca cations with lime-rich hornfels. Tilley (1935) and Floyd (1965) both argue that all of the hornfels are genetically related and have been metasomatically derived from a hornblende volcanic parent during contact metamorphism. Floyd notes that both vertical and lateral intercalation are seen in the field between the various hornfels associated with the Lands End granite. Reynolds (1947) advocated a protolith of calcareous sediments to which Fe and Mg were metasomatically introduced from an advancing basic front during contact metamorphism.

(4) Finally, Chinner and Fox (1974), in their interpretation of the cordierite-anthophyllite assemblages, argue for pre-metamorphic redistribution of Mg, Fe, Ca probably due to hydrothermal alteration of basalt that may be resulted to sulfide mineralization.

Since unmetamorphosed equivalents to the hornfels of the Lands End aureole are not exposed, it is difficult to distinguish between pre-metamorphic redistribution of cations (hydrothermal alteration or weathering) and syn-metamorphic redistribution (contact metamorphic redistribution or introduction of Mg and Fe from the granite) (Vallance, 1967; Chinner and Fox, 1974).

Ferromagnesian Granofels/Schist Synthesis. Field and petrographic observations and inferences in the Pinto gneiss place two apparent constraints on hypotheses for the origin of its ferromagnesian schists. The first constraint is the stratigraphic setting of the schists: they occur in the Lost Horse lithologic belt in thin layers that are consistently conformable to compositional layering within the pelitic gneiss. Moreover, they seem to be confined to a narrow stratigraphic zone that may form a diachronous sub-belt within the Lost Horse facies, a few meters from its contact with the

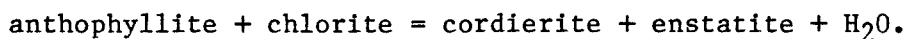
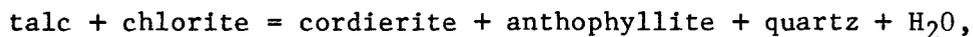
Music Valley facies. There is no evidence that the ferromagnesian schists are intrusive. If the ferromagnesian schists are indeed limited to a small time-transgressive zone, then their protolith must be sedimentary. If, contrary to observations to date, they actually lay across facies boundaries, then other protoliths such as hydrothermally altered mafic volcanic or volcanoclastic rocks are possible. Since there are no other metavolcanics recognized in the terrane, an altered volcanic ash might be a more likely ferromagnesian precursor under those circumstances. Based on the observations and inferences made to date, however, a volcanic protolith for the cordierite-anthophyllite rocks seems to be ruled out in the Pinto gneiss by the stratigraphically restricted occurrence of these lithologies.

The second constraint is the metamorphic setting of the ferromagnesian schists as defined by the mineral assemblages of the interlayered pelitic gneiss: because only one prograde metamorphic event has been recognized, the ferromagnesian assemblages must have developed under the same P_T - T conditions as did the pelitic assemblages. Other metamorphic conditions, however, such as P_F in a mixed volatile environment or f_{O_2} may have varied along with the change in bulk composition.

The northwest-southeast distribution of cordierite-orthoamphibole and chlorite-talc rocks is parallel to the protolithic compositional belts and orthogonal to the metamorphic zones. In the simplest sense, these relationships preclude syn-metamorphic concentric metasomatic zones of cation emanation or redistribution in some regionally developed aureole. In any case, the scale of such an aureole would have to be of improbable proportions to be a contact phenomenon.

As discussed above, the pelitic assemblages of the Pinto gneiss indicate a southeast to northwest decreasing P_{H_2O}/P_T ratio along the regional

P_T - T trajectory during the metamorphic episode, with concomitant asymmetric distribution of more hydrous assemblages toward the southeast. Within this context, the experimental sequence of dehydration curves for talc to anthophyllite + quartz with increasing temperature in the $MgO-SiO_2-H_2O$ system (Figure 2-23) is consistent with the observed south to north distribution of talc-chlorite versus orthoamphibole-cordierite in the ferromagnesian zone of the Lost Horse lithosome. However, at $P_T \approx 2$ to 4 kb the stability field of anthophyllite for $P_{H_2O} = P_T$ in the system $MgO-SiO_2-H_2O$ occur at temperatures (700-800°C) that are incompatible with those indicated by the pelitic assemblages (500-600°C). The experimental results in the system $MgO-Al_2O_3-SiO_2-H_2O$ (Figures 2-23, 2-24) show a succession of dehydration curves beginning with a chlorite + quartz paragenesis would yield the following reactions with increasing temperature:



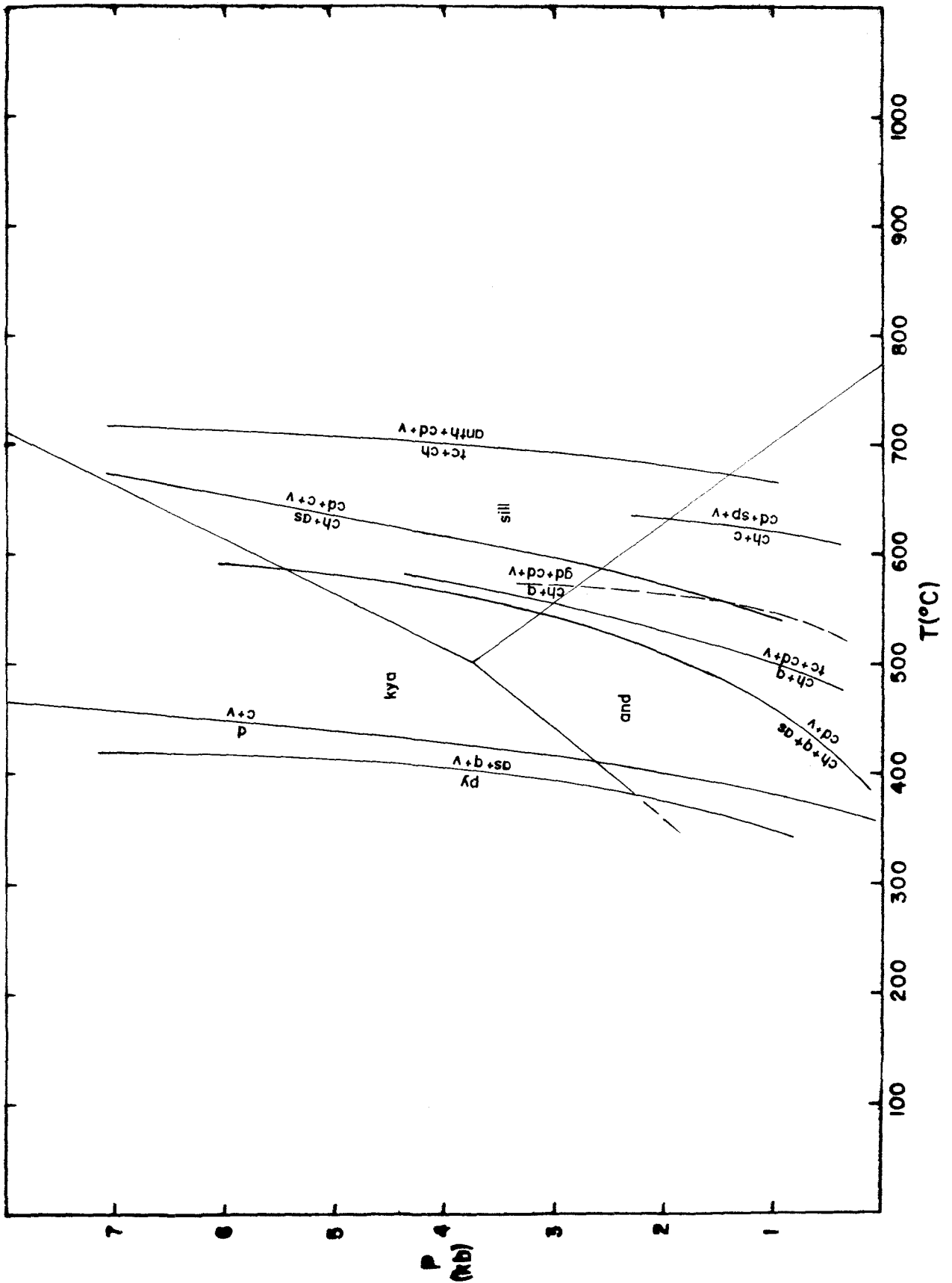
The stability field of anthophyllite in this system at $P_F = P_T \approx 2$ to 3.5 occurs at slightly lower temperatures (675-725°C) than in the alumina-free system, but still higher than the 500-600°C range of the pelitic assemblages.

Two environmental factors would tend to reduce the temperature at which cordierite + anthophyllite become stable:

- 1) The addition of iron as a component in the chemical system;
- 2) Lowering of water pressure in the physical environment such that $P_{H_2O} < P_T$.

Figure 2-24. Combined experimental curves for the system $\text{MgO/FeO-Al}_2\text{O}_3\text{-SiO}_2\text{-H}_2\text{O}$ (chlorite + quartz) pertinent to the metamorphism of the ferromagnesian rocks of the Pinto gneiss. Curves are referenced in Figures 2-13 and 2-23.

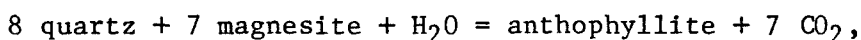
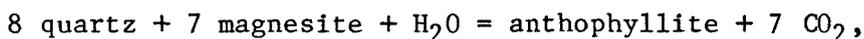
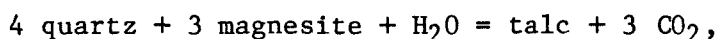
and	andalusite	gd	gedrite
anth	anthophyllite	kya	kyanite
as	aluminosilicate	py	pyrophyllite
c	corundum	q	quartz
cd	cordierite	sill	sillimanite
ch	chlorite	sp	spinel
d	diaspore	v	vapor



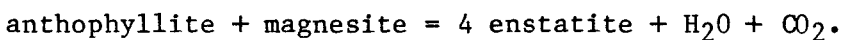
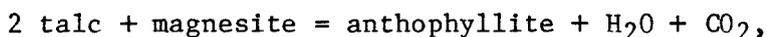
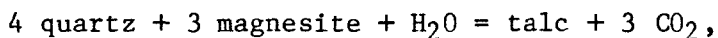
In a qualitative sense, some iron is clearly involved in the natural system as indicated by the presence of staurolite and hercynite in the ferroaluminous enclaves. The quantitative effect of iron in lowering the temperatures at which the above dehydration reactions go is not known, although reductions of 100–200°C from the experimental curves are needed to bring the curves into the P_T - T region indicated by the pelitic assemblages. The experimental results of Akella and Winkler (1966) on Fe-Mg chlorite + quartz indicate that Mg-rich, Al-rich or Al-poor chlorites react with quartz to yield talc followed at higher temperatures by anthophyllite. Chlorites with appreciable iron and aluminum react with quartz to give gedrite, with no stability field for talc. In the Pinto gneiss, the composition has to contain enough Mg to produce talc. For their experimentally determined curves, using a system with $Fe/(Fe + Mg) = 0.44$, Akella and Winkler (1966) formed gedrite within the range of Pinto P_T - T conditions, but the suppressed stability field of talc in their experiment is inconsistent with the Pinto gneiss assemblages. Within the context of these experiments, the viability of an iron component as a controlling or contributing factor to lower the reaction temperatures into alignment with those of the pelitic assemblages cannot be evaluated until analytical data or phase compositions are obtained for the Pinto gneiss assemblages. Although the effect has not been calculated, a metamorphic condition of $P_{H_2O} < P_T$ would also yield the dehydration reaction at lower temperatures than those experimentally determined for $P_{H_2O} = P_T$.

If the gradient in P_{H_2O}/P_T , in conjunction with an Fe component in the natural system, is not sufficient to produce orthoamphibole + cordierite at the temperatures indicated by the pelitic assemblages, then at least one supplementary contributing means of lowering the reaction temperatures of the orthoamphibole-forming reaction can be suggested from the results of

experimental work in the mixed volatile system $\text{MgO-SiO}_2\text{-H}_2\text{O-CO}_2$. One means of further reducing $P_{\text{H}_2\text{O}}$ below P_{T} is to introduce another volatile component, such as CO_2 , so that $P_{\text{T}} = P_{\text{H}_2\text{O}} + P_{\text{CO}_2}$. In terms of experimental studies (Greenwood, 1967; Johannes, 1967, 1969), a starting assemblage of magnesite + quartz in a mixed volatile ($\text{MgO-SiO}_2\text{-H}_2\text{O-CO}_2$) environment of $0.9 < X_{\text{CO}_2} < 1.0$ at $P_{\text{F}} = P_{\text{H}_2\text{O}} + P_{\text{CO}_2} = 2\text{kb}$ would yield a decarbonation array of talc/anthophyllite/enstatite in the temperature range of $500\text{-}600^\circ\text{C}$ by either the array of reactions



or the sequence of reactions



If the temperature ranges for the stability fields of talc, anthophyllite, and enstatite at $X_{\text{CO}_2} = 0.95$ on the $P_{\text{F}} = 2 \text{ kb}$ isobaric $T\text{-}X_{\text{CO}_2}$ section are plotted on a $P_{\text{T}}\text{-}T$ diagram, and if these points are extrapolated as approximate dehydration curves at $P_{\text{H}_2\text{O}} \approx 0.5 P_{\text{T}}$ (cf. Schreyer et al., 1972), then the approximate stability fields for the observed magnesian minerals (at $X_{\text{CO}_2} = 0.95$) agree very well with the $P\text{-}T$ ranges for the associated pelitic assemblages. Temperatures of dehydration at a given pressure can be increased by increasing $P_{\text{H}_2\text{O}}$ relative to P_{CO_2} , and vice versa. A

similar lowering of the temperature of dehydration reactions and stability fields occurs in a preliminary T-X_{CO₂} grid constructed for the mixed volatile system MgO-Al₂O₃-SiO₂-H₂O-CO₂ from a combination of experimental curves and curves calculated from thermodynamic data, but the necessary reactions proceed at lower mole percent CO₂. Addition of an FeO component would further lower the mole percent CO₂ required for a given temperature of dehydration.

Because CO₂, along with H₂O, is one of the two most likely volatile components to be found in a sedimentary rock, it is not unreasonable to seek a carbonate-bearing sedimentary protolith for cordierite-orthoamphibole rocks of the Pinto gneiss that would give rise to a mixed volatile system during metamorphism. The requisite components for such a rock are Mg(Fe)O, Al₂O₃, SiO₂, H₂O, CO₂, which mineralogically translates to chlorite, quartz, and Mg(Fe)-carbonate, i.e. magnesite-breunnerite-sideroplesite-siderite. Sedimentary magnesite- to sideroplesite-rich units have been described in several iron-formations of the Russian platform (Alexandrov, 1973). In the Krivoy Rog region, sideroplesite units also contain varying amounts of interlaminated chlorite, biotite, quartz, magnetite, dolomite, and graphite. The validity of this hypothetical protolith is difficult to test because the carbonate is consumed at relatively low temperatures.

It should be commented also that if the andalusite = sillimanite phase boundary of Richardson, Gilbert, and Bell (1969) is used to interpret that isograd within the Pinto gneiss, then the temperatures indicated by the pelitic assemblages can be increased from 100° to 200°C within the range of P_T = 2 to 4 kb. In this case, with the addition of an iron component plus a condition of P_{H₂O} < P_T, orthoamphibole would be compatible with the P_T-T

conditions indicated by the pelitic assemblages without recourse to a mixed volatile environment.

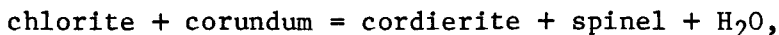
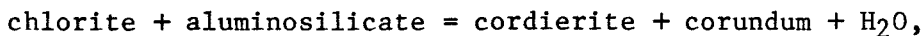
Aluminous enclaves. The origin of the ferro-aluminous enclaves observed in thin-section poses an intriguing problem. They seem to be a rather common phenomenon in cordierite-anthophyllite rocks, having been described in southwestern New Hampshire (Robinson and Jaffe, 1968), Manitouwadge, Ontario (James et al., 1978), Coronation Mine, Saskatchewan (Froese, 1969), Cornwall (Tilley, 1935; Floyd, 1965; Chinner and Fox, 1974), and Orijärvi, Finland (Eskola, 1914). Approximately 75 kilometers northeast of the Eastern Transverse Ranges, aluminous enclaves have been described in cordierite-anthophyllite rocks in the Old Woman Mountains (Stoddard, 1979; Stoddard and Miller, 1979). This widespread occurrence of aluminous enclaves in cordierite-anthophyllite rocks suggests that some explanation for their formation must be an integral part of any hypothesis for the origin of the rock as a whole.

From mutual contact relationships, it can be argued that corundum, spinel, and staurolite found in the enclaves are in equilibrium with the enveloping cordierite at the final stage of metamorphism. Conversely, the enclave minerals are not in equilibrium with orthoamphibole or chlorite, since they share no common boundaries through the armoring cordierite. Cordierite, however, is in equilibrium with chlorite and orthoamphibole. It is also evident that at an earlier stage of metamorphism corundum, spinel, and staurolite must have coexisted within some pre-cordierite paragenesis. In that earlier paragenesis, quartz was not initially available for reaction with the silica-deficient corundum-spinel assemblage, although the later growth of staurolite followed by cordierite suggests

that it was increasingly available with time. Furthermore, the intimate intergrowths of cordierite and orthoamphibole suggest that they formed simultaneously.

If biotite is ignored as the only phase containing K_2O , then the ferromagnesian assemblages can be represented by the model systems $MgO/FeO-Al_2O_3-SiO_2-H_2O$. For these systems, a hypothetical scheme for the development of ferro-aluminous enclaves can be shown qualitatively in the triangular diagrams of Figure 2-25. The proposed development will work only if the bulk composition of the protolith lies within a fairly restricted range. Although the bulk compositions of the ferromagnesian rocks in the Pinto gneiss are not known, the domain defined by those analyzed from other regions appear to include the hypothetical range needed in Figure 2-25.

The reaction sequence probably includes early reactions between an early ferromagnesian phase and an early aluminous phase to produce corundum followed by spinel. The early ferromagnesian phase was probably chlorite which, as the Pinto gneiss advanced along the $P-T$ trajectory proposed above for development of the pelitic assemblages, could have reacted with aluminosilicate to form cordierite + corundum, then reacted with corundum to form cordierite + spinel by the reactions



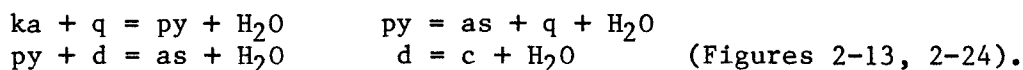
respectively curves (5) and (6, 6') in Figure 2-23 (see also Figure 2-24). In order for the second reaction to have proceeded, chlorite and aluminosilicate must have been present in excess of quartz so that any quartz present would be consumed by the lower grade reaction

Figure 2-25. Schematic topologies for MgO-SiO₂-Al₂O₃ and FeO-SiO₂-Al₂O₃ ternary faces (represented on parallel planes) of the MgO-FeO-SiO₂-Al₂O₃ tetrahedron. Changing topologies with increasing temperature are shown at about 2 kb to conform with the reactions shown in Figures 2-13, 2-23, 2-24, and with the experimental study of Fleming and Fawcett (1976).

A. Mineral compositions represented on the MgO/FeO-SiO₂-Al₂O₃ ternary faces:

q	quartz	tc-mn	talc-minnesotaite
ka	kaolinite	oa	orthoamphibole
as	aluminosilicate	en-fs	enstatite-ferrosilite
c	corundum	alm	almandine
cd	cordierite	ch	chlorite
st	staurolite	sp-h	spinel-hercynite

B. Schematic topologies at ~350°C, after reactions such as



C. Schematic topologies at ~500°C, after the reactions $\text{ch} + \text{as} + \text{q} = \text{cd} + \text{H}_2\text{O}$ (MgO/FeO), $\text{ch} + \text{q} = \text{tc} + \text{cd} + \text{H}_2\text{O}$ (MgO), $\text{ch} + \text{q} = \text{oa} + \text{cd} + \text{H}_2\text{O}$ (FeO) (Figures 2-23, 2-24).

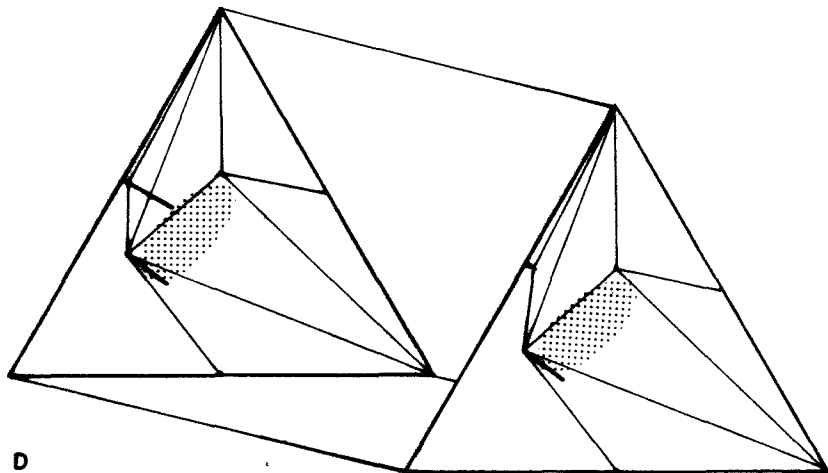
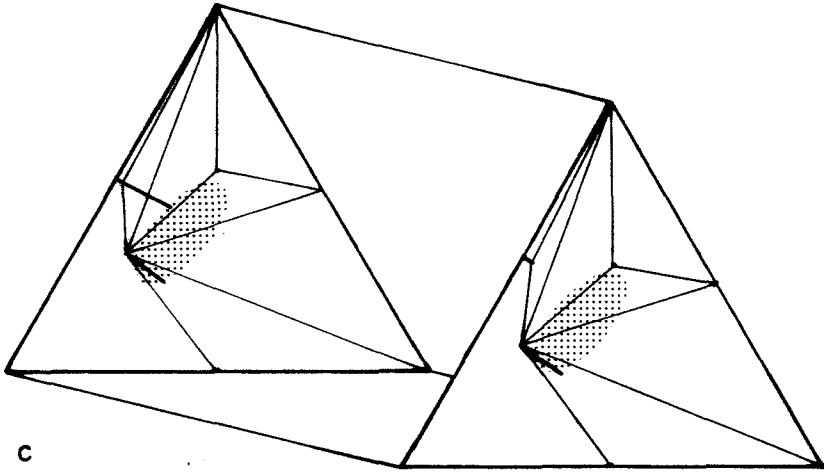
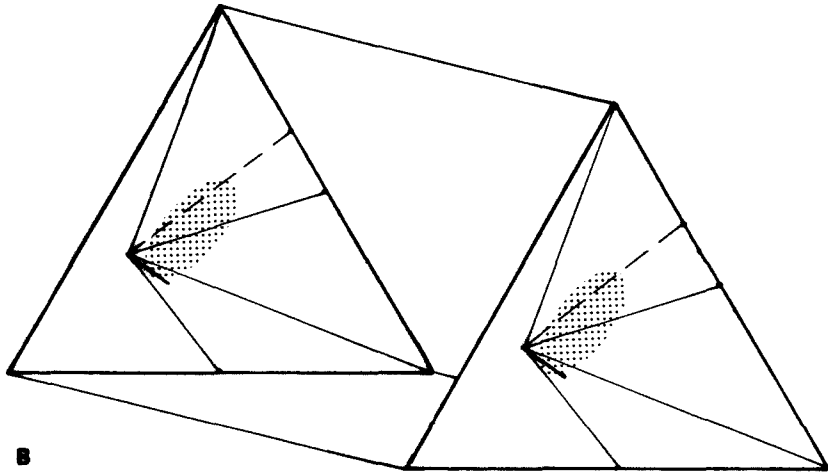
D. Schematic topologies at ~550°C, after the reaction $\text{ch} + \text{as} = \text{cd} + \text{c} + \text{H}_2\text{O}$ (Figures 2-23, 2-24).

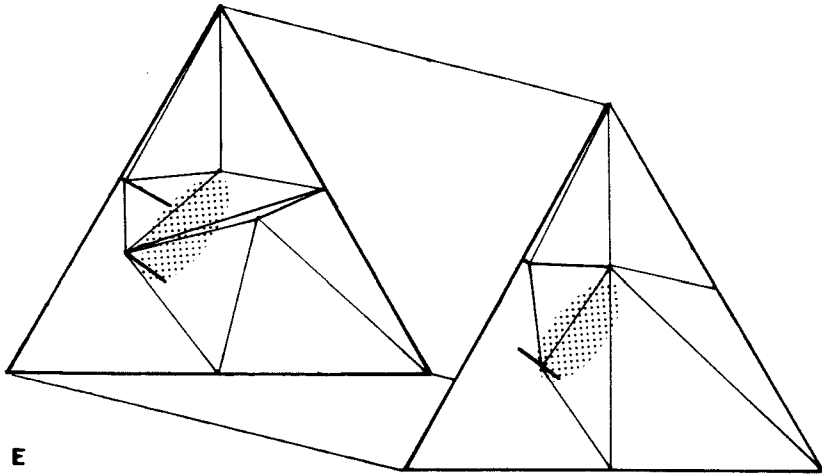
E. Schematic topologies at ~575°C to 600°C, after the reactions $\text{ch} + \text{c} = \text{cd} + \text{sp} + \text{H}_2\text{O}$ (MgO) and one such as $\text{cd} + \text{c} + \text{q} + \text{h} + \text{H}_2\text{O} = \text{st}$ (FeO).

F. Schematic topologies at ~600°C, after reactions such as $\text{cd} + \text{c} = \text{as} + \text{sp}$ (MgO), $\text{ch} + \text{as} = \text{cd} + \text{st} + \text{H}_2\text{O}$ and $\text{ch} + \text{st} = \text{cd} + \text{h} + \text{H}_2\text{O}$ (FeO).

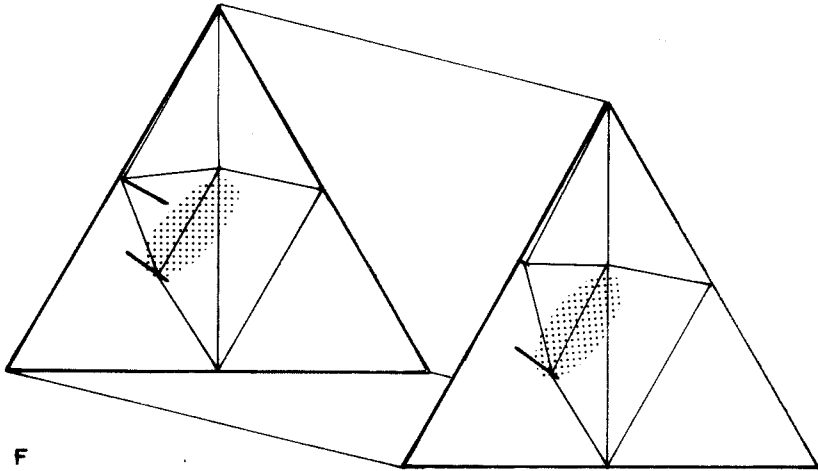
G. Schematic topologies at ~650°C, after the reactions $\text{tc} + \text{ch} = \text{oa} + \text{cd} + \text{H}_2\text{O}$ (MgO) and an alm-forming reaction involving ch, cd, oa (FeO) (Figures 2-23, 2-24).

H. Schematic topologies at ~700°C (cf. Turner, 1968, p. 227, 230, 250, 253), after reactions such as $\text{ch} + \text{oa} = \text{opx} + \text{cd} + \text{H}_2\text{O}$ (MgO/FeO) (Figure 2-23).

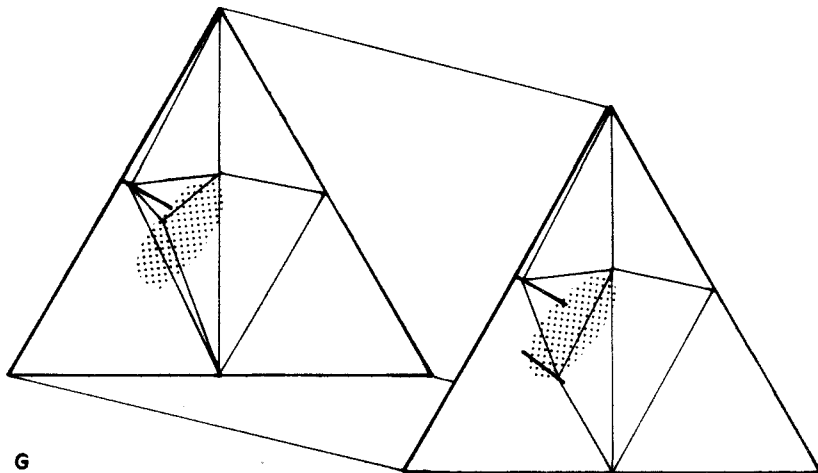




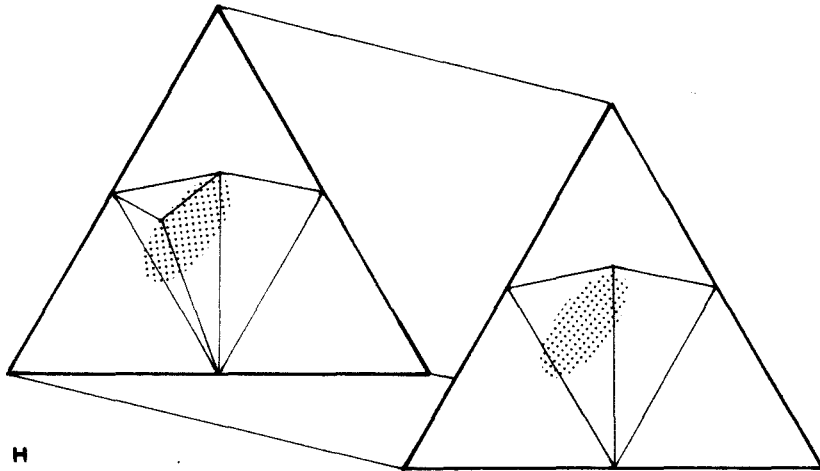
E



F



G

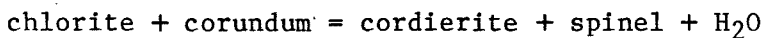




curve (1) in Figure 2-23. The amount of quartz present in the protolith would determine the nature of the early aluminous phases. Depending on the amount of quartz initially available, any of several sequences could develop (see curves (1, 2, 3, 4), Figure 2-13, and curve (1), Figure 2-23):

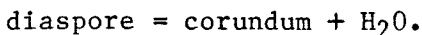
1. kaolinite + quartz = pyrophyllite + H₂O
 pyrophyllite = aluminosilicate + quartz + H₂O
 chlorite + aluminosilicate + quartz = cordierite + H₂O
 chlorite + aluminosilicate = cordierite + corundum + H₂O;
2. kaolinite = diaspore + pyrophyllite + H₂O
 diaspore + pyrophyllite = aluminosilicate + H₂O
 pyrophyllite = aluminosilicate + quartz + H₂O
 chlorite + aluminosilicate + quartz = cordierite + H₂O
 chlorite + aluminosilicate = cordierite + corundum + H₂O;
3. kaolinite = diaspore + pyrophyllite + H₂O
 diaspore + pyrophyllite = aluminosilicate + H₂O
 diaspore = corundum + H₂O
 chlorite + aluminosilicate = cordierite + corundum + H₂O;

With continuing increase in P_T-T, the reaction



would proceed (Figure 2-24).

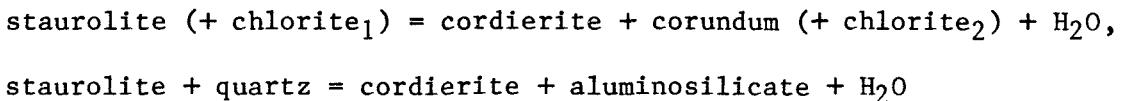
By this stage in the metamorphic history of the rock, aluminous microdomains of corundum and spinel have been established. Enclaves including corundum mantled by spinel within cordierite-anthophyllite rocks are described in Finland (Eskola, 1914, fig. 37), New Hampshire (Robinson and Jaffe, 1969), and California (Stoddard, 1979). Diaspore could be present instead of corundum if it persisted metastably above the dehydration curve



Diaspore enclaves in cordierite and spinel have been reported from the Land's End aureole in Cornwall (Tilley, 1935, p. 189, 196; Chinner and Fox, 1974). Tilley (1935, p. 186; Tilley and Flett, 1929, pl. II) notes the association of clinocllore with spinel and diaspore prior to the appearance of cordierite.

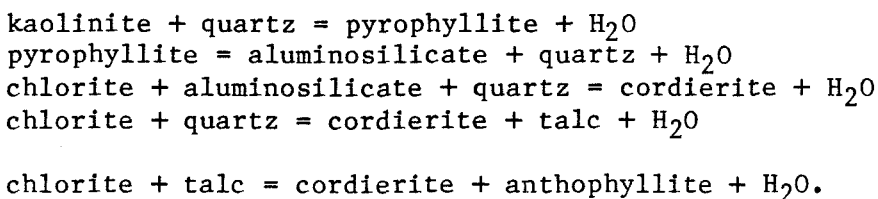
Although not yet found in the Pinto gneiss, andalusite and sillimanite are described in enclaves within cordierite-anthophyllite rocks in Finland (Eskola, 1914, p. 179-181, p. 188, fig. 37). Kyanite and sillimanite are described in enclaves from New Hampshire (Robinson and Jaffe, 1969). Kyanite enclaves with rare sillimanite are reported with corundum in cordierite-talc (\pm rare gedrite) schist from Afghanistan (Kulke and Schreyer, 1973).

If at this juncture P_{H_2O}/P_T increased sufficiently, then staurolite could form by retrograde crossing at relatively high pressure of a reaction such as



in the $\text{FeO-Al}_2\text{O}_3\text{-SiO}_2\text{-H}_2\text{O}$ system (Richardson, 1968). Staurolite-bearing enclaves in cordierite-anthophyllite rocks are reported in New Hampshire (Robinson and Jaffe, 1969), Ontario (James et al., 1978), Saskatchewan (Froese, 1969), and California (Stoddard, 1979).

Along a similar $P_T\text{-T}$ trajectory, less aluminous bulk compositions would undergo a sequence of reactions such as



There is some experimental evidence to indicate that with increasing temperature the cordierite + chlorite + quartz three-phase field slides toward more magnesian chlorites, while the talc + chlorite + quartz three-phase field slides toward more aluminous chlorite (see Fleming and Fawcett, 1976). If the direction of sliding for the talc + chlorite + quartz three-phase field is continued by the talc + cordierite + chlorite or orthoamphibole + cordierite + chlorite three-phase field after the breakdown of chlorite + quartz such that either of these fields displaced the chlorite-cordierite-spinel field, then for rocks with bulk compositions within the restricted range mentioned above, these sliding reactions would permit lower grade "alumina-sequence" assemblages to be replaced by higher grade "magnesia + quartz sequence" assemblages. The final step in the development and isolation of the enclaves would occur when either of the fields

chlorite-talc-cordierite,

chlorite-orthoamphibole-cordierite

encompassed the bulk composition of the system. Along the cordierite-chlorite join, cordierite will be in equilibrium with both spinel and talc or orthoamphibole (or nearly so, if there is only a small two-phase field between the two). Since cordierite has already begun to form around the aluminous domains by the earlier reactions, at least some of the cordierite formed by the later reaction should continue to grow at these previously nucleated sites. Thus, once the chlorite and quartz within and touching any aluminous domain that is to become an enclave is consumed, the remaining reactants (corundum, spinel, staurolite) are left in equilibrium with the cordierite that has formed around them. Similarly, any of either quartz or chlorite left in the domain surrounding the cordierite-armored

enclaves after the other is used up will also be in equilibrium with cordierite. In effect, the aluminous enclaves are buffered by the formation of cordierite.

Further increase of temperature would lead to complete dehydration of chlorite, talc, and anthophyllite, yielding phase assemblages of the pyroxene-hornfels facies (cf. Turner, 1968, p. 227,230)(Figure 2-25H).

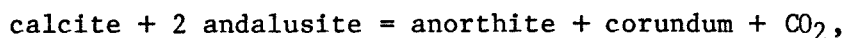
In an alternative interpretation, the sliding effect of the talc- or orthoamphibole-cordierite-chlorite three-phase field could be generated by metasomatic influx of MgO into the system, thereby shifting its bulk composition rather than shifting phase compositions within a constant bulk composition.

If, as discussed earlier, the ferromagnesian rocks of the Pinto gneiss are derived from a sedimentary protolith, then the bulk composition requires some sedimentary mineral, or combination of minerals, rich in Al_2O_3 , MgO/FeO, and SiO_2 . A marl of kaolinite and a Mg/Fe carbonate, or a clay of the palygorskite-sepiolite type both approximate the compositional requirement. It seems unlikely that quartz was initially abundant.

A qualitative appraisal of the enclaves within the context of a Mg-Fe carbonate marl protolith suggests a series of metamorphic reactions that would lead to early-stage formation of microdomains of aluminous minerals and later-stage armoring and isolation as the protolith was progressively metamorphosed in a mixed volatile ($H_2O - CO_2$) system. The enclaves could have been produced from such a marl through the succession of mixed volatile reactions encountered along an appropriate trajectory in a T-X $_{CO_2}$ diagram, beginning with a wet system composed of magnesite and kaolinite at $P_T = 2$ kb. Such a diagram has been preliminarily constructed from

experimental curves (Greenwood, 1967; Johannes, 1967, 1969), and from calculated dehydration and decarbonation curves using the equations developed by Greenwood (1967; see also, Kerrick, 1974). The systematics are analogous to $T-X_{CO_2}$ diagrams constructed for the system $FeO-SiO_2-H_2O-CO_2$ to model the metamorphism of iron-formations (see Frost, 1979).

If some calcium component had been present in either the carbonate or the clay protolith, then its association with the aluminous domains would lead to the reaction



which Nitsch and Storre (1972) have experimentally located between about 400 and 600°C on a $T-X_{CO_2}$ diagram at $P = 2\text{kb}$. Calcic plagioclase (anorthite or bytownite) is found in aluminous enclaves in New Hampshire (Robinson and Jaffe, 1969), Ontario (Grieve et al., 1978), and California (Stoddard, 1979).

Age of Metamorphism

The timing of the metamorphism that affected the Joshua Tree terrane can be bracketed in a relative sense. It must have occurred at some time following the accumulation of the protolith for the Pinto gneiss; it must also have occurred at some time prior to the emplacement of the San Gabriel allochthon. As shown in Chapter IV, the mangerite-jotunite, retrograded granulites, and sillimanite-garnet-biotite-K-feldspar-bearing pelitic gneiss of the San Gabriel terrane are thrust over all the northeast-trending metamorphic facies belts of the Pinto gneiss. In addition, at least some of the metamorphic minerals formed during the thermal event were foliated, folded, and broken during the overprint of a thrust-related fabric locally super-

imposed on the rocks of the Joshua Tree terrane (see following section). As discussed above, however, there is some evidence that the metamorphic mineral growth and deformation related to the emplacement of the allochthon overlapped in time.

In terms of absolute ages, the metamorphism occurred prior to the intrusion of the Mesozoic batholithic rocks, which have been dated as old as 160 to 165 m.y. for the Jurassic monzogranite plutons (see Chapter V). That the metamorphism is not an effect of either the Jurassic or the Cretaceous batholiths is apparent from the truncation of the metamorphic facies belts by the Red Cloud thrust system, which in turn is intruded by the Mesozoic batholithic rocks. The lack of a causal relationship is also emphasized by the regionally consistent orthogonal intersection of the northwest-trending batholiths of two ages with the northeast-trending isograds. The metamorphism must be younger than the age of the Joshua Tree granite-granite gneiss (≥ 1650 m.y.), which lies nonconformably beneath the Pinto Mountain quartzite.

Geothermal Gradient

The geothermal gradient estimated from the pelitic assemblages for metamorphism in a temperature range of 500° to 550°C and pressure range of 3.5 to 4 kb would have been in the range of $40^{\circ}\text{C}/\text{km}$ to $55^{\circ}\text{C}/\text{km}$. Because $P_{\text{H}_2\text{O}} < P_{\text{T}}$, this gradient is less than gradients estimated for other areas in which cordierite-sillimanite-biotite assemblages are found or are thought to have occurred. In the Bosost area of the central Pyrenees, Zwart (1962) estimated a gradient of $150^{\circ}\text{C}/\text{km}$; in the Panamint Mountains of California, Labotka (1978) estimated a gradient of $60^{\circ}/\text{km}$.

DEFORMATION

Deformational patterns within the Joshua Tree terrane fall into at least three settings. A pervasive cataclastic fabric has been superimposed parallel to the early Red Cloud thrust fault. This fabric has cross-cut all lithologies within the Joshua Tree terrane in proximity to the thrust, and will be discussed in Chapter IV. It should be emphasized here, however, that all cross-bedding sets observed within the Pinto Mountain quartzite are upright, both in the little-deformed rocks of the Pinto Mountains and in the intensely deformed section of the Eagle Mountains. Furthermore, the nonconformity between granite-granite gneiss and quartzite is everywhere upright in the Pinto, Eagle, and Chuckwalla Mountains. Implied in this consistency of up-indicators is the absence of isoclinal or, with one exception, overturned folds, an inference that constrains interpretation of the pre-batholithic structure (see Chapter IV). Asymmetric to overturned minor folds are observed only internally within schist or gneiss units. This deformation developed after at least some of the metamorphic minerals had formed.

The second structural setting appears to be a deformation confined to the Music Valley lithofacies of the Pinto gneiss. The Music Valley gneiss is contorted with abundant minor folds that have no apparent systematic orientation. At present, this chaotic deformation is thought to reflect an incompetency related to the migmatitic nature of the unit. The deformation is probably synmetamorphic. Flanking pelitic lithofacies are granofelsic with little deformation.

The third structural pattern is represented by a quaquaversal stereo-net arrangement of bedding attitudes within the Pinto Mountain quartzite. This deformation does not appear to be related to the Red Cloud thrust

system, but it is ambiguous whether the pattern was imposed before or after the emplacement of the San Gabriel allochthon.

III. SAN GABRIEL TERRANE

INTRODUCTION

In the Eastern Transverse Ranges, the San Gabriel terrane is an allochthonous remnant of a deep-seated crustal section comprising three distinct lithologic layers. The highest layer consists of upper amphibolite facies metasedimentary gneiss (Hexie gneiss) intruded by monzogranite (Soledad orthogneiss). The middle layer is an underplating of retrograded granulite facies gneisses (Augustine gneiss) that intrude and incorporate both lithologies of the upper layer. The lowest preserved layer consists of syenite, mangerite, and jotunite intrusive into the retrograded granulites. The regional layering, inferred here to have been originally subhorizontal, defines a lower crustal section that has been structurally superposed above the Joshua Tree terrane along the Red Cloud thrust. The three layers of the section are structurally truncated at the Red Cloud thrust system, so that it is not clear whether the syenite-mangerite-jotunite layer was originally a continuous layer throughout an area equivalent to that over which the San Gabriel terrane is presently exposed in the Eastern Transverse Ranges.

The concept of crustal layering developed for these rocks during the course of this study is consistent with their spatial distribution in the Eastern Transverse Ranges as deformed by the structures of the Red Cloud thrust system. As discussed in Chapters II and IV, the geometry of these structures is also consistent with the spatial distribution of the various elements of the stratigraphic package of the Joshua Tree terrane. It is important to emphasize this synthesis and the conceptual resonance between structure and stratigraphy. The concept of crustal layering of the San Gabriel terrane, together with its deformed geometry, can also be used to test Cenozoic palinspastic reconstructions involving the San Andreas

fault system and the San Gabriel Mountains block, as discussed in Chapter VI.

The informal name San Gabriel terrane is used to emphasize the lithologic and geochronological links that have been established between these rocks of the Eastern Transverse Ranges and the Precambrian rocks of the San Gabriel Mountains and Soledad Basin (Crowell and Walker, 1962; Silver, 1971). Constituent lithologic suites of the San Gabriel terrane were first identified in the San Gabriel Mountains and Soledad Basin. The anorthosite-gabbro suite has been mapped and described by several geologists (Miller, 1934; Higgs, 1954; Oakeshott, 1958). Most recently, Carter has conducted a comprehensive study of the structure and petrology of the anorthosite massif, including both the anorthosite-gabbro and syenite-mangerite-jotunite suites, and its tectonic relationships to the surrounding crystalline rocks of the San Gabriel Mountains (Silver and Carter, 1965; Carter, 1970; Carter and Silver, 1972; Carter, 1980b).

Prior to the present study, Silver had characterized rocks of the Precambrian San Gabriel terrane throughout much of the Transverse Range province (Silver et al., 1963; Silver, 1971). In the basement rocks of the Soledad Basin, granodioritic to monzogranitic augen gneiss intruded amphibolite-grade quartzo-feldspathic gneiss and amphibolite at about 1655 m.y. (Silver, 1971). Lithologically and geochronologically identical granodiorite and granodioritic augen gneiss is found in the Eastern Transverse Ranges in the western Orocofia, Chuckwalla, and Little Chuckwalla Mountains (Silver, 1971).

At about 1400 m.y. in the San Gabriel Mountains and Soledad Basin, granulite grade metamorphism affected the pre-existing rocks, followed by retrograding into amphibolite facies, to produce the Mendenhall Gneiss

(Oakeshott, 1958; Silver et al., 1963; Silver and Carter, 1965; Silver, 1971; Carter, 1980b). Contact or transitional relationships between the Mendenhall Gneiss and the Soledad augen gneiss and its country rock are not described in the literature. Anorthosite and gabbro were emplaced into the granulites, culminating in the intrusion of a syenite-mangerite-jotunite suite of rocks at about 1200 m.y. (Oakeshott, 1958; Silver and Carter, 1965; Silver, 1971; Carter, 1980b). Because the rocks of the anorthosite suite show evidence of deuteric alteration, it is possible that this alteration and retrogradation of the granulites occurred together during or after intrusion of the syenite. The rocks of the anorthosite complex clearly intrude the Mendenhall gneiss, but have not been observed in contact with the older gneisses. This apparent enveloping relationship has led some observers to argue that the granulites represent a contact metamorphic effect related to the intrusion of the anorthosite (Ehlig, personal comm.). The 200 m.y. age difference between the granulite-grade metamorphism and syenite intrusion appears incompatible with such an interpretation. Prior to the start of this study, syenitic rocks in the Orocofia and Little Chuckwalla Mountains had yielded ages identical to those in the San Gabriel Mountains-Soledad Basin block, and during its course, the lithology has also been dated in the Eagle Mountains (Silver, 1971, and personal comm.)

It is within the context of Silver's regional geochronological studies in southwestern North America that this assemblage of Precambrian rocks has emerged as a distinctive and apparently exotic terrane juxtaposed outboard of his two regionally extensive Precambrian cratonic provinces (Silver, 1968, 1969, 1971; Silver and Anderson, 1974; Silver et al., 1977a).

HEXIE GNEISS

The Hexie gneiss of the San Gabriel terrane is exposed in the Chuckwalla, Eagle, Cottonwood, Hexie, and central Pinto Mountains. The name is derived from its most extensive area of exposure in the Hexie Mountains. Prior to this study, the Hexie gneiss was an undifferentiated part of the Chuckwalla complex. It is predominantly, if not exclusively, metasedimentary, in contrast to the country rock for the Soledad augen gneiss in the San Gabriel Mountains, Soledad Basin basement, and Frazier Mountain exposures of San Gabriel terrane, which contain stratified quartzo-feldspathic gneisses of possible metavolcanic derivation (Silver, 1971). As such, the Hexie gneiss has not yet been mapped as a distinct lithologic unit outside of the area of this study in the Eastern Transverse Ranges. It is inferred to be the highest and oldest of three lower crustal layers comprising the San Gabriel terrane.

In outcrop, the metasedimentary Hexie gneiss is layered biotite-quartzo-feldspathic gneiss (Figure 3-1A) and pelitic sillimanite-garnet-biotite-feldspar-quartz gneiss. Texturally and mineralogically distinguishable layers a few meters to a few tens of meters thick occur sporadically, but no marker units were found that would enable a reliable distinction of stratigraphically continuous section from that which has been structurally repeated through isoclinal folding, or faulting parallel to the layering. Aluminous layers within the Hexie gneiss are relatively coarse-grained and light-colored, with sillimanite porphyroblasts typically retrograded to bluish-white pseudomorphs and elongate clots of white mica (Figure 3-2B). Garnet commonly occurs as large porphyroblasts (1-3 cm). Biotite-rich layers tend to be fine-grained and dark in color, commonly migmatitic with multiple generations of concordant and discordant

Figure 3-1. Photographs of Hexie and Soledad gneisses in outcrop:

- A. Folded layered biotite-quartz-feldspar Hexie paragneiss with thin layer of Soledad orthogneiss above hammer head, Red Cloud Canyon gorge, Chuckwalla Mountains. Up is toward the left of the photograph.
- B. Layered biotite-quartz-feldspar Hexie gneiss intruded by Soledad augen gneiss in Red Cloud Canyon gorge, western Chuckwalla Mountains. Contact is folded.
- C. Undeformed Soledad granodiorite with inclusion of Hexie(?) gneiss, upper Fried Liver Wash, Hexie Mountains.
- D. Undeformed Soledad granodiorite with inclusion and rapakivi-textured K-feldspar phenocrysts, upper Fried Liver Wash, Hexie Mountains.
- E. Deformed Soledad granodioritic augen gneiss with oriented tabular phenocrysts of K-feldspar, southwestern Eagle Mountains.
- F. Mylonitic Soledad granodioritic augen gneiss with true augen of K-feldspar, Red Cloud Canyon gorge, western Chuckwalla Mountains.
- G. Mylonitic Soledad augen gneiss in Red Cloud Canyon gorge, western Chuckwalla Mountains.
- H. Soledad augen gneiss partially transformed to Augustine gneiss, Ship Creek, southeastern Chuckwalla Mountains.

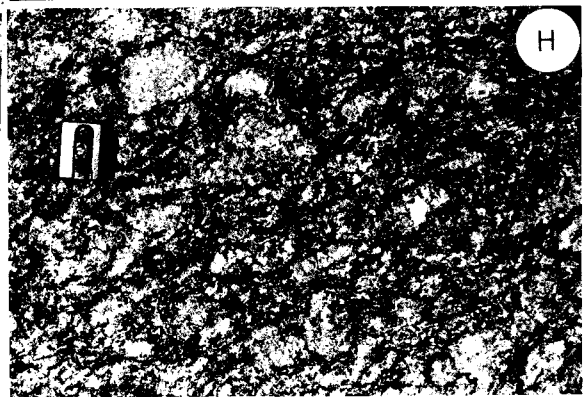
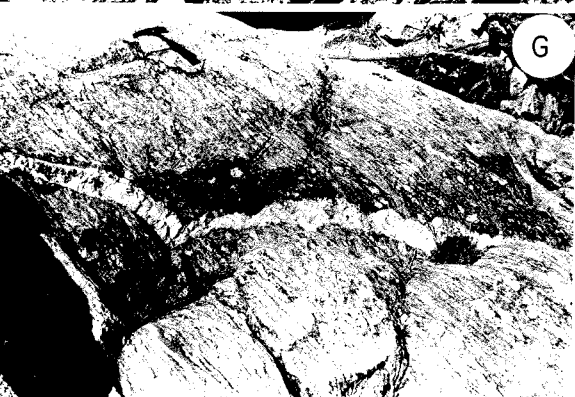
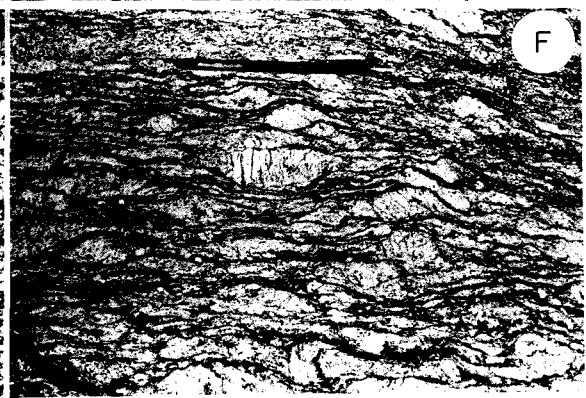
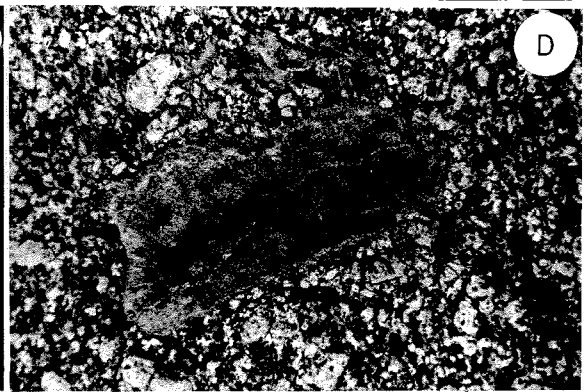
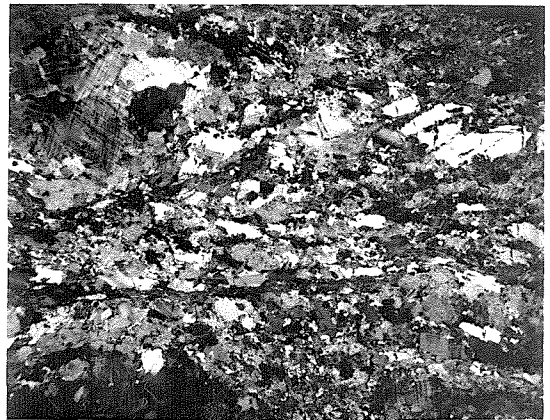
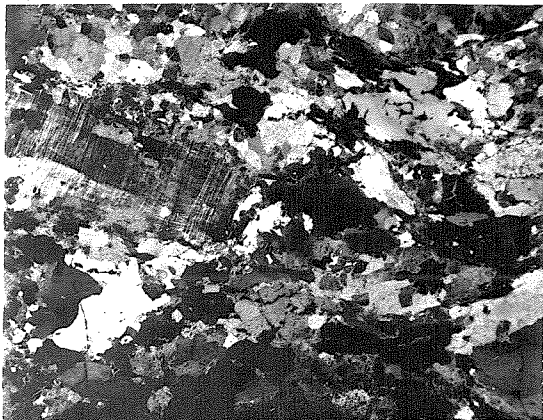
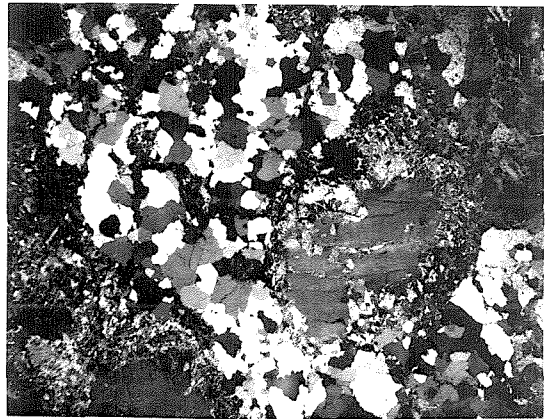
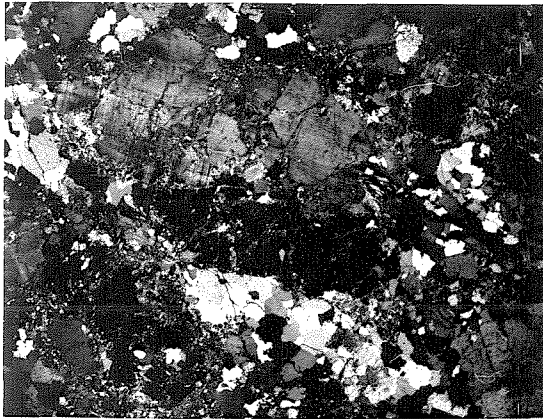
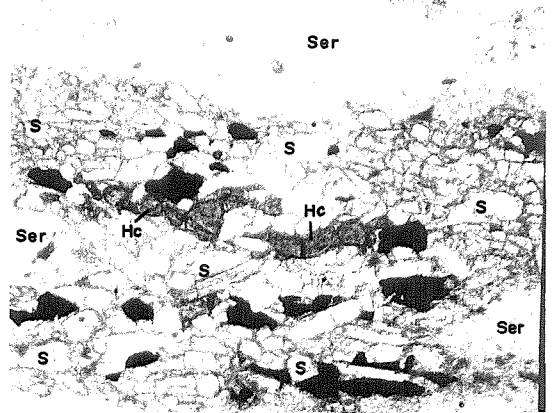
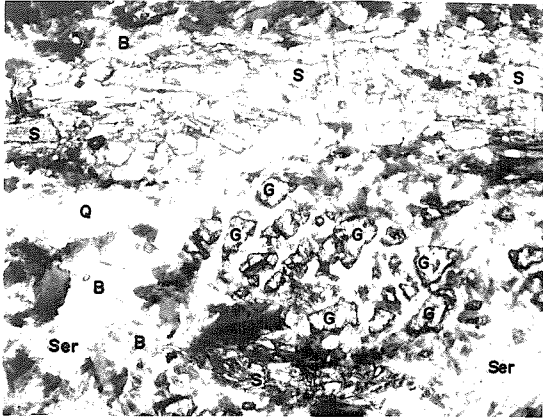


Figure 3-2. Photomicrographs of Hexie and Soledad gneisses from the San Gabriel terrane:

- A. Hexie gneiss: sillimanite(S)-garnet(G)-biotite(B)-quartz(Q) assemblage, partially retrograded to chlorite and sericite (Ser). Plagioclase is also present, but not shown within the field of view. Sample Hexie-7P: uncrossed nicols, horizontal field of 2 mm.
- B. Hexie gneiss: sillimanite(S) with enclosed green spinel (hercynite?: Hc). Sample Cotton-13P: uncrossed nicols, horizontal field of 2.2 mm.
- C. Undeformed Soledad granodiorite. Sample Chkwal-101-1LTS: crossed nicols, horizontal field of 2.2 cm.
- D. Undeformed Soledad granodiorite. Sample Chkwal-101-3LTS: crossed nicols, horizontal field of 1.9 cm.
- E. Soledad augen gneiss. Sample Eagle-6P: crossed nicols, horizontal field of 2.6 cm.
- F. Soledad augen gneiss. Sample Chkwal-41P, crossed nicols, horizontal field of 2.6 cm.



white quartzo-feldspathic veins a few millimeters to a few centimeters thick. The white veins contrasted in dark gneiss display spectacular ptigmatic folding at many localities. Gneissic segregations generally occur in laminae a few millimeters thick. Near its contact with the Augustine gneiss, the Hexie gneiss is highly migmatized and intensely deformed (Figure 3-4A,B). As will be discussed following the description of the Augustine gneiss, the deformational zone is also a zone of lithologic transition from Hexie and Soledad gneiss into the subjacent Augustine gneiss.

Petrographically, the Hexie gneiss is characterized by high grade metamorphic mineral assemblages. For pelitic layers, the diagnostic paragenesis is quartz-biotite-K-feldspar-garnet-sillimanite-plagioclase (Figure 3-2A). In three thin-sections, relics of green spinel (hercynite?) are observed within sillimanite grains (Figure 3-2B). Sericite and coarse muscovite are commonly present as retrograde replacements of sillimanite (Figure 3-2A,B). Biotite and garnet may be partially or completely retrograded to chlorite. Less aluminous layers consist of quartz-biotite-feldspar. Typical modes for the Hexie gneiss are tabulated in Table 3-I. The mineral parageneses for the Hexie gneiss are similar to descriptions for uppermost amphibolite-facies pelitic and semi-pelitic gneiss in amphibolite-granulite transition zones in the Adirondacks (Engel and Engel, 1960; Stoddard, 1976) and in the Willyama complex of the Broken Hill district, New South Wales (Binns, 1964, 1965).

Table 3-I. Parageneses for samples of Hexie gneiss:

Sample:	Chuckwalla Mts.							Eagle Mts.				
	Chk-12	Chk-22	Chk-25,26	Chk-40	Chk-42	Chk-43	Chk-291	E-8	E-38	E-64	E-119	E-192
Quartz	x	x	x	x	x	x	x	x	x	x	x	x
Muscovite	x	x	x	x	x	x	x	x	x	x	x	x
K-feldspar	-	x	-	x	x	x	x	-	-	-	-	-
Sillimanite [†]	(p?)	-	(p?)	-	x	x	(p?)	(p?)	(p?)	x	(p?)	-
Biotite	x	x	x	x	x	x	x	x	x	x	x	x
Garnet	x	x	-	x	x	x	-	-	x	-	-	-
Plagioclase	x	x	x	x	x	x	x	x	x	x	x	x
Spinel	-	-	-	-	-	-	-	-	-	-	-	-
(hercynite?)												
Chlorite [†]	(a)	(a)	(a)	-	(a)	(a)	(a)	(a)	-	-	-	(a)
Accessories*	z,a,o e	z,o e-a	z,o,a e	z,o,a e-a	z,o,a e	z,o,a e	z,o	z,o	-	z,o e	z	o

Sample:	Cottonwood Mts.						Hexie Mts.			Pinto Mts.	
	Co-1	Co-2	Co-4	Co-7	Co-10	Co-11	Co-13	H-7	H-14 B	H-39	P-22
Quartz	x	x	x	x	x	x	x	x	x	x	x
Muscovite	x	x	x	x	x	x	x	x	x	x	x
K-feldspar	-	-	-	-	-	-	-	-	-	-	-
Sillimanite [†]	-	-	-	-	-	-	x	x	(p?)	-	x
Biotite	x	x	x	x	-	x	x	x	x	x	x
Garnet	x	-	-	x	x	-	x	x	-	-	(p?)
Plagioclase	x	x	x	x	(p?)	x	x	x	x	x	x
Spinel	-	-	-	-	-	-	x	x	-	-	-
(hercynite?)											
Chlorite [†]	-	(a)	(a)	(a)	(a)	-	-	(a)	-	-	(a)
Accessories*	z,o,a e-a	z,o,a e-a	z,o,a	o	z,o e-a	z,o e-a	z,o	z,o,a	-	z,a e-a	o

* a apatite
 e-a epidote-allanite
 o opaques
 z zircon

[†] (p) pseudomorphed
 (a) retrograde alteration

SOLEDAD GRANODIORITE-AUGEN GNEISS

The Soledad granodiorite-augen gneiss has been informally named for exposures in the Soledad Basin basement, where it was first recognized as a mappable intrusive unit and characterized geochronologically (Silver, 1971). Additional exposures were subsequently dated in the Frazier Mountain area, the south-central Orocopia Mountains in Salton Wash, and the Chuckwalla Mountains in Gulliday Wash and Red Cloud Wash. At each of these localities the age is about 1655 m.y. (Silver, 1971). During the course of this study, the areal distribution of exposures of the Soledad granodiorite-augen gneiss has been extended northwestward from the Chuckwalla Mountains in a nearly continuous belt through the Eagle, Cottonwood, and Hexie Mountains. The unit includes the quartz monzonite (monzogranite) gneiss mapped by Hope (1966, 1969) in the Hexie and Cottonwood Mountains.

Generally resistant to erosion, the Soledad granodiorite-augen gneiss supports physiographic ridges and escarpments throughout the area of its exposures in the Eastern Transverse Ranges. In outcrop and hand-specimen, it is a dark-colored, coarse-grained megacrystic granitic rock that ranges texturally from undeformed porphyritic igneous (Figure 3-1C,D) to foliated porphyroclastic metamorphic (Figure 3-1E,F,G). Large pink to white tabular megacrysts of microcline (1 to 6 cm long) are set in a dark matrix of quartz, feldspar, and biotite. The unit is mostly augen gneiss that has undergone varying degrees of cataclastic deformation from slightly deformed porphyritic through mylonitic augen gneiss to mylonite (Figure 3-1E to G). Microtexturally, the feldspars have behaved in a brittle fashion, showing cracked and broken grains and bent twin lamellae, whereas quartz and biotite have responded in a more ductile fashion involving both crystalline deformation and recrystallization (Figure 3-2E,F). Both

of these latter minerals occur as fine-grained lenticular aggregates in a matrix around the feldspar augen. In the less deformed augen gneiss, euhedral tabular potassium feldspar megacrysts are aligned parallel to foliation within the matrix (Figure 3-1E). In the more deformed gneiss, the feldspar megacrysts become more rounded and, enhanced by finer-grained "pressure-shadow" aggregates of quartz and feldspar, take on a typical eye-shaped morphology (Figure 3-1F,G).

Significant areas of undeformed plutonic rock occur in both the southern Chuckwalla Mountains (in the vicinity of Gulliday Wash) and northern Hexie Mountains (in the upper reach of Fried Liver Wash). In each of these areas, the rock consists of randomly oriented phenocrysts of potassium feldspar in a dark, medium-grained matrix of quartz, biotite, and feldspar. The phenocrysts commonly exhibit a rapakivi texture, rimmed with overgrowths of plagioclase (Figure 3-1C). Xenoliths of Hexie gneiss, as well as amphibolitic inclusions of unknown derivation are locally abundant and easily recognized in the undeformed rock (Figure 3-1C,D). Deformed, flattened equivalents to these inclusions can be found in the augen gneiss. Even where stretched out and folded within the Hexie gneiss, Soledad augen gneiss can locally be found to cross-cut foliated Hexie gneiss. One well-exposed example to such a relationship is found in Red Cloud Wash gorge in the western Chuckwalla Mountains as it enters a northward kink just before it swings southsoutheastward toward Red Cloud Mine (Figure 3-1B).

In thin section (Figure 3-2C to F), the potassium feldspar is microcline and perthitic microcline. The exsolved plagioclase occurs as spindle or string and patch perthites. Myrmekitic intergrowths of quartz and plagioclase occur where plagioclase feldspar abuts microcline. The

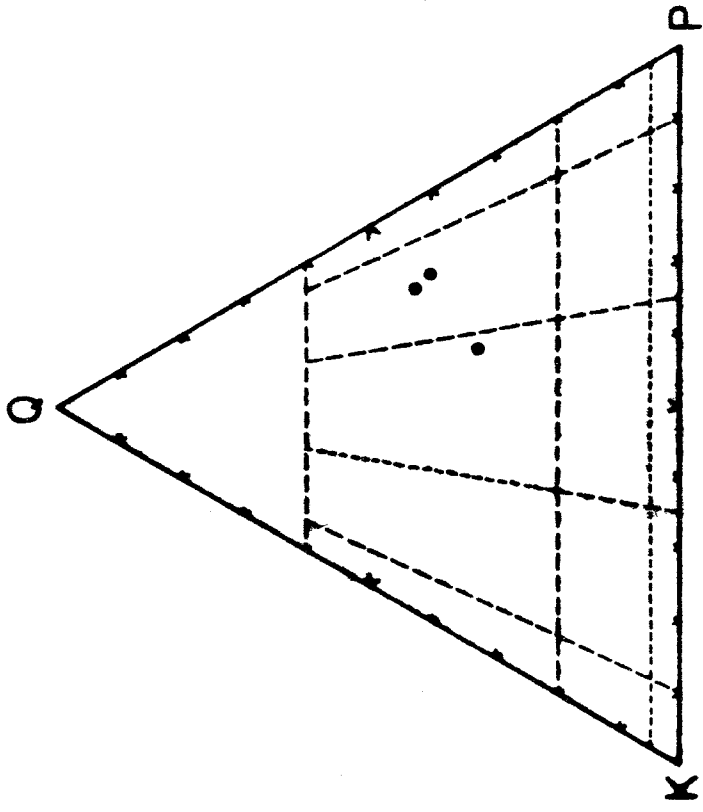
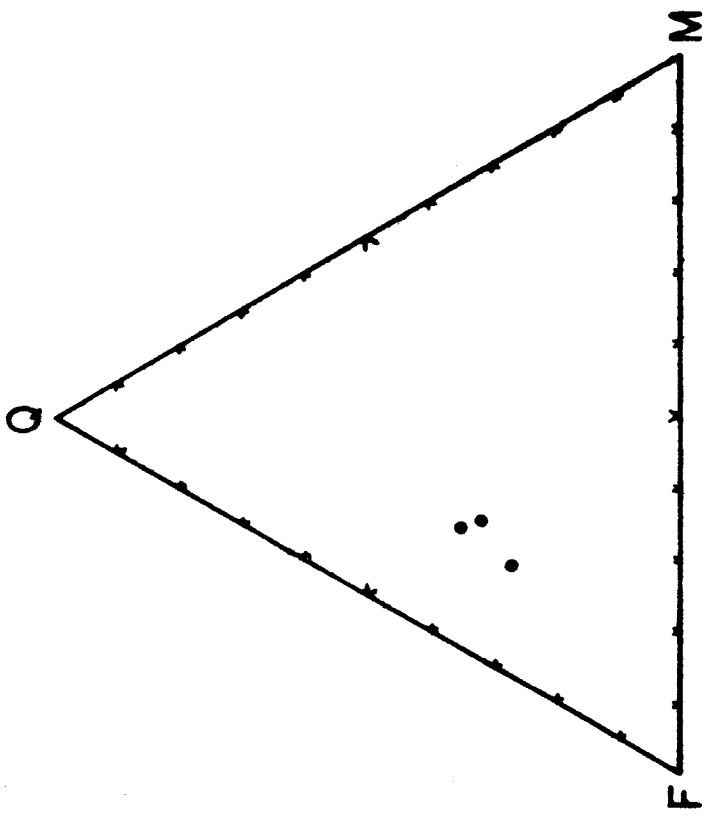
plagioclase is oligoclase-andesine with optically determined anorthite content approximately in the range An_{28} - An_{38} . The plagioclase is more or less altered to sericite and epidote. Feldspar generally forms about 50% of the rock, quartz about 30%, and biotite 15-20%. Biotite usually occurs as recrystallized fine-grained aggregates, pleochroic green to greenish brown. Chlorite occurs rarely as an alteration product of biotite. Coarse-grained muscovite may occur in addition to sericite as a replacement of plagioclase. Accessory minerals include sphene, apatite, epidote, allanite, zircon, and opaques. Modal abundances of sphene and apatite commonly comprise a percent and half a percent, respectively. Epidote and allanite occur in trace amounts, with epidote commonly rimming cores of allanite. Carbonate occurs rarely. Opaque minerals constitute 0.5 to 1 % of the rock and include magnetite-ilmenite (?) and hematite. Based on three point counts in standard-sized thin sections (Table 3-II), modes on the Soledad gneiss range from granodioritic to monzogranitic in Streckeisen's (1967) igneous rock classification (Figure 3-3).

In general, the Soledad augen gneiss is foliated parallel to the foliation of the Hexie gneiss. In detail, however, especially in less-deformed exposures, the Soledad gneiss cross-cuts the Hexie gneiss and locally contains rotated xenoliths of Hexie gneiss, as well as amphibolitic xenoliths of unknown derivation. The Soledad augen gneiss is inter-layered within the Hexie gneiss. In part, the interlayering is due to isoclinal folding, and in part it seems to represent an original sill-like intrusive geometry. It is likely, though, that this apparent sill-like geometry is enhanced by a stretching deformation during which originally more equant intrusive masses were severely flattened into layers

Table 3-II. Modal compositions for samples of Soledad granodiorite and augen gneiss:

	Hexie Mts.	Eagle Mts.	Chuckwalla Mts.
Sample: (Points)	<u>H-3</u> (1617)	<u>E-6</u> (1488)	<u>Chk-41</u> (1982)
Quartz	30.9	35.3	26.5
K-feldspar	9.2	10.3	21.2
Plagioclase	37.2	37.4	34.1
Biotite	19.0	17.0	15.4
Sphene	0.8	tr	1.5
Epidote	0.3	tr	tr
Allanite	--	tr	0.1
Apatite	0.4	tr	0.6
Zircon	0.3	tr	0.1
Opaques	1.3	tr	0.4
Carbonate	0.2	--	--
White Mica	0.4	tr	tr
Chlorite	--	tr	--

Figure 3-3. Modal compositions of samples of Soledad granodiorite and augen gneiss from the San Gabriel terrane, plotted on quartz-K-feldspar-plagioclase (QKP) and quartz-feldspar-mafics (QFM) diagrams. Classification from Streckeisen (1967).



of augen gneiss. This interpretation is not inconsistent with the pervasive mylonitic gneiss fabric of the Soledad augen gneiss (Figure 3-1G). It is apparent that at least one early pervasive Precambrian deformational fabric was superimposed on the Hexie gneiss prior to intrusion of the Soledad granodiorite, and at least one pervasive fabric was superimposed following its intrusion. This fabric was also Precambrian since it must have been developed prior to the intrusion of the syenite-mangerite. In addition, later fabrics have been locally developed parallel to large faults including those of the Red Cloud thrust system.

In terms of its regional distribution, the Soledad augen gneiss can be interpreted to occur as a layer or series of layers in a single zone subparallel to and within a few hundred meters of the underlying contact with the Augustine gneiss. The thickness of this layer in Red Cloud Wash in the Chuckwalla Mountains and in the Hayfield area of the Eagle Mountains is about 250 meters, but in the southern Hexie Mountains it appears to be at least 1500 meters thick. In the structure sections and block diagrams (Plate III, Figure 4-11), the Soledad augen gneiss is treated as a single, continuous lithologic sheet.

Although the origin of their geometry is ambiguous, similar sheets of originally intrusive orthogneiss have been mapped in the Precambrian rocks of the Baldwin Lake area of the San Bernardino Mountains, although the quartzo-feldspathic gneisses of the country rock are not pelitic (R. Powell, unpub. map) and the age is somewhat older than that of Soledad augen gneiss (Silver, 1971). Similarly, Chapman (1939) has interpreted the Bethlehem orthogneiss of western New Hampshire as a great sheet several thousand feet thick intrusive into Paleozoic schists.

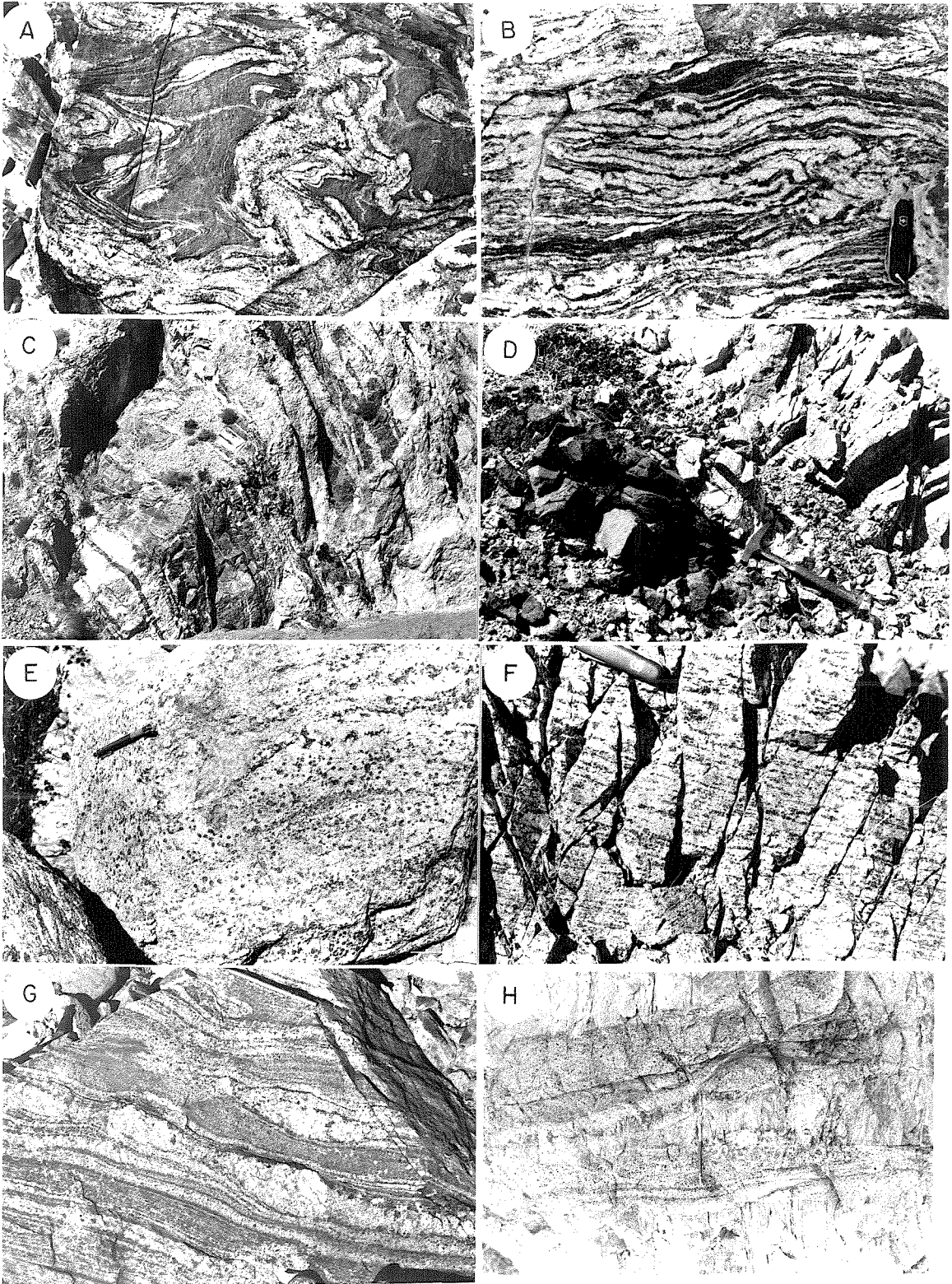
AUGUSTINE GNEISS

The Augustine gneiss is a heterogeneous mixture of intrusive mafic to felsic orthogneisses. The mafic gneisses show granoblastic and amphibolitic textures, whereas the felsic gneisses are typically foliated granoblastic. Relict and replacement textures and relict mineralogy indicate that at least some of the gneisses were elevated to granulite facies and subsequently retrograded to upper-amphibolite facies. The gneiss is named for extensive exposures in the Chuckwalla Mountains in the vicinity of St. Augustine Pass. It also occurs in the easternmost Orocopia Mountains, the southern Cottonwood and Eagle Mountains and in the northern Hexie and south-central Pinto Mountains. In addition, it has been mapped in the Orocopia Mountains west of the Clemens Well fault (Crowell and Walker, 1962). Lithologically, the gneiss is equivalent to the Mendenhall gneiss in the San Gabriel Mountains (see Oakeshott, 1958; Carter, 1980b) (Figure 3-5).

In a transitional zone between Augustine gneiss and Hexie-Soledad gneiss, retrograded granulitic gneisses are intermingled with pelitic and augen gneiss in a variety of ways. In places, the two are interlayered, with sheets of retrograded granulite interlayered within Hexie and Soledad gneisses. The sheets include felsic quartz-microcline-perthite-plagioclase-biotite granulites as seen in the Eagle Mountains on the west wall of Cholla Wash (T5S, R13E, Sec.30, E1/2), and amphibolites as seen at the southwestern corner of the Chuckwalla Mountains at the Red Cloud thrust contact a few kilometers north of the Old Baumonk Mill site (T7S, R15E, Sec.21, SE1/4). In most places, these sheets are sill-like parallel to the plane of foliation in the Hexie-Soledad gneiss with ambiguous cross-cutting relationships. At a few localities, however,

Figure 3-4. Photographs of Hexie and Augustine gneisses in outcrop:

- A. Hexie gneiss: migmatitic layered gneiss near contact with Augustine gneiss, Chuckwalla Mountains.
- B. Hexie gneiss: migmatitic layered gneiss near contact with Augustine gneiss, Chuckwalla Mountains.
- C. Augustine gneiss: interlayered retrograded felsic and mafic granulites in the southern Chuckwalla Mountains.
- D. Augustine gneiss: interlayered retrograded felsic and mafic granulites in the southwestern Cottonwood Mountains.
- E. Augustine gneiss: retrograded granulite in the southeastern Hexie Mountains. Dark spots are garnets and garnet pseudomorphs.
- F. Augustine gneiss: close-up of retrograded felsic granulite from upper right corner of Photograph 3-4D.
- G. Augustine gneiss: retrograded felsic granulite showing pinch-and-swell texture of blocky-textured quartzo-feldspathic layers, and wispy, discontinuous biotite-quartz-feldspar layers, southeastern Chuckwalla Mountains.
- H. Augustine gneiss cross-cut by dikes of syenite-mangerite-jotunite in southeastern Chuckwalla Mountains. Up is toward the left of the photograph.



dikes of retrograded granulite are found to cross-cut foliation. One of these localities occurs a couple of hundred meters south of the Red Cloud Mine Road just after it has dropped into Red Cloud Wash at the lower end of its gorge in the western Chuckwalla Mountains (T6S, R15E, Sec.30, SW1/4).

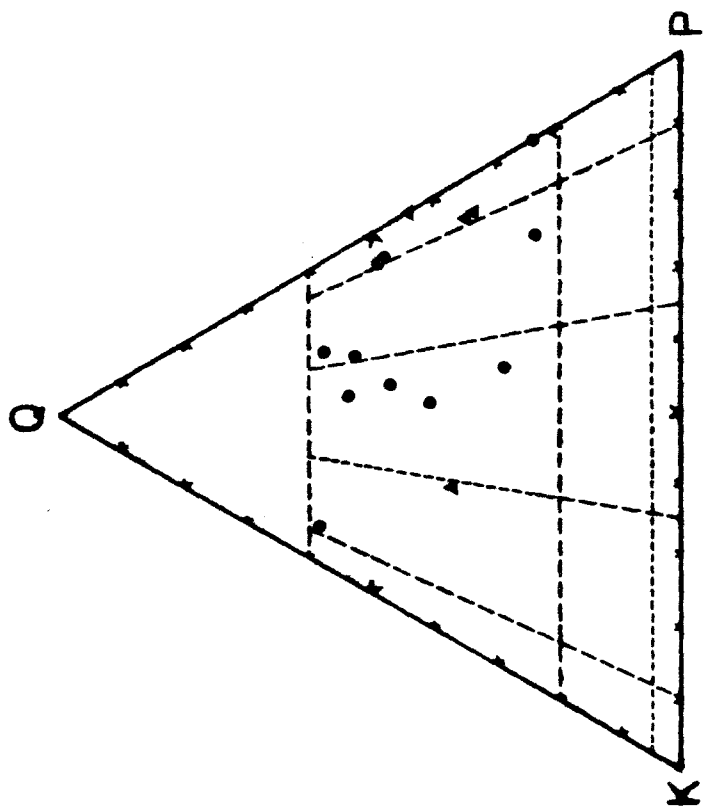
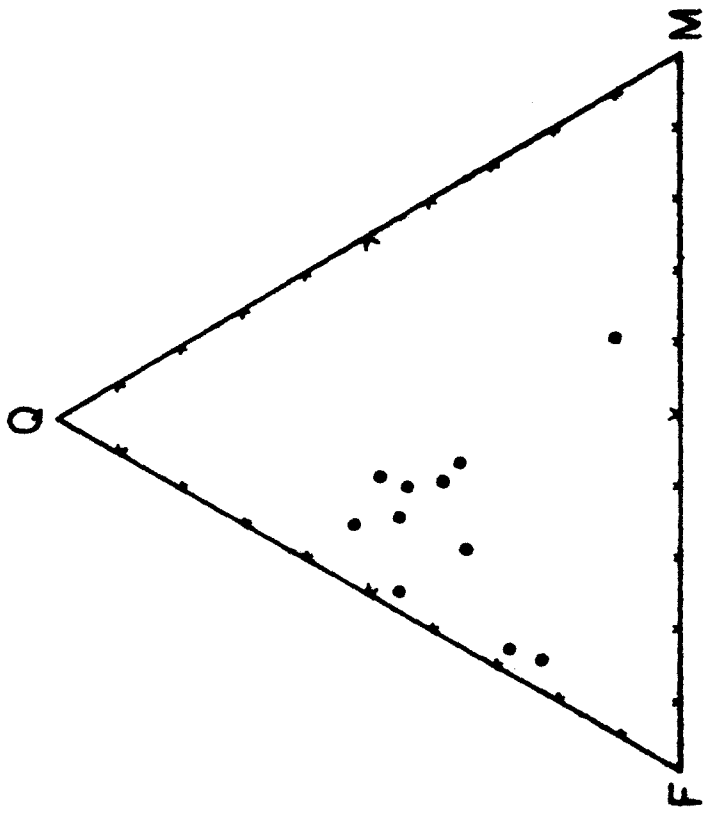
Layers of Soledad augen gneiss can be traced from intrusive relationships with the Hexie gneiss into the granulitic gneisses where they become progressively more deformed and granulitic until they are lost in the granulites (Figures 3-1H, 3-6A). Relics of both Soledad augen gneiss and sillimanite-garnet-biotite Hexie gneiss are found as isolated inclusions within the Augustine gneiss. At some localities, the felsic granulitic rocks invade the Hexie gneiss with progressive migmatization until only wisps of Hexie gneiss remain as schlieren within felsic granulites. Commonly, however, local contacts from a layer of granulite to a layer or inclusion of Hexie gneiss are knife-sharp. From these relationships, the Augustine gneiss is inferred to have intruded the superjacent Hexie and Soledad gneisses. The nature of this intrusion is complex and is discussed further below.

In outcrop, the retrograded granulites of the Augustine gneiss present a somewhat varied appearance. Felsic and mafic gneisses, where equally abundant such as locally in the southern Chuckwalla Mountains, are interlayered in alternating light and dark layers 1 to 10 meters thick (Figure 3-4C,D). Where the mafic gneisses are less abundant, they are found as inclusions, commonly in strings, within the felsic gneisses. Two classes of felsic gneiss occur. One variety is characterized by coarse- to very coarse-grained blotchy-textured gneiss composed of quartz, feldspar, garnet, and biotite (Figure 3-4E,F). The blotchy texture is

Table 3-III. Modal compositions for samples of Augustine gneiss:

Sample: (Points)	Chuckwalla Mts.					Orocopia Mts. Pinto Mts.			Hexie Mts.		
	Chk-8 (2007)	Chk-131 (2111)	Chk-244 (2078)	Chk-249 (2185)	Chk-253 (1731)	Chk-289 (1613)	O-12 (1809)	P-4 (1508)	P-15 (1438)	H-5 (1480)	H-45 (2002)
Quartz	44.0	27.4	10.5	22.2	35.1	44.5	37.4	33.9	51.5	43.9	44.1
K-feldspar (perthitic microcline)	21.1	27.7	--	12.8	3.1	13.8	3.7	24.2	11.3	x	27.3
Mesoperthite	--	--	--	--	--	x	--	--	--	28.1	--
Plagioclase	28.7	40.0	33.2	58.7	35.3	26.7	35.5	26.2	26.5	9.9	4.0
Antiperthite	--	--	--	x	--	--	--	x	--	--	--
Hornblende	--	--	50.5	--	--	--	--	--	--	--	--
Uralite (hastingsite?)	--	--	--	--	0.05	--	--	--	--	--	--
Biotite	2.7	3.6	3.2	4.6	23.2	6.0	21.0	11.4	8.5	14.9	6.1
Garnet	--	--	--	--	1.7	7.1	--	2.2	0.3	3.1	0.5
Sphene	--	0.2	1.0	tr	--	--	--	--	--	--	--
Apatite	--	0.1	0.1	tr	tr	--	--	--	--	tr	--
Epidote	1.0	0.5	1.3	tr	0.1	--	0.3	1.0	--	--	--
Allanite	0.3	tr	--	--	0.2	--	tr	?	--	--	--
Zircon	tr	tr	0.2	tr	0.05	0.1	0.2	0.1	0.3	0.1	0.1
Opques	1.7	0.5	tr	1.5	1.0	1.8	0.1	0.3	0.4	--	0.2
Carbonate	--	--	--	tr	tr	--	--	--	--	--	--
Chlorite	0.1	--	tr	0.2	0.2	tr	0.3	0.3	--	--	9.2
Muscovite	0.4	--	--	--	--	--	1.5	0.4	1.0	--	8.5

Figure 3-5. Modal compositions of samples of Augustine gneiss from the San Gabriel terrane, plotted on quartz-K-feldspar-plagioclase (QKP) and quartz-feldspar-mafics (QFM) diagrams. Classification from Streckeisen (1967). Solid circles represent samples of Augustine gneiss; triangles represent samples of Mendenhall gneiss from the San Gabriel Mountains (Oakeshott, 1958).



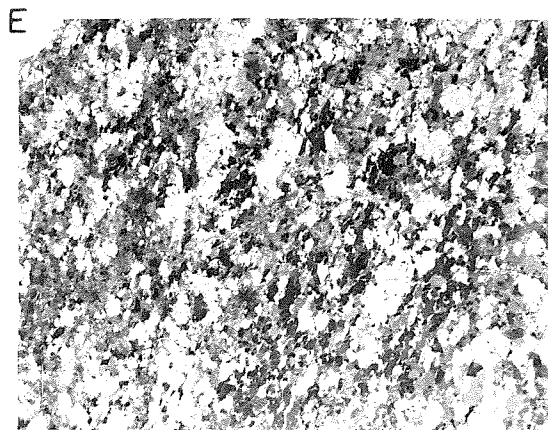
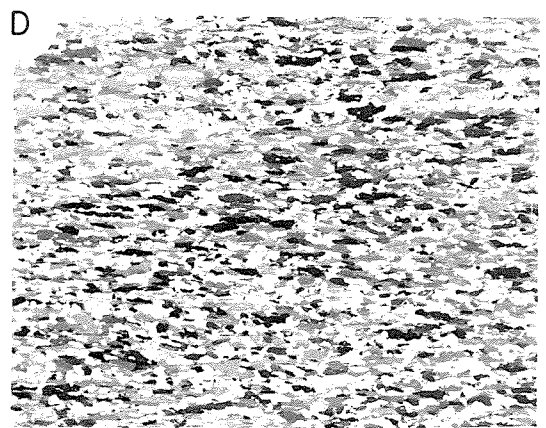
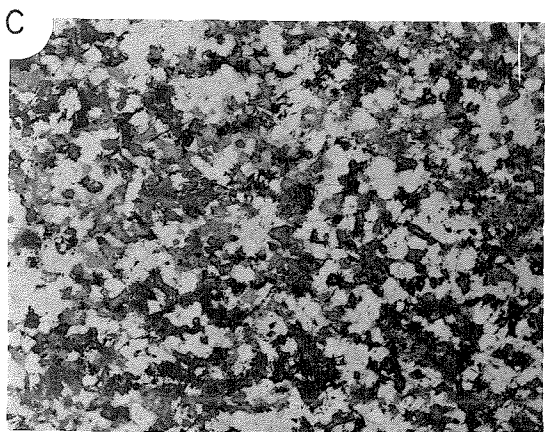
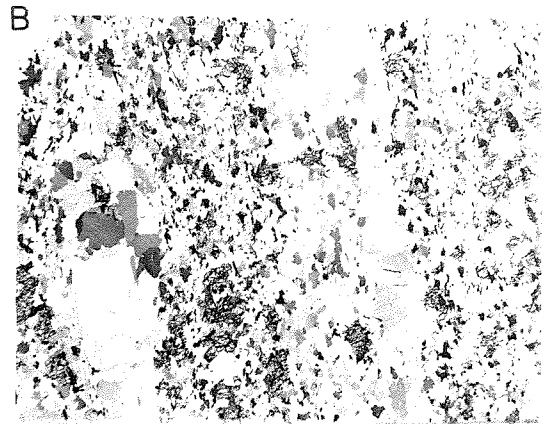
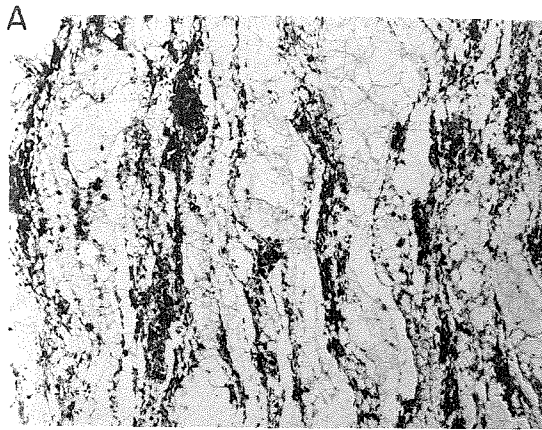
produced by aggregates of equant, blocky quartz and feldspar, and by garnet porphyroblasts and biotite aggregates pseudomorphous after garnet and/or pyroxene(?). The foliation in the gneiss consists of alternating layers richer in quartz + feldspar or in biotite + garnet. The thickness of these segregations is irregular on the scale of 1 to 10 cm. Within the biotite-garnet-quartz-feldspar layers, subsidiary segregations occur with thicknesses of 1 to 2 mm. In general, the more felsic segregations are coarser grained than the more mafic layers. Layered segregations at all scales pinch and swell and have short lateral continuity, imparting a wispy character to the rock (Figure 3-4G). The other class of felsic gneiss within the Augustine gneiss consists of fine-grained, slightly to moderately foliated granitic rock with biotite and garnet (Figure 3-4C,D).

The mafic retrograded granulites consist of varying proportions of hornblende, biotite, plagioclase, and quartz, and range texturally from granoblastic to amphibolitic (Figure 3-6C to E). Within the Augustine gneiss, wherever relationships can be established, the felsic gneisses invariably intrude the mafic gneiss.

In detail, the Augustine gneiss is a complex intrusive unit. Part of this complexity is due to the internal deformation that the gneiss has undergone; and part is due to lithologic variability within the unit. Viewed as a whole, however, the Augustine gneiss is composed of a series of lithologies that range in modal composition from quartz-rich granite to tonalite (Figure 3-5). In thin-section, however, granoblastic and amphibolitic textures indicate metamorphic recrystallization. Not all samples are characterized by the presence of mesoperthite, antiperthite, garnet, or relict corona textures indicative of retrograded orthopyroxene. These minerals are characteristic of granulite facies metamorphism and

Figure 3-6. Photomicrographs of samples of Augustine gneiss from the San Gabriel terrane:

- A. Transition of Soledad augen gneiss to felsic granulite (retrograded): quartz, K-feldspar, and plagioclase are light-colored; biotite and hornblende are dark-colored. Sample Chkwal-290P: uncrossed nicols, horizontal field of 2.1 cm.
- B. Retrograded felsic granulite: garnet (high relief) with K-feldspar (perthite), plagioclase, and quartz. Sample Chkwal-289P: partially crossed nicols, horizontal field of 2.5 cm.
- C. Retrograded mafic granulite: plagioclase, K-feldspar, and quartz are light-colored; the dark mineral is hornblende, much of which occurs in coronas suggesting replacement of pyroxene. Sample Chkwal-220P: uncrossed nicols, horizontal field of 6.9 cm.
- D. Amphibolite: hornblende is dark-colored; plagioclase and quartz are light-colored. Located at early Red Cloud thrust and probably derived from retrograded mafic granulite. Sample Chkwal-244P: uncrossed nicols, horizontal field of 1.9 cm.
- E. Retrograded mafic granulite: hornblende is dark-colored; plagioclase and quartz are light-colored. Sample Chkwal-286P: uncrossed nicols, horizontal field of 1.4 cm.



allow at least some of the rocks to be classified as retrograded granulites.

The literature on the nomenclature of rocks from granulite terranes is rife with terms that are at once parochial and exotic, including charnockites (India), enderbites (Australia), and birkremites, farsundites, and opdalites (Norway), all indicative of hypersthene-bearing rocks that range in composition from granite to quartz diorite. Several classifications have been devised (Hødal, 1945; de Waard, 1969) that fit these names to quartz-K-feldspar-plagioclase ternary diagrams. In essence, they are all similar to that shown in Figure 3-5 in which the granulite-terrane names are superimposed on Streckeisen's (1967) modal subdivision of that ternary. For the purposes of this discussion, however, the rocks will be considered as retrograded granitic to tonalitic granulites, with mesoperthite, antiperthite, garnet, and hypersthene(?) available as modifiers. Modes are listed in Table 3-III.

Quartz is ubiquitous in the Augustine gneiss, ranging in modal abundance from 10 to 52%. In thin-section, it occurs as amoeboid grains and aggregates of grains, highly embayed by surrounding grains of feldspar, mafic minerals, and opaques. It also occurs as a constituent of the fine-grained aggregates inferred to have replaced orthopyroxenes. In hand-specimen, under bright sunlight, quartz in the retrograded granulite gneisses commonly has a lavender to bluish-gray tint.

Plagioclase is present in modal abundances that range from 4 to 60%. It occurs as anhedral grains that are typically twinned but unzoned. Compositionally, the plagioclase is oligoclase-andesine. It is commonly antiperthitic with spindles or pod-shaped to stubby tabular blebs of potassium feldspar volumetrically forming up to 10% of some feldspar

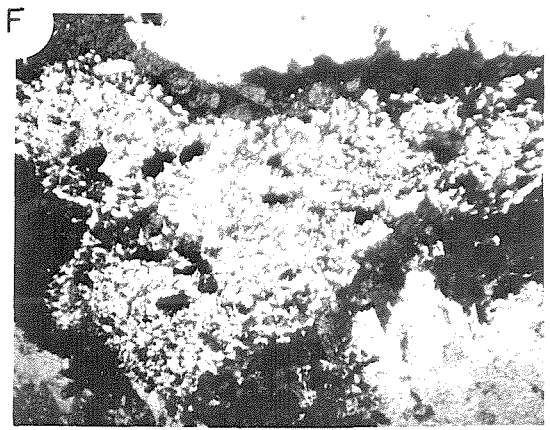
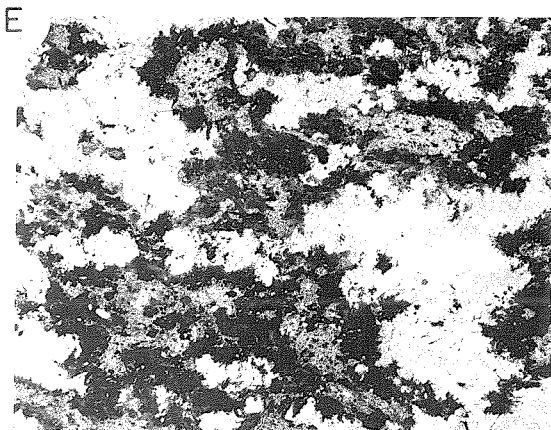
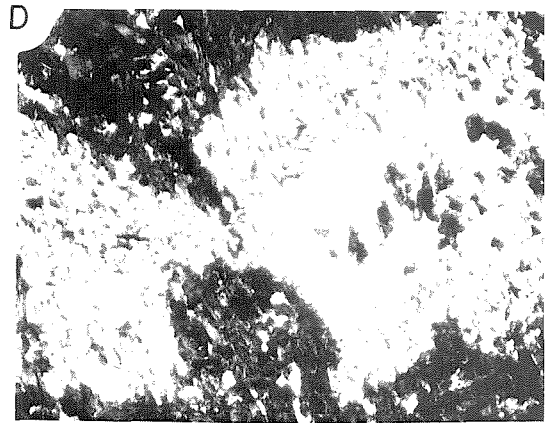
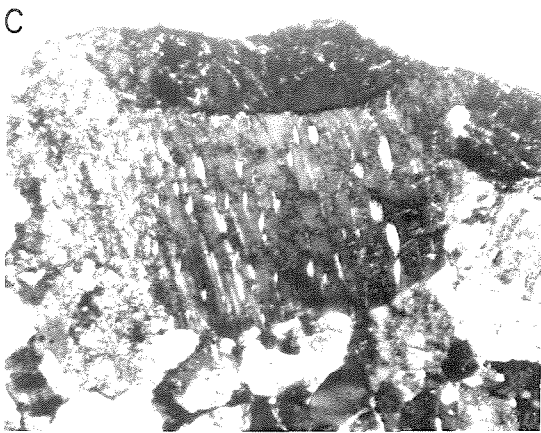
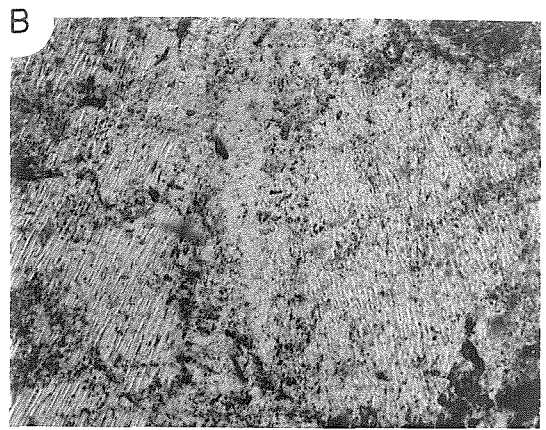
grains (Figure 3-7C). Such antiperthite has been described by Eskola (1952, p. 148, fig. 16) in the granulites of Lapland. Myrmekitic intergrowths of quartz in plagioclase occur sporadically along plagioclase-potassium feldspar boundaries. Plagioclase is typically altered to sericite and epidote.

Potassium feldspar occurs as anhedral grains of microcline and perthitic microcline. In some thin-sections, small amounts of mesoperthite exist (Figure 3-7A,B). Mesoperthite, consisting of subequal amounts of K-feldspar and plagioclase, occurs commonly in granulite terranes. If it is interpreted to have exsolved from an originally homogeneous feldspar, then the granulite must have once been at a temperature high enough to form such a feldspar (de Waard, 1967; Morse, 1968). Microcline is commonly embayed by surrounding plagioclase grains; rarely, it is found in large poikiloblastic (or relict poikilitic) megacrysts with plagioclase inclusions. The modal abundance of potassium feldspar varies from 0 to 35-40%. In general, it is less altered than coexisting plagioclase.

No pyroxene has been observed in any thin-section of Augustine gneiss yet examined, although relict kelyphitic reaction rim textures indicate that orthopyroxene probably was present at least locally when the rocks crystallized. Green hornblende occurs in both the amphibolitic gneisses (50%) and in the granoblastic gneisses as part of the mafic clots that have replaced orthopyroxene(?). Blue-green uralitic amphibole (hastingsite?) occurs in some sections probably as a retrograde alteration reaction product between plagioclase and hypersthene. The uralite occurs radiating clusters partially or completely rimming fine-grained aggregates of quartz, opaque minerals (magnetite-ilmenite?), blue-green amphibole,

Figure 3-7. Photomicrographs of samples of Augustine gneiss and mangerite from the San Gabriel terrane:

- A. Augustine gneiss: mesoperthite in retrograded felsic granulite.
Sample Chkwal-211P: uncrossed nicols, horizontal field of 1 mm.
- B. Augustine gneiss: mesoperthite in retrograded felsic granulite.
Sample Chkwal-298P: uncrossed nicols, horizontal field of 1 mm.
- C. Augustine gneiss: antiperthite in retrograded felsic granulite.
Sample Pinto-4P: crossed nicols, horizontal field of 1 mm.
- D. Augustine gneiss: retrograde corona texture with rims of blue-green uralitic amphibole around cores of quartz, amphibole, and opaques. The texture suggests the former presence of orthopyroxene.
Sample Chkwal-288P: uncrossed nicols, horizontal field of 2 mm.
- D. Mangerite: light-colored plagioclase and dark-colored blue-green uralitic amphibole in coronas around cores of quartz, amphibole, opaques, and apatite. The coronas suggest the former presence of orthopyroxene. Sample Chkwal-298P: uncrossed nicols, horizontal field of 2 cm.
- E. Mangerite: close-up of corona of blue-green uralitic amphibole around a core of quartz, amphibole, and opaques. Sample Chkwal-298P: uncrossed nicols, horizontal field of 2 mm.



and biotite (Figure 3-7D). These mafic clots are interpreted as coronas or kelyphitic reaction rims produced in retrogressive reactions between plagioclase and pyroxene involving water. Green to greenish-bluish biotite occurs in the felsic granulitic rocks both dispersed and as a constituent of the mafic replacement clots. Biotite is locally partly replaced by chlorite. Minor yellow- to red-brown biotite is present in the amphibolitic gneisses, typically as a replacement of hornblende. Garnet, more or less altered to chlorite, is present along with biotite in many of the felsic granulitic gneisses (Figure 3-6B). It is commonly entrained in the more intensely foliated rocks.

Accessory minerals for the Augustine gneisses include ilmenite-magnetite, hematite, apatite, sphene, zircon, allanite, epidote, and carbonate. Ilmenite-magnetite is characteristically rimmed by retrograde overgrowths of sphene, which also occurs as inclusions in biotite aggregates. Ilmenite-magnetite and sphene are rarely euhedral. Apatite and zircon are commonly subhedral to euhedral. Reddish-brown pleochroic allanite is typically rimmed by epidote, although the inverse relationship also occurs. Carbonate, along with sericite, chlorite, and much of the epidote, occur as alteration products.

Mineralogically, the Augustine gneiss with abundant hornblende, sphene, and plagioclase relative to the Hexie gneiss cannot have been derived by melting or isochemically (ultra)metamorphosing the Hexie gneiss. Moreover, the common occurrence of sharp contacts argues against a metamorphic front involving sharp P-T gradients alone. Because the source of the magma is not apparent, it is not known how far it traveled prior to intruding the Hexie and Soledad gneisses: it may be largely new material introduced by some deeper-seated melt-generating process,

or it may be locally-derived by melting or mobilization of a more calcium-rich sedimentary or volcanic layer beneath the pelitic gneiss. No relict features were observed that might lead to the latter interpretation. If the latter situation obtains, then tectonic intrusion of the mobilized gneisses may account for the observed contact relationships (L. Silver, personal comm.). If the former situation obtains, then the regional occurrence of the granulites suggests that intrusive material from an unknown, relatively deep source was being underplated beneath the high-grade pelitic gneisses at deep crustal levels.

SYENITE-MANGERITE-JOTUNITE

Rocks of the syenite-mangerite-jotunite suite are found in Big Wash in the Eagle Mountains and along the east flank of the Chuckwalla Mountains. Together with an occurrence in the Little San Bernardino Mountains, these isolated exposures are distributed within a northwest-trending belt about 55 kilometers long and 5 kilometers wide. As discussed above, another area of exposure occurs in the Orocopia Mountains west of the Clemens Well fault.

Syenite, mangerite, and jotunite are used to refer to plutonic rocks of roughly syenitic, monzonitic, and monzodioritic composition, respectively, that are characterized by the presence of hypersthene and mesoperthite. These terms are commonly applied to rocks associated with massif anorthosites. The modal percentages of quartz, K-feldspar, and plagioclase assigned to each of these rock names has varied somewhat among investigators from different regions (Buddington, 1939; Hødal, 1945; Philpotts, 1966; de Waard, 1969; Carter, 1980b). A further complication is introduced by the alternative plotting of mesoperthite all as alkali feldspar or as a weighted combination of K-feldspar and plagioclase. In this study, the modal percentages of Streckeisen (1967) are used to limit the fields of each rock type and mesoperthite is equally divided between K-feldspar and plagioclase (see Figure 3-8). Because these compositional subdivisions are not readily distinguishable in the field in the Eastern Transverse Ranges, they have been mapped as a single unit. The range of modal abundances for this unit is shown in Figure 3-8. Modes are tabulated in Table 3-IV.

Syenite-mangerite-jotunite is seen to intrude Augustine gneiss on

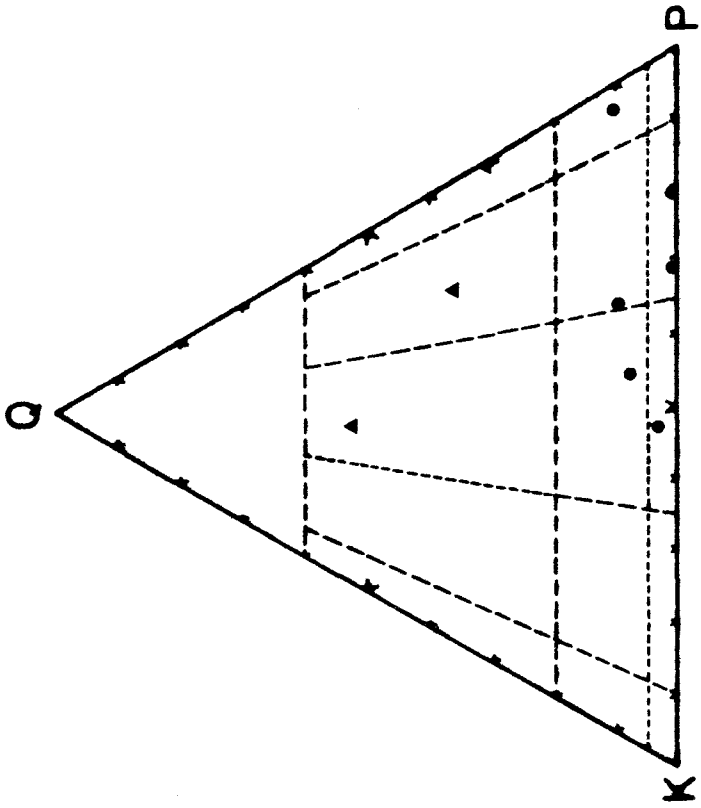
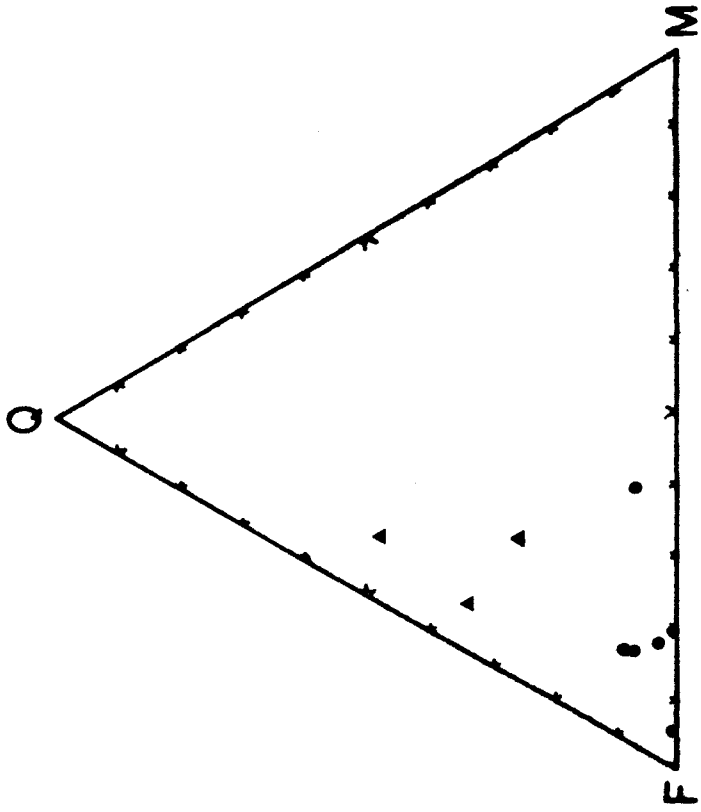
Table 3-IV. Modal compositions of samples of syenite-mangerite-jotunite:

Sample: (Points)	Chuckwalla Mts.					Eagle Mts.			
	Chk-80 (1918)	Chk-224* (1973)	Chk-229* (2053)	Chk-237* (1830)	Chk-298 (1940)	E-20 (1637)	E-91 (2093)	E-98 (1578)	E-100 (1593)
Quartz	8.4	33.5	23.4	46.8	6.3	0.9	0.4	2.9	6.8
K-feldspar	26.6	14.1	tr	22.9	2.3	29.1	16.2	42.4	35.4
Mesoperthite [†]	x	--	--	x	x	--	x	x	x
Plagioclase	50.9	44.5	49.9	19.1	52.2	64.6	62.8	37.3	43.1
Clinopyroxene	0.4	--	--	--	--	--	0.5	--	0.3
Pyroxene? pseudomorphs	x	--	--	--	x	x	x	x	x
Hornblende/ Uralite	11.0	4.0	2.2	5.2	21.4	5.3	15.7	16.2	11.2
Biotite	1.7	3.1	16.3	4.5	13.1	--	3.0	0.2	2.1
Apatite	0.3	0.5	0.9	0.2	1.6	--	0.4	0.3	tr
Sphene	--	--	3.2	--	0.6	0.1	--	--	--
Epidote	--	--	0.3	--	--	--	--	--	--
Allanite	--	0.1	tr	tr	--	--	--	--	--
Zircon	0.3	0.1	0.3	0.1	0.3	tr	0.3	0.3	0.1
Opauques	0.4	0.1	3.5	1.2	2.0	--	0.7	0.4	1.0
Carbonate	tr	0.1	--	--	0.2	--	--	--	--

* Domains of porphyritic quartz dioritic to monzogranitic composition within the syenite-mangerite-jotunite unit.

† Mesoperthite abundances have been divided equally between K-feldspar and plagioclase.

Figure 3-8. Modal compositions of samples of mangerite-jotunite plotted on quartz-K-feldspar-plagioclase (QKP) and quartz-feldspar-mafics (QFM) diagrams. Classification from Streckeisen (1967). Solid circles represent samples of equigranular mangerite-jotunite; triangles represent samples of porphyritic tonalite-granodiorite-monzogranite that is part of the syenite-mangerite-jotunite unit.



the southwestern flank of the Chuckwalla Mountains between Ship Creek Wash and the Aztec Mines. It also intrudes the retrograded granulites in the klippe of San Gabriel terrane preserved in Big Wash in the Eagle Mountains. At this latter locality, dikes of syenite-mangerite cross-cut Augustine gneiss (Figure 3-4H).

Whereas the Hexie, Soledad, and Augustine gneisses each have at least one superimposed penetrative deformation, the syenite-mangerite-jotunite has no superimposed pervasive deformation (Figure 3-7E). The implication is that much of the deformation of older gneisses occurred prior to the intrusion of the syenite-mangerite-jotunite at about 1195 m.y. ago. The unit does, however, contain localized deformation zones, one of which is related to the early break of the Red Cloud thrust system discussed below.

In outcrop and hand-specimen, the syenite-mangerite-jotunite is characterized by a rusty-brown color on weathered surfaces. On freshly broken surfaces, the brown color persists as cream-colored or brown-tinted gray feldspar with interspersed rusty-brown spots of iron oxide. The rock is extensively fractured and weathers readily, leaving few fresh exposures.

Three textural variants of syenite-mangerite-jotunite occur within the field area. Most abundant is light brown, sugary-textured, feldspathic, equigranular rock with varying abundance of mafic clots. The feldspars and mafic clots are roughly equant in a size-range of 0.5 to 3 mm, but the mafic clots consist of fine-grained aggregates of hornblende and biotite. The feldspar is white to cream-colored. Quartz is locally present in varying abundance, generally less than 5%, but in places up to 20%. It occurs as individual equant grains or aggregates and in coarse-

grained lenticular aggregates with a bluish-gray color.

The second most common textural variety is a darker colored, more mafic-rich rock (Figure 3-7E,F). Feldspar is cream-colored to a slightly brownish gray. Within a given hand-specimen, the rock is roughly equigranular, but the grain size varies from 1 to 3 mm to 5 to 10 mm. Mafic clots are generally equal in size to the feldspar, but consist of fine-grained aggregates of biotite, hornblende, and pyroxene. In hand-specimen, the larger mafic clots commonly show dark olive greenish cores enclosed within black rims. In thin-section, the mafic clots exhibit corona textures (Figure 3-7F).

The third textural variety of "syenite-mangerite-jotunite" is actually a very coarse-grained, porphyritic tonalitic to monzogranitic rock that occurs as scattered isolated domains of uncertain sequencing relationship within rocks of the first textural variety.

At one locality 3 kilometers westnorthwest from the Aztec Mines in the Chuckwalla Mountains, a small amount of gabbroic anorthosite is exposed beneath the syenite-mangerite-jotunite unit. With the exception of this one exposure, the syenite-mangerite-jotunite is the lowest crustal unit exposed within the area mapped. Since it has been truncated along the Red Cloud thrust, the original lateral extent of the unit beyond the limits of its present exposure are not known. Augustine gneiss is everywhere present as an intervening layer between syenite-mangerite-jotunite and Hexie-Soledad gneiss.

REGIONAL CORRELATION

As noted by Silver (1971), the rocks of the San Gabriel terrane have not been identified outside of the Transverse Ranges and vicinity in southern California. This observation is based on exhaustive geochronologic and petrologic study within the Precambrian rocks of southwestern North America (see, for instance, Silver et al., 1961; Silver et al., 1963; Silver, fide Bishop, 1964; Silver, 1968, 1969; Silver, fide Miller, 1970; Silver, 1971; Silver and Anderson, 1974; Silver et al., 1977a). Within the Eastern Transverse Ranges, rocks of the San Gabriel terrane have now been found in the Chuckwalla, Little Chuckwalla, Oro-copia, Eagle, Cottonwood, Little San Bernardino, Hexie, and Pinto Mountains, based on the work of Silver (1971), Silver and his students (unpub. maps), and Crowell and Walker (1962), as well as the present study. None, however, has yet been recognized in the San Bernardino Mountains.

IV. PRE-BATHOLITHIC DEFORMATION

RED CLOUD THRUST SYSTEM

Introduction

The San Gabriel terrane is an allochthonous crustal slab regionally emplaced above the Joshua Tree terrane along the Red Cloud thrust system. The thrust system is a major composite structural feature exposed in the Chuckwalla, Orocopia, Eagle, Cottonwood, Hexie, and Pinto Mountains. Subsequent extensive Mesozoic batholithic emplacement, younger faulting, and erosion, however, have left only isolated thrust segments preserved. Remnants of the fault system are discussed individually below, followed by their integration into a coherent tectonic feature. The connections among these segments, and structural interpretations based on such interpolations are of necessity inferential. The Red Cloud thrust system is named for thrust traces exposed on both sides of Red Cloud Canyon in the western Chuckwalla Mountains (Plate I; Figure 4-1C).

Folded thrust faults of the Red Cloud system, and stacked repetitions of the two crystalline terranes, require a structural interpretation that is more complex than a single thrust. It seems clear that the sequence of pre-batholithic deformation must be (1) overthrusting followed by (2) folding, then (3) renewed thrusting across the folded initial thrust, and finally (4) continued or renewed folding. These stages of deformation are inferred to represent an ongoing, though perhaps episodic, orogenic event, but an unrelated origin for the initial thrust emplacement cannot be ruled out.

The initial emplacement along the Red Cloud thrust involved superposition of the San Gabriel terrane over the Joshua Tree terrane. The direction and magnitude of displacement of the allochthon are not direct-

Figure 4-1. Photographs of the Red Cloud thrust system:

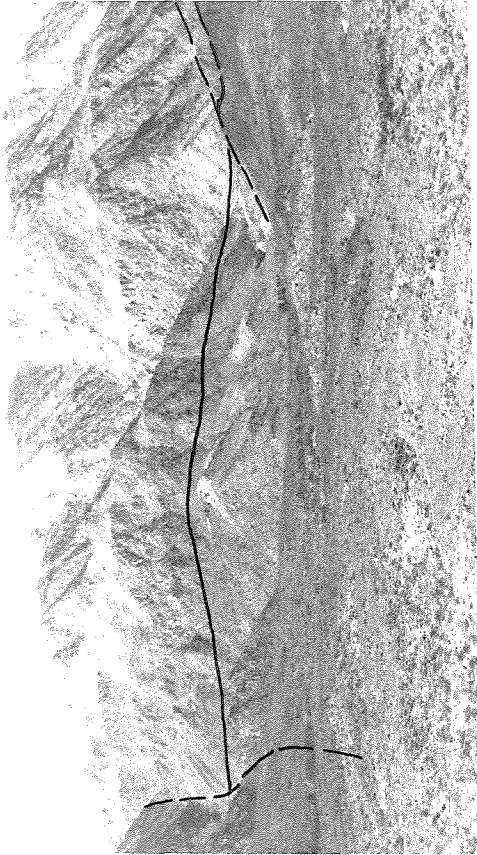
- A. Early Red Cloud thrust on the west flank of the synformal klippe in the Big Wash area of the Eagle Mountains; view to the south. Dark-colored syenite-mangerite-jotunite of the San Gabriel terrane is superposed on light-colored quartzite of the Joshua Tree terrane. Joshua Tree granite gneiss is exposed beyond the ridge crest at the right margin of the photograph. The thrust (shown with arrow) is broken by a younger high-angle fault. Cretaceous(?) monzogranite, forming the mountain in the background, intrudes the thrust.
- B. Later Red Cloud thrust on the east flank of Pilot Mountain in the southern Chuckwalla Mountains. The thrust superposes light-colored Joshua Tree granite gneiss of the Joshua Tree terrane over dark-colored syenite-mangerite-jotunite of the San Gabriel terrane. The thrust is broken at the left of the photograph by the left-lateral Ship Creek fault, and at the right of the photograph by another high-angle fault.
- C. The Red Cloud thrust system at the south end of Red Cloud Canyon in the western Chuckwalla Mountains; view to the southeast. The early Red Cloud thrust in the foreground (with barbs on the upper plate) superposes Hexie gneiss of the San Gabriel terrane over Joshua Tree granite gneiss of the Joshua Tree terrane. High-angle faults in the background juxtapose Soledad augen gneiss and Hexie gneiss against Joshua Tree granite gneiss. The later Red Cloud thrust is truncated by the high-angle faults just off the left edge of the photograph. The left-lateral Ship Creek fault offsets the thrust fault in the

Figure 4-1 (cont.).

upper right corner of the photograph.

- D. Later Red Cloud thrust fault along the east margin of Red Cloud Canyon, at a location just off the left edge of Photograph 4-3C; view to the north. Here, the thrust is undeformed and dips 70° eastward, with Joshua Tree granite gneiss on the left juxtaposed against Hexie gneiss on the right.

B



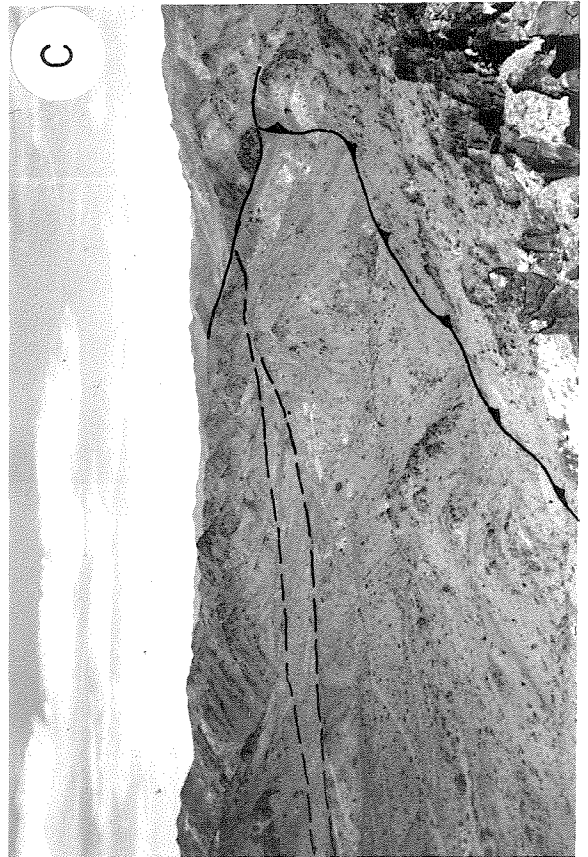
D



A



C



ly ascertainable within the area mapped. Parallel stretched pebbles and mineral lineations above and below the thrust in the Eagle Mountains may be interpreted to indicate a sense of linear movement oriented roughly eastnortheast-west southwest, but not unique direction.

Later stages of emplacement involve folding then compounding of the thrust to produce stacked repetition of the two pre-batholithic crystalline terranes. The thrust formed during this stage is subparallel to, and appears to merge with, the earlier thrust. It is inferred to represent a new break that formed after the initial thrust became folded. Displacement during this stage was roughly 15 to 25 kilometers west-southwestward, based on offset lithologic patterns in both terranes.

Continued or renewed folding was coincident with and followed the later thrusting episode in the final emplacement stage. This folding produced a northnorthwest-trending, westward-vergent, asymmetric to overturned regional fold in the structurally layered section of stacked thrust plates. The lineations cited above alternatively may have developed during this overturned folding episode.

If this sequence of initial emplacement, folding, compounded thrusting, and continued folding does indeed represent stages of a single orogenic epoch, then the vergence for the entire epoch was apparently west-southwestward. This pre-batholithic tectonic evolution is developed in a series of block diagrams in Figure 4-11B to F. In the present tectonic setting, there is no recognized source terrane lying to the east-northeast from which the San Gabriel terrane could have been structurally displaced.

Early Thrusting Stage

Big Wash Area, Eagle Mountains. In the Big Wash area of the southeastern Eagle Mountains (T4,5S, R14E), a klippe of San Gabriel terrane syenite-mangerite-jotunite and Augustine gneiss occurs in a southward-plunging synform truncated to the south by Cretaceous quartz monzonite (Plate I, Figure 4-1A). The thrust fault is a mylonite zone that varies in thickness from less than a meter to perhaps 50 meters (Figure 4-3A). The underlying Pinto Mountain quartzite has a gradationally superimposed mylonite fabric for even greater distances beneath the thrust. The upright cross-bedding of the subjacent quartzite, together with its nonconformable stratigraphic position above Joshua Tree granite gneiss, indicates that the tectonic superposition of mangerite over quartzite is also upright. At the northernmost tip of the klippe, the quartzite is structurally missing, and Augustine gneiss rests directly upon Joshua Tree granite gneiss.

Hayfield Area, Eagle Mountains. Another segment of the initial Red Cloud thrust is exposed in the southern Eagle Mountains north of the Hayfield pumping station. Here the fault dips westward at 45° to 60°, with Hexie gneiss, Soledad gneiss, and Augustine gneiss above Pinto Mountain quartzite and Joshua Tree granite gneiss (Plate I). Basal rocks of the upper plate have been mylonitized (> 50 m) along the thrust (Figure 4-2A,B).

Red Cloud Canyon Area, Chuckwalla Mountains. In the Chuckwalla Mountains, the contact relationship between rocks of the San Gabriel terrane and those of the Joshua Tree terrane is not a single thrust. The upright stratigraphic and structural superposition as described in the

Figure 4-2. Photographs of mylonites in the Red Cloud thrust system:

- A. Minor folds in mylonite along the Hayfield segment of the early Red Cloud thrust in the southern Eagle Mountains north of Hayfield.
- B. Mylonite near the early Red Cloud thrust in the southern Eagle Mountains north of Hayfield.
- C. Mylonite of later Red Cloud thrust in the central Chuckwalla Mountains.
- D. Mylonite near the Red Cloud thrust in the southwestern Hexie Mountains.

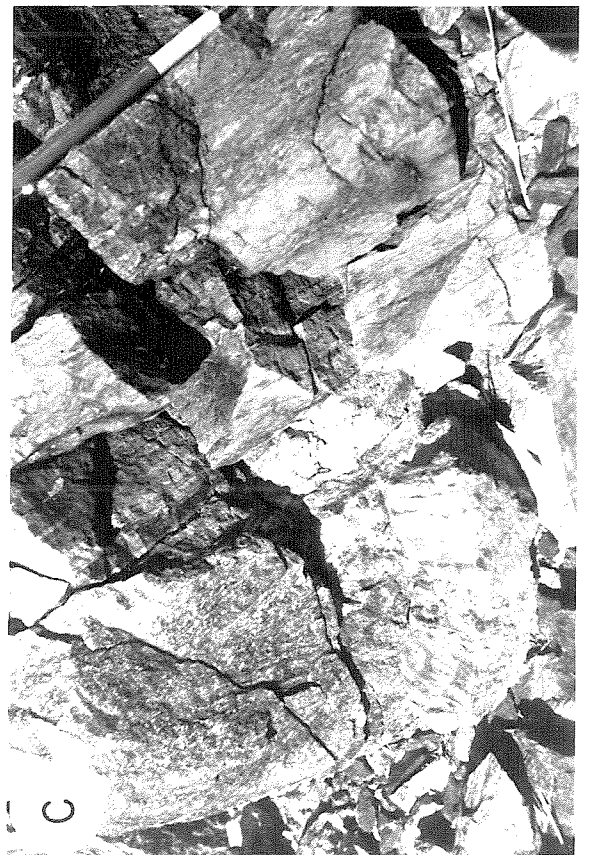
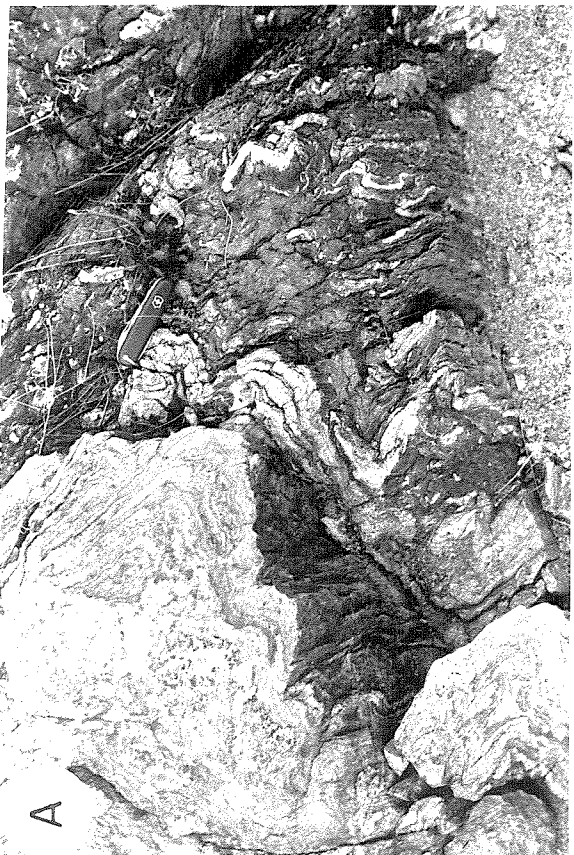


Figure 4-3. Photomicrographs of mylonite samples from the Red Cloud thrust system:

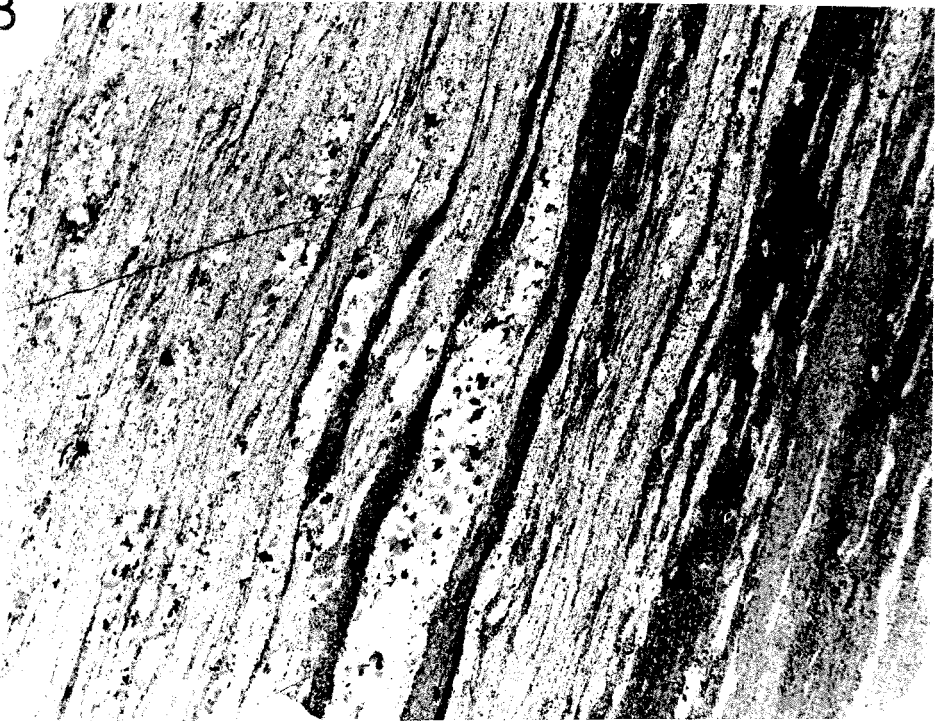
- A. Mylonitized Soledad augen gneiss near the early Red Cloud thrust in the Big Wash area of the Eagle Mountains. Sample Eagle-125P: uncrossed nicols, horizontal field of 2.4 cm.

- B. Mylonite from the later Red Cloud thrust in the central Chuckwalla Mountains at the locality of Photograph 4-2C. Sample Chkwal-167-2P: partially crossed nicols, horizontal field of 2.0 cm.

A



B



Eagle Mountains is present in the southwestern corner of the range, north of the Old Baumonk Mill site. At this locality, Hexie gneiss intruded by Soledad augen gneiss is thrust over Joshua Tree granite gneiss nonconformably overlain by a thin remnant of basal Pinto Mountain quartzite. At this locality, the fault is a zone of interlayered quartzite and gneiss a few meters thick. This fault can be traced nearly continuously northnorthwestward along the west side of Red Cloud Canyon, then along the west flank of the northern Chuckwalla Mountains (Plate I, Figure 4-1C).

At the southwest corner of the range, the thrust fault dips 35° to 45° westward. Northnorthwestward, the attitude of the fault plane is steepened to overturned to about 70° eastward, then is rotated back to about vertical at the north end of the range. The Pinto Mountain quartzite has been structurally removed between the southwesternmost Chuckwalla Mountains and the Eagle Mountains, so that Hexie, Soledad, and Augustine gneiss are juxtaposed against Joshua Tree granite gneiss (Plate I).

Within the Chuckwalla Mountains, the fault trace is left-laterally offset along the Quaternary Ship Creek and Corn Springs Wash faults. North of the Chuckwalla Mountains, the fault is inferred to be offset 11 kilometers left-laterally along the Chiriaco fault to the thrust trace in the Eagle Mountains north of Hayfield (Plate I, Figure 1-2A).

Cottonwood Pass Window. A small window of Pinto Mountain quartzite is exposed beneath Hexie gneiss of the San Gabriel terrane just northwest of the Pinto Basin Road at the crest of Cottonwood Pass (T5S, R11E, sec. 16) (Plate I). The quartzite is clean, coarse-grained white quartzite. The thrust contact above the quartzite is involved in overturned folds

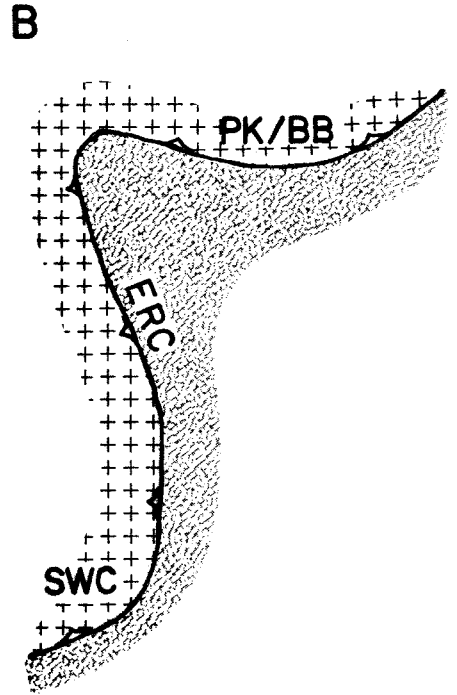
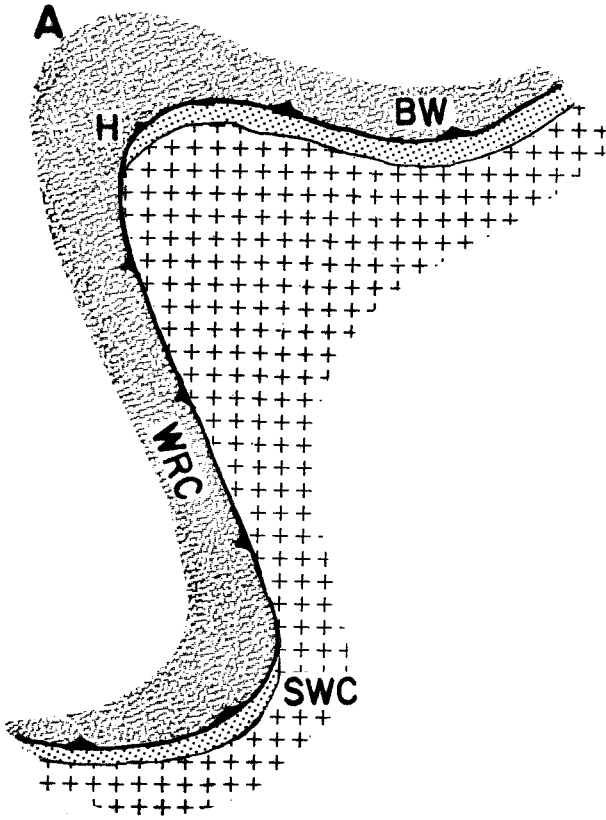
with an anomalous eastward vergence. Because the tectonic superposition of San Gabriel terrane over Pinto Mountain quartzite or Joshua Tree granite gneiss is found only along the early Red Cloud thrust, this exposure is interpreted to be part of that structure.

Synthesis of Early Thrust Segments. In overview, the early Red Cloud thrust can be interpreted as a folded thrust fault. If offset is restored along the Cenozoic left-lateral faults, the folded thrust can be viewed down-structure northnorthwestward from an aerial perspective south of the Chuckwalla Mountains. The Chuckwalla, Hayfield, and Big Wash fault segments can be seen to be parts of a regionally folded thrust fault (Figure 4-4A). The fold axis trends northnorthwestward and the fold is overturned toward the westsouthwest. The Pinto Mountain quartzite has been structurally excised on the overturned limb. Geometrically, Figure 4-4A can be considered either as a plan view with north at the top of the page, or as a cross-section viewed from the south.

A pronounced lineation is present in the rocks of both plates in each of the areas discussed above. It is defined by stretched pebbles in the Pinto Mountain quartzite conglomerates (Figures 2-2H, 4-5D), by mineral lineations in the deformational fabric of the quartzites and interbedded schists (Figure 4-5C), by mineral lineations in the Joshua Tree granite gneiss and Pinto gneiss (Figure 4-5E,F), by elongate quartz aggregates in the quartz-augen schist (paleo-weathered zone), by aligned hornblendes in the syenite-mangerite-jotunite of the San Gabriel terrane (Figures, 4-5A), and by other mineral lineations in the Hexie, Soledad, and Augustine gneisses (Figure 4-5A,B). The average orientation of the combined mineral lineations is about N70E and varies

Figure 4-4. Schematic down-structure views of the Red Cloud thrust system, viewed from south of the Chuckwalla Mountains. Each of the diagrams can be interpreted either as a cross-sectional view toward the north, or as a plan view with north toward the top of the page. For scale, compare locations of identified areas to the same locations on Plate I. San Gabriel terrane rocks are represented by the wavy pattern, Joshua Tree granite gneiss by crosses, and the nonconformably overlying Pinto Mountain quartzite by dots. The thrust faults are indicated with barbs on the upper plates.

- A. Early Red Cloud thrust: segments discussed in the text consist of
- BW - Big Wash area, Eagle Mountains,
 - H - Hayfield area of the southern Eagle Mountains,
 - WRC - western margin of Red Cloud Canyon in the western Chuckwalla Mountains,
 - SWC - southwestern Chuckwalla Mountains, north of the Old Baumonk Mill site.
- B. Later Red Cloud thrust: segments discussed in the text consist of
- PK/BB - Pilot Knob and Black Butte area of the central and southern Chuckwalla Mountains,
 - ERC - eastern margin of Red Cloud Canyon in the western Chuckwalla Mountains,
 - SWC - southwestern Chuckwalla Mountains, north of the Old Baumonk Mill site.
- C. Figure 4-4A and B are combined to show the tectonic slice of Joshua Tree terrane between slices of San Gabriel terrane. Location of Red Cloud Canyon (RCC) is shown, other locations are shown in Figure 4-4A,B. A north arrow and the approximate location of the present Eagle and Chuckwalla Mountains are shown for plan view.



CHUCKWALLA MOUNTAINS
EAGLE MTS.

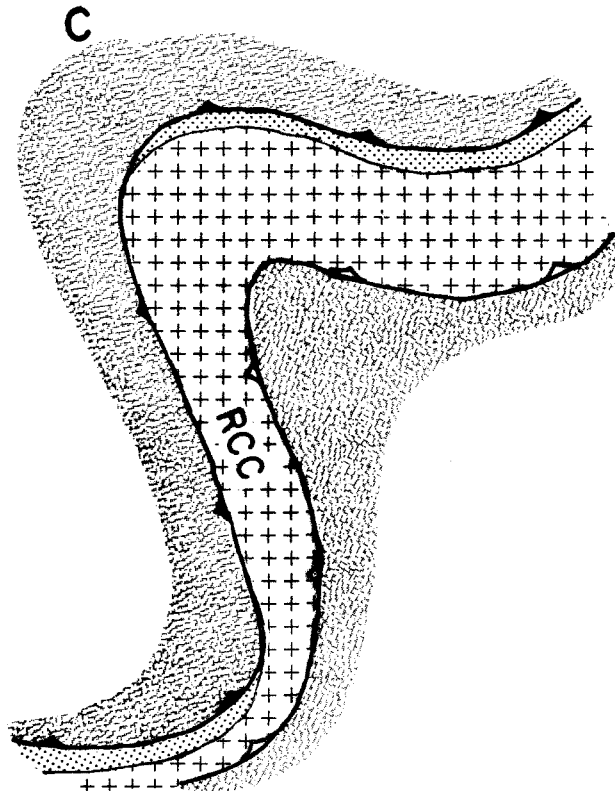
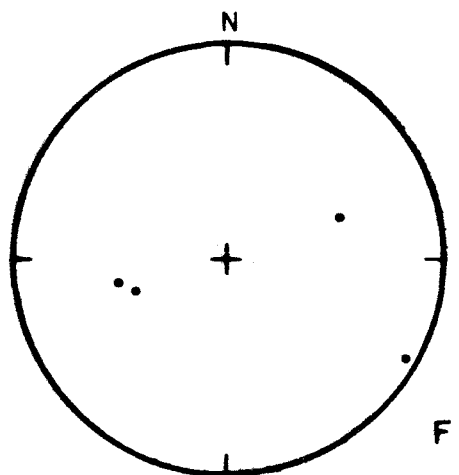
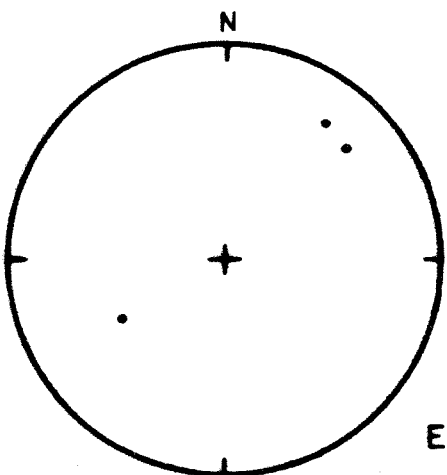
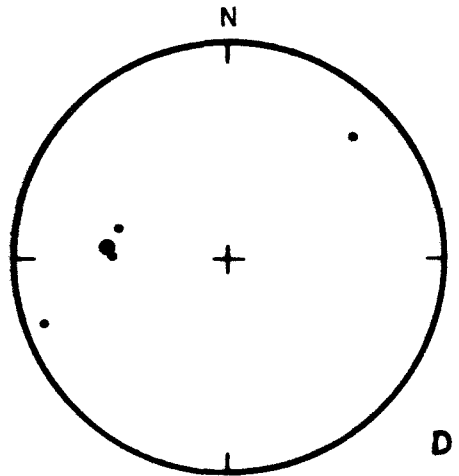
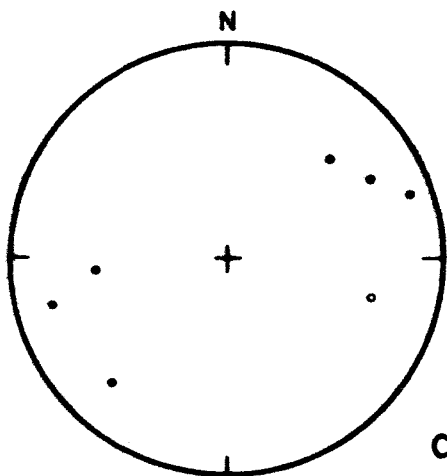
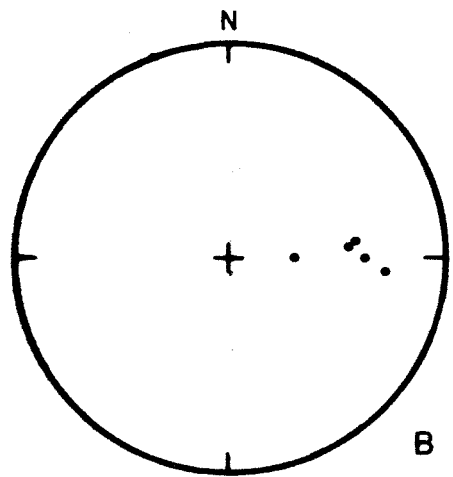
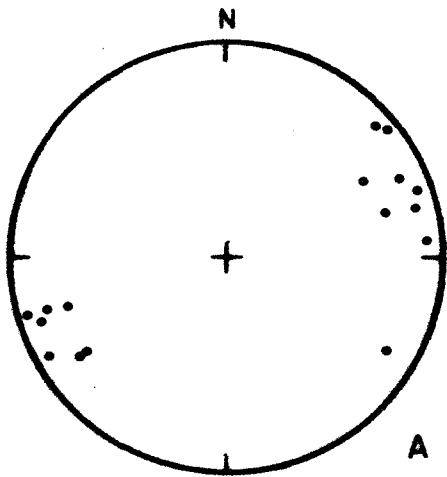


Figure 4-5. Mineral and pebble lineations within the deformational fabric related to the emplacement of the San Gabriel allochthon, plotted on lower hemisphere equal area stereographic projections:

- A. Mineral lineations in the rocks of the San Gabriel terrane in the Big Wash area of the Eagle Mountains: syenite-mangerite-jotunite in solid circles; Augustine gneiss in open circles.
- B. Mineral lineations in the Hexie and Soledad gneisses of the San Gabriel terrane in the western Chuckwalla Mountains.
- C. Mineral lineations in the Pinto Mountain quartzite of the Joshua Tree terrane in the Big Wash area of the Eagle Mountains and in the southwesternmost Chuckwalla Mountains: quartzite in solid circles; interbedded schist in open circles.
- D. Quartz/quartzite-pebble lineations in the Pinto Mountain quartzite of the Joshua Tree terrane in the Big Wash and Hayfield areas of the Eagle Mountains and in the central Pinto Mountains: circled dot represents two measurements.
- E. Mineral lineations in the Joshua Tree granite gneiss in the Eagle Mountains.
- F. Mineral lineations in the Pinto gneiss in the central Pinto Mountains.



from N45E to east-west (Figure 4-6F). The plunge varies from eastnorth-east to westsouthwest depending on position with respect to the synformal and antiformal fold axes (Figure 4-11D,E).

Minor fold axes within the rocks of the San Gabriel terrane (Figure 4-6A to D) are orthogonally oriented with respect to the mineral lineations of both terranes (Figure 4-6F). Minor fold axes within the rocks of the Joshua Tree terrane are either orthogonal to the mineral lineations (Figures 4-6E, 4-7E) or parallel to them (Figure 4-7E,F). Similarly, the minor fold axes within the thrust mylonite (Figure 4-7A to D) appear to comprise two populations: one orthogonal to the mineral lineations and one parallel to them. The number of fold axis measurements is not sufficient to warrant emphasis of these apparent patterns, especially in the San Gabriel terrane for which some of the deformation must have occurred prior to intrusion of the syenite-mangerite-jotunite. An attempted Hansen-type analysis (Hansen, 1967) of the minor folds within the thrust mylonite did not yield a slip line.

From the observation that parallel lineations exist in lithologies of presumably different mechanical properties, it can be argued that the deformation reflects a primary strain distribution directly related to allochthon emplacement, as opposed to an internal response to a secondary strain distribution generated within a specific unit. If the axis of maximum strain is parallel to the direction of tectonic transport during emplacement, then the common eastnortheast-westsouthwest direction of elongation of divers indicators may be interpreted as a bidirectional manifestation of movement. In terms of the geographic distribution of deformed and undeformed rocks, and proximity to the proposed structures, it appears that the lineations are related to thrust-

Figure 4-6. Minor fold axes and mineral lineations within the deformational fabric related to emplacement of the San Gabriel allochthon, plotted on a lower hemisphere equal area stereographic projections:

- A. Fold axes in the Hexie and Augustine gneisses of the San Gabriel terrane in the Hexie and Cottonwood Mountains.
- B. Fold axis in the Augustine gneiss of the San Gabriel terrane in the easternmost Orocopia Mountains.
- C. Fold axes in the Hexie and Augustine gneisses of the San Gabriel terrane in the western Chuckwalla Mountains.
- D. Combination of fold-axis stereonet plots of Figure 4-6A,B,C.
- E. Fold axes in the Pinto gneiss of the Joshua Tree terrane in the easternmost Orocopia Mountains.
- F. Combination of mineral-lineation stereonet plots of Figure 4-5A to F.

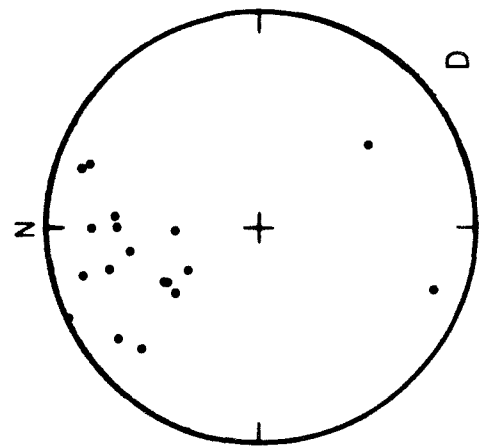
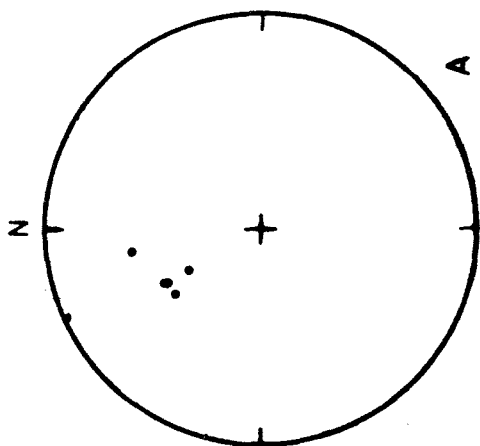
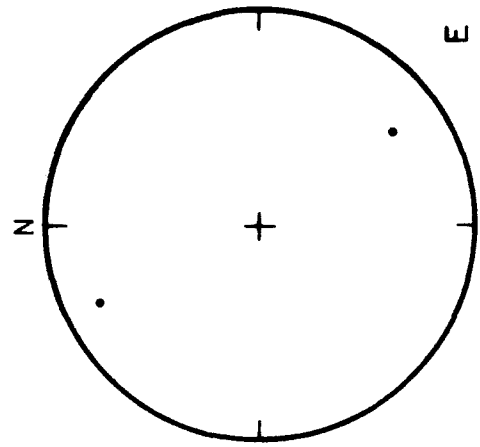
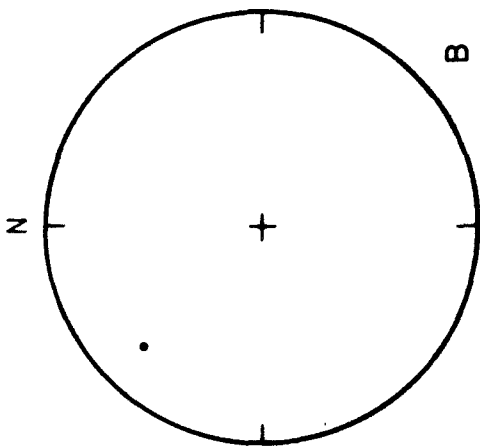
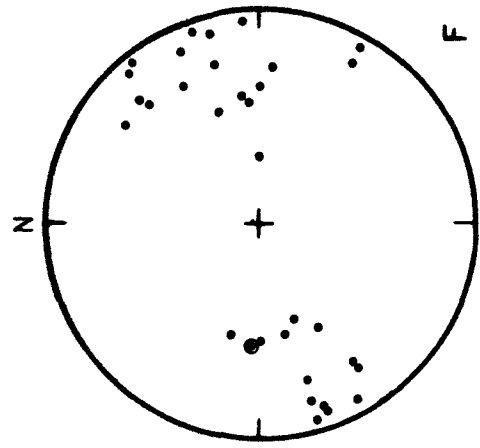
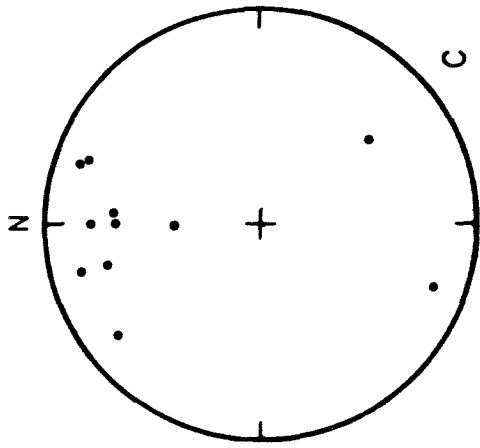
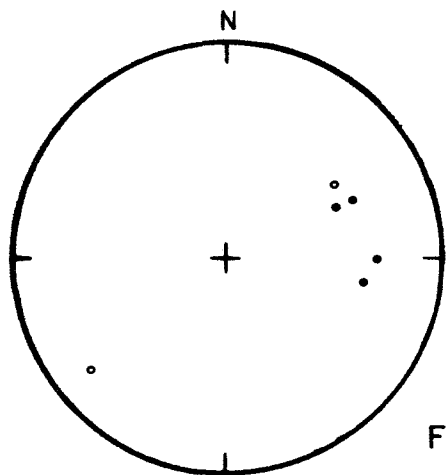
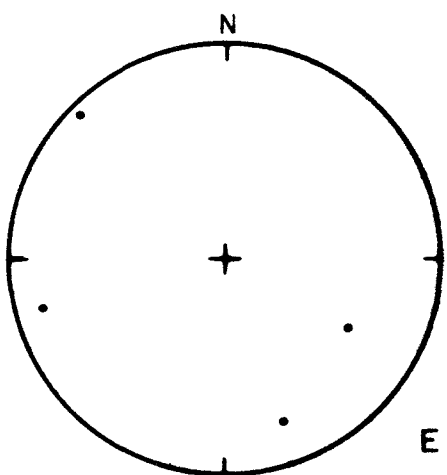
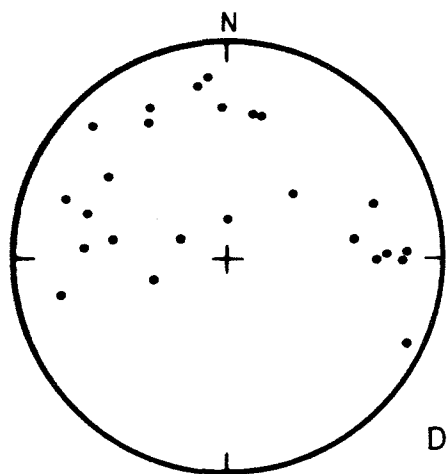
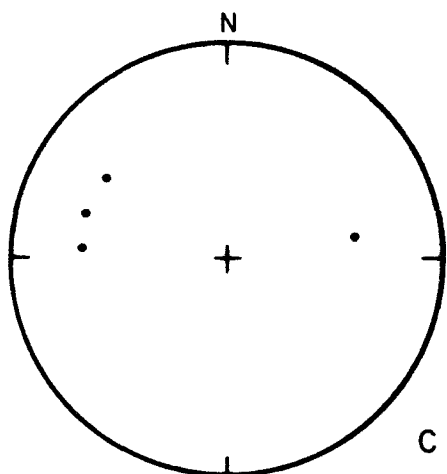
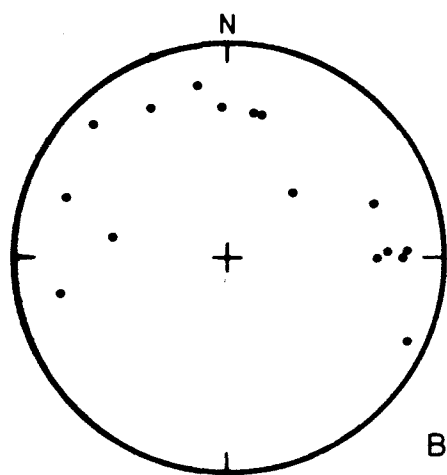
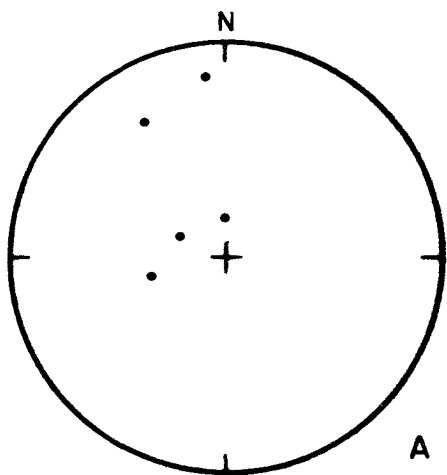


Figure 4-7. Minor fold axes within the deformational fabric related to emplacement of the San Gabriel allochthon, plotted on lower hemisphere equal area stereographic projections:

- A. Fold axes in the Red Cloud thrust mylonite in the Hayfield area of the Eagle Mountains.
- B. Fold axes in the Red Cloud thrust mylonite in the Big Wash area of the Eagle Mountains.
- C. Fold axes in the Red Cloud thrust mylonites in the Orocopia, Cottonwood, and Hexie Mountains.
- D. Combination of fold-axes stereonet plots of Figure 4-7A,B,C.
- E. Fold axes in the Joshua Tree granite gneiss in the Chuckwalla and Eagle Mountains.
- F. Fold axes in the Pinto gneiss of the Joshua Tree terrane in the Orocopia, Eagle, and Pinto Mountains: solid circles represent schist of the paleo-weathered zone and that interbedded in quartzite; open circles represent dolomite.



ing associated with the initial emplacement of the San Gabriel allochthon. Alternatively, however, they may be related to the overturned folding at the final stage of deformation. In terms of proximity, it is unlikely that the lineation is related to the renewed thrusting event.

In similar structural settings, thrust-related interpretations have been advanced for the lineations in the deformed Ben Thutaig conglomerates above the Moine thrust in Scotland (Wood, 1973; Peach et al., 1907) and for the deformed Bygdin conglomerates beneath the Jotun nappe of south-central Norway (Hossack, 1968; Wood, 1973). Kvale (1953) concludes from a synthesis of thrust-related lineations throughout the length of the Norwegian Caledonides that the lineations are parallel to the emplacement direction of the Caledonian nappes. He cites stratigraphic offsets to support his conclusion. McIntyre (1951) and Christie (1963), on the other hand, argue that the principal transport direction along the Moine thrust in the Scottish highlands is perpendicular to the lineation direction. It would seem, therefore, that at the present level of understanding, interpretation of the results of small-scale structural analysis in relationship to the direction of tectonic movement of major structures is ambiguous without independent stratigraphic evidence for magnitude and direction of transport.

In light of this ambiguity, the interpretation of the Big Wash lineations is not unique. If the lineations are related to the regionally overturned fold with its westsouthwest vergence, then they are oriented parallel to the direction, or at least a component of the direction, of tectonic transport of the major structure. If, however, the lineations are related to the initial thrusting event, then they

may be interpreted as having developed perpendicular to a northnortheast or southsouthwest transport of the allochthon, or parallel to an east-northeast or westsouthwest transport. The perpendicular interpretation requires different transport directions for the initial thrusting episode and the folding episode, whereas the parallel interpretation permits a common transport direction for both episodes (Figure 4-8A,C).

Combined theoretical, experimental, and observational petrofabric studies of plastic flow in high temperature metamorphic rocks have been conducted at the tectonophysics laboratory at the Univ. de Nantes, France (Nicolas and Poirier, 1976). In particular, a study of quartzites plastically deformed along the Main Central thrust of the central Himalaya Mountains in Nepal supports a transport direction parallel to the quartz lineation (Bouchez and Pécher, 1976). Conceptually applied to the early Red Cloud thrust, the results of their work favor a tectonic transport direction subparallel to the quartzite lineation and stretched quartzite pebbles, and provide a means for determining the sense of shear related to the initial emplacement of the San Gabriel allochthon. In thin-sections oriented parallel to the field-measured lineation in a plane perpendicular to the plane of shear, the sense of shear is indicated by the angular discordance between the measured lineation (maximum axis of strain ellipsoid) and the normal to subgrain boundaries which are dislocation walls that form perpendicular to the deformational slip line or flow line. A systematic collection of oriented quartzite samples is planned to test the westward to southwestward emplacement proposed for the initial emplacement of the San Gabriel allochthon. For the Main Central thrust of the Himalaya, 7 out of 10 samples analyzed using this technique indicated a shear sense in agree-

Figure 4-8. Directions of inferred movement along the Red Cloud thrust system:

A. Early Red Cloud thrust.

1. Schematic block diagram showing stretched-pebble and mineral lineations inferred to have developed during the emplacement of the San Gabriel allochthon.
2. Compass with heavy diameters marking the limits (on a lower hemisphere stereographic projection) of the orientations of stretched-pebble and mineral lineations (from Figure 4-6F) dashed diameters mark the limits of the orientations of minor fold axes in the upper and lower plates (from Figure 4-6D,E). If the movement direction along the early thrust was parallel to the lineation direction and perpendicular to the fold axes, then the San Gabriel terrane was emplaced either toward the eastnortheast or toward the westsouthwest.
3. Alternatively, if movement on the thrust was perpendicular to the lineations and parallel to the fold axes, then the San Gabriel terrane was emplaced either toward the northnorthwest or toward the southsoutheast.

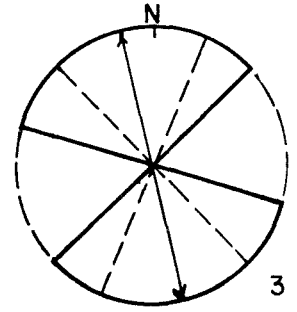
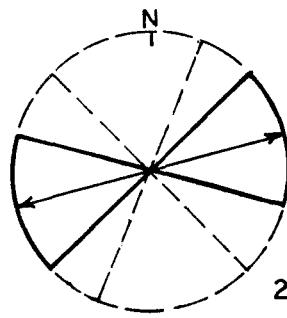
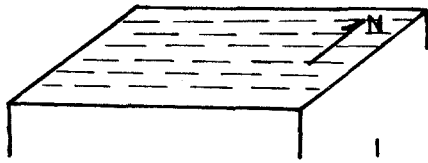
B. Later Red Cloud thrust.

1. Schematic block diagram showing Joshua Tree granite gneiss (crosses) overlain by quartzite (dots) that interfingers with and is overlain by Pinto gneiss. This stratigraphic package is broken by the later Red Cloud thrust, as are the northeast-trending metamorphic isograds.

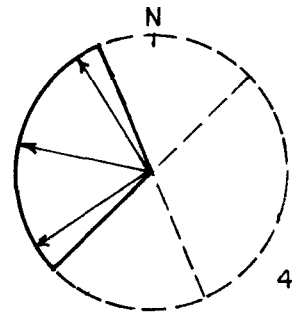
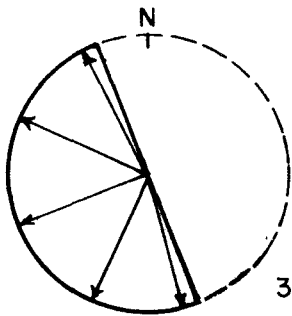
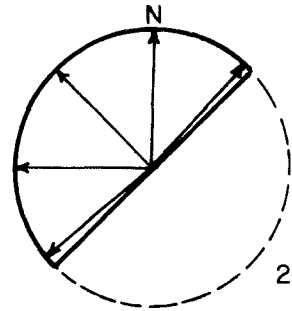
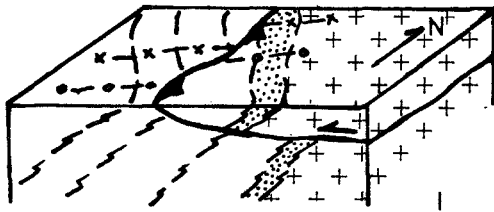
Figure 4-8 (cont.).

2. Compass showing the semicircular range of movement directions compatible with stratigraphic offsets across the later thrust.
 3. Compass showing the semicircular range of movement directions compatible with apparent offsets in the metamorphic isograds across the later thrust.
 4. Compass showing the overlap of the semicircles of Figure 4-8B-1 and 2.
- C. Overturned folding of Red Cloud thrust system.
1. Schematic perspective diagram showing the orientation of the overturned regional fold.
 2. Compass showing the semicircular range of movement directions compatible with the asymmetry of the fold.

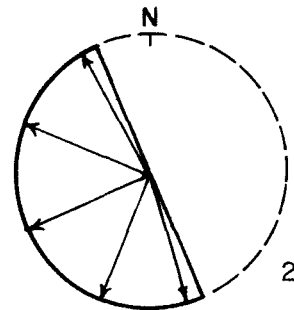
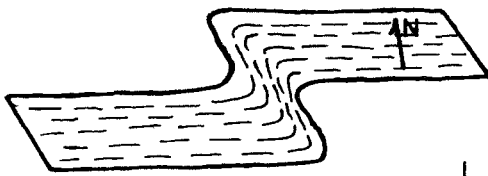
A. EARLY RED CLOUD THRUST



B. LATE RED CLOUD THRUST



C. OVERTURNED FOLDING OF RED CLOUD THRUST SYSTEM



ment with that which is stratigraphically indicated; 2 out of 10 samples gave an inverse shear sense and one sample gave ambiguous results (Bouchez and Pécher, 1976).

It is evident that the granite, paleo-weathered zone, and quartzite of the Joshua Tree terrane, as well as the syenite-mangerite-jotunite of the San Gabriel terrane have been penetratively deformed during the emplacement of the San Gabriel terrane allochthon. Inasmuch as both undeformed and deformed domains of each lithology are present in the map area, this setting provides an excellent opportunity for a detailed structural analysis to characterize the deformational response of each crystalline unit involved in the large structures proposed in this study. It provides an opportunity to make a systematic empirical comparison between directional indications of flow within monomineralic rocks which are linked to theoretically understood experimental work (see Nicolas and Poirier, 1976) and those within polymineralic rocks where the understanding of deformational mechanisms together with consequent predictive ability is complicated by the presence of crystalline species of different crystallographic systems.

Late Thrusting Stage

Chuckwalla Mountains. Along the east side of upper Red Cloud Canyon, an eastward-dipping through vertical to westward-dipping fault (Figure 4-1C,D) can be traced northward almost to the Corn Springs Wash fault, where its trace swings southeastward along the west flank of Pilot Knob to the Ship Creek fault (Plate I). This leg of the fault dips northeastward. South of the Ship Creek fault, the same structure can be traced up and around the top of Black Butte where it dips northward. At Black

Butte, its trace swings northeastward back to the Ship Creek fault, then along the east flank of Pilot Knob, where it dips northwestward (Figure 4-1B). As the fault nears Corn Springs Wash, it becomes vertical. This structure is nearly continuously exposed, and for its entire length Joshua Tree granite gneiss rests structurally above the gneisses of the San Gabriel terrane. No Pinto Mountain quartzite is found along the fault. Mylonite along this thrust varies in thickness from 10 cm (Figures 4-2C, 4-3B) to about 100 m.

Once again viewed down-structure to the north, this break can be seen as a folded and overturned thrust fault (Figure 4-4B), but with the Joshua Tree terrane thrust over the San Gabriel terrane. No inter-relationship between the two thrusts has been found in the Chuckwalla Mountains. The effect of these two thrust faults in the Chuckwalla Mountains is to structurally interlayer a great slice of Joshua Tree granite gneiss within the San Gabriel terrane (Figure 4-4C). This structural superposition of Joshua Tree terrane over San Gabriel terrane is not seen again to the north of the Chuckwalla Mountains.

Central Pinto Mountains. In the central Pinto Mountains, a folded thrust fault exists within the Joshua Tree terrane (Plate I). On the upper plate, Joshua Tree granite is nonconformably overlain by Pinto Mountain quartzite with some intercalation of the inner facies of the Pinto gneiss. The lower plate consists of the vitreous white outer quartzite facies and Pinto gneiss. The thrust is stratigraphically required, but where quartzite is faulted against quartzite, it is extremely difficult to identify at the outcrop scale. Along this thrust, more easterly or shoreward lithosomes of the stratigraphic facies model described above are superposed

over more westerly or basinward lithosomes (Figure 4-9). Because the stratigraphic trends are roughly northnorthwest-southsoutheast, a direction of tectonic transport anywhere within the NNW-WSW-SSE semi-circle would have yielded the observed basinward component of movement (Figure 4-8B).

The most convincing exposure of this thrust fault occurs in the Pinto Mountains at longitude $115^{\circ} 48'W$ between the north edge of the Hexie Mountains quadrangle (15') and the northern boundary of Joshua Tree National Monument (Plate I). At this locality, the Joshua Tree granite overlain by the paleo-weathered zone and quartz/quartzite pebble conglomerate occurs synformally above very coarse grained white quartzite with interbedded pelitic schist. The simplest interpretation of this relationship is a folded low-angle fault beneath the granite.

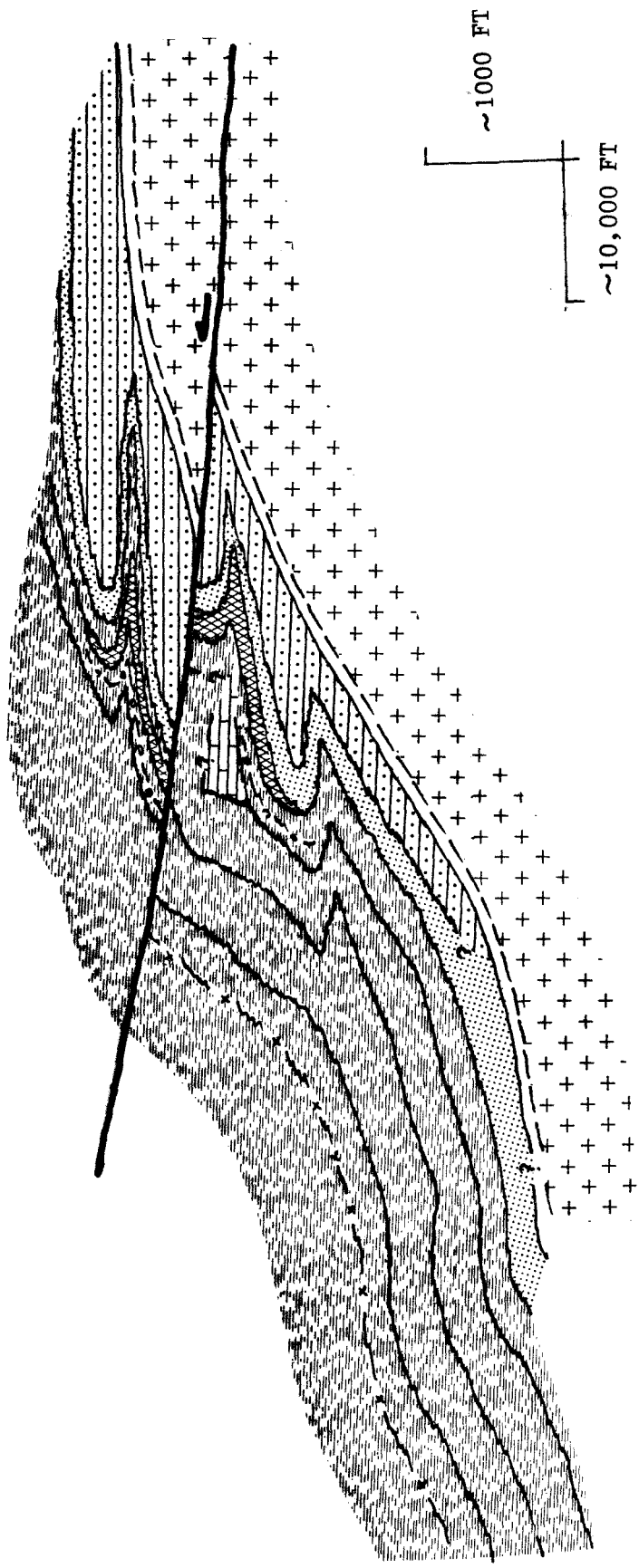
A similar stratigraphic discontinuity can be seen on the southwest flank of the ridge that intersects the boundary between the Hexie Mountains and Valley Mountain quadrangle (15') at longitude $115^{\circ}49'W$. The steep dips on the discontinuity at both of these localities indicate that the thrust was folded during or following its development. No systematic pattern of folding has been established, but the massive white quartzite has been folded up into the overlying thrust sheet. Steep dips on the folded thrust contact (see Plate I), localized non-stratigraphic zones of coarse-grained white quartz that cross-cut quartzite units above the granite gneiss at the second locality cited above, and brecciated quartzites with no obvious genesis require further evaluation.

Because mapping is incomplete along the eastern slopes of Pinto Mountain, this intra-Joshua Tree terrane thrust in the Pinto Mountains

Figure 4-9. Schematic cross-section diagramming the disruption of the stratigraphy of the Joshua Tree terrane by the later Red Cloud thrust. Compare Figure 2-11. See text for discussion.

E

W



has not been carried south to the alluvium of Pinto Basin. There are, however, no observations to limit such an extrapolation.

Northern Eagle Mountains. A similar stratigraphic discontinuity within the Joshua Tree terrane is present in the Eagle Mountains between the Big Wash area and the vicinity of the Eagle Mountain iron mines of Kaiser Steel Corporation (Plate I). Although intrusive rocks of the older batholithic suite have obliterated the trace of the bounding thrust, it is nevertheless inferred to have traced southeast through the northern Eagle Mountains from the Black Eagle Mine Road in Pinto Basin to the Eagle Mountain Pumping Station on the Colorado River Aqueduct.

Cottonwood Pass. Just west of the crest of Cottonwood Pass, a west-dipping thrust fault has superposed Hexie gneiss over the interfingering(?) Music Valley and Baumonk Mill lithofacies of the Pinto gneiss, although the contact is largely obliterated by intrusive Cretaceous quartz monzonite. This contact crops out a few hundred meters east of the window of Pinto Mountain quartzite described earlier and must project westward beneath the window. This structure is inferred to represent a remnant of the later Red Cloud thrust that has telescoped Pinto Mountain quartzite westward and basinward over Pinto gneiss. The thin sliver of quartzite together with the absence of quartzite farther west implies that the bounding early and late thrusts merge westward.

Synthesis of Late Thrust Segments. Displacement on the intra-Joshua Tree terrane thrust fault in the Pinto and Eagle Mountains can be estimated by using offsets of both the protolithic sedimentary facies belts (Figure 4-9) and the superimposed metamorphic reaction boundaries. Both disrup-

tions indicate a westward component of displacement of the upper plate relative to the lower plate.

The northnorthwestward trending facies belts of the stratigraphic model presented in Chapter II are displaced basinward on this thrust in the Pinto and Eagle Mountains; that is, basement (Joshua Tree granite) and the shoreward Pinto Mountain quartzite facies are thrust out over the basinward quartzite facies and the offshore facies of the Pinto gneiss. This displacement requires a direction of tectonic transport somewhere in the semicircle NNW-WSW-SSE (Figure 4-8B).

Similarly, since the metamorphic reaction boundaries described above trend northeast, the occurrence of metamorphic minerals on the upper plate northwest of their limiting boundaries implies a direction of tectonic transport somewhere in the semicircle NE-NW-SW (Figure 4-8B). The actual direction of transport should lie within the overlap of these two semicircles (Figure 4-8B) in the NNW-WSW quadrant. The magnitude of displacement indicated by the disruptions of both the stratigraphic and metamorphic facies patterns is at most 20-30 kilometers. The westward structural superposition of shoreward Joshua Tree terrane over basinward Joshua Tree terrane is not found south of the northern Eagle Mountains. The facies change from Pinto Mountain quartzite to Pinto gneiss (see Figures 2-11, 4-9) may have been a factor in localizing the break of the younger Red Cloud thrust.

Although the westward structural superposition of different parts of the Joshua Tree terrane is not found south of the northern Eagle Mountains, the superposition of Joshua Tree terrane over San Gabriel terrane as discussed above is found at the equivalent structural level. Thus, the late Red Cloud thrust that placed Joshua Tree granite gneiss

above rocks of the San Gabriel terrane in the Chuckwalla Mountains is hypothesized to represent the same structure as the intra-Joshua Tree terrane thrust of the Eagle and Pinto Mountains. Such a correlation implies that both the lithologic patterns within the San Gabriel terrane and the early Red Cloud thrust that separates the two terranes are offset at most a few tens of kilometers by the later Red Cloud thrust. As shown in the block diagrams of Figure 4-11, the predicted offsets of that magnitude are consistent with the mapped distribution of units in the San Gabriel terrane.

Combined Early and Late Thrusting Stages

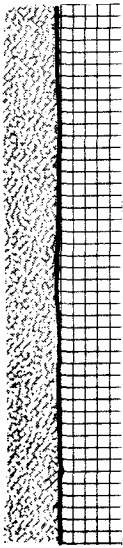
Along the western flank of the Eastern Transverse Ranges, the Red Cloud thrust seems to consist of a single fault plane rather than the compound structure seen to the east. The eastward-dipping trace of this fault is exposed in the easternmost Orocochia Mountains and in the Cottonwood and Hexie Mountains (Plate I). Westward-dipping exposures in the Cottonwood Pass area between the Eagle and Cottonwood Mountains and in the central Pinto Mountains indicate that the thrust surface has been folded. In all of these areas, the thrust is a mylonite zone a meter to 50 meters thick with incipient mylonitization superimposed outside the zone (Figure 4-2D).

In view of the pre-batholithic structural development discussed above, the westward disposition of the early and late thrust planes of the Red Cloud fault system can be expected to conform to one of three geometries (Figure 4-10):

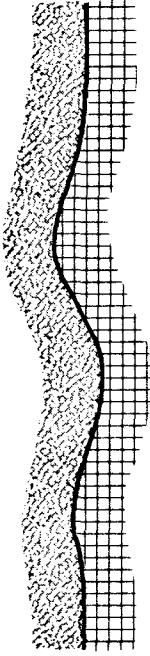
- 1) The later thrust surface passes westward within the rocks of the San Gabriel terrane structurally above the plane of the early thrust and

Figure 4-10. Alternative cross-sectional interpretations for the relationship between the early and late strands of the Red Cloud thrust system. East is toward the right of each sketch, west toward the left. See text for discussion.

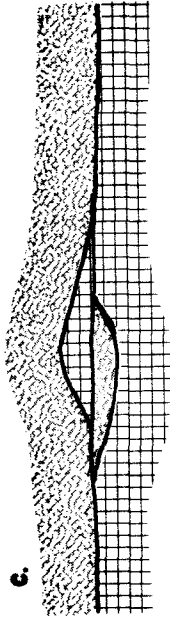
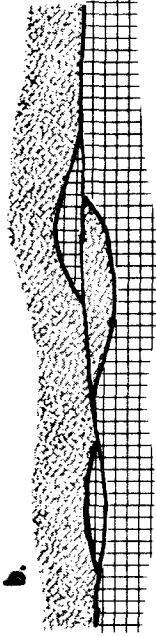
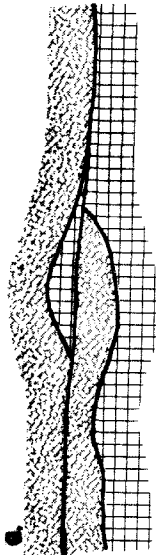
1. Early Thrusting



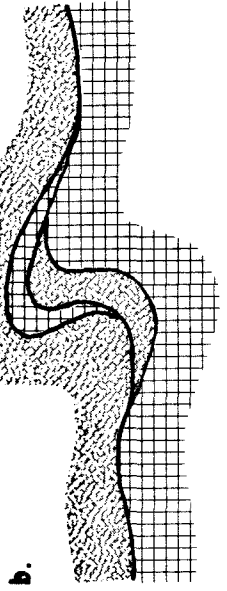
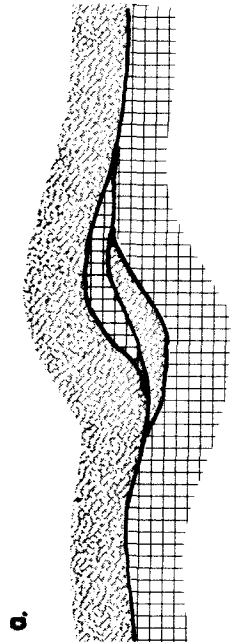
2. Folding



3. Renewed Thrusting



4. Continued Folding



has not been recognized (Figure 4-10-3a);

2) The later thrust to the west again breaks across the folded early thrust and continues westward within the rocks of the Joshua Tree terrane structurally below the plane of the early thrust (Figure 4-10-3b);

3) The late and early thrust surfaces are part of an anastomosing thrust system that merges both eastward and westward into a single fault surface, having diverged only where the initial fault surface became folded (Figure 4-10-3c).

The first interpretation can probably be ruled out by an argument based on the occurrence of a small window of Pinto Mountain quartzite exposed beneath rocks of the San Gabriel terrane a kilometer west of the Pinto Basin Road at the crest of Cottonwood Pass. The thrust beneath which the quartzite is exposed must be part of the early Red Cloud thrust since only that structure has been shown to superpose San Gabriel terrane above Joshua Tree terrane. The base of the quartzite in the window is not observed. However, immediately east of this window a thrust is exposed which places San Gabriel terrane over rocks of the Baumonk Mill facies of the Pinto gneiss. It seems probable that the base of the quartzite is truncated by a thrust fault which places it over the Baumonk Mill facies. Because this structure places a shoreward facies of the Joshua Tree terrane westward over a more basinward facies of the Joshua Tree terrane, it can be inferred to be part of the later Red Cloud thrust. This geometry is inconsistent with that of the first interpretation (Figure 4-10-3a), in which the westward extension of the younger Red Cloud thrust must place Joshua Tree terrane over San Gabriel terrane and must occur at a structurally higher level than the early Red

Cloud thrust.

The observations presented in the preceding paragraph are handled equally well by either the second or the third interpretation. Not enough of the pre-batholithic record may have survived the Mesozoic batholithic intrusions to distinguish between these two interpretations. Because the distributional pattern of the San Gabriel terrane will be the same in either interpretation, the distinction hinges on the distribution of lithologies within the Joshua Tree terrane, and on the number of thrust traces observed or obscured in the west. At this time the second interpretation is subordinate in favor to the third interpretation for three reasons:

- 1) No thrust trace has yet been identified within the Joshua Tree terrane west of that which places it beneath the San Gabriel terrane in the Cottonwood, Hexie, and Pinto Mountains (see Plate I);
- 2) The distribution of lithofacies so far recognized within the Pinto gneiss can be accommodated without recourse to such a western intra-Joshua Tree terrane thrust;
- 3) However, should a western intra-Joshua Tree terrane thrust eventually be found or stratigraphically required, the second alternative can be brought forward to replace the one discussed below.

In the third interpretation, the single thrust plane exposed in the western ranges is inferred to accommodate the displacement of both the early- and late-stage thrusts described above for the eastern ranges. Combined with the folding described below, this interpretation is consistent with the distribution of lithologies of both terranes and for the intervening thrust faults so far observed. The later thrust of the

eastern ranges formed only in conjunction with the folding; elsewhere all movement occurred along a single thrust plane.

Folding Phase

The Red Cloud thrust system is folded in a regional overturned antiform that trends from the southern Chuckwalla Mountains northwest through the Eagle Mountains into the central Pinto Mountains. The pre-batholithic fold is asymmetric to overturned toward the southwest (see Figure 4-4). The evolution of the fold appears to overlap in time with the development of the thrust system as shown in Figure 4-11, and is inferred to be genetically related to the thrusting.

The record of the folding events probably initiated prior to the development of the late-stage thrusting events (Figure 4-11D). This sequence is suggested required by the synformal distribution of the crustal layers of the San Gabriel terrane beneath the overthrust slab of Joshua Tree terrane (granite gneiss) which must also lie folded beneath the synformal allochthonous San Gabriel terrane. A later folding event occurred during and after movement along the later Red Cloud thrust as indicated by overturned folding of the slab of Joshua Tree granite gneiss superjacent to the San Gabriel terrane (Figure 4-11C). It is apparent in Figures 4-11 and 4-4 that construction of these block diagrams required that the antiformal axis of the later folding event be at least partially superimposed on the synformal axis of the earlier folding event.

Probable constraints are placed upon the transport direction of allochthon emplacement by the westsouthwest vergence of the overturned fold. The fold affects a tectono-stratigraphy which includes Joshua

Figure 4-11. Tectonic evolution of the Red Cloud thrust system. The history of thrusting is presented in a series of block diagrams constructed from Figure 1-2A using a single-point perspective south of the field area. Figure 4-11F was constructed first, then E, D, C, and B were palinspastically developed from F. Details are discussed in the text.

- A. Schematic block diagrams representing the stratigraphic relationships established within the Joshua Tree and San Gabriel terranes in Chapter II and III, respectively.
- B. Inferred crustal layers of the San Gabriel terrane scaled to the area of the block diagram constructed from Figure 1-2A.
- C. Stratigraphic model for the Joshua Tree terrane scaled to the area of the block diagram constructed from Figure 1-2A. The block diagram has been palinspastically extended.
- D. Superposition of San Gabriel terrane above Joshua Tree terrane during the early Red Cloud thrusting event, followed by folding. The later Red Cloud thrust will break approximately along the surface of this diagram and carry the antiformal crest cored with Joshua Tree terrane (upper diagram) westward over top of the synform cored with San Gabriel terrane. The new break results in an interlayering of the two terranes (see Figure 4-11E).
- E. The later Red Cloud thrust has displaced the stratigraphy of both terranes and the earlier thrust plane westward. Folding of both thrust planes continued during this event until deformation ceased, leaving a regionally overturned, westward-vergent structure.

Figure 4-11 (cont.).

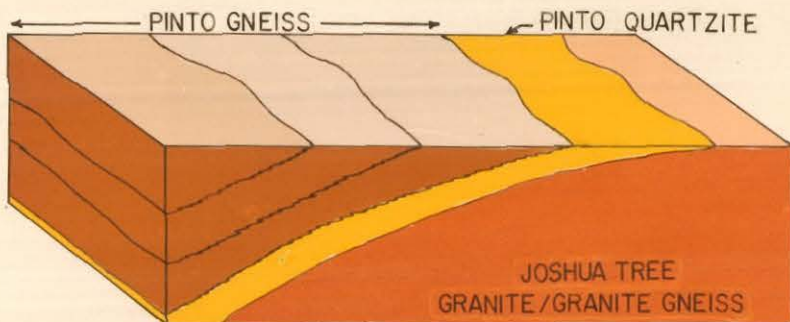
F. Intrusion of the Mesozoic batholiths left isolated pendants of pre-batholithic terranes from which the preceding diagrams were inferred. Mesozoic rocks include a Jurassic(?) belt shown in salmon-color with a speckled pattern and a Cretaceous(?) belt shown in pink: dashes--hornblende-biotite-sphene granodiorite; vees--porphyritic monzogranite; crosses--medium- to coarse-grained nonporphyritic monzogranite (see Chapter V). At some time after the intrusion of the Mesozoic batholiths, the crystalline complex of the Eastern Transverse Ranges is inferred to have been thrust over Pelona-type schist (wavy gray pattern).

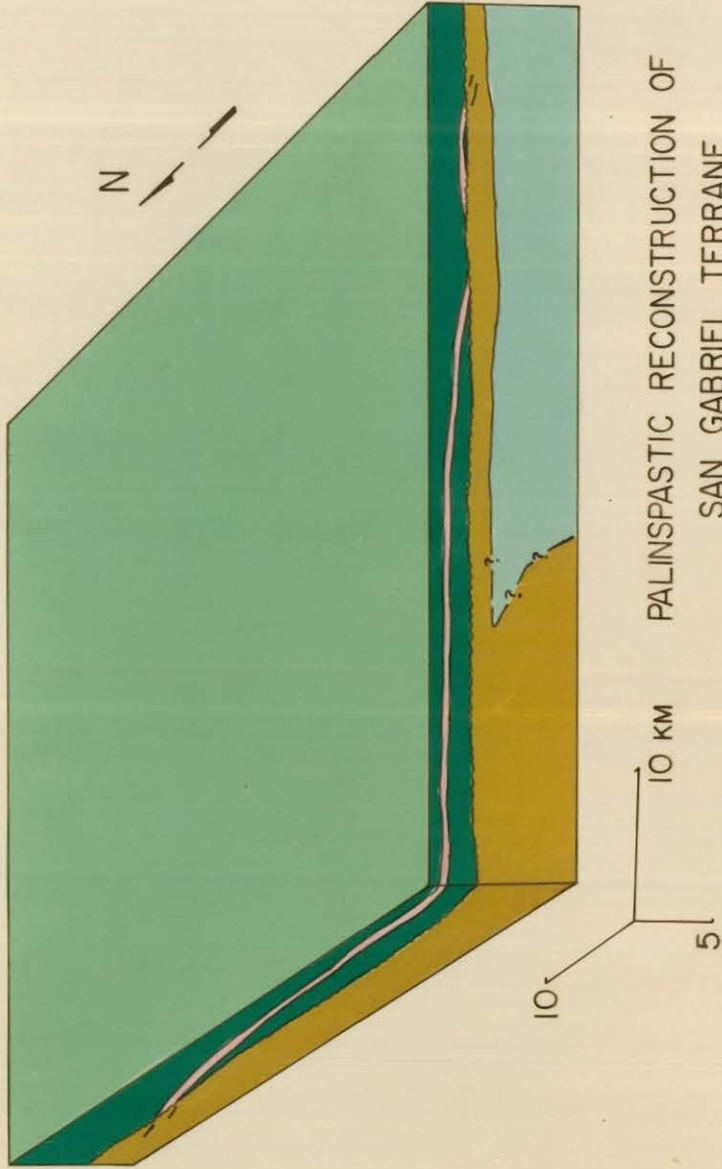
SAN GABRIEL TERRANE



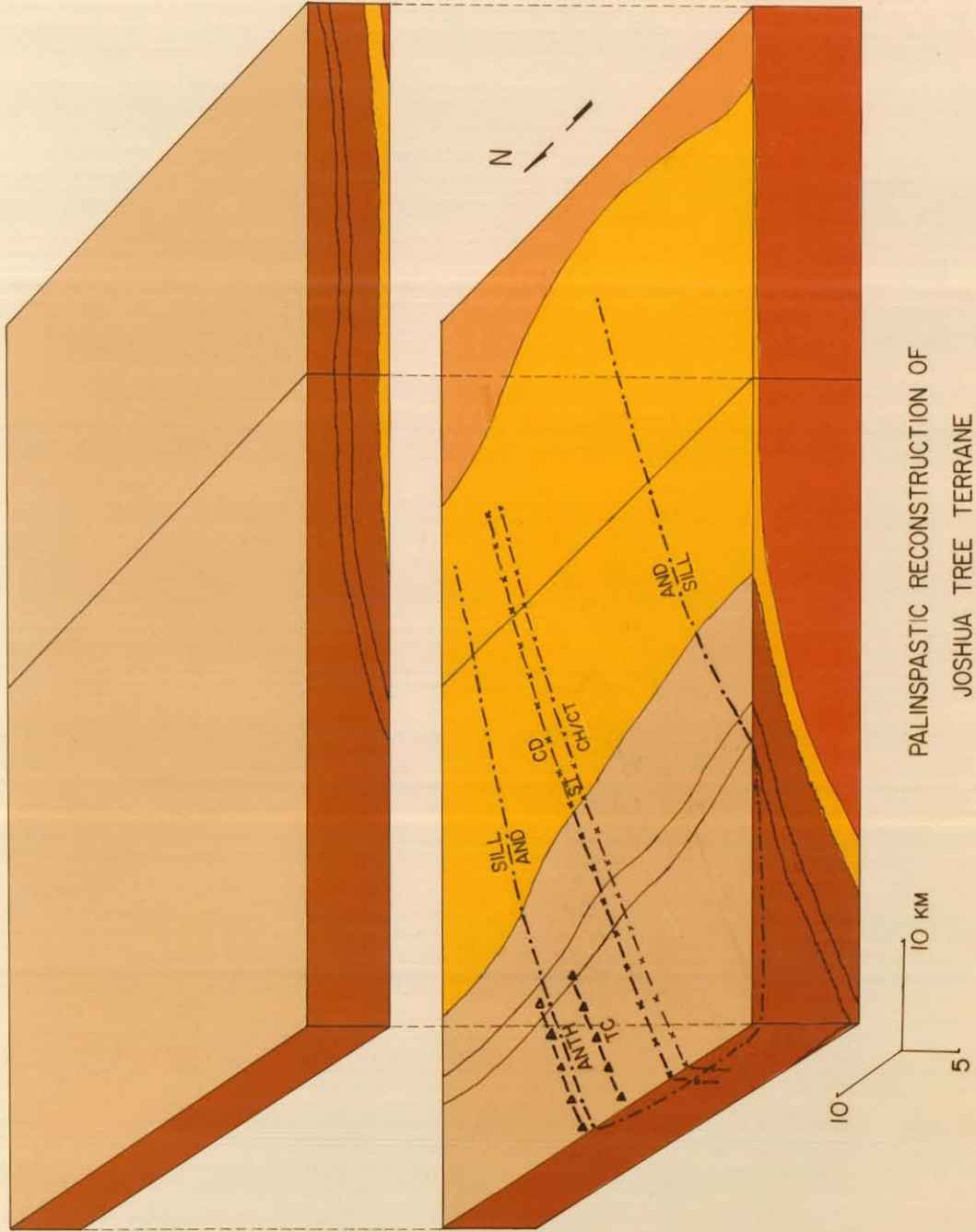
RED CLOUD THRUST SYSTEM

JOSHUA TREE TERRANE

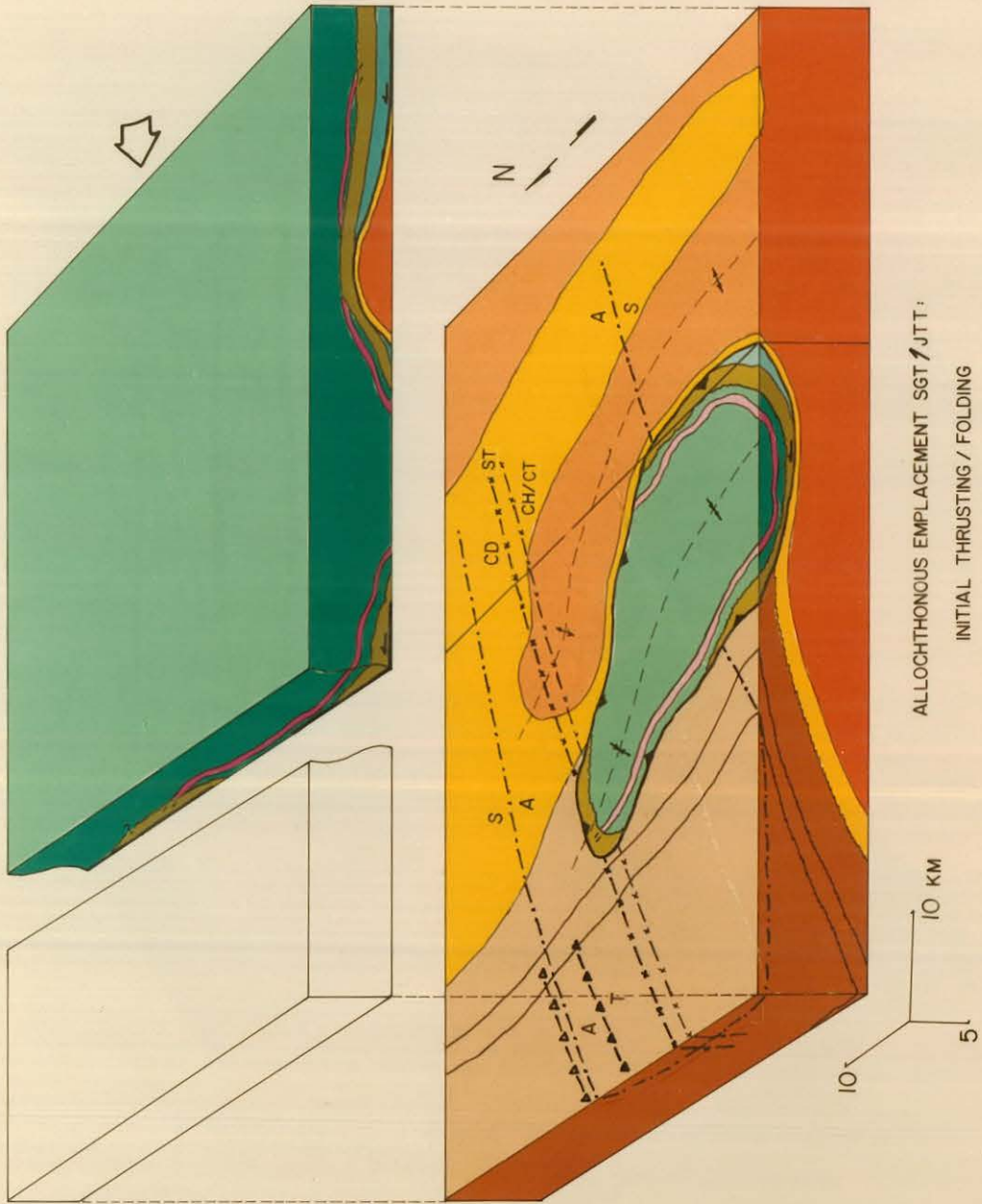


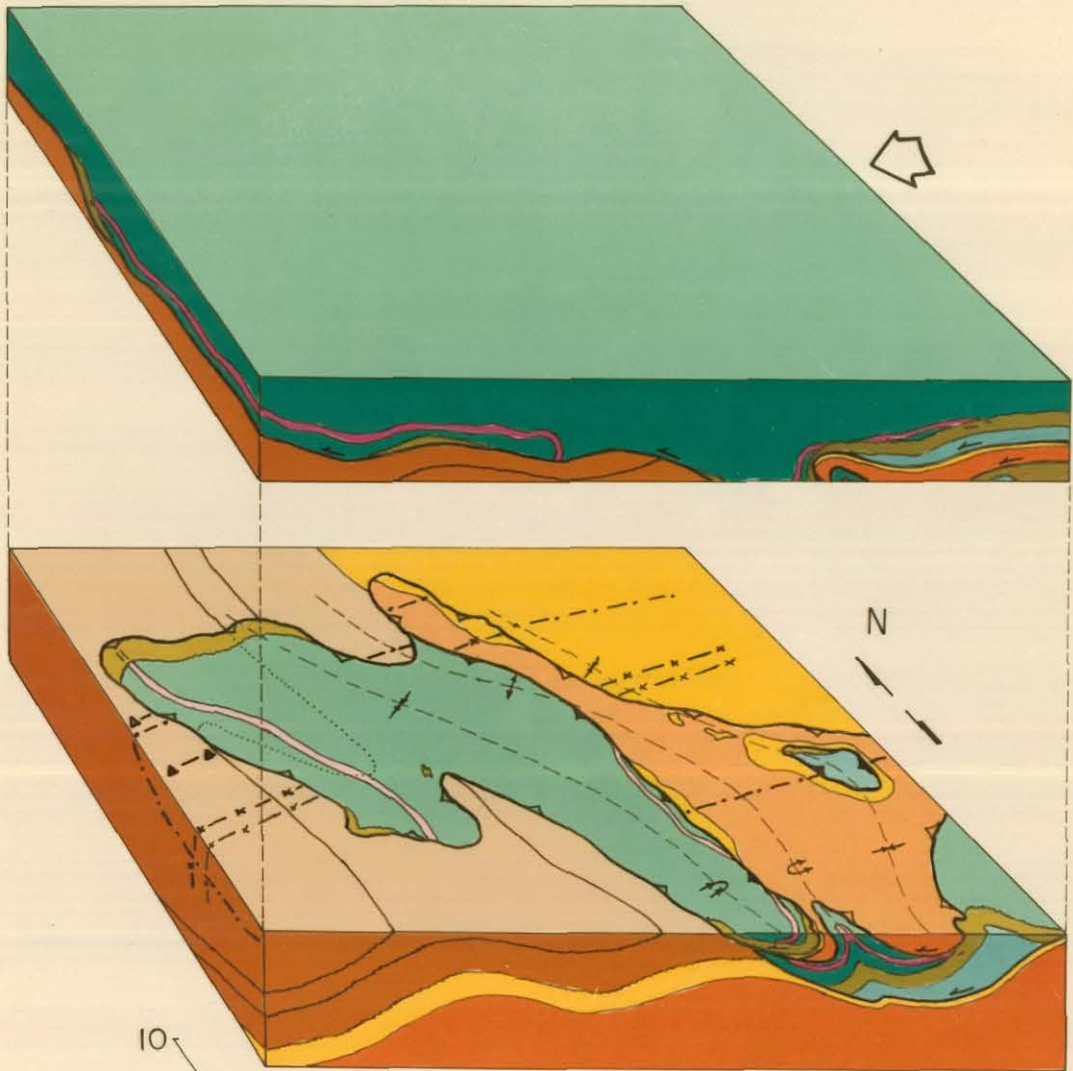


PALINSPASTIC RECONSTRUCTION OF
SAN GABRIEL TERRANE



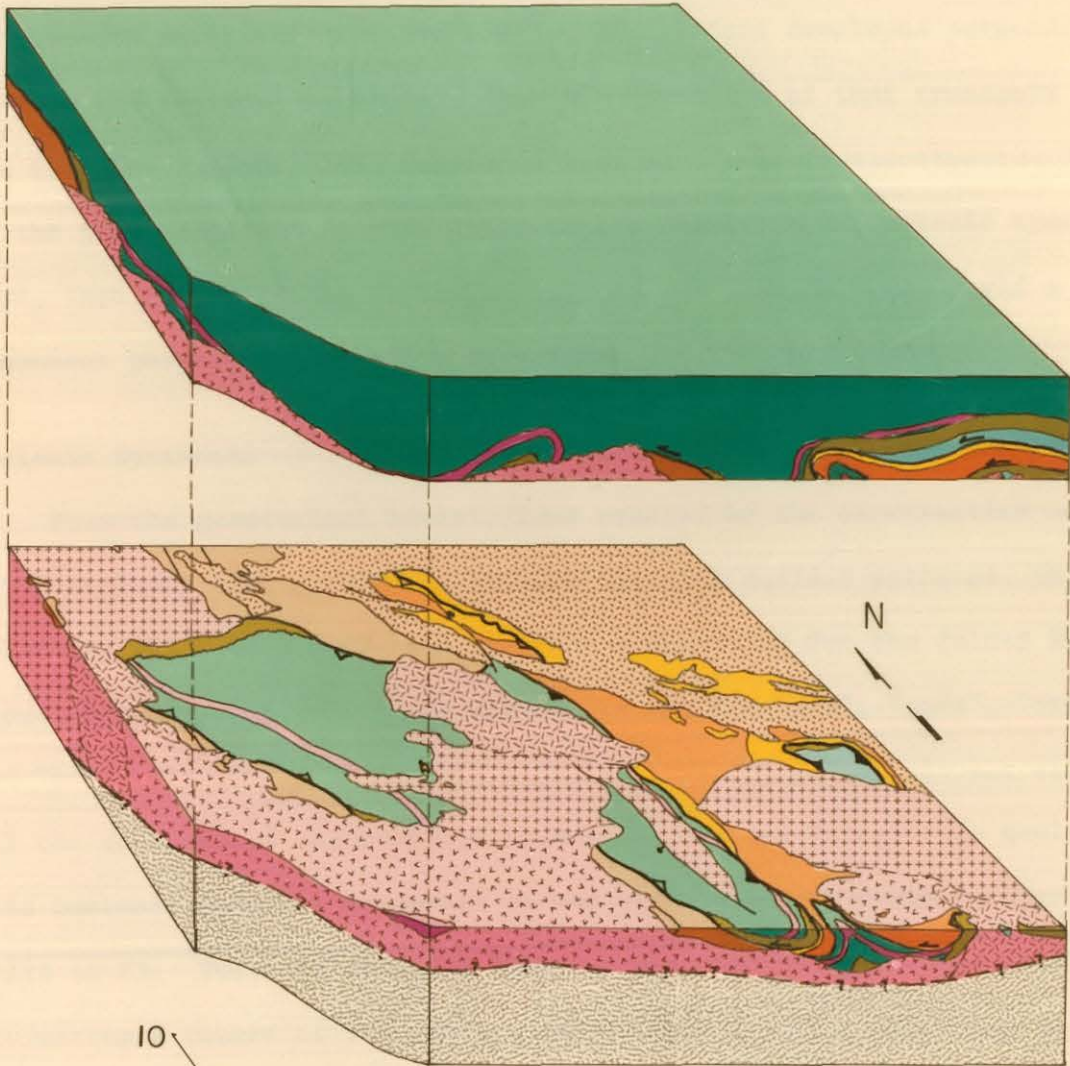
PALINSPASTIC RECONSTRUCTION OF
JOSHUA TREE TERRANE





10
5
10 KM

ALLOCHTHONOUS EMPLACEMENT SGT/JTT:
RENEWED THRUSTING / FOLDING



MZ BATHOLITHIC INTRUSION
 FOLLOWED BY
 EMPLACEMENT OF CRYSTALLINE COMPLEX
 OVER PELONA/OROCOPIA SCHIST

Tree granite gneiss overlain by upright Pinto Mountain quartzite overthrust by rocks of the San Gabriel terrane. If the sense of asymmetry in the overturned fold is assumed to represent at least a component of the transport direction, then that transport direction must lie in the NNW-WSW-SSE semicircle (Figure 4-8C). If the fold developed perpendicular to the tectonic transport, then the direction of that transport at the time the regional fold developed must have been westsouthwestward. If the fold developed at some angle to the direction of tectonic transport, then any direction in the semicircle NNW-WSW-SSE would yield a component perpendicular to the fold axis.

Tectonic Synthesis

From the geometrical restrictions exacted by the construction of cross-sections that accurately reflect plunging surface patterns, the following structural evolution has been synthesized for the folded Red Cloud thrust system. Although subject to all the "ifs", "ands", "ors", and "buts" discussed above, this model is nevertheless consistent with all the accumulated observations concerning the pre-batholithic geology. This tectonic model is presented in the block diagrams shown in Figure 4-11A to F). The last of these diagrams was rigorously constructed by projecting a square of the eastern two-thirds of the geologic map at a scale of 1:250,000 (Figure 1-2A) from a one-point perspective (see, e.g., Raisz, 1962, p. 226-227). Prior to construction, however, offsets were restored along the left-lateral faults (Chiriaco and Blue Cut) as described in Chapter VI. The earlier block diagrams in the sequence were then constructed by extracting the Mesozoic batholithic rocks and successively unravelling the deformations described above. Thus the

earlier diagrams are palinspastically extended by removing the compressional events recorded in the later diagrams. The break in each block is shown at the present earth's surface, with above-ground projections of material inferred to have been structurally and erosionally removed shown in the upper blocks. Figure 4-11A summarizes the stratigraphic and structural relationships within and between the San Gabriel and Joshua Tree terranes. Figures 4-11B and 4-11C are schematic block diagrams that scale the general stratigraphic relationships within the Joshua Tree and San Gabriel terranes, respectively, to the ensuing block diagrams.

The earliest structural event was the initial emplacement of the San Gabriel allochthon, probably with some component of westward movement (Figure 4-11D). The magnitude of this displacement is not known, but a minimum of 80 kilometers is required to superpose entirely distinct lithologic terranes within the Eastern Transverse Ranges province.

The next event was the initiation of folding along a northwest to northnorthwest axis that produced a wrinkle in the early Red Cloud thrust (Figure 4-11D). The development of this wrinkle is inferred to have been related to a compressional stress regime associated with the emplacement of the allochthon. Eventually, the wrinkle reached an amplitude that was sufficient to impede further movement along the early thrust plane in the vicinity of the growing fold. Thrust movement, however, was presumably continuing in areas removed from the fold, resulting in a new break across the fold (Figure 4-11E). In Figure 4-11D, this break will occur along the surface of the lower block.

The later break eventually moved a maximum of about 30 kilometers with a westward component of displacement. The result of this displace-

ment was to move the antiformal crest in the upper block of Figure 4-11D westward over the synformal trough in the lower block. This later thrust is thus responsible for the interlayering of the Joshua Tree and San Gabriel terranes seen in the Chuckwalla Mountains. However, during this westward emplacement, the fold continued to develop along the same axes as it had prior to the breaking of the younger thrust. Consequently, the thrust sheet of the later Red Cloud thrust folded as it advanced, rolling over until eventually it locked as movement associated with the emplacement of the San Gabriel allochthon ceased (Figure 4-11E).

The final block diagram of the series shows the intrusion of the Mesozoic batholithic rocks with a tendency to favor emplacement along old thrust faults (Figure 4-11F). These intrusive rocks are discussed in Chapter V. The diagram also hypothetically shows the tectonic superposition of both of the pre-batholithic terranes, as well as the batholithic rocks, over Pelona-type schist. This structure evolved in a latest Cretaceous to early Cenozoic post-batholithic event and is discussed further in Chapter VI.

Age of the Red Cloud Thrust System

Within the Eastern Transverse Ranges, the faults and fold of the Red Cloud thrust system are clearly intruded by all of the lithologic units of both batholithic belts discussed in Chapter V (Plate I; Figure 1-2A). The oldest cross-cutting batholithic rock yet dated is the monzogranite of the older suite, that yielded an age of 165 m.y. U-Pb on zircons (L. Silver, personal comm.) and 163 m.y. K-Ar (Geochron, fide Bishop, 1964), both located in the north-central Pinto Mountains. Undated gabbros, diorites, and monzodiorites older than the monzo-

granite also cross-cut the thrust system. The youngest unit of the San Gabriel terrane broken by the thrust system is the syenite-mangerite-jotunite unit dated by U-Pb on zircons at 1195 m.y. (L. Silver, personal comm.) in Big Wash in the Eagle Mountains. Therefore, currently, the movement along the thrust can only be bracketed between 165 m.y. and 1195 m.y.

Sequentially, however, thrust movement also is partially coincident with or post-dates the metamorphism of the Pinto gneiss and quartzite. As shown in Figure 4-11D and Plate I, retrograded granulite facies rocks (Augustine gneiss) and upper amphibolite grade rocks (Hexie gneiss) of the San Gabriel terrane are thrust on top of the entire zonal pattern of metamorphic facies assemblages of the Pinto gneiss, including a wide belt of andalusite-bearing rocks. Furthermore, the thrust-related deformational fabric superimposed on the rocks of the Joshua Tree terrane in the Eagle and Chuckwalla Mountains, breaks folds, and retrogrades minerals of the Pinto metamorphism. Thus, the thrust system at least partially post-dates the metamorphism. The metamorphism is younger than the Pinto stratigraphic package that rests nonconformably on Joshua Tree granite with an age interpreted from U-Pb in zircons of at least 1650 m.y. (see Chapter II). In terms of relative timing, then, the Red Cloud thrust system must have occurred between metamorphism of the Pinto gneiss and intrusion of the mafic rocks of the older Mesozoic batholithic suite.

An Analogy in Tectonic Style

The lithologies and allochthonous tectonic setting of the San Gabriel terrane are remarkably similar to the Caledonian Jotun and Bergen

nappes of southern Norway. The upper Jotun and Bergen nappes are sheets of deep-seated crystalline rocks that consist of anorthosite, syenite-mangerite-jotunite, and granulites (Hødal, 1945) thrust along a mylonite zone over para-autochthonous to autochthonous quartzites, conglomerates, schists and subjacent crystalline basement (Holtedahl, 1960). Similarities in structural style near the thrust have been alluded to in earlier sections of this chapter. The striking correspondence in the character and scale (at least in preserved remnants) of the San Gabriel allochthon to the Jotun nappe suggests that during its emplacement, the San Gabriel allochthon experienced a tectonic environment similar to that of the Jotun-Bergen nappes during the Caledonian orogeny in Scandinavia. If additional fragments of the San Gabriel and Joshua Tree terranes can be found, the development of this analogy might provide insights into the North American Cordilleran tectonic evolution.

REGIONAL TECTONIC SETTING (PRE-BATHOLITHIC)

The relationship between the pre-batholithic rocks of the map area and those of the San Bernardino Mountains is particularly important because the Cenozoic disruption between the two regions is limited to 16 kilometers of left-lateral displacement along the Pinto Mountain fault. As discussed above (Chapter II), none of the specific lithologies described in either the Joshua Tree terrane or the San Gabriel terrane is found in the pre-batholithic rocks of the Baldwin Lake area of the San Bernardino Mountains. In addition to the lithologic and stratigraphic discontinuities across the intervening Mesozoic intrusive rocks, there is a major contrast in pre-batholithic tectonic vergence (Figure 4-12). The regional antiform in which San Gabriel terrane rocks and Pinto Mountain quartzite are folded around a basement core of Joshua Tree terrane granite gneiss in the Chuckwalla, Eagle, and Pinto Mountains is overturned toward the west, whereas the regional anticline in which Saragossa quartzite is folded around a basement core of Baldwin gneiss in the Baldwin Lake area is overturned and thrust toward the east to northeast (Dibblee, 1964a,d; 1967f,g; R. Powell, unpub. map).

It is proposed here that the spatial coincidence of discontinuities between Joshua Tree granite and Baldwin gneiss, the Pinto gneiss/quartzite stratigraphic package and the Saragossa quartzite/Furnace limestone stratigraphic column, the presence versus absence of San Gabriel terrane rocks and the opposing vergence of major pre-batholithic structures collectively provide strong circumstantial evidence for the existence of a fault between the Pinto and San Bernardino Mountains. Because the Mesozoic batholithic trends are not disturbed beyond the effect of the Cenozoic Pinto Mountain fault, this proposed structure must be pre-batho-

Figure 4-12. Discontinuity in the basement rocks of the Eastern Transverse Ranges and Mojave Desert. The discontinuity is represented by the heavy line superimposed on a map of the crystalline basement rocks of southern California. In the Eastern Transverse Ranges the discontinuity is older than 165 m.y. Also shown are Cenozoic strike-slip faults that disrupt the older feature (compare Figure 6-1). All of the pre-Mesozoic and pre-Mesozoic(?) rocks in southern California that have been proposed to be exotic lie west of the heavy line; all of the pre-Mesozoic and Mesozoic rocks correlated with rocks of the Great Basin and Colorado Plateau lie east of the line. See text for discussion and references.

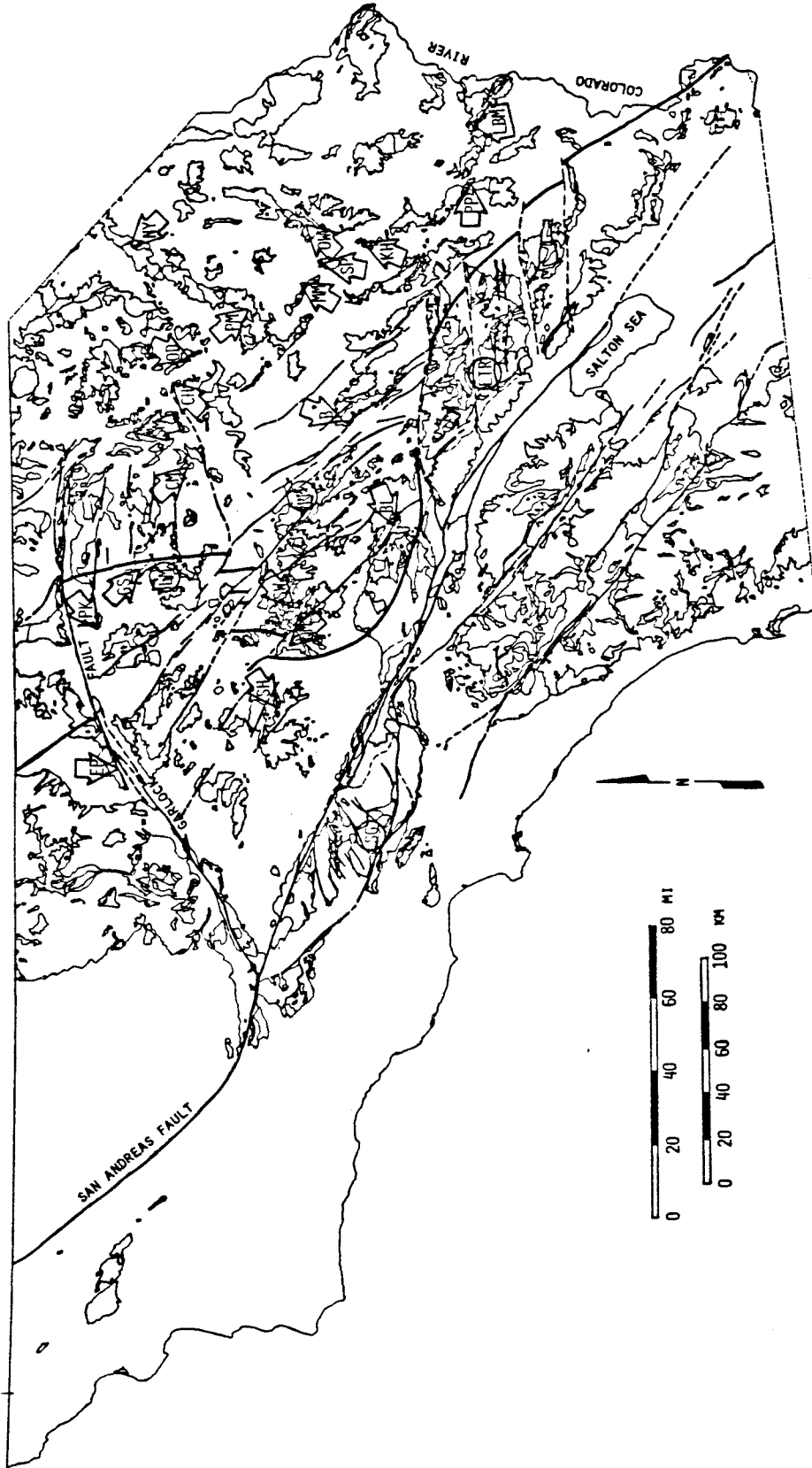
Localities with rocks thought to be exotic:

EP	El Paso Mountains
ETR	Eastern Transverse Ranges
GS	Goldstone
LM	Lane Mountain
PK	Pilot Knob
SG	San Gabriel Mountains
SH	Shadow Mountains

Localities with rocks thought to be indigenous:

BL	Baldwin-Big Bear Lakes area of the San Bernardino Mountains
CH	Cow Hole Mountain
KH	Kilbeck Hills
LBM	Little and Big Maria Mountains
MM	Marble Mountains
NY	New York Mountains
OD	Old Dad Mountain
OW	Old Woman Mountains
PM	Providence Mountains
PP	Palen Pass
QM	Quartzite Mountain
SM	Soda Mountains
SW	Sidewinder Mountain

B	Bullion Mountains
CM	Cave Mountain
RM	Rodman Mountains.



lithic. In fact, direct evidence for its existence has apparently been obliterated by intrusion of both the Jurassic and Cretaceous plutonic rocks (Figure 4-12).

Scattered pendants of pre-batholithic gneiss along the southwestern flank of the San Bernardino Mountains include quartzose and pelitic gneiss that, in reconnaissance, have textural and mineralogical (sillimanite + cordierite) affinity to the Pinto gneiss. If this tentative assignment is valid, then the pre-batholithic line or zone dividing rocks of the Baldwin Lake terrane from those of the Joshua Tree and San Gabriel terranes extends southeastward through the southwestern San Bernardino Mountains, swings eastward through the southeastern San Bernardino and northern Pinto Mountains subparallel to the Pinto Mountain fault, then possibly southeastward again through the eastern Pinto Mountains. The relatively straight trend of this zone, in contrast to the serpentine trace of the Red Cloud thrust system, implies a high-angle fault.

It is possible that this discontinuity in pre-batholithic trends is a manifestation of a segment of the Jurassic(?) Mojave-Sonora continental transform proposed by Silver and Anderson (1974; Anderson and Silver, 1979); or it may be a reflection of some older structure responsible for the Permo-Triassic(?) truncation of the Paleozoic geosynclinal lithologic belts of the Great Basin proposed by Hamilton (1966, 1969) and Burchfiel and Davis (1972). The location of both proposed structures are blurred within the Mesozoic and Cenozoic deformation of the Mojave Desert region. At present, it is ambiguous whether the two proposed pre-batholithic structures are synonymous or synchronous, and if not, what their temporal and spatial relationships are within the Mojave

Desert region. In either case, the presence of cratonic rocks (San Gabriel and Joshua Tree terranes) outboard of the proposed San Bernardino-Pinto Mountains structure would require a translational truncation of Paleozoic paleogeology, rather than the rifted truncation favored by Burchfiel and Davis (1972). It is considered here that one structure is sufficient to account for all the paleogeologic truncations and translations (in agreement with Silver and Anderson), and that the apparent gap in timing of truncation will eventually disappear.

There are several implications inherent in the inference that the proposed pre-batholithic discontinuity in the northern Eastern Transverse Ranges is a segment of a continental margin transform fault:

- 1) The timing of this structure, whatever it represents, must precede emplacement of the monzogranites of the older batholithic suite, which continue from the Eastern Transverse Ranges north into the Mojave Desert (Dibblee, 1964b,c, 1966, 1967b,c,d,e,g, 1968c, 1970a; Dibblee and Bassett, 1966a,b) without major disruption and with no recognized throughgoing zone of deformation.

- 2) The present trace of this proposed fault segment is displaced from the small circle path proposed by Silver and Anderson to traverse northwest from Sonora through the Mojave Desert. Because oceanic and continental transform faults generally define small circles, a deviation from such a path may be an indication of later deformation, in this case a westward shift accompanied by counterclockwise rotation. Such a deformation is consistent with the Cenozoic tectonics described in Chapter VI.

3) The trace of the proposed fault segment, interpreted as a displaced fragment of the Mojave-Sonora megashear, would reconcile the conflict between the offset Precambrian-Paleozoic relationships between Sonora and the southern Great Basin advocated by Silver and Anderson, and the Precambrian-Paleozoic correlations propounded by Stewart and Poole (1975) between the San Bernardino Mountains-Victorville area and the southern Great Basin (Figure 4-12). Between the southern Great Basin of southern Nevada and southeastern California and the vicinity of Caborca, Sonora, Silver and Anderson propose a $700\pm$ kilometer left-lateral disruption of a once coherent northern Precambrian basement terrane (Silver et al., 1962; Anderson and Silver, 1970, 1971; Silver et al., 1977a; Anderson et al., 1979) nonconformably overlain in both regions by correlative miogeoclinal Eocambrian-Paleozoic quartzites and marbles (Anderson et al., 1979). The rocks in Sonora have been juxtaposed outboard of a more southerly Precambrian basement terrane that is slightly younger than that underlying the Eocambrian-Paleozoic miogeoclinal section (Silver et al., 1977a; Anderson and Silver, 1971, 1979). The northern age province consists of eugeosynclinal graywackes and volcanic rocks (1730-1770 m.y. old) intruded by batholiths (1700-1740 m.y. old); the younger southern age province (1610-1700 m.y. old) also consists of eugeosynclinal graywackes and volcanics intruded by batholiths (Silver, 1969; Silver et al., 1977a). The boundary between these two provinces trends approximately northeastward from about the confluence of the Colorado and Gila Rivers. Silver and Anderson delineate a hypothetical small circle trace for the disrupting transform fault. Stewart and Poole, however, propose a match between the supracrustal miogeoclinal Eocambrian-Paleozoic quartzites and carb-

onates in the southern Great Basin and those in the San Bernardino Mountains across the small circle projection of the Mojave-Sonora megashear (Figure 4-12). This correlation is consistent with northern province Precambrian dates for the crystalline basement underlying both sections (Silver et al., 1962; Silver, 1971). Silver and Anderson (1974) anticipated some such younger structural dislocation of the megashear in the Mojave Desert.

If this San Bernardino-Pinto Mountains discontinuity is a disrupted segment of the Mojave-Sonora megashear, then it must be displaced in some specific way from the small circle path indicated by Silver and Anderson (1974). Within the context of the Cenozoic deformation of the Transverse Ranges and Mojave Desert as discussed in Chapter VI, this displacement must follow a pattern similar to that shown in Figure 4-12. It is immediately apparent that all the exotic terranes of the Mojave Desert and Transverse Ranges can be mapped to lie outboard of this segmented megashear. These exotic terranes include not only the San Gabriel and Joshua Tree terranes described above, but also the Shadow Mountains-Lane Mountain-Pilot Knob terrane distinguished by several investigators (McCulloh, 1952, 1954; Rich, 1971, 1977; Miller, 1977, 1979; Smith and Ketner, 1970). The Pilot Knob rocks have been correlated with the rocks of the El Paso Mountains across the Garlock fault (Smith and Ketner, 1970; M. D. Carr, personal comm.). Indeed, the pre-batholithic discontinuity indicated by the juxtaposition of the El Paso Mountains-Pilot Knob-Lane Mountain eugeosynclinal terrane against the southern Great Basin miogeosynclinal-shelf terrane from the Panamint Mountains south-southeastward to the Marble and Ship Mountains formed one of the original constraints used by Silver and Anderson to locate the transform. Thus,

if all the above stratigraphic correlations are valid, then the trace of the transform must approximate that shown in Figure 4-12. The segmented pattern shown in Figure 4-12 is also consistent with the Mesozoic correlations proposed by Miller and Carr (1978) and Cameron et al. (1979), all of which fall inboard of the segmented megashear.

No link between the Joshua Tree and San Gabriel terranes and other pre-batholithic rocks that lie outboard of the segmented discontinuity has been established. These other rocks include the Shadow Mountains-Lane Mountain-Pilot Knob terrane as well as pre-batholithic rocks in the Salinian block, parts of the southern and southwestern San Gabriel Mountains, and the Peninsular Ranges. It is possible that some of these rocks may be stratigraphically linked to the Pinto gneiss as additional northwest-trending lithofacies belts basinward of those described in Chapter II. Other possibilities include stratigraphic onlap over a basement of Joshua Tree terrane or tectonic discontinuities involving either thrust or strike-slip faults. If it is possible to establish one or more of these relationships, then the determination of the tectonic relationship of these terranes and the San Gabriel terrane might further constrain the timing of the emplacement of the latter. Such rocks that have not been assigned to a particular terrane include the pre-batholithic granulites in the southeasternmost San Gabriel Mountains (Hsu, 1955) and the Placerita formation in the southwesternmost San Gabriel Mountains (Miller, 1934; Oakeshott, 1958).

V. MESOZOIC BATHOLITHIC TERRANE

INTRODUCTION

Mesozoic batholithic rocks comprise at least 75% of the pre-Tertiary basement outcrop area in southern California (cf. Jennings, 1977). This observation emphasizes the importance of understanding lithologic and sequencing relationships within this vast intrusive terrane in any effort to unravel the syn- or post-batholithic tectonic evolution of the region. In the Eastern Transverse Ranges, the ratio of Mesozoic batholithic rocks to older rocks is closer to 1:1, which makes the area one of the most favorable in southern California for establishing pre-batholithic relationships. The approach in this study has been to map lithologies within the batholithic terrane and to establish relative age relationships among the mapped units.

In this study, the Mesozoic batholithic rocks in the Eastern Transverse Ranges south of the Pinto Mountain fault have been mapped in two distinct lithologic suites. Within each suite, several lithologies have been distinguished as mappable units. None of these individual lithologic units is continuously exposed throughout the area mapped, but rather each occurs as a belt of isolated plutons. Between plutons of a given lithology, the intervening geologic units consist of pre-batholithic rocks, other batholithic units, and younger cover that includes Tertiary terrestrial deposits as well as extensive Quaternary alluvium. Although the various batholithic units cannot be traced continuously, consistent intrusive sequencing of lithologic units within each batholithic suite is observed from range to range throughout the field area, and the oldest lithology of the younger group intrudes the youngest lithology of the older group. In general, the distribution of the batholithic suites defines two belts, with units of the older suite exposed to the northeast

in the northeastern Eagle Mountains and eastern and central Pinto Mountains, and with units of the younger suite exposed to the southwest in the Chuckwalla, Orocopia, Eagle, Cottonwood, Hexie, Little San Bernardino, and western Pinto Mountains (Plate I, Figure 1-2A). Petrographically, the older batholithic group has an alkalic character, whereas the younger group is calc-alkaline.

Based on a few radiometric age determinations on individual units within each suite, the younger batholithic suite is tentatively assigned a Cretaceous(?) age, and the older suite a Jurassic(?) age. The ages include both U-Pb dates (L. Silver, personal comm.) and K-Ar dates (Bishop, 1964; Armstrong and Suppe, 1973). To the north of the field area, an extensive domain of anomalously young K-Ar ages has been identified in the San Bernardino Mountains and southern Mojave Desert (Miller and Morton, 1980). Because the present study area lies athwart the southeastward projection of the axis of this domain of reset emplacement ages, any uncorroborated K-Ar date may indicate the resetting thermal event rather than a cooling age related to batholithic emplacement. However, in the north-central Pinto Mountains, the porphyritic monzogranitic lithology of the older batholithic suite has yielded Jurassic dates in both radiometric systems (Bishop, 1964; L. Silver, personal comm.), and in the southernmost Chuckwalla Mountains, the hornblende-biotite-sphene-bearing granodioritic lithology of the younger batholithic suite has yielded Cretaceous dates in both radiometric systems (Armstrong and Suppe, 1973; L. Silver, personal comm.). Within the context of his regional geochronological and petrologic studies of the Mesozoic batholithic rocks of southwestern North America, Prof. Silver has collected several samples from both suites of Mesozoic batholithic

rocks within the area of this study. These samples, currently being processed in the laboratory, will in part test the batholithic interpretation presented herein.

The petrographic nomenclature of the plutonic described in this study generally follows the classification of Streckeisen (1967). The one exception pertains to the use of the term quartz monzonite, which is used synonymously with monzogranite. This deviation from Streckeisen's classification is a concession to the prevalent prior usage of quartz monzonite for Cordilleran granites in the monzogranitic composition field.

JURASSIC(?) BATHOLITHIC SUITE

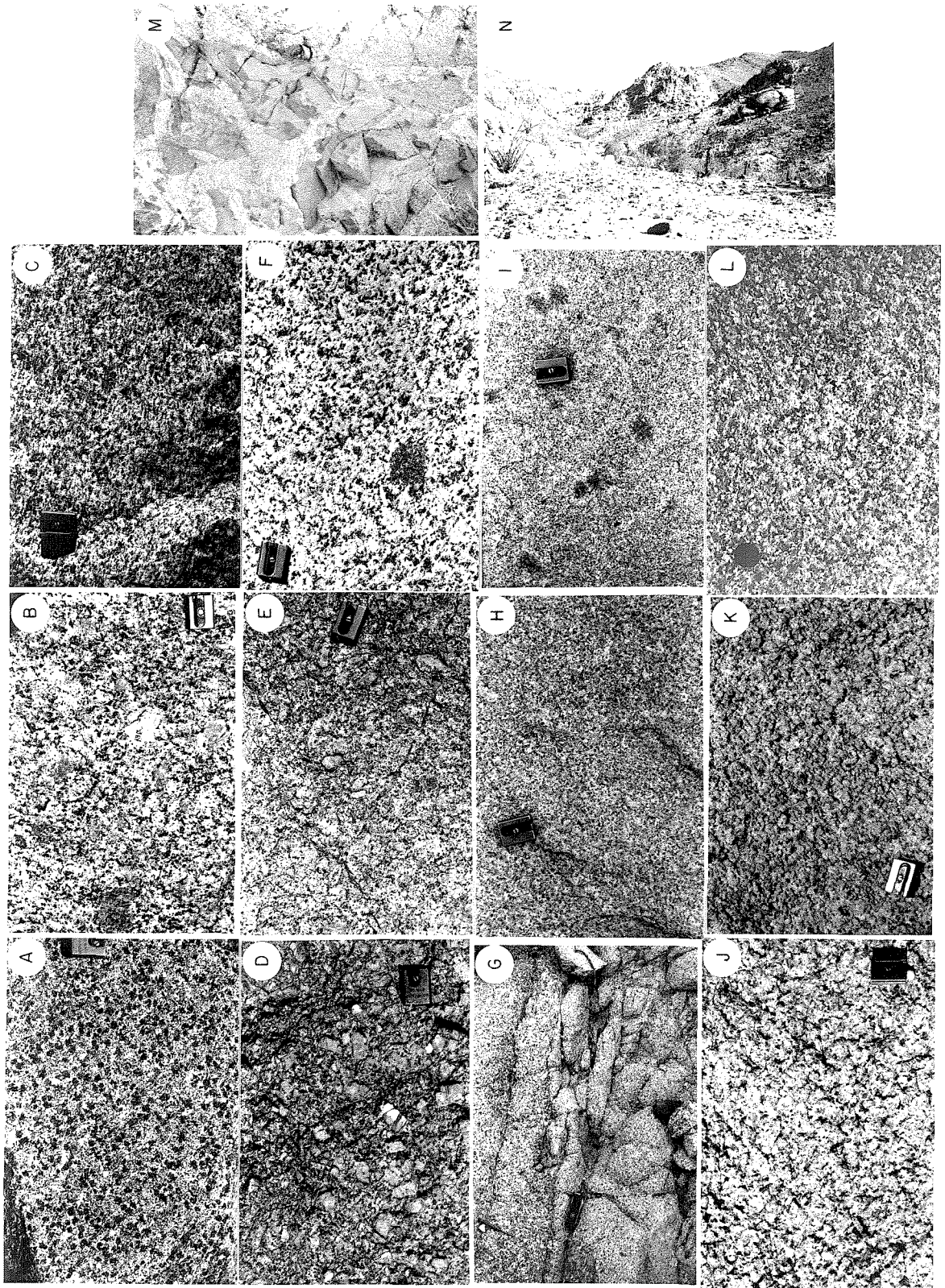
Two groups of rocks are assigned to the older batholithic suite. The older of these groups is composed of mafic to intermediate rocks including mafic hornblende-pyroxene and hornblende-biotite gabbros, diorites, and dark-colored monzodiorites. The younger group includes porphyritic monzogranite (quartz monzonite), equigranular monzogranite, and light-colored monzodiorites all characterized by the presence of hornblende and sphene in addition to biotite. Chlorite and epidote are ubiquitous and abundant alteration products in both groups. Both groups of rocks occur in a broad belt from the northeastern Eagle Mountains northward and northwestward through the central and western Pinto Mountains (Plate I). Still farther north, the rocks continue into the Mojave Desert (Dibblee, 1964b,c, 1966, 1967b,c,d,e,g, 1968c, 1970a; Dibblee and Bassett, 1966a,b). In general, the gabbro-diorites lie to the southwest and the monzogranites to the northeast within this belt. Fragments of the belt of gabbro-diorite occur as pendants and screens within the Cretaceous(?) batholithic belt from the southeastern Chuckwalla Mountains northwestward through the Chuckwalla and Eagle Mountains (Plate I).

Gabbro-Diorites

Field Relations. From diking and inclusion relationships, it is clear that the gabbro-diorites are the oldest lithologic unit of the two suites of Mesozoic intrusive rocks outlined above. In the Chuckwalla and southern Eagle Mountains, gabbro-diorites are intruded by all of the Cretaceous(?) plutonic lithologies (e.g., Figure 5-1M); in the northern Eagle and central Pinto Mountains gabbro-diorites are intruded by Jurassic porphyritic quartz monzonite. No systematic distribution of textural or

Figure 5-1. Outcrop photographs of textures and intrusive relationships of plutonic rocks of the Mesozoic batholithic suites.

- A. "Leopard-spot" hornblende gabbro-diorite of the older batholithic suite, northeastern Chuckwalla Mountains.
- B. Porphyritic monzogranite of the older batholithic suite, central eastern Chuckwalla Mountains.
- C. Lineated hornblende-biotite-sphene granodiorite of the younger batholithic suite, Corn Springs Wash, Chuckwalla Mountains.
- D. Coarse-grained porphyritic monzogranite of the younger batholithic suite, central northern Orocochia Mountains.
- E. Coarse-grained porphyritic monzogranite of the younger batholithic suite, northeastern Chuckwalla Mountains.
- F. Coarse-grained porphyritic monzogranite of the younger batholithic suite, southwestern Cottonwood Mountains.
- G. Coarse-grained porphyritic monzogranite intruded by finer-grained porphyritic monzogranite with scattered pea-sized phenocrysts of K-feldspar, upper Corn Springs Wash, central Chuckwalla Mountains. Contact is nearly vertical with up toward the right of the photograph.
- H. Finer-grained porphyritic monzogranite with scattered pea-sized phenocrysts of K-feldspar.
- I. "Polka-dot" granite phase of finer-grained porphyritic monzogranite, upper Corn Springs Wash, central Chuckwalla Mountains. Bluish-black clots of biotite + quartz rimmed by leached zones of quartz + feldspar.
- J. Coarse-grained nonporphyritic monzogranite of the younger batholithic suite, northeastern Chuckwalla Mountains.
- K. Coarse-grained nonporphyritic monzogranite of the younger batholithic suite, northeastern Orocochia Mountains.
- L. Coarse-grained nonporphyritic monzogranite of the younger batholithic suite, northwesternmost Hexie Mountains.
- M. Inclusions of hornblende gabbro of the older batholithic suite in coarse-grained porphyritic monzogranite of the younger suite, northwestern Chuckwalla Mountains.
- N. Jointed medium- to coarse-grained nonporphyritic monzogranite of the younger batholithic suite intrusive into dark-colored Augustine gneiss, Ship Creek, eastern Chuckwalla Mountains.



mineralogic varieties has been recognized within the gabbro-diorite map unit (Plate I), but the rocks were not mapped in detail sufficient to exclude the possibility of a pattern.

Petrography. Modally, the gabbro-diorites range from quartz-bearing mafic-rich hornblende gabbro to diorite and monzodiorite. Modes are tabulated in Table 5-I, and plotted on QPK and QFM ternary diagrams in Figure 5-2. Texturally, most of the mafic rocks can be classified as one of two varieties: one characterized by stubby equant to tabular hornblende crystals, the other by prismatic to acicular hornblende crystals. Both categories contain rocks that range in color index from about 50 to >95. Where its color index is relatively low, the stubby hornblende unit has a spotted, leopard-skin appearance (Figure 5-1A). The rocks with high color index are hornblendites. Mafic-rich gabbros with acicular hornblende sporadically show an igneous layering defined by planes of otherwise randomly oriented hornblende crystals. This layered texture elsewhere has been interpreted to indicate crystal accumulation. More commonly, hornblendes in the prismatic-acicular unit are unoriented in three dimensions. The grain-size of the stubby hornblende unit ranges from 3-5 mm to 3-4 cm. Grain-size in the prismatic hornblende unit is generally medium-grained.

Mafic minerals in the gabbro-diorites are, in the order of their abundance, hornblende, biotite, pyroxene, and rarely olivine. Hornblende is pleochroic from brown to greenish-brown. In some thin-sections, the brown pleochroic hornblende is partially rimmed by green pleochroic hornblende; in other sections, green to brown pleochroic hornblende surrounds cores of secondary chlorite, epidote, and sphene. Where pyroxene

Table 5-I. Modes of samples from the older batholithic suite.

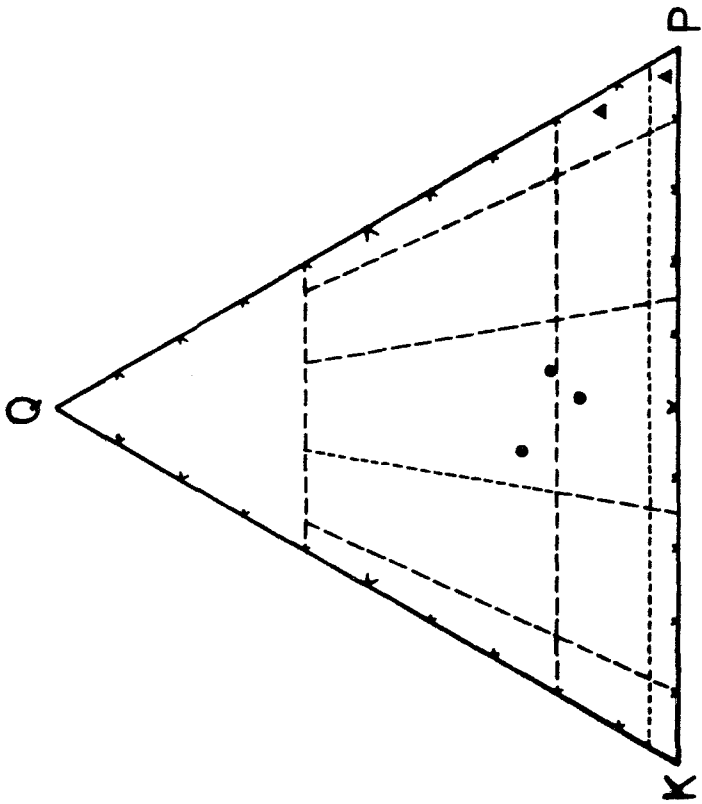
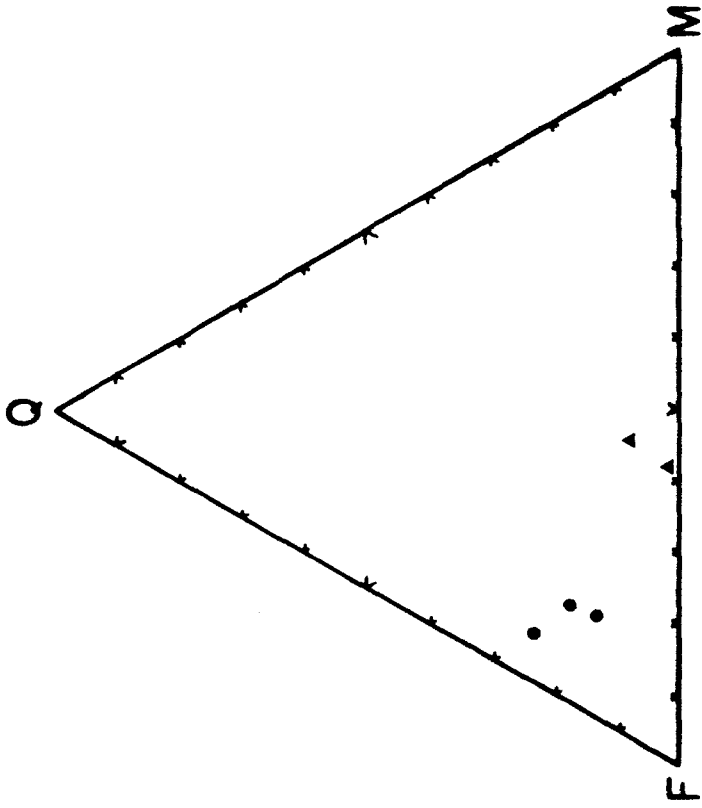
Sample*: (Points)	Gabbro-diorite		Porph. Monzogranite		
	<u>E-33</u> (1858)	<u>Chk-36</u> (2062)	<u>P-1</u> (3080)	<u>P-2</u> (3091)	<u>E-19</u> (1522)
Quartz	1.0	7.3	14.8	17.4	13.3
K-feldspar	1.7	1.2	31.1	29.2	34.2
Micrographic intergrowths	--	--	16.5	--	--
Plagioclase	52.0	48.5	28.5	37.8	36.7
Clinopyroxene	3.6	--	--	--	--
Hornblende	28.3	24.6	5.4	9.0	4.2
Biotite	--	10.7	--	4.0	6.2
Chlorite	1.4	0.1	0.1	0.2	3.1
Epidote	4.4	2.2	0.9	0.7	tr
Sphene	1.0	3.0	0.7	--	1.0
Apatite	0.3	0.8	--	0.05	tr
Opaques	6.3	1.6	1.8	1.6	1.3
Zircon	--	tr	0.1	0.05	tr
Allanite	--	--	0.1	--	tr

* Chk - Chuckwalla Mountains

E - Eagle Mountains

P - Pinto Mountains

Figure 5-2. Modes of older batholithic suite plotted on quartz-K-feldspar-plagioclase (QKP) and quartz-feldspar-mafics (QFM) ternary diagrams. Classification follows Streckeisen (1967). Triangles represent gabbro-diorites; circles represent porphyritic monzogranite.



or olivine is present, hornblende is invariably younger, generally rimming the pyroxene or olivine and replacing the pyroxene along fractures (Figure 5-3D). Where biotite is present, it is invariably younger than the hornblende (Figure 5-3C). Biotite is typically pleochroic from green to brown, and rarely from brown to red-brown. It has been observed in 2-3 cm poikilitic grains at some localities. Olivine and clinopyroxene occur sporadically, most commonly within hornblende crystals. Chlorite is usually present as an alteration product.

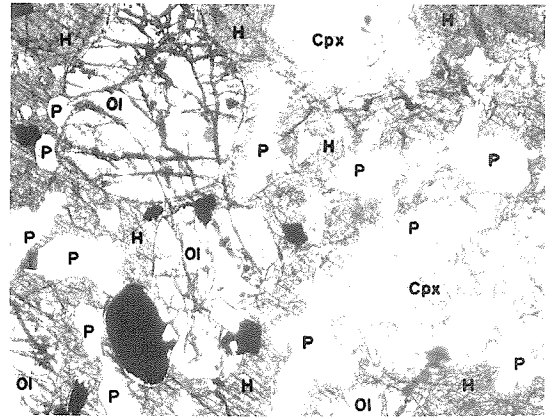
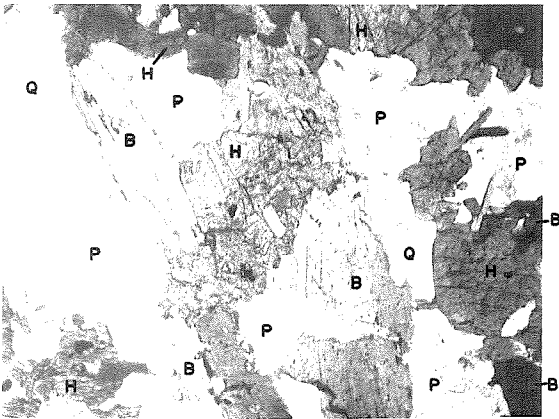
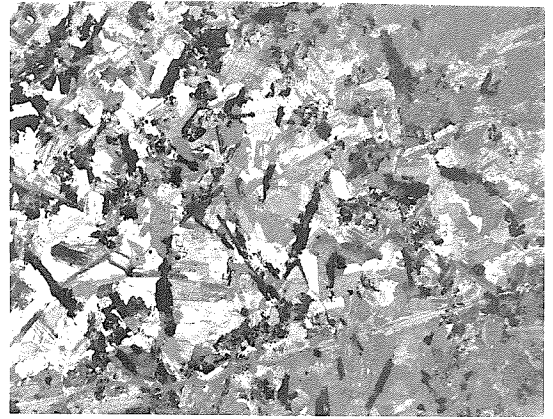
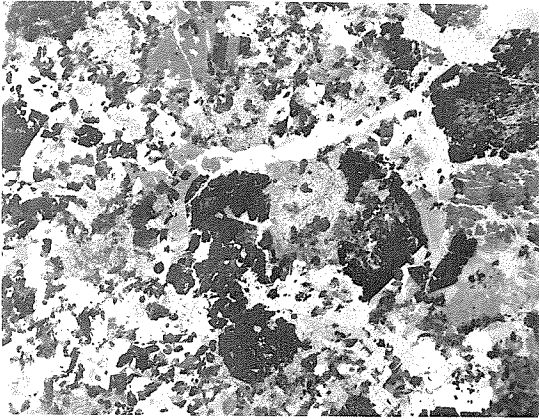
Plagioclase occurs as subhedral to euhedral zoned crystals or optically determined labradorite with saussuritized calcic cores of epidote, sericite, and chlorite. Oscillatory zoning is rare. Interstitial microcline is rarely microperthitic. Quartz is ubiquitous, but generally is present interstitially in volumes of less than 10%. Abundant epidote, euhedral sphene, and apatite are invariably present as accessories or alteration minerals. Opaques include probably magnetite-ilmenite with sphene overgrowths. Zircon is usually present; allanite and carbonate may be present.

Monzogranites (Quartz Monzonites)

Field Relations. At least three varieties of monzogranitic rock cross-cut the gabbro-diorite suite. The most abundant is porphyritic quartz monzonite that constitutes much of the northeastern Eagle and eastern Pinto Mountains. Locally, this lithology is complexly intermingled with finer-grained equigranular quartz monzonite and hypabyssal quartz monzonite porphyries throughout the two ranges, apparently related to proximity to the roof of the pluton. The porphyritic quartz monzonite is in turn intruded by a coarse- to very coarse-grained leuco-monzogranite in the

Figure 5-3. Photomicrographs of samples from the older batholithic suite.

- A. Top left. Gabbro-diorite: hornblende and sphene are dark-colored; plagioclase, K-feldspar, and quartz are light-colored. Sample Chkwal-31P: partially crossed nicols; horizontal field of 2.3 cm.
- B. Top right. Diorite: biotite, hornblende, and sphene are dark-colored; plagioclase, quartz, and K-feldspar are light-colored. Sample Chkwal-15P: partially crossed nicols; horizontal field of 2.3 cm.
- C. Center left. Gabbro-diorite: biotite (B) crystallized after hornblende (H); quartz (Q) + plagioclase (P). Sample Chkwal-33P: uncrossed nicols; horizontal field of 2 mm.
- D. Center right. Gabbro: hornblende (H) poikilitically enclosing olivine (Ol), clinopyroxene (Cpx), and euhedral plagioclase (P). Sample Eagle-116P: uncrossed nicols; horizontal field of 2 mm.
- E. Bottom. Porphyritic monzogranite: K-feldspar + plagioclase + quartz + biotite + hornblende + sphene. Sample Eagle-19P: crossed nicols; horizontal field of 2.7 cm.



Eagle Mountains, and possibly in the Pinto Mountains as well where the lithology has been seen in float. Intrusive quartz porphyry cross-cuts the gabbro-diorites in the Eagle and Pinto Mountains along a trend roughly parallel to and slightly southwest from their contact with the porphyritic quartz monzonite. No sequencing relationship was found between the quartz porphyry monzogranites and the porphyritic quartz monzonites, however, nor was an exhaustive effort made to find a mutual contact.

Petrography. The porphyritic quartz monzonite and quartz monzonite porphyry are both characterized by 1-4 cm euhedral, tabular phenocrysts of pink potassium feldspar with a distinct lavender cast. The leucomonzogranite has similarly colored potassium feldspar. Carlsbad twinning is common. In thin-section (Figure 5-3E), the phenocrysts are microcline, in places microperthitic. Microcline also occurs in the groundmass. Plagioclase occurs as subhedral to euhedral zoned grains, usually sericitized. Quartz is present as interstitial grains in the groundmass of the porphyritic quartz monzonite and also as phenocrysts in the quartz monzonite porphyry. Locally, the quartz grains are recrystallized sutured aggregates of subgrains showing the effect of slight deformation. Hornblende is pleochroic green to yellowish-brown, subhedral to euhedral, and usually somewhat altered. Biotite is pleochroic green to brown, rarely red-brown. Both hornblende and biotite are partially altered to chlorite. Veinlets and anhedral of epidote and carbonate are also secondary. Sphene occurs as large euhedral to subhedral crystals and as rims around opaques (magnetite-ilmenite?). Zircon, apatite, and allanite are present as accessories. Modal abundances for the porphyritic quartz monzonite are listed in Table 5-I, and presented in ternary diagrams

in Figure 5-2.

In hand specimen, the intrusive quartz porphyry is a very fine-grained gray rock characterized by scattered 2-5 mm rounded phenocrysts of quartz. This rock has not been examined in thin-section.

Summary

The modal mineralogy of rocks assigned to the Jurassic(?) batholithic suite shows a continuous variation on both the QKP and QFM ternary diagrams. In correspondence with the intrusive sequence, the rocks become more potassic and more silicic; less calcic and less ferromagnesian. The relatively high abundance of K_2O -bearing minerals (biotite and K-feldspar) in the gabbro-diorites with low silica and the relatively low quartz content of the monzogranites suggest that the suite is alkalic. Characteristic alteration gives the rocks of this suite a distinct green cast and has yielded abundant chlorite, epidote, and calcite, the latter two found in veins as well as disseminated within the rock. In addition to being more altered, the Jurassic(?) intrusives are more extensively fractured and usually weather darker (more thoroughly coated with desert varnish) than the Cretaceous(?) intrusive rocks.

Localized zones of gneissose plutonic rocks occur within the Jurassic(?) batholith, but since there is no evidence for throughgoing external deformational zones, the fabrics are thought to represent internal protoclastic deformation.

CRETACEOUS(?) BATHOLITHIC SUITE

The younger suite of batholithic rocks within the field area comprise three principal lithologies that are distributed in northwest-southeast-trending belts (Plate I). At the present level of exposure, these lithologies are not continuous, but rather consist of a series of aligned, commonly elongate plutons. Throughout the length of the Eastern Transverse Ranges south of the Pinto Mountain fault, these lithologies have consistent intrusive sequencing relationships. All of the plutons are epizonal with sharp, clear-cut contacts. Xenoliths, where they occur, are well-defined, unassimilated blocks.

Hornblende-Biotite Granodiorite

Field Relations. The oldest intrusive lithology within the younger batholithic suite is hornblende-biotite-sphene granodiorite (Figure 5-1C). It is exposed in four separate elongate plutons that comprise a belt from the Little Chuckwalla Mountains through the Chuckwalla, Eagle, Hexie, and Little San Bernardino Mountains (Plate I). The southeasternmost pluton is situated just north of Graham Pass at the juncture of the Little Chuckwalla and Chuckwalla Mountains. It intrudes mangerite-jotunite and retrograded granulites of the San Gabriel terrane. Texturally, the rock is medium-grained, hypidiomorphic granular with stubby to acicular hornblende and euhedral biotite, which is characteristic of this lithology where it is undeformed.

A larger pluton occurs farther north in the eastern Chuckwalla Mountains from just south of the Aztec Mine fault northward across the Ship Creek and Corn Springs Wash faults. It has intruded both the San Gabriel and Joshua Tree terranes and the Red Cloud thrust system. The

southern two-thirds of this pluton is undeformed, the northern third has been pervasively lineated (with a westnorthwest orientation; see Plate I) and foliated (Figure 5-1C). The cause of this deformation is not understood, but it must post-date the intrusion of the granodiorite and pre-date the intrusion of undeformed quartz monzonite. It seems likely that the deformation is related to the emplacement of the hornblende-biotite granodiorite.

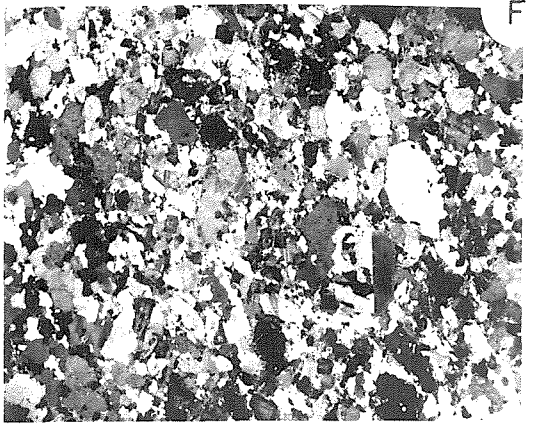
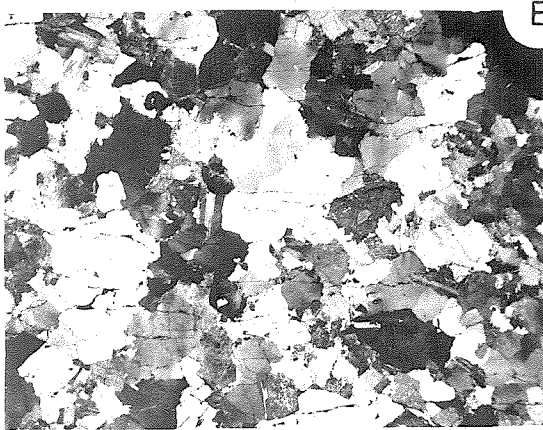
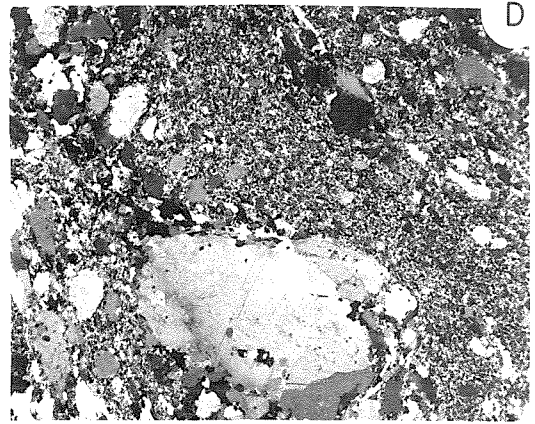
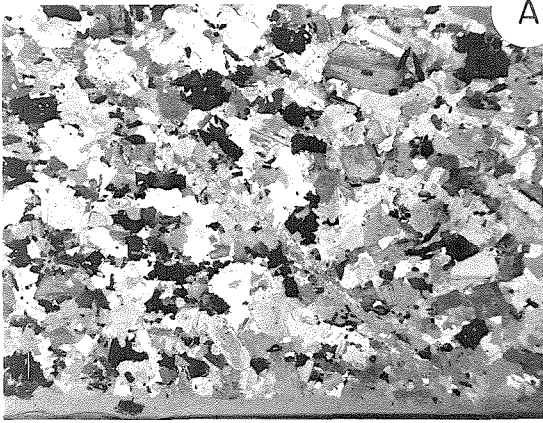
At the south margin of the Pinto Basin in the Eagle and Hexie Mountains in Joshua Tree National Monument another deformed pluton of granodiorite intrudes rocks of both the San Gabriel and Joshua Tree terranes and the Red Cloud thrust system. The eastern margin of this pluton in the northwestern Eagle Mountains has a more mafic-rich border phase. Granodiorite dikes from this body cross-cut both gabbro-diorite and quartz monzonite of the Jurassic batholithic suite in the north-central Eagle Mountains. This granodiorite has been described by Hope (1966, 1969). In addition a small pluton intrudes the Jurassic plutonic rocks at the western margin of the Eagle Mountain Mine area (Plate I).

The fourth granodiorite pluton cross-cuts rocks of the San Gabriel and Joshua Tree terranes and the Red Cloud thrust system in Pleasant Valley between the Hexie and Little San Bernardino Mountains south of the Blue Cut fault and in the Little San Bernardino Mountains north and south of the fault. This pluton has also been described by Hope (1966, 1969). Approaching the lip of the Little San Bernardino escarpment, this pluton becomes increasingly foliated and lineated until it is pervasively and intensely cataclased in the face of the escarpment (Figure 5-4A,B).

Petrography. Modes of thin-sections from each of the hornblende-biotite

Figure 5-4. Photomicrographs of undeformed and cataclastic samples from the younger batholithic suite.

- A. Undeformed hornblende-biotite-sphene granodiorite. Sample Eagle-62P: partially crossed nicols; horizontal field of 2.7 cm.
- B. Deformed granodiorite from the cataclastic zone of the Little San Bernardino Mountains. Sample L. San Berdo-20P: crossed nicols; horizontal field of 1.8 cm.
- C. Undeformed coarse-grained porphyritic monzogranite. Sample Orocop-26P: crossed nicols; horizontal field of 2.1 cm.
- D. Deformed porphyritic monzogranite from the cataclastic zone of the Little San Bernardino Mountains. Sample L. San Berdo-5P: crossed nicols; horizontal field of 1.8 cm.
- E. Undeformed coarse-grained nonporphyritic monzogranite. Sample Eagle-61P: crossed nicols; horizontal field of 2.5 cm.
- F. Deformed nonporphyritic monzogranite from the cataclastic zone of the Little San Bernardino Mountains. Sample L. San Berdo-13P: crossed nicols; horizontal field of 1.7 cm.



granodiorite plutons are tabulated in Table 5-II, and plotted in Figure 5-5. The rock is hypidiomorphic-granular and medium-grained (Figure 5-4A). Homogeneously distributed biotite (5-10%), hornblende (5-10%), and sphene (< 1%) in a light matrix of more abundant quartz-feldspar (75-85 %) give the rock a speckled appearance. Subhedral to euhedral plagioclase is oscillatory zoned sodic andesine compositionally within the range An 30-38. More calcic cores tend to be saussuritized. Myrmekite may be present. Potassium feldspar is microcline and micro-perthitic microcline that is interstitial and poikilitic. Anhedral interstitial quartz constitutes 20-30 % of the rock.

Hornblende is subhedral to euhedral, prismatic, and pleochroic green to greenish brown. It commonly contains inclusions of biotite as well as quartz and feldspar. Biotite is also pleochroic green to brown, but somewhat ragged and typically intersheaved with secondary chlorite. Euhedral to subhedral sphene is invariably present. Apatite, zircon, and opaques are always present as accessories. Allanite is usually present.

Porphyritic Monzogranite (Quartz Monzonite)

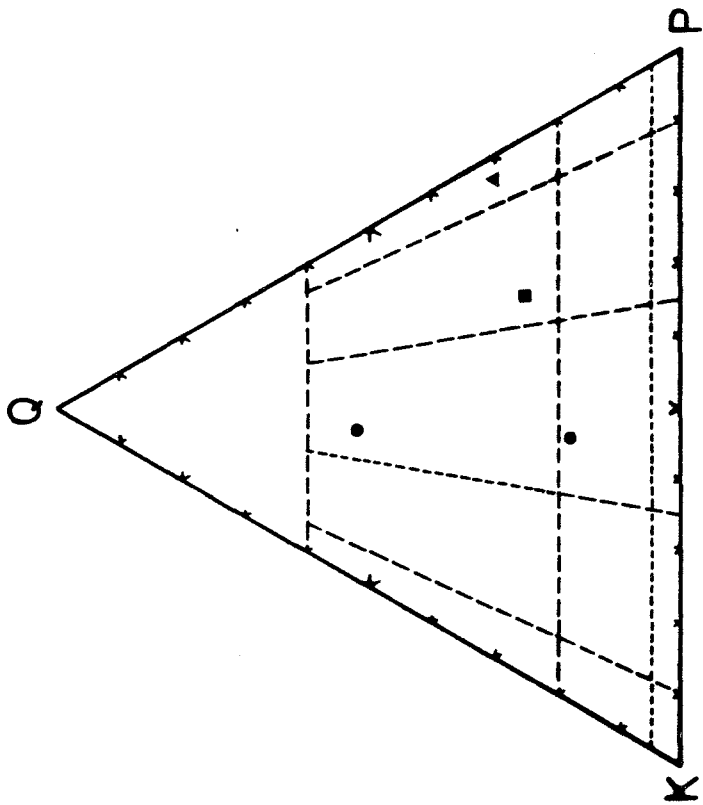
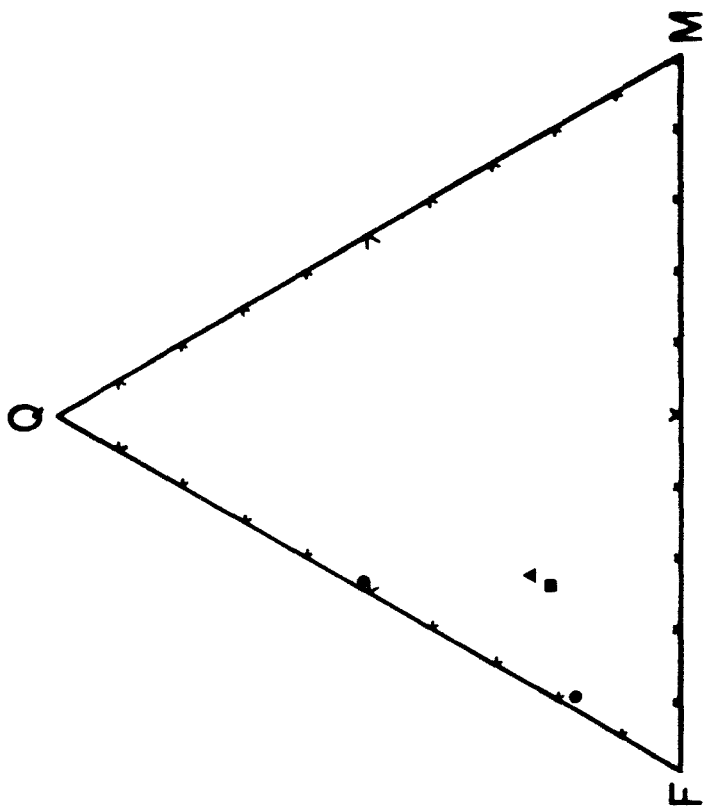
Field Relations and Petrography. The next youngest lithology within the Cretaceous(?) batholithic suite is porphyritic monzogranite. This lithology occurs in plutons in the northern Chuckwalla, Orocopia, Eagle, Cottonwood, and Little San Bernardino Mountains (Plate I). It appears equivalent to the Fargo quartz monzonite farther north in the Little San Bernardino Mountains (Hope, 1966, 1969) and porphyritic parts of the White Tank quartz monzonite in Pinto and Little San Bernardino Mountains (Rogers, 1961; Dibblee, 1967d, 1968c). In the Chuckwalla, Eagle, and Little San Bernardino Mountains, apophyses and inclusions clearly indicate

Table 5-II. Modes of samples from the younger batholithic suite.

Sample*: (Points)	Tonalite	Granodiorite	Monzogranite	
	<u>LSB-1</u> (1090)	<u>E-62</u> (2163)	<u>E-39</u> (2116)	<u>E-61</u> (1713)
Quartz	24	21.1	17.4	50.8
K-feldspar	4	18.6	44.0	26.1
Plagioclase	56	43.9	35.4	20.5
Hornblende	9	7.8	—	—
Biotite	6	7.6	0.9	1.7
Sphene	1	0.3	—	0.2
Chlorite	—	—	1.1	—
Epidote	tr	tr	tr	0.1
Apatite	—	0.1	0.1	tr
Opaques	tr	0.6	1.0	0.6
Zircon	tr	tr	0.1	tr

* LSB - Little San Bernardino Mountains
E - Eagle Mountains

Figure 5-5. Modes of younger batholithic suite plotted on quartz-K-feldspar-plagioclase (QKP) and quartz-feldspar-mafics (QFM) ternary diagrams. Classification follows Streckeisen (1967). Circles represent monzogranite, squares represent granodiorite, and triangles represent tonalite.



that this lithology intrudes the hornblende-biotite granodiorite. The porphyritic monzogranite consists of two subunits, each of which varies somewhat in mineralogy and texture. The older of these subunits is coarse- to very coarse-grained porphyritic monzogranite with 2- to 8-cm, zoned, Carlsbad-twinning phenocrysts of potassium feldspar (Figure 5-1D, E,F). Rapakivi overgrowths of plagioclase are locally present. The potassium feldspar phenocrysts are usually a light flesh-colored pink, but at a few localities, such as the northeastern Chuckwalla Mountains, they have a lavender cast similar to those of the Jurassic(?) monzogranites. (The intrusive sequencing with respect to the hornblende-biotite granodiorite is unmistakable). Biotite is the typical mafic mineral, but hornblende may be present. Quartz is usually abundant, but at a few restricted localities it is sufficiently scarce to render the rock a monzonite. In thin-section (Figure 5-4C), the rock is hypidomorphic porphyritic.

The younger sub-unit consists of a finer-grained porphyritic monzogranite with scattered pea-sized (.5 to 1.5 cm) phenocrysts of potassium feldspar (Figure 5-1G,H). This lithology can be seen to cross-cut the coarser-grained porphyritic monzogranite in the upper reaches of Corn Springs Wash (Figure 5-1G), in the central and eastern Orocopia Mountains, and in the southernmost Little San Bernardino Mountains. It grades transitionally into fine-grained, equigranular monzogranite to granodiorite (Figure 5-1I). At localities in the central and eastern Orocopia Mountains, in the north-central and eastern Orocopia Mountains, and in the north-central Chuckwalla Mountains in Corn Springs Wash, this last lithology contains spherical bluish-gray clots of quartz, biotite, and muscovite commonly surrounded by white zones from which all mafics have

been removed (Figure 5-1I). These clots, generally 2-5 cm in diameter, have not been examined in thin-section, but similar clots have been studied in detail by Ehlert and Ehlig (1977), who have sought to use occurrences of this distinctive "polka-dot granite" in outcrop and as clasts in conglomerates to constrain offset along the San Andreas fault (see also Smith, 1977). These authors report relict cordierite in some clots. The results of this study extend the known exposure of "polka-dot granite" into the Chuckwalla Mountains, and place the "polka-dot" rock in a temporal and spatial relationship to regional batholithic belts.

All of the above lithologies are shown on Plate I as part of the porphyritic monzogranite unit. Each of them becomes increasingly cataclasized westward over the lip of the Little San Bernardino escarpment (e.g., Figure 5-4D; see Chapter VI).

Monzogranite (Quartz Monzonite)

Field Relations and Petrography. The youngest lithology within the Cretaceous(?) batholithic suite consists of medium- to very coarse-grained non-porphyritic monzogranite (Figure 5-1J,K,L). The unit occurs as a belt of two or three plutons in the northern Chuckwalla and Orocopia Mountains, in the southern Eagle and Cottonwood Mountains, and in the western Pinto Mountains where it includes most of the White Tank quartz monzonite (Miller, 1938; Rogers, 1961; Hope, 1966, 1969; Dibblee, 1968c) (Plate I). The lithology takes on little desert varnish so that it forms light-colored exposures in contrast to the generally much darker country rock (Figure 5-1N). In fresh hand-specimen, the rock is pinkish-gray. This unit typically contains abundant quartz (20 to 50%) and subequal amounts of potassium feldspar (microperthitic microcline), and

plagioclase (zoned oligoclase), with potassium feldspar slightly more abundant. Biotite, usually altered to chlorite, is present in very small amounts (< 5%). Modes are listed in Table 5-II and plotted in Figure 5-5. In thin-section, (Figure 5-4E), the monzogranite is hypidiorhombic-granular coarse-grained equigranular to seriate porphyritic. Microcline phenocrysts are rare, and the weathered rock disintegrates to guss. Apophyses and inclusions clearly indicate that this lithology intrudes the hornblende-biotite granodiorite and the porphyritic monzogranite in the northern Chuckwalla Mountains, in the southern Eagle Mountains, in the Cottonwood Mountains, and in the Orocopia Mountains. In the Orocopia Mountains, the biotite monzogranite grades transitionally into very coarse-grained muscovite monzogranite. This lithologic unit also becomes cataclased at the lip of the Little San Bernardino escarpment (Figure 5-4F; see Chapter VI).

Summary

Petrographically, the lithologies of the younger batholithic suite have a calc-alkaline character, with abundant K_2O -bearing minerals (biotite and K-feldspar) in rocks with intermediate to abundant quartz content. This character contrasts with that of the older batholithic suite in which abundant K_2O -bearing minerals are present in rocks with relatively low quartz content.

Within the southern Eastern Transverse Ranges, each of the three lithologies of the younger batholithic suite occurs in multiple plutons. The plutons of each lithology are aligned in belts that trend approximately southeast from the Little San Bernardino-Pinto Mountains to the Orocopia and Chuckwalla Mountains. The discontinuous belts formed by

the three lithologic types of plutons are braided so that the relative spatial position of the different lithologies changes along strike. At the present level of exposure, average contact attitudes, where they can be obtained (Plate I), consistently dip southwestward at approximately 40 to 50° (except at the tops of the plutons). In cross-section, the units of the Cretaceous batholithic suite are shown with this dip. Extensive distribution of plutonic units with distinct mineralogical and textural characteristics and a consistent sequence of relative ages is common in subduction-related magmatic arcs and has been reported in the Peninsular Ranges (Larsen, 1948; Everhart, 1951), the Sierra Nevada (Bateman and Dodge, 1970), and the Coastal batholith of Peru (Cobbing and Pitcher, 1972; Cobbing et al., 1977; Pitcher, 1978). The recognition of lithologic belts within the Mesozoic batholithic suites through a large portion of the Eastern Transverse Range provides potential constraints for palinspastic reconstructions along the Cenozoic faults that bound the province. This potential will be discussed further in Chapter VI.

DIKES

Introduction

The crystalline basement terrane of Province II (Figure 6-1) is cross-cut by a variety of post-batholithic dikes, presumably related to the Tertiary volcanism in the eastern and southern bounding regions of Province I (see Dibblee, 1967a; Crowe, 1978). Although no comparative petrography, geochemistry, or geochronology has yet been undertaken to test the validity of this presumption, most of the dikes do intrude plutons of the younger batholithic (K?) suite. Within the context of this study, the dikes have been mapped in five categories for the purpose of constraining offsets on the left-lateral fault system (Plate I):

1. Light-gray quartz latite dikes that intrude in a great dike swarm along the eastern flank of the Chuckwalla and Eagle Mountains and at scattered localities elsewhere in the Eastern Transverse Ranges;
2. Dark-gray trachyte dikes that intrude in swarms in the Chuckwalla Mountains;
3. A single popylitized dacite dike that is used as a displacement indicator for the Chiriaco fault;
4. Undifferentiated mafic to intermediate dikes;
5. Undifferentiated fine-grained felsites.

Quartz Latite Dikes

A swarm of northwest-trending, southwest-dipping silicic dikes intrudes the Cretaceous monzogranites in the northeasternmost Chuckwalla Mountains and the southeasternmost Eagle Mountains. These dikes weather light- to dark-brown with well-developed patinas of desert

varnish. Within the monzogranite plutons, the orientation of most of the dikes is parallel to a prominent joint set. To the southeast, the swarm disappears under the alluvium of Chuckwalla Valley on the northwestern flank of the Chuckwalla Mountains. To the northwest, it continues into the central Eagle Mountains, where it dies out before reaching the southern Pinto Basin. These dikes in the central Eagle Mountains, emplaced into Precambrian and Jurassic rocks, are near vertical and strike a little west of north. No quartz latite dikes have been mapped in the Pinto Mountains, but dikes of identical lithology and trend crop out north of the Pinto Mountain fault at Valley Mountain and sporadically to the northwest along the alluviated east flank of the westernmost ridge of the Bullion Mountains.

In hand specimen, fresh quartz latite is light to medium gray with a thin rind of chalky white altered rock (1 to 2 mm thick) covered with brown desert varnish (~ .2 mm thick) on weathered surfaces. The rock characteristically fractures conchoidally. Phenocrysts of quartz and feldspar are set in a siliceous aphanitic groundmass. In thin section, the rock is 80 to 85% matrix and 15 to 20% phenocrysts. Somewhat resorbed quartz phenocrysts are commonly euhedral and dipyramidally terminated. Potassium feldspar phenocrysts are perthitic microcline, commonly showing Carlsbad twinning. Plagioclase phenocrysts are sericitized zoned oligoclase. Yellowish green pleochroic biotite phenocrysts are slightly more abundant than hornblende and are typically partially altered to chlorite. White mica and opaques occur in trace amounts. The groundmass contains quartz, feldspar, micrographic intergrowths of quartz and feldspar, biotite, and white mica. Garnet may be present. Based on modal abundances of the phenocrysts, the

dikes are quartz latite (Table 5-III), although the composition of the matrix might make them rhyolite, as they were identified by Hope (1966).

The continuity of the voluminous northwest-trending quartz latite dike swarm indicates a regional extensional regime with the minimum principal stress axis oriented parallel to a northeast azimuth. In the eastern Chuckwalla Mountains, the trachyte swarm discussed below occurs with the same strike as the quartz latite swarm. Together, the swarms occur in a belt along the eastern margin of the Eastern Transverse Ranges south of the Blue Cut (see Chapter VI).

Trachyte Dikes

The trachyte occurs as dike swarms and long through-going dikes in the Chuckwalla Mountains. In hand specimen, it is a distinctive rock with creamy white to pinkish white potassium feldspar set in a very dark-gray, aphanitic groundmass. The feldspar phenocrysts are typically embayed and appear to be skeletal. They range in size from 2-3 mm to 2 cm and commonly make up 20-25% of the rock. Small phenocrysts of hornblende, biotite and rare quartz also occur. The rock has not been studied in thin-section.

Dacite Dike

A northeast-trending, vertical dacite dike forms the spine of Alligator Ridge immediately southwest of Desert Center. The dike, with a somewhat sinuous trace, is nearly continuous for a distance of 4 kilometers along the length of Alligator Ridge, extending from a few hundred meters southwest of Desert Center to the north-central flank of the Chuckwalla Mountains. Near the range, the surface expression of the dike is exposed in two or three en echelon segments. Northeast-

Table 5-III. Modes of samples from the quartz latite dike swarm.

	Chuckwalla Mts.	Eagle Mts.
Sample: (Points)	<u>Chk-3</u> (3790)	<u>E-16</u> (3756)
Matrix	80.5	84.3
Phenocrysts	<u>19.5</u>	<u>15.7</u>
Quartz	30.7	13.3
K-feldspar	32.2	38.8
Plagioclase	31.3	36.7
Hornblende	0.1	0.5
Biotite	3.5	1.7
Garnet	--	8.0
Chlorite	--	--
White mica	1.2	--
Opagues	1.0	1.0

trending exposures of an identical dacite dike in the southwesternmost Eagle Mountains also occur in apparently discontinuous segments inferred to have been offset from Alligator Ridge along the Chiriaco fault. For most of its length, the dike is 2-6 m thick.

In hand specimen, the dike is very light mottled greenish gray. The weathered surface is pitted with a well-developed layer of desert varnish about 0.1 mm thick, underlain by a 1 to 2 mm thick zone in which feldspar phenocrysts have a chalky white altered appearance. Texturally, the rock is 50-60% roughly equigranular phenocrysts (1-3mm) set in 40-50% siliceous, very fine-grained (0.1-0.3mm) matrix. Compositionally, the phenocrysts are approximately 50-60% feldspar, 20% biotite and chlorite, 10-20% quartz, and 5-10% epidote and sphene. Amphibole and garnet occur in trace amounts. In thin-section, the phenocrysts include zoned plagioclase, rare orthoclase, deeply embayed quartz, and biotite nearly completely altered to chlorite. The plagioclase is extensively sericitized, but where the degree of alteration permits, its composition has been optically determined to be oligoclase. The rock is propylitized, containing abundant secondary calcite, epidote, and chlorite in addition to sericite. Zircon, opaques, and euhedral sphene occur in trace amounts. Rutile occurs as inclusions in biotite and chlorite. No other dikes of this texture and mineralogy were found in the Chuckwalla or southern Eagle Mountains.

Other Dikes

Other dikes in the field area exhibit a variety of compositions and ages. They include undifferentiated mafic dikes throughout the field area that probably represent more than one age, but at least some of which

are younger than the dike swarms discussed above. Intermediate andesitic to dacitic dikes are found in the Chuckwalla and Eagle Mountains where they cross-cut plutons of both batholithic suites (see Hope, 1966). Undifferentiated fine-grained felsitic dikes without phenocrysts may also include more than one generation, but at least some dikes are younger than Cretaceous(?) plutons in the Chuckwalla Mountains.

VI. POST-BATHOLITHIC TECTONICS

INTRODUCTION: PRELIMINARY STATEMENT OF CONCLUSIONS

The argument has been presented earlier (Chapter I) that the Eastern Transverse Ranges, as a physiographic and structural province, evolved entirely within the Cenozoic era. Not only is the east-west physiographic grain of the ranges controlled by movement and erosion along Cenozoic left-lateral and normal faults, but the boundaries of the province occur along zones of transition from this left-lateral structural regime into contrasting adjacent Cenozoic structural regimes. This chapter will deal with the nature of these structural regimes and their boundaries, as well as with constraints for palinspastic reconstruction of Cenozoic structures imposed by lithologic and tectonic patterns within the pre-Cenozoic crystalline terranes. The framework for this discussion is presented briefly below, then elaborated upon in the sections that follow.

In terms of its Cenozoic geology, southeastern California, as bounded by the San Andreas and Garlock faults and by the Colorado River, can be classified in two parts (Figure 6-1):

1. A province characterized by the presence of extensive Cenozoic terrestrial volcanic and sedimentary deposits of Oligo-Miocene age that overlie a pre-Cenozoic crystalline basement;
2. A province characterized by pre-Cenozoic crystalline basement rocks with a virtual absence of lower to mid-Tertiary terrestrial volcanic and sedimentary deposits.

The transitions between the two provinces are abrupt, typically marked by buttress nonconformable overlap of the Tertiary stratigraphic sections of Province I onto the crystalline basement of Province II.

Figure 6-1. Index map of southern California showing the distribution of crystalline basement exposures, Cenozoic strike-slip faults, Cenozoic cataclastic zones (C), Cenozoic Vincent-Orocopia-Chocolate Mountain thrust (V, O, CM), and Provinces I (extensive Tertiary terrestrial sedimentary and volcanic cover) and II (devoid of Tertiary cover). See text for discussion.

Right-lateral faults:

San Andreas fault system: SA San Andreas fault
 SG San Gabriel fault
 SJ San Jacinto fault

Inferred to be right-lateral and part of the San Andreas fault system:

CW Clemens Well fault
 F Fenner fault
 SF San Francisquito fault

Mojave Desert:

BW Blackwater fault
 CA Calico fault
 CR Camp Rock fault
 H Harper fault
 HD Helendale fault
 HL Harper Lake fault
 L Ludlow fault
 LH Lockhardt fault
 LW Lenwood fault
 P Pisgah fault
 SH Sheep Hole fault

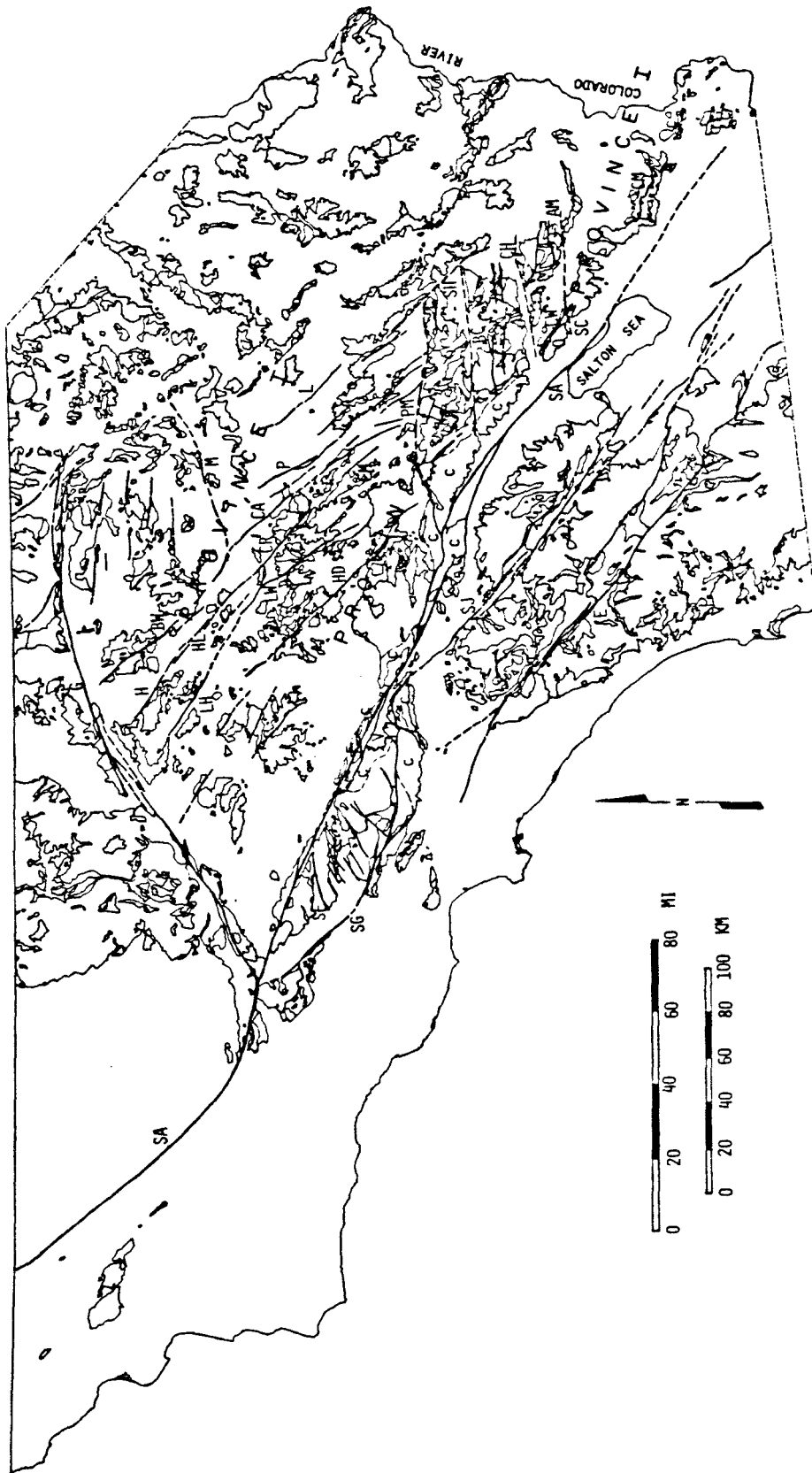
Peninsular Ranges:

E Elsinore fault
 SJ San Jacinto fault

Left-lateral faults:

Mojave Desert:

AM Aztec Mines Wash fault
 BC Blue Cut fault
 CH Chiriaco fault
 G Garlock fault
 M Manix fault
 PM Pinto Mountain fault
 SC Salton Creek fault



One segment of the provincial boundary, somewhat modified by younger faulting, occurs at the southern boundary of the Eastern Transverse Ranges.

As shown in Figure 6-1, the area mapped for this study lies within Province II, which consists of both the Eastern Transverse Ranges and the westernmost Mojave Desert from the Tehachapi Mountains southeastward to the Colorado River at Blythe. Each of these subregions of Province II forms a northwest-trending physiographic-structural belt roughly 50 kilometers wide. The Eastern Transverse Range belt is characterized by east-west left-lateral faults, whereas the western Mojave Desert belt is characterized by northnorthwest-trending right-lateral faults. The boundary between these two subprovinces marks the eastern limit of the Eastern Transverse Ranges. The pattern of the right- and left-lateral faults permits the interpretation that they form a conjugate set of strike-slip faults. Because these faults cross-cut the Tertiary stratigraphy of Province I and the bounding buttress nonconformities, their development must be at least partly younger than the evolution of the boundary between the two provinces.

The western margin of the Eastern Transverse Ranges occurs at a structural transition of a different nature than the change in fault orientation (from east-west left-lateral to northnorthwest right-lateral) that marks the eastern boundary. Ostensibly the western margin is marked by the San Andreas fault, but observations made in this study suggest that the east-west left-lateral faults lose their definition within a zone of cataclastic deformation a short distance east of the San Andreas fault (Figure 6-1). Deformation within this zone is at least partially synchronous with movement along the left-lateral faults.

With the exception of the Pinto Mountain fault, these faults do not appear to intersect the San Andreas fault, appearing rather to be absorbed within this zone of intensely fractured and brecciated rocks that trends northwest along the Little San Bernardino escarpment. As such, the Little San Bernardino Mountains are not strictly part of the Eastern Transverse Ranges province, insofar as that province is defined by the left-lateral faults.

Recorded within the cataclastic zone along the western margin of the Eastern Transverse Ranges is a sequence of Cenozoic deformational events that has been superimposed on some of the Mesozoic and Precambrian crystalline rocks described in preceding chapters. The earliest event produced a cataclastic foliation that has been imprinted on rocks as young as late Cretaceous(?). The fabric developed during this cataclastic event has been subsequently folded and, finally, severely fractured and brecciated. These structural responses are hypothetically linked to two regional tectonic features.

The cataclastic foliation is inferred to be related to the tectonic emplacement of the crystalline rock allochthon along the regional Vincent-Chocolate Mountain Thrust fault above a substrate of Pelona-type schist that is not exposed at the present level of erosion in the Little San Bernardino Mountains. During or following the emplacement of this allochthon, a regional antiform developed which folded the cataclastic fabric across what is now the Little San Bernardino escarpment (Figure 6-1). It is suggested here that this antiform, with its inferred core of mylonite and Pelona-type schist, together with all the antiformal exposures of Pelona-type schist recognized in southern California and southwesternmost Arizona, formed a continuous structural feature prior

to disruption by the Cenozoic strike-slip fault systems. If valid, the reconstruction of the antiform explicitly constrains offset along these faults, including the San Andreas fault. More precisely, rather than a single, regionally continuous antiformal structure, the feature is interpreted to consist of at least three en echelon doubly plunging(?) antiforms arranged nose-to-nose (see Plate VI-C). The northwest orientation of the reconstructed antiformal array implies a stress regime with a northeast-oriented maximum principal stress axis and a vertical minimum principal stress axis. Mid-Tertiary terrestrial and volcanic rocks are deformed in the synforms flanking the antiforms.

Later, under a continued or reactivated stress regime, the folded crystalline thrust plate appears to have been reactivated in the Eastern Transverse Ranges, with the mechanical response of the crystalline allochthon producing the array of left-lateral faults that defines the Eastern Transverse Ranges. The pattern and nature of these faults suggest the passive break-up of a brittle crystalline plate riding above a less brittle substrate. The substrate is inferred to be Pelona-type schist, and reactivation of a zone at or near the pre-existing Vincent-Chocolate Mountain thrust hypothesized to absorb differential deformation between the brittle plate and its substrate. It is further inferred that the differential mechanical response which results in the break-up of the crystalline plate into discrete, through-going faults is obstructed across the antiformal fold, resulting in a deformational response characterized by pervasive fracturing and brecciation.

Because the right-lateral faults of the westernmost Mojave Desert are interpreted to form a conjugate set with the left-lateral faults,

it can logically be concluded from the preceding arguments that a Pelona-type (Rand) schist substrate is implied for a region that extends as far north as the Garlock fault and at least as far northeast as a line from the Rand Mountains through Rice Valley near the Colorado River into Arizona. The axis of maximum principal stress for the conjugate fault system has the same northeast to eastnortheast orientation as that for the fold system described above, whereas the minimum principal stress axis is oriented northnorthwest.

This chapter concludes with an attempt to place these geologic observations and structural interpretations within the tectonic context of the plate margin interaction of North America and the Farallon and Pacific plates.

LEFT-LATERAL FAULTS IN THE EASTERN TRANSVERSE RANGES

Introduction

As discussed above, the east-west physiography that defines the Eastern Transverse Ranges is controlled by a series of parallel left-lateral strike-slip faults, including from north to south the Pinto Mountain, Blue Cut, Porcupine Wash-Substation, Smoke Tree Wash-Big Wash, Chiriaco, Corn Springs Wash, Ship Creek, and Salton Wash-Aztec Mines Wash faults (Figure 6-1; Plate I). Exceptions are the east-west thrust systems that delineate the northern and southern flanks of the San Bernardino Mountains. The reverse character of these thrust boundaries is more akin to the tectonic style of the western and central Transverse Ranges than to the high-angle strike-slip faults described below.

The east-west grain of this province was first noted by Hill (1928, p. 144-146, pl. I/II), who recognized three prominent physiographic lineaments that he concluded were fault-controlled. From north to south, Hill named these breaks the Pinto Mountain fault, Eagle Mountain lineament, and Orocopia lineament. They are discussed below as the Pinto Mountain, Blue Cut, and Chiriaco faults, respectively.

Hill (1928, p. 136-144, pl. I/II) incorporated these desert lineaments with several east-west coastal faults and lineaments into a physiographic-structural province that he called the great Transverse Belt. The coastal features include the Santa Ynez and Bouquet Canyon (San Francisquito) faults, and the Anacapa lineament, a prominent topographic break that includes the submerged escarpment south of the northernmost channel islands and the southern margins of the Santa

Monica and San Gabriel Mountains. Also included were the Banning fault in San Geronio Pass and an uncertain link between the Anacapa lineament and the Pinto Mountain fault through the southern San Bernardino Mountains. This synthesis constitutes the earliest recognition of the Transverse Ranges province.

Hill (1928, p. 137, 147-148) speculated that this transverse belt continued still farther southeastward as a lineament across southeastern California to the Colorado River between Blythe and Parker, then across Arizona and New Mexico along the southern edge of the Colorado Plateau, thus taking first note of much of the trace of what was later to be called the Texas lineament (Albritton and Smith, 1956). More recent maps (Bishop, 1964; Hope, 1966, 1969; Jennings, 1967, 1977) invalidate Hill's eastward extrapolation of Transverse Range structures. The eastern termination of the east-west structures at the Sheep Hole and Coxcomb Mountains is also apparent in Skylab orbital photographs (Silver et al., 1977b, figs. 4-4, 4-5) (Figure 1-1A,B).

Pinto Mountain Fault

The northern margin of the Little San Bernardino and Pinto Mountains forms a prominent east-west lineament from Yucca Valley on the west to Dale Lake and the Sheep Hole Mountains on the east, a distance of about 85 kilometers. West of Yucca Valley, Allen (1957) mapped the trace of the Pinto Mountain fault along the northwest side of Morongo Valley into Big Morongo Canyon, then through the southernmost San Bernardino Mountains to merge with the Mission Creek fault near the confluence of the North and South forks of Whitewater River. Allen notes scarps, springs, and ground water damming indicative of recent activity on the Pinto

Mountain fault at the north of Big Morongo Canyon. Dibblee (1967f) has mapped similar relationships.

More recent studies (Hope, 1966; Dibblee, 1967d, 1968c) indicate that the Pinto Mountain fault has also been recently active between Yucca Valley and its juncture with the northwest-trending right-lateral Mesquite fault just east of Twentynine Palms. Scarps in alluvial fans are found along this segment, and ground-water damming occurs at the linear Twentynine Palms oasis. No indications of recent activity have been recognized east of the Mesquite fault, although the continued linear escarpment along the north edge of the Pinto Mountains is probably fault-controlled. Since there is no east-west break through the crystalline rocks of the southern Sheep Hole or Coxcomb Mountains immediately east of the Pinto Mountains, the Pinto Mountain fault and its eastward extension must terminate at the northwest-trending Sheep Hole fault.

Approximately 16 kilometers of post-Cretaceous(?) left-lateral strike-slip displacement along the Pinto Mountain fault has been documented by Dibblee (1967d,f, 1968b,c) based on offset crystalline-rock contacts and a quartzite-clast gravel inferred to have been shed from the San Bernardino Mountains across the Pinto Mountain fault prior to its movement. The quartzite clasts, however, may well have been derived from the Pinto quartzite in the central Pinto Mountains (Plate I).

Blue Cut Fault

The trace of the Blue Cut fault extends about 80 kilometers eastward from the central Little San Bernardino Mountains, through Pleasant Valley, between the Pinto and Hexie Mountains, then on through the length

of Pinto Basin. The fault is named for its exposure in Blue Cut in the Little San Bernardino Mountains (Pruss et al, 1959; Hope, 1966, 1969) and forms the central break in an array of faults responsible for Hill's (1928, p. 147) Eagle Mountain lineament (Hope, 1966, 1969).

The Blue Cut fault zone has been studied in detail by R.A. Hope (1966, 1969). Where the fault zone transects the Little San Bernardino and Hexie Mountains, erosion has produced fault-line valleys along Blue Cut and El Dorado Canyon, respectively. West of Blue Cut in the Little San Bernardino Mountains, scarps cut an old conglomerate. At the eastern end of Pleasant Valley and in the central Pinto Basin, deformed old alluvial sediments occur along the Blue Cut fault. Gouge zones a few meters thick are exposed in Blue Cut itself.

Hope (1966, 1969) has documented a left-lateral displacement of 5 to 6.5 kilometers along the Blue Cut fault zone. Additional crystalline-rock contacts established during the course of this study corroborate this offset (Plate I). There is some suggestion that the displacement increases eastward from 3 kilometers in the Little San Bernardino Mountains to 8 kilometers in the eastern Pinto Basin (Hope, 1966, p. 81-83).

At its western end, the Blue Cut fault has been interpreted to merge with the northwest-trending, steeply northeast-dipping Dillon fault (Hope, 1966, p. 86; 1969, p. D117). It seems likely, however, that the Dillon fault is merely one break or series of breaks within an extremely complex structural zone that forms the Little San Bernardino Mountain escarpment (see below).

As in the case of the Pinto Mountain fault, the eastern termination of the Blue Cut fault must occur at the Sheep Hole fault inasmuch as no trace of the fault occurs within the crystalline rocks of the Coxcomb

Mountains. Either the Blue Cut fault has been offset by the presumably right-lateral Sheep Hole fault, or the left-lateral displacement has been accommodated by penecontemporaneous right-lateral displacement along the Sheep Hole fault (cf. Hope, 1966, p. 89; 1969, p. D117).

The left-lateral displacement of crystalline bedrock patterns across the Blue Cut fault zone is attributed by Hope to movement along a main fault strand that is exposed in Blue Cut and El Dorado Canyon but is buried beneath Pinto Basin. In addition to this main break, Hope (1966, p. 56-67) describes several west-trending, normal-separation faults along the Blue Cut fault zone. These are range-bounding faults with scarps that face south along the north margin of the Blue Cut fault zone and north along its south margin. South-facing fault and/or fault-line scarps include the south flank of the northern Hexie Mountains facing Pleasant Valley, the south flank of the central Pinto Mountains facing the western Pinto Basin, and the south flank of the eastern Pinto Mountains facing the central Pinto Basin. North-facing range-front scarps include the north flank of the southern Hexie Mountain facing the western Pinto Basin and the north flank of the Eagle Mountains facing the eastern Pinto Basin. Vertical separation of Plio-Pleistocene(?) sediments and basalt flows on discontinuous faults along both margins of Pinto Basin provide evidence for young graben-like faulting associated with the Blue Cut fault (Hope, 1966, p. 61, 67, 91-2) (Plate I). The Blue Cut fault zone is thought to be seismically active (see Fuis et al., 1977, pl. 10).

Porcupine Wash and Substation Faults (Hexie and Eagle Mountains)

The Porcupine Wash fault extends eastward from the lip of the

Little San Bernardino escarpment for about 26 kilometers through the Hexie Mountains to the paved Pinto Basin Road through Joshua Tree National Monument, where it disappears within the alluviated granodiorite of the southernmost Pinto Basin (Plate I). Porcupine Wash has been eroded along the fault. Within the Hexie Mountains, the fault shows several splays and at its eastern end it becomes lost within the brecciated cataclastic zone of the Little San Bernardino Mountains. Hope (1966, p. 94) described a left-lateral separation of 2.4 kilometers based on the offset of a steep intrusive contact between granodiorite and gneiss. He observed small scarps in older alluvium, indicative of Quaternary(?) movements. The offsets shown on Plate I corroborate Hope's work.

The Substation fault transects the east-central Eagle Mountains in an east-west break that is 19 kilometers long. Hope (1966, p. 95) argues for 3 kilometers of left-lateral offset of the north-trending quartz latite (rhyolite) dike swarm. This displacement has been corroborated with additional contacts identified during the course of this study (Plate I).

Although the Porcupine Wash and Substation faults are aligned (Hope, 1966, 1969; Merifield and Lamar, 1975; Silver et al., 1977b) (Plate I) and their displacements are nearly equal, the two faults cannot be joined at the surface. As shown in Plate I, the intervening lithologies and contacts are not broken. Both of these fault zones are thought to be seismically active (see Fuis et al., 1977, pl. 10).

Smoke Tree Wash and Victory Pass Faults (Cottonwood-Hexie and Eagle Mountains)

The east-west reaches of Smoke Tree Wash and Pinkham Canyon are eroded along a left-lateral fault that disappears eastward beneath alluvium and dies out westward as it nears the Little San Bernardino Mountains. The fault offsets crystalline rock contacts about a kilometer, and has produced scarps in all but the youngest alluvium. The fault appears to offset the young basalt in the Cottonwood and Hexie Mountains (Plate I). To the east, evidence of faulting can be seen on the south margin of the narrow alluviated gap traversed by the jeep trail from Cottonwood Spring to Conejo Well. If this break is part of the Smoke Tree Wash fault, then the structure is about 25 kilometers long. A more northerly buried branch of the Smoke Tree Wash fault may pass through Smoke Tree Well, then east along the abandoned jeep trail across the Pinto Basin Road (Plate I).

The Victory Pass fault is situated in the southeastern Eagle Mountains 4 kilometers south of the Substation fault (Plate I). It controls much of the course of Big Wash and has a length roughly equal to that of the Substation fault (19 kilometers). At its eastern end, the fault passes beneath the alluvium of Chuckwalla Valley; at its western end, it dies out along the north margin of Big Wash. The fault left-laterally offsets the quartz latite (rhyolite) dike swarm and the trace of the early Red Cloud thrust 1.5 kilometers (Plate I).

As in the case of the Porcupine Wash and Substation faults, the Victory Pass and Smoke Tree Wash faults are not continuous at the surface (Plate I). Also, both faults appear to be seismically active (see Fuis et al., 1977, Pl. 10).

Chiriaco Fault

The linear physiographic rift that marks the course of the Chiriaco fault was first noted by Hill (1928, p. 147, pl. I/II) as part of his Orocopia Lineament. In order to avoid confusion with the Orocopia thrust, this name was abandoned during the course of this study in favor of Chiriaco fault. The name was chosen because the fault must pass approximately beneath Chiriaco Summit. Following Hill's lead, a number of investigators cited the linearity of the valley and its bounding escarpments, and, more recently, parallelism with known faults to the north, as evidence of fault-control (Hope, 1966, p. 97; Merifield and Lamar, 1975, p. 18). An east-west negative Bouguer gravity anomaly at the eastern end of the valley has been interpreted to reflect the presence of a fault in the subsurface (Biehler et al., 1964; Rotstein et al, 1976). Documentation of a left-lateral displacement of 11 kilometers for the Chiriaco fault marked the initial phase of this study (Powell, 1975) (Plate I).

The valley along the fault is relatively flat-bottomed with steep flanking escarpments that bound ranges to the north and south. Coalescing alluvial fans have been shed from both escarpments to merge in roughly axial topographic lows that drain both east and west. West of Chiriaco Summit the valley drainage is channelled westward to the Salton trough; east of the east end of Hayfield Lake it is channelled eastward to the Colorado River. Between Chiriaco Summit and the east end of Hayfield Lake, the drainage is channelled east or west into the small interior basin of Hayfield Lake. Hayfield Lake may be either a sag feature related to movement on the Chiriaco fault or a depression due

to aggradation of alluvial fans that block or dam exterior drainage. It is interesting to notice that the Salton Sea/Colorado River drainage divide in the Chuckwalla Mountains appears to be offset about 14 kilometers left-laterally from the equivalent drainage in the Eagle Mountains (Plate I), suggesting that movement on the Chiriaco fault may post-date the development of the divide. The intervening drainage divides in the Eagle and Orocopia Mountains are Colorado River/interior and Salton Sea/interior, respectively.

No surface expression of the Chiriaco fault has been found, except perhaps the rather straight southern margin of the west half of the Hayfield Lake aligned with the roughly linear northern margin of the eastern part of the lake. On aerial photographs, there appears to be a linear feature in the dry lake along a line between these aligned margins, but this feature has not been investigated on the ground.

Left-lateral separation along the Chiriaco fault is indicated by the consistent offset of a number of geologic features, including the trace of the steeply-dipping portion of the early Red Cloud thrust, the western contact of a Cretaceous(?) monzogranite pluton in the northern Chuckwalla and southern Eagle Mountains, and the quartz latite dike swarm in the southeasternmost Eagle Mountains and northeasternmost Chuckwalla Mountains (Plate I). Another important offset marker is the distinctive propylitized dacite dike that supports Alligator Ridge projecting from the north-central Chuckwalla Mountains and that transects the ridge-toes between the mouths of Difficult and Boulder Canyons in the southeasternmost Eagle Mountains (Plate I).

The northeast-trending, vertical dacite dike exposed along the crest of Alligator Ridge intersects the Chiriaco fault at an acute

angle that renders it a particularly effective indicator of offset along the fault. The continuity of the dike, together with its lithologic uniqueness in the Chuckwalla and southern Eagle Mountains leave little doubt that it was once a continuous or near-continuous feature. The dike is discussed in detail in a previous section of this chapter. If the dike exposures in the northern Chuckwalla and southeasternmost Eagle Mountains are interpreted as disrupted parts of a single prophyllitized dacite dike, and if the exposed traces are projected beneath the alluvium of Chuckwalla Valley to the subsurface trace of the Chiriaco fault shown in Plate I, then a left-lateral separation of 11 kilometers is indicated.

A roughly equivalent separation is indicated by the offset trace of the early Red Cloud thrust from Cholla Wash in the southern Eagle Mountains to the northwesternmost tip of the Chuckwalla Mountains (Plate I). This portion of the thrust, involved in a pre-batholithic overturned fold (Chapter IV), is vertical in the Chuckwalla Mountains and dips steeply westward in the lower reach of Cholla Wash. Precambrian granite gneiss of the Joshua Tree terrane is exposed east of the thrust; Hexie gneiss intruded by Soledad augen gneiss of the San Gabriel terrane occurs to the west.

The gently southwestward dipping quartz latite dike swarm exposed in the southeasternmost Eagle Mountains and in the northeasternmost Chuckwalla Mountains is offset only 9.5 kilometers. If there is no eastward decrease in strike-slip separation along the short (3 kilometer) segment of fault between its respective intersections with the prophyllitized dacite dike and the quartz latite dike swarm, then the

reduced offset of the dike swarm (with a dip of 30° SW) indicates a vertical component of displacement with the north side of the fault dropped approximately 1500 feet relative to the south side. Since the evidence for vertical separation exists only at the east end of the Chiriaco fault, it is possible that the magnitude or sense of vertical displacement changes along the fault.

Timing of fault movement is only broadly bracketed by offset of the TK(?) dikes and continuity of Holocene alluvium across the fault. None of the dikes involved has been dated isotopically, but they cross-cut Cretaceous(?) monzogranite. Along the south side of the fault, lithologies with offset equivalents are recognized only as far west as Chiriaco Summit (11 km farther west on the north side). Extrapolation of the fault to the west of Chiriaco Summit permits a narrower age bracket in that it appears to truncate the Eocene Maniobra and lower Miocene Diligencia formations first described by Crowell and Susuki (1959), and is covered by the Pleistocene(?) Ocotillo fanglomerate mapped by Dibblee (1954), Hays (1957), and Ware (1958). No seismic activity is known to occur along the Chiriaco fault or any of the more southerly left-lateral faults.

Corn Springs Wash Fault (Chuckwalla Mountains)

The course of Corn Springs Wash is largely controlled by erosion along another break of the east-west fault set. Left-lateral separation of about 2.5 to 3 kilometers can be seen in the offset of several contacts and lithologies associated with the Mesozoic batholithic rocks (Plate I). The western end of the fault swings northwestward to disappear beneath alluvium, after which it may either merge with the

Chiriaco fault in the subsurface, or swing westward again to connect with a fault along the north flank of the Orocopia Mountains.

At Corn Springs in the eastern Chuckwalla Mountains and at the point where the road to the microwave relay tower crosses the fault in the western part of the range, exposed segments of the fault plane show alluvial material to the south and southwest faulted against shattered Mesozoic batholithic rocks to the north and northeast. At both of these localities, three geomorphologic events post-date the most recent movement along the fault: deposition of a colluvial(?) unit a meter or two thick, then deposition of caliche, followed by fluvial downcutting to the present stream level. Superimposed alluvial fan systems in the Eastern Transverse Ranges exhibit spectacular differences in degree of development of desert pavement and desert varnish and in degree of dissection that seem to recur from range to range. A regional alluvial stratigraphy has been characterized by Shlemon and Purcell (1976) for the southeastern Mojave Desert and the Colorado River area. Although it has not been attempted during the course of this study, it may be possible to correlate the units which bracket movement on the Corn Springs Wash fault with this alluvial stratigraphy.

Ship Creek Fault (Chuckwalla Mountains)

Ship Creek Wash in the Chuckwalla Mountains is eroded along the east-west Ship Creek fault. The offsets of Precambrian and Mesozoic lithologies and contacts show about 2 kilometers of left-lateral separation (Plate I). Alluvial material is faulted against crystalline rock at at least two localities. At its west end, fault displacement dies out in a fold which left-laterally bends steeply-dipping lithologic

units within the San Gabriel terrane (Plate I). The magnitude of the bending matches the magnitude of displacement along the Ship Creek fault. The east end of the fault disappears beneath alluvial material east of the Chuckwalla Mountains.

Salton Wash and Aztec Mines Wash Faults

Just south of the main mass of the Chuckwalla Mountains, an unnamed wash cuts through the range. Because the Aztec Mines are situated just north of this wash where it debouches from the eastern flank of the range, it is informally referred to here as Aztec Mines Wash. The wash has eroded along an east-west fault that left-laterally offsets an intrusive contact between Cretaceous hornblende-biotite granodiorite and Precambrian rocks of the San Gabriel terrane about 8 kilometers (Plate I). The fault also appears to truncate interbedded lower Miocene volcanics and terrestrial sedimentary rocks overlying the crystalline basement south of the fault. The volcanic rocks in this section are about 25 m.y. old (Crowe et al., 1979). The fault does not appear to significantly offset the relatively old alluvial unit exposed at the drainage divide southeast of Gulliday Wash.

The Aztec Mines Wash fault is aligned with the Salton Creek fault between the Orocopia and Chocolate Mountains as mapped by Crowell (1962). Murray, Bell, and Crowe (1976) cite evidence that crystalline rocks in the Chocolate Mountains south of the fault are juxtaposed against old fanglomerates to the north. However, younger alluvium is not affected by the fault. Between the two fault segments is a marked lineament that runs along the north margin of the volcanic rocks of the Chocolate Mountains through Tabaseco Well, then along the northern limit of the

older alluvium shown on the Salton Sea sheet of the geologic map of California (Jennings, 1967) past the isolated exposure of Pluto gneiss at the old Baumonk Hill site. This lineament is especially visible on Skylab orbital photographs (Silver et al., 1977b). No surface break in alluvium, however, has been recognized east of the Salton Creek fault.

Summary

The system of left-lateral faults that defines the Eastern Transverse Ranges is presented in dramatic overview on the Skylab orbital photographs (Merifield and Lamar, 1975, fig. 3; Silver et al., 1977b, figs. 4-3, 4-4). The left-lateral faults disrupt the crystalline rocks of the Eastern Transverse Ranges as discrete fault zones up to 80 kilometers long. From south to north, cumulative westward displacement across these faults amounts to about 50 kilometers.

Certain pairs of the smaller zones, specifically the Porcupine Wash and Substation faults, and the Smoke Tree Wash and Victory Pass faults, are aligned and are seismically active, yet they do not connect at the surface. Transformation of fault displacement into folding may occur in these gaps, as demonstrated at the western end of the Ship Creek fault in the Chuckwalla Mountains. There does not appear to be an equivalent gap in the seismicity associated with either pair of faults (see Fuis et al, 1977, pl. 10), perhaps indicating that the faults are continuous in the subsurface.

The pattern and continuity of the left-lateral faults suggests that they have formed as a brittle mechanical response within a crystalline plate riding atop a substrate of less brittle material. The situation may be analogous to the results of clay model experiments

designed for analysis of fracture patterns (see Cloos, 1955), in which strike-slip fracture patterns have been produced in thin clay sheets that are deformed by stretching or twisting the base on which they rest.

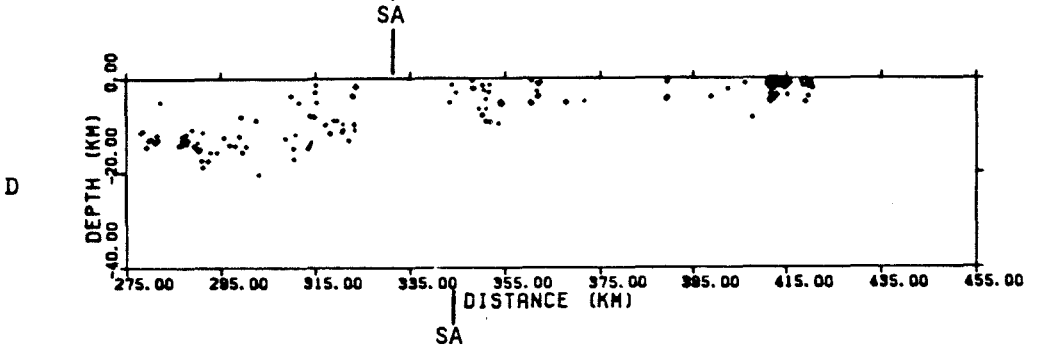
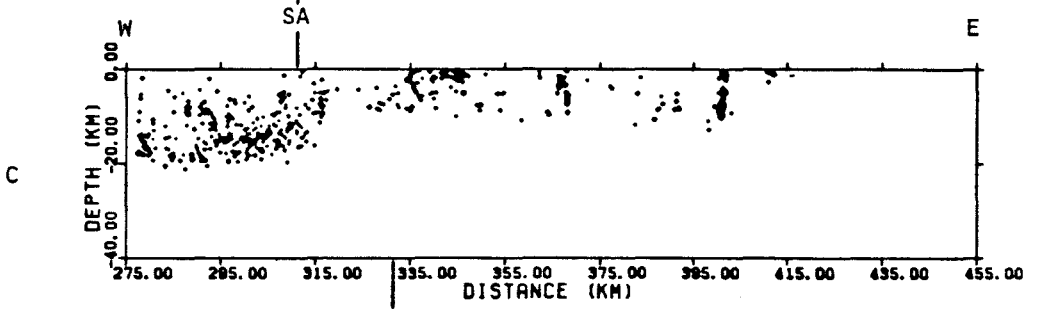
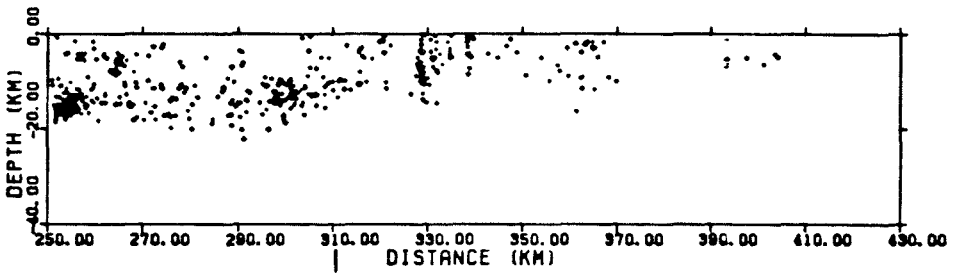
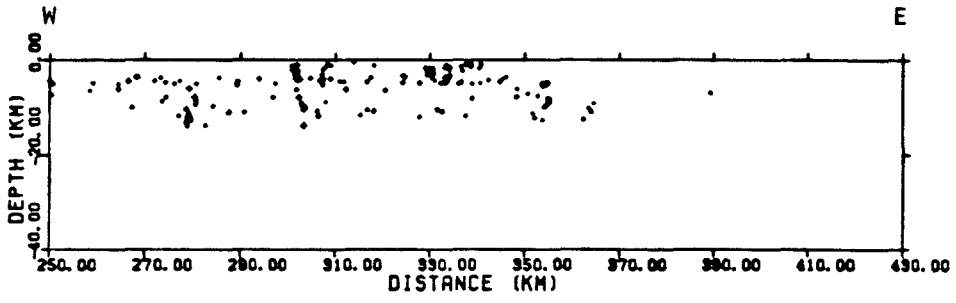
If such a brittle plate interpretation is correct, then it would seem reasonable to expect that hypocenters for earthquakes along the left-lateral faults within this plate would occur no deeper than the base of the plate. In other words, the maximum hypocentral depths for earthquakes beneath the Eastern Transverse Ranges might be expected to define a plane at the base of the brittle crystalline plate. Figure 6-2 shows a series of east-west profiles across the Eastern Transverse Ranges in which earthquake hypocenters are plotted against horizontal position east of 120° W longitude. Earthquakes located within latitudinal intervals of 0.1 degree are plotted on mid-interval cross-sections at distances measured from pole positions at 120° W longitude and latitudes midway between the boundaries of the 0.1° latitude intervals. Only "A" quality earthquakes located since the 1974 installation of the USGS seismograph network in the Eastern Transverse Ranges and Mojave Desert are plotted in the profiles. The San Andreas fault, trending northwest, cuts obliquely through the latitude intervals, so that it defines a zone within the profiles. It is interesting to observe that the San Andreas fault at depth shows the least seismic activity of the region, just as it does at the surface (Fuis et al., 1977).

A striking contrast in maximum hypocentral depth is apparent on opposite sides of the San Andreas fault. Whereas the maximum depth of seismic activity beneath the Peninsular Ranges occurs below 20 kilometers,

Figure 6-2. Earthquake hypocenter profiles in the Eastern Transverse Ranges, showing abrupt shallow lower limits of seismicity. The profiles are oriented east-west and include events within latitudinal intervals of 0.1° plotted at mid-interval. Earthquake hypocenters are plotted against horizontal distance east of 120° W longitude. The profiles include only "A" quality events located by the USGS seismograph networks in the Eastern Transverse Ranges and Mojave Desert during the interval between the 1974 installation of the networks and mid-1980 (see Fuis et al., 1977). The latitudinal intervals represented are

- A. 34.2° to 34.1° N
- B. 34.1° to 34.0° N
- C. 34.0° to 33.9° N
- D. 33.9° to 33.8° N.

The San Andreas fault (SA) transects the profiles obliquely from southeast to northwest, swinging west off the diagram within the latitudinal interval of Profile B. See text for additional discussion.



it is as shallow as 12 kilometers beneath the southern Eastern Transverse Ranges (Figure 6-2). From south to north, the base of seismicity as shown on the profiles increases in depth from 12 through 15 to 17 or 18 kilometers, then rises again to about 15 kilometers. The apparently abrupt and shallow cessation of seismic activity at 12 to 18 kilometers beneath the Eastern Transverse Range is consistent with, but does not prove, the brittle plate interpretation.

The crustal structure beneath the northern Eastern Transverse Ranges shown by Hadley and Kanamori (1977, fig. 3) shows a seismic velocity contrast between 6.7 and 6.2 km/sec along a sloping discontinuity from about 20 kilometers beneath the east end of the San Bernardino Mountains to about 15 kilometers beneath the San Andreas fault. The crustal structure is based on travel-time data from a reversed refraction profile using signals from two magnitude 4.5 earthquakes located at the east end of the San Bernardino Mountains and the west end of the San Gabriel Mountains (Hadley and Kanamori, 1977; cf. Kanamori and Hadley, 1975). The depth of this velocity discontinuity is very close to the maximum depth of hypocenters at the same latitude, so that they may be manifestations of the same crustal zone. It will be speculated later that this geophysical discontinuity may represent a horizon close to the subsurface projection of the Vincent-Chocolate Mountain thrust, with superjacent batholithic and pre-batholithic crystalline rocks and subjacent Pelona-type schist.

There is some suggestion, in terms of sequencing relationships with respect to various ages of alluvium, of a south to north decrease in age of the left-lateral fault zones. This trend has been suggested informally by a number of investigators who have proposed that the left-lateral

faults developed sequentially, each as it was in alignment with the southern bend (San Geronio Pass) in the San Andreas fault, as the Eastern Transverse Ranges migrated southeastward relative to the southern bend. The seismicity associated with the northern faults in contrast to the aseismic nature of the southern faults is consistent with such an interpretation. Hadley and Kanamori (1977) predict a south to north younging as the relatively southeastward-moving crust of the Eastern Transverse Ranges is progressively wrinkled above a mantle ridge moving relatively northwestward. It should be noted, however, that a more conservative, and perhaps more precise, interpretation of the pattern and timing of the left-lateral faults would infer a penecontemporaneous inception to the faulting with south to north younging of the cessation of activity.

RIGHT-LATERAL FAULTS IN THE MOJAVE DESERT

Introduction

The western Mojave Desert has been sliced by numerous northwest- to northnorthwest-trending right-lateral strike-slip faults arrayed en echelon in a belt that reaches from the Garlock fault in the northwest at least to the eastern end of the Pinto Mountains and probably to the Colorado River at Blythe, then farther southeastward into Arizona. This belt corresponds to a subregion of Province II in Figure 6-1. It was first recognized as a structural province by Hill (1928, p. 152-159, pl. I/II). Subsequently, Hewett (1954, 1955) indentified additional faults within this province in the northwestern Mojave Desert and interpreted their movement as dip slip, with the sense of displacement scissoring along strike. Dibblee (1961a, 1967a) presented evidence for predominant right-lateral displacement along these faults, documented in the output of his prodigious mapping effort in the Mojave Desert (Dibblee, 1964a,b, c, 1966, 1967a,b,c,d,e,g, 1968c, 1970a; Dibblee and Bassett, 1966a,b).

Northwestern Mojave Desert

Arguments for components of right-lateral movement along the north-northwest-trending faults are most convincing in the northwestern Mojave Desert, where the major throughgoing faults within this system, shown on the geologic map of California (Jennings, 1977, 1:750,000), include the Helendale, Lockhart-Lenwood, Harper-Harper Lake-Camp Rock-Emerson, Blackwater-Calico-Mesquite, Pisgah-Bullion, Old Woman Springs, and Johnson Valley faults. There are no published detailed displacement studies along these faults, but from Dibblee's maps, the cumulative displacement across them can be estimated to sum to between 25 kilometers

and 65 kilometers. The minimum figure is derived from the conservative offset estimates of both the middle Tertiary buttress nonconformity (Dibblee, 1971) that forms part of the northeastern provincial boundary shown in Figure 6-1, and the apparent trends in the distribution of Mesozoic volcanic rocks and Paleozoic miogeoclinal rocks within Province II. The maximum figure depends on more liberal estimates of offset of the trends of these features. Several investigators have noted the spatial termination of many of these right-lateral faults of the northwestern Mojave Desert at the Pinto Mountain fault (Hewett, 1954; Allen, 1957; Dibblee, 1968c; Hope, 1966). The possibility of linked displacements for the right-lateral Mesquite fault and the left-lateral Pinto Mountains faults was suggested by Hope (1966, p. 111).

The right-lateral faults of the Mojave Desert northwest of the Bullion Mountains (Figures 4-12, 6-1) show evidence of more recent movement than those farther southeast. Many of these faults have produced scarps in young alluvium and are seismically active (see Fuis et al., 1977, pl. 10). Recent earthquakes at Galway Lake and in Homestead Valley were accompanied by right-lateral ground-breakage. The orientation and sense of displacement along these faults have been modeled in various ways as a deformational response within a crustal wedge between the San Andreas and Garlock faults (Garfunkel, 1974; Cummings, 1976). Evidence will now be discussed, however, that suggests a related physiographic and structural province extending farther southeast through the Mojave Desert into southwestern Arizona (Figure 6-1). This extended belt is affected by faults with orientation and sense of displacement equivalent to those of the northwestern Mojave Desert, but with no indication of current activity and indications of less recent last movement. An areally

expanded deformational model with some spatial variation of time of activity will be required to encompass this enlarged province.

Southeastern Mojave Desert

A number of lines of evidence may be marshalled to argue that the northwestern Mojave Desert system of right-lateral faults extends in a belt still farther to the southeast:

1. The linear physiography of the ranges to the southeast, including the Coxcomb, Palen, McCoy, and Little Maria Mountains, suggests that they are fault-bounded, and the northnorthwest trend of the ranges is consistent with the trend of the northwestern Mojave faults.

2. On the basis of a discontinuity in crystalline bedrock patterns involving both batholithic and pre-batholithic rocks, it can be argued that the Coxcomb Mountains must be separated from the Eastern Transverse Ranges by a high-angle, northwest-trending fault. Other evidence for this break, called the Sheep Hole fault by Hope (1966), includes an up-faulted sliver of olivine basalt capped by alluvium at the southeastern corner of the Pinto Basin (Hope, 1966, p. 103-104). Subparallel faults within the Coxcomb Mountains exhibit right-lateral separation up to one kilometer (Hope, 1966; Jennings, 1967). The magnitude of displacement along the Sheep Hole fault has not been resolved. A possible right-lateral displacement of 32 kilometers was inferred from Skylab IV orbital photographs, but subsequent ground study failed to corroborate the photointerpretation (Silver et al., 1977b). The contrast in batholithic rocks across the fault may eventually be accommodated with small to moderate displacement of up to a few tens of kilometers to match in some way the granitic rocks of the Coxcomb Mountains with

those of the Bullion Mountains. However, the profound discontinuity in pre-batholithic rocks implies the existence of at least one earlier break, inter- and/or pre-batholithic, that has been subsequently masked by movement along the Sheep Hole fault as well as by batholithic emplacement. One candidate structure was discussed in Chapter IV.

3. Right-lateral separation of 1.5 kilometers has been demonstrated on a northnorthwest-trending fault in the southern Palen Mountains, and a small right-lateral separation of about 3 kilometers may exist between the Palen and McCoy Mountains (Pelka, 1973).

4. It may be possible to demonstrate right-lateral offset between fragments of the gypsum-bearing Upper Paleozoic stratigraphic section that crops out in Palen Pass (Hoppin, 1954) and in the southwestern Little Maria Mountains (Shklanka, 1963; Hamilton, 1964, and fide Jennings 1967). An estimated disruption in trend of 16 kilometers along the intervening valley separates the similar areas of two ranges.

5. Several unsubstantiated northnorthwest-trending faults have been mapped in reconnaissance within the basement rocks of the Coxcomb, Iron, Palen, and Little Maria Mountains (Bishop, 1964; Jennings, 1967).

6. Terrain-corrected Bouguer gravity maps in the southeastern Mojave Desert have been interpreted to indicate northnorthwest-trending faults beneath the alluviated valley between the Big and Little Maria Mountains and the McCoy Mountains, and flanking the southwestern margin of the McCoy Mountains (Rotstein et al., 1976). These two geophysically inferred faults could accommodate the right-lateral displacements proposed above in paragraphs (4) and (3), respectively.

7. Physiographic evidence supported by some detailed geologic mapping suggests that the system of northnorthwest-trending faults continues

across the Colorado River into the Dome Rock and Plomosa Mountains of Arizona. Right-lateral offset on some of these structures has been documented in the Plomosa Mountains (Miller, 1970), with a cumulative displacement of perhaps 10 kilometers distributed over several faults.

Summary of Right- and Left-lateral Strike-slip Fault Pattern

In summary, northwest- to northnorthwest-trending right-lateral faults characterize a northwest-trending physiographic and structural belt in the western Mojave Desert. Cumulative displacement across this structural zone, falling perhaps within a range from as little as 60 kilometers to as much as 140 kilometers, is not rigorously constrained. The Garlock fault limits the northern extent of the Mojave Desert system of northwest-trending right-lateral faults. With a maximum left-lateral separation of 60 kilometers (Smith, 1962; Michael, 1966; Smith and Ketner, 1970), the Garlock fault absorbs a change in tectonic style from these right-lateral strike-slip faults to a regime of Cenozoic extensional tectonics north of the fault (Davis and Burchfiel, 1973; Garfunkel, 1974; Wright, 1976). Much of this displacement has occurred in Plio-Pleistocene time (Carter, 1971, 1980a; Clark, 1973; Clark and Lajoie, 1974; Burke and Clark, 1978).

The southern limit of the western Mojave Desert structural province is ambiguous. Although the northnorthwest-trending fault system apparently continues into Arizona, imparting a grain that transects the Dome Rock and Plomosa-New Water Mountains, the physiographic orientation of the ranges themselves is northnortheast. Geologic mapping within the Tertiary volcanic province in the ranges south of Dome Rock and New Water Mountains is not sufficiently detailed to ascertain whether the

right-lateral fault system extends still farther to the southeast. It is not known whether or not the northwest-trending ranges southeast of Yuma are controlled by faults related to the western Mojave system. Tectonic models developed below predict that they are not cogenetic.

It is consistent with all of the earlier observations concerning the left-lateral Eastern Transverse Ranges faults and the right-lateral Mojave Desert faults to propose that they represent complementary elements of a conjugate shear system superimposed on the crystalline rocks of the region. The complementary strike-slip faults intersect with acute angles of 40 to 60 degrees bisected by a westnorthwest azimuth. The regional stress field can be inferred from the conjugate fault system to have a principal stress axis oriented about northeast. The conjugate shear planes are inferred to have initiated in the Transverse Ranges-Mojave Desert block with roughly north-south and eastnorth-east orientations, then rotated with increasing deformation into their present orientations (cf. deformational patterns in clay-cake experiments: Cloos, 1955; Badgely, 1965, p. 108-112). To produce the faults of the Mojave Desert and Eastern Transverse Ranges, a left-lateral couple is inferred at the Garlock fault on the north and approximately at the Gila lineament to the south.

Both the right- and left-lateral faults exhibit more recent activity to the northwest versus inactivity to the southeast, in terms of both faulted young alluvium and seismicity. This temporal commonality, with apparent progressive cessation of activity from southeast to northwest, is consistent with a cogenetic interpretation for the faults.

ZONE OF CATACLASIS AND BRECCIATION IN THE LITTLE SAN BERNARDINO MOUNTAINS

The rocks in the Little San Bernardino Mountains include a variety of batholithic and pre-batholithic lithologies that have been severely cataclasized, fractured, and brecciated, yielding a geologic terrane that is extremely complex in its lithologic and structural detail. Rapid erosion of the pulverized rock has resulted in a rugged physiographic terrane with a topography that is characterized by steep-walled canyons and ravines incised within a broad, headward-steepening escarpment. A few of the major canyons breach the lip of the escarpment and drain parts of an old erosion surface, now warped, broken and dissected in the Eastern Transverse Ranges. Most drainages, however, head in the steep upper slopes of the escarpment.

A number of investigators have dealt with the detailed geologic complexity of portions of this pervasively deformed zone by delineating composite lithologic units amenable to expedient mapping (MacLellan, 1936; Miller, 1944; Rogers, 1961; Hope, 1966, 1969; Dibblee, 1967f; Proctor, 1968). A similar zone of deformation, continuous with that of the Little San Bernardino Mountains, has been mapped in the southernmost San Bernardino Mountains, north of San Geronimo Pass (Vaughan, 1922; Allen, 1957; Dibblee, 1964d, 1967f). These complexes have been integrated on the Santa Ana and San Bernardino sheets (Rogers, 1966; 1969) of the 1:250,000 geologic map of California and on the 1:750,000 geologic map of California (Jennings, 1977) into an undifferentiated Precambrian (-Mesozoic?) igneous-metamorphic gneiss complex. The present study will also treat these rocks as an amalgamation, but as a post-batholithic structural unit rather than a Precambrian gneiss complex (Figure 6-1).

In a map of the area along the East Coachella Tunnel of the Colorado River aqueduct on the southwestern flank of the Little San Bernardino Mountains, MacLellan (1936) divided the terrane into metasedimentary gneiss and schist (Berdoe Series), "granitoid replacement" rocks (Thermal Canyon Series), and granitic intrusives. The Santa Ana sheet of the Geologic map of California (Rogers, 1966) shows the contact between the two series, as mapped by MacLellan, just south of Berdoe Canyon. In a more realistic assessment, however, rocks of both series in the southern Little San Bernardino Mountains are predominantly cataclasized Mesozoic plutonic rocks. Older gneisses are present, however, as cataclasized screens and pendants within the plutonic rocks (Plate I).

Similarly, in a reconnaissance strip map from Palen Springs to Blythe, Miller (1944, p. 16-17) included the foliated rocks of the southernmost Little San Bernardino Mountains within his polygenetic Chuckwalla Complex, which in this area he inferred to be derived from igneous rocks. Miller (1944, p. 59-60) described the Fargo Canyon diorite, of probable Mesozoic age, as intrusive into the Chuckwalla Complex. In detail, although older gneisses do occur as pendants and screens, most of the Chuckwalla Complex in the southernmost Little San Bernardino Mountains consists of foliated quartz diorite (equivalent to Fargo Canyon diorite) or foliated quartz monzonite rock actually younger than Miller's Fargo Canyon diorite (Plate I).

Farther north, in the southernmost San Bernardino Mountains, Vaughan (1922, p. 344-352, map) mapped an undifferentiated crystalline complex of schist and gneiss derived from mixed sedimentary and plutonic protoliths. In places, Vaughan mapped heterogeneous plutonic rocks as

a distinct unit, but he recognized gradational intermingling between granitic rocks and the schist complex. Allen (1957, p. 318, 322, pl. I) later described these crystalline rocks north of San Gorgonio Pass as a hybrid migmatitic terrane which he referred to as the San Gorgonio igneous-metamorphic complex. Allen (p. 319) classified most of the complex as a "biotite-hornblende-quartz-andesine gneiss with varying amounts of potassium feldspar," that shows local textural gradations into schist or foliated quartz diorite. These intermediate rocks are intimately intruded and migmatized by foliated quartz monzonite rocks.

Proctor (1968, p. 12-15) has extended the San Gorgonio complex southeastward into the northern Little San Bernardino Mountains, where he has recognized gneisses with the same mineralogy and texture as those described by Allen. Dibblee (1964d, 1967d, 1967f) has mapped the gneisses in both the southern San Bernardino and northern Little San Bernardino Mountains as laminated quartz dioritic to quartz monzonite gneiss (quartz-plagioclase-potassium feldspar-biotite-hornblende) that ranges texturally to foliated quartz diorite and quartz monzonite.

Rogers (1961) and Hope (1966, 1969) include most of the cataclastic rocks of the central and northern Little San Bernardino Mountains in an undifferentiated gneiss unit (unrestricted Pinto gneiss) that includes several of the pre-batholithic gneisses to the east as well. In contrast to Rogers, Hope distinguishes a foliated quartz monzonite from the remainder of the gneiss along the lip of the escarpment in the central Little San Bernardino Mountains, a treatment that agrees with Dibblee's (1967d,f) mapping in the northernmost part of the range. In fact, much of the gneiss in the Little San Bernardino Mountains below the lip of

the escarpment is also derived from plutonic rocks, with screens of cataclasized metasedimentary gneiss.

A thorough understanding of the Little San Bernardino structural zone will require field study and a lithologic map of sufficiently large scale and a structural map of sufficient density of structural measurements to do justice to the detailed complexity of the terrane. Since I have not studied this zone in the detail it requires, I will emphasize some general relationships about the Little San Bernardino terrane as a whole, which place temporal and geometric constraints on results that might be anticipated from a more exhaustive study.

First, and perhaps most significant, the distinctive character of the rocks of the Little San Bernardino Mountains results primarily from a superimposed cataclasis and brecciation. Lithologic units of the Little San Bernardino escarpment are the same as those of the Eastern Transverse Ranges east of the escarpment, except that they have been imprinted with a pervasive cataclastic fabric, then fractured and brecciated at all scales. Pre-batholithic lithologies include Pinto gneiss, recognized in float at the mouth of East Deception Canyon in the Thousand and Palm 15' quadrangle, and in place just west of State Highway 62 where it enters the Little San Bernardino Mountains. Probably the garnet-sillimanite schist described by Proctor (1968, p. 15) in the northeastern Little San Bernardino Mountains and as clasts in terrace deposits in the Desert Hot Springs area of the northwestern Little San Bernardino Mountains is also part of the Pinto gneiss, although from his terse description it is also possible that the rock is Hexie gneiss. Cataclasized screens and pendants of Augustine gneiss are found in the southernmost Little San Bernardino Mountains.

Batholithic rocks overprinted by the cataclasis include large, sheared inclusions of the dark-colored, coarse-grained, porphyritic hornblende gabbro of the Jurassic(?) batholithic suite that crop out at the mouth of Long Canyon just southeast of Desert Hot Springs. This occurrence lies on trend with the southwestern limit of the belt of Jurassic(?) mafic rocks in the Pinto, Hexie, Eagle, and Chuckwalla Mountains (see Plate I). Each of the units mapped in the Cretaceous(?) batholithic suite can be traced from undeformed states into the zone of cataclasis in the Little San Bernardino Mountains. However, much of deformed rock in the cataclastic zone of the northern Little San Bernardino and southern San Bernardino Mountains is foliated quartz diorite to quartz dioritic gneiss that does not crop out in an undeformed state farther east. In the southernmost Little San Bernardino Mountains, foliated quartz diorite (Fargo Canyon) grades eastward into foliated porphyritic quartz monzonite of probable Cretaceous(?) age.

Secondly, the cataclastic fabric must therefore have been superimposed on the rocks of the Little San Bernardino escarpment at some time after the emplacement of the Cretaceous batholithic rocks. Because there are also some unfoliated fine-grained felsic dikes that cross-cut the cataclastic foliation (for instance, a third of the way up Berdoo Canyon), it may be possible to bracket the cataclastic deformation absolutely in time.

Thirdly, although the penetrative cataclastic foliation is pervasively developed in the Little San Bernardino Mountains, the preservation of delicate intrusive relationships (dikes and apophyses) at several plutonic contacts examined in Berdoo Canyon indicate that incremental

displacements within the shear zone were small during the deformational event that produced the cataclasis. However, larger displacements probably did occur along localized schistose and mylonitic zones within the cataclastic granitic rocks. Nor does cumulative displacement across the whole escarpment seem to have been very great, since the trends of the major lithologic units that enter the zone from the east do not seem to be greatly disrupted. However, it must be noted that the complete shear zone is not observed because it has been antiformally folded then truncated by faults of the San Andreas system at the base of the escarpment.

The Cenozoic(?) cataclastic foliation within the crystalline rocks of the Little San Bernardino Mountains may have developed in one of two ways: either parallel to a regional post-batholithic thrust fault or parallel to the axial plane of an intracrystalline fold. Because the antiform that runs the length of the Little San Bernardino Mountains is largely defined by its folding of the foliation, the latter interpretation seems untenable. In a thrust-related interpretation, however, the cataclastic foliation, in terms of both timing and position, may be linked to the regional Vincent-Chocolate Mountain thrust fragmentarily exposed in the Sierra Pelona, San Gabriel Mountains, Crafton Hills, Banning Canyon in the southernmost San Bernardino Mountains, Orocopia Mountains, and Chocolate Mountains. Such an interpretation is supported by established relationships in the Chocolate Mountains (Dillon, 1975; Haxel, 1977), San Gabriel Mountains (Ehlig, 1958, 1975; Morton, 1975; Dibblee, 1970b), Banning Canyon (Dibblee, 1964d; cf. Allen, 1957), and Crafton Hills (Dibblee, 1970b), where cataclastic crystalline rocks including Mesozoic plutonic rocks overlie thick mylonite zones at the

Vincent-Chocolate Mountain thrust. Ramifications of this interpretation are discussed below in a tectonic synthesis section.

Fourthly, based on a limited number of foliation attitudes (Plate I) in the southern Little San Bernardino Mountains, it appears that the cataclastic foliation has been antiformally folded across the escarpment. The axis of the fold is colinear with the antiformal axes mapped by Hope (1966, 1969) in the central Little San Bernardino Mountains and by Dibblee (1967f) in the northern part of the range. Furthermore, rocks of the San Gabriel terrane (Augustine gneiss) occur as pendants and screens within the cataclastic zone of the southern Little San Bernardino Mountains at a structural level that is too low to be accommodated by the pre-batholithic structures described in Chapter IV (Figure 4-11). The post-batholithic antiform perfectly accounts for the anomalous distribution of these rocks. The exposure of Soledad augen gneiss in the vicinity of Canyon Spring just east of the Clemens Well fault in the Orocopia Mountains is also structurally too low to be accommodated by the pre-batholithic structures, but is correctly positioned if folded across both an extension of the Little San Bernardino antiform and its complementary synform through the eastern and central Orocopia Mountains.

The synform is also indicated by a synclinorium of Tertiary sedimentary rocks that rest nonconformably on crystalline basement underlying Maniobra Valley (Crowell and Susuki, 1959; Crowell, 1962). It lies parallel to and southwest of the antiform, and appears to be truncated by the Clemens Well fault. Cataclastic foliation is only locally developed in the folded Mesozoic plutonic rocks of the Orocopia Mountains, although most of the crystalline rocks underlying and flanking Maniobra Valley are intensely brecciated.

The marine Maniobra formation (Eocene) rests nonconformably on the Cretaceous quartz monzonite of the Orocopia Mountains. It contains clasts of the quartz monzonite, including some that are cataclasized. If the localized cataclasis in the crystalline rocks of the central Orocopia Mountains is part of the cataclasis inferred to be thrust-related, then it must already have been formed and was beginning to be folded by about 40-45 m.y. ago, a figure that is consistent with earlier arguments for the age of thrusting. Alternatively, the cataclastic clasts in the Maniobra formation may be derived from intra-batholithic shear zones unrelated to the thrusting.

The terrestrial Diligencia formation rests with angular unconformity across both the Maniobra formation and crystalline basement. Deposition in a tectonically active basin is indicated by thick beds of megaconglomerate and megabreccia underlying and interbedded with red beds, lacustrine deposits, and andesitic to basaltic volcanics, linked by abrupt lateral facies changes and intraformational unconformities.

Fifthly, at some time after the development of the cataclastic foliation and probably during the time interval when the foliation was antiformally folded, the cataclastic zone along the Little San Bernardino escarpment was severely fractured and brecciated. The scale of the fragmentation ranges from gouge particles less than a millimeter in diameter to fault blocks tens to hundreds of meters across and probably larger. Faults and gouge zones with no apparent systematic orientation are ubiquitous. The spatial coincidence of the two deformations suggests that they may be linked in some way. Extremely fractured and brecciated crystalline rocks that underlie the Tertiary rocks of both Maniobra Valley and the southern Chuckwalla Mountains between Aztec Mines Wash

and St. Augustine Pass (Plate I) are inferred to be part of the same deformation. The overlying sedimentary rocks were folded and faulted rather than brecciated.

Sixthly, the antiformal axis is offset by left-lateral faults, including the Pinto Mountain fault (Dibblee, 1975, p. 134), the Blue Cut fault (Hope, 1966, p. 75; 1969), and the Chiriaco fault (Plate I). Thus, the left-lateral faults at least partially post-date the development of the antiform.

REVIEW OF PELONA-TYPE SCHIST AND THE VINCENT-CHOCOLATE MOUNTAIN THRUST

Introduction

Pelona-type schist is used in this study to designate a package of lithologies that is discontinuously exposed in fifteen geographically distinct bodies in southern California and southwesternmost Arizona. These separate exposures share distinctive lithologic and structural features which have prompted most investigators to correlate them and to incorporate them into a single tectonic-stratigraphic package. No evidence has yet been presented which contradicts this correlation. Although the separate exposures of this package of lithologies have been variously named Pelona, Rand, Orocopia, and Chocolate Mountain schist, they are herein collectively referred to as "Pelona-type schist" to emphasize their apparent consanguinity. Pelona-type schist does not crop out within the area mapped during the course of this study, but because it is extensively exposed immediately to the south and southwest of that area, the contact relationships between the crystalline rocks of the Eastern Transverse Ranges and the Pelona-type schist terrane will be addressed. Protolithologic, metamorphic, and tectonic attributes of the occurrences of Pelona-type schist, with reference to earlier studies of each body, have been regionally synthesized by Ehlig (1968) and Haxel and Dillon (1978). The present review is drawn largely from these syntheses. Inasmuch as the tectonic evolution of the Pelona-type schist terrane remains ambiguous, it is intended below to highlight those aspects of the terrane for which any tectonic model must rigorously account. This review of the structural setting of the Pelona-type schist terrane leads into the tectonic synthesis presented in a later section, which attempts to integrate aspects of this setting with the

Cenozoic structural features described above for the crystalline rocks of the Eastern Transverse Ranges.

Lithology

The predominant lithology within Pelona-type schist is gray flaggy quartzo-feldspathic schist characterized by metamorphic mineral assemblages of muscovite-albite (or oligoclase)-quartz \pm chlorite \pm biotite \pm microcline (Ehlig, 1958, 1968; Muehlberger and Hill, 1958; Crowell, 1962; Haxel, 1977; Dillon, 1975; Haxel and Dillon, 1978; Hulin, 1925). Albite typically occurs as distinctive gray to black poikilitic porphyroblasts colored by included graphite. Thin compositional and textural layering represents bedding, although it is generally overprinted by a strong bedding-plane schistosity (Ehlig, 1958, 1968) and is probably transposed (Haxel and Dillon, 1978), especially near overlying thrust contacts. The protolith for this lithology was probably gray-wacke with interbedded shale. Graded bedding has been identified in little-deformed sections far removed from the Vincent thrust in the eastern San Gabriel Mountains and at scattered other localities (Ehlig, 1958, 1968; Haxel and Dillon, 1978). Locally abundant greenschist is characterized by a metamorphic mineral assemblage of chlorite-actinolite-albite-clinozoisite (Hulin, 1925; Muehlberger and Hill, 1958; Crowell, 1962; Ehlig, 1968; Haxel and Dillon, 1978). Nodules of coarse-grained, light-green actinolite are common. The protoliths for the greenschists were probably volcanic or volcanoclastic. Relict pillow structures have been observed at one locality in the Sierra Pelona (P. Ehlig, fide Haxel and Dillon, 1978, p. 464). Thin beds of marble (limestone) and ferruginous and manganiferous quartzite (meta-

chert) occur sporadically within the greenschist and less commonly within the metagraywacke (Ehlig, 1968; Haxel and Dillon, 1978). Talc, talc-actinolite, and talc-serpentine (meta-ultramafic?) rocks occur rarely.

No stratigraphic or structural base has been observed for any exposure of Pelona-type schist, although Ehlig (1958, 1968, 1975) estimates that a section of more than 3000 m is preserved beneath the Vincent thrust in the eastern San Gabriel Mountains. No direct paleontologic or isotopic evidence has been found to bear on the age of the protolith. Indirectly, however, the age of the protolith must be older than the age of thrusting and metamorphism discussed below. It may also be older than a discordant K-Ar date on hornblende (74.2 m.y.; coexisting biotite: 18.2 m.y.) from a metamorphosed granitic rock intrusive into Pelona-type schist in the Rand Mountains (R. Kistler, fide Miller and Morton, 1977), if the hornblende date is interpreted as a minimum plutonic crystallization age.

The graywacke (turbidite)-volcaniclastic-chert association of the protolith for Pelona-type schist indicates a depositional environment related to a convergent continental margin, with sedimentary accumulation occurring either outboard (trench slope) or inboard (back-arc basin) from a volcanic arc. The regional dimensions of such deposomes are typically greater than the area circumscribed by all the exposures of Pelona-type schist, let alone any one body. Depositional models that propose protolith accumulation in troughs formed along the San Andreas fault, such as those advocated by Ehlig (1968), and Haxel and Dillon (1977), followed by compressional overthrusting related to later movements along the strike-slip faults, are inconsistent with the lithologic nature of the

protolith. Furthermore, no conglomeratic facies, as might be expected within an intracontinental basin, has been recognized in Pelona-type schist.

Tectonic Setting

All mapped boundaries between Pelona-type schist and other pre-Cenozoic rocks in the region are structural. Tectonically, the schist consistently lies subjacent to low-angle faults with upper plates of pre-Cenozoic crystalline rocks, or else juxtaposed along younger strike-slip faults against either pre-Cenozoic crystalline rocks or Cenozoic sedimentary and volcanic rocks. Pelona-type schist overridden by crystalline rocks has been observed in several ranges in southern California, including the Sierra Pelona (Ehlig, 1968), eastern San Gabriel Mountains (Ehlig, 1958, 1968), Crafton Hills east of Redlands (Dibblee, 1970b; Ehlig, 1968), Banning Canyon in the southernmost San Bernardino Mountains (Dibblee, 1964d), Orocopia Mountains (Crowell, 1962; Ehlig, 1968), Chocolate Mountains (Haxel and Dillon, 1978), and Rand Mountains (Ehlig, 1968). The low-angle structure(s) will be referred to as thrust fault(s). At most of those localities, a zone of extreme cataclasis a few meters to several hundred meters thick immediately overlies the thrusts. The mylonite zone is characterized by retrograde chloritization (Ehlig, 1968; Haxel and Dillon, 1978). Inverted metamorphic gradients have been proposed in Pelona-type schist beneath the thrust contacts (Ehlig, 1958, 1968; Vargo, 1972; Graham, 1975; Graham and England, 1976; Haxel and Dillon, 1978), ranging upward from lower greenschist through epidote-amphibolite as high as lower amphibolite facies over an interval of two to three thousand feet.

Pelona schist metamorphism is interpreted to have occurred within a pressure range of 6-7.5 kb (20-27 km) and temperature ranges of 500 to 550° C for the amphibolite facies rocks immediately beneath the thrust and 420 to 500± °C for the epidote-amphibolite facies rocks below (Graham, 1975; Graham and England, 1976). Graham and England (1976) calculate transient shear heating effects for subhorizontal overthrusting to model an inverted thermal gradient capable of producing the metamorphic assemblages observed in the Pelona schist. They rule out a hot allochthonous slab as the exclusive cause of the metamorphism, because the temperature required would exceed granitic melting temperatures.

As discussed by Haxel and Dillon (1978), the subsurface extent of Pelona-type schist can be interpreted in one of two ways:

1. The original distribution of Pelona-type schist is related to Cenozoic strike-slip faults (San Andreas and Garlock). In this interpretation, once advocated by Ehlig (1968) and later by Haxel and Dillon (1977), the protolith for Pelona-type schist accumulated in troughs formed along the San Andreas and Garlock faults. Compressional stresses related to later movements along the strike-slip faults produced isolated thrust faults at each geographic locality. As noted above, this interpretation is not consistent with the lithologic-stratigraphic association of the protolith.

2. Subsequent to accumulation of the Pelona-type schist protolith in an arc-related depositional environment, an allochthon consisting of the crystalline rocks of the western Mojave Desert and Transverse Ranges was regionally thrust over the deposome. This interpretation requires integration of the several disconnected segments of low-angle structures

above Pelona-type schist into a single regional structure. Such structural continuity permits stratigraphic continuity in a substrate of Pelona-type schist. It also permits postulation of a single deep-seated inverted thermal gradient beneath the regional allochthon to account for widely separated occurrences of inverted metamorphic facies. Haxel and Dillon (1978) refer to this thrust as the Vincent-Chocolate Mountain thrust (see also Ehlig, 1958; Crowell, 1962).

The timing of the thrusting event is bracketed by regional intrusion of the Cretaceous(?) batholithic rocks (~ 70-90 m.y.) that are inferred to be cut by the thrust in the eastern San Gabriel Mountains, (Ehlig, 1958, 1968), Mesozoic intrusives in the Orocochia and Chocolate Mountains (Crowell, 1962; Dillon and Haxel, 1978), and by intrusion of Tertiary quartz monzonites (~ 20-25 m.y.) in the Chocolate Mountains (Miller and Morton, 1977; Haxel and Dillon, 1978) into the thrust. If metamorphism of the schist did occur during emplacement of the allochthon, then K-Ar whole rock and Rb-Sr mineral isochron dates in the San Gabriel Mountains and Sierra Pelona on the mylonite (K-Ar: 53 ± 0.5 m.y.; Rb-Sr: 58.5 ± 4 m.y.) and immediately subjacent schist (K-Ar: 47 ± 1 m.y., 52 ± 1 m.y.; Rb-Sr: 53 ± 2 m.y., 59 ± 1 m.y.) may indicate the age of thrusting (Ehlig et al., 1975; Conrad and Davis, 1977; Haxel and Dillon, 1978).

The tectonic vergence of the crystalline allochthon is an issue of some debate. Haxel and Dillon (Dillon, 1975; Haxel, 1977; Haxel and Dillon, 1978) have measured the orientation and sense of rotation of S and Z minor folds at 25 localities throughout the southern Chocolate and Picacho-Peter Kane Mountains. By using Hansen's (1967) method of slip analysis on these measurements, Haxel and Dillon (1978) infer a northeastward direction of tectonic transport of the upper plate along

the thrust.

Some crystalline lithologies of the allochthon, however, have apparent affinities with crystalline rocks of the Sierra Nevada, southernmost Great Basin, and eastern Mojave Desert that belie allochthonous emplacement from the southwest across an extensive terrane of Pelona-type schist. Correlations have been proposed between the Precambrian and Paleozoic pre-batholithic rocks in the Baldwin Lake area of the San Bernardino Mountains and in the vicinity of Victorville in the western Mojave Desert and equivalent sections in the southern Great Basin in eastern California and southern Nevada (Stewart and Poole, 1975; see also Silver, 1971; Silver et al., 1962). In addition, Jurassic quartz monzonites are distributed across the Eastern Transverse Ranges and the Mojave Desert, through the southern Great Basin just east of the Sierra Nevada, into the central Sierra Nevada (Silver, personal comm.; Evernden and Kistler, 1970; Morton and Miller, 1980). Similarly, Cretaceous quartz monzonites and granodiorites occur through the Eastern Transverse Ranges and the Mojave Desert, and along the crest of the Sierra Nevada (Evernden and Kistler, 1970; Morton and Miller, 1980). This seeming continuity of some of the crystalline lithologies can be used to argue that the direction of crystalline overthrusting must have had southerly and westerly components, diametrically opposed to the direction indicated by the minor fold analysis (Yeats, 1968; an idea also discussed informally by a number of investigators, including L. Silver, J. Crowell, G. A. Davis, and B. C. Burchfiel).

In the Orocopia Mountains, gouge and breccia along the Orocopia thrust indicate that this segment of the Vincent-Chocolate Mountain thrust has been reactivated as a relatively shallow later Cenozoic

fault (Crowell, 1974; Haxel and Dillon, 1978).

Pelona-type schist is exposed in thirteen geographically distinct bodies in a belt that extends from Mt. Pinos through the Sierra Pelona, eastern San Gabriel, Orocochia, and Chocolate Mountains, and on into southwestern Arizona. Two additional exposures occur along the Garlock fault in the Tehachapi and Rand Mountains. The linear array of the main belt of schist bodies is subparallel to but tectonically disrupted by the San Andreas and San Gabriel faults. The Tehachapi and Rand Mountains exposures are offset along the Garlock fault. The linear occurrence of the schist bodies in proximity to the major strike-slip faults of southern California has been explained by a model that genetically links the schist and its protolith to the San Andreas fault (Ehlig, 1968; Haxel and Dillon, 1977) and by one that uses the strike-slip faults to uplift and expose linear arrays as a structural substrate of Pelona-type schist (Haxel and Dillon, 1978).

Each occurrence of Pelona-type schist is structurally exposed in the core of an antiform (Haxel and Dillon, 1978), although many of these antiforms have been truncated by younger faults. Foliation and bedding within Pelona-type schist of the Sierra Pelona define a broad, southwestward-plunging asymmetric antiform with a steeper south limb (Muehlberger and Hill, 1958; Dibblee, 1961b; Harvill, 1969). The Vincent-Chocolate Mountain thrust fault with the overriding crystalline allochthon may be exposed on the south flank of the range in Soledad Basin, but the north limb of the antiform is truncated by the San Francisquito faults (Muehlberger and Hill, 1958; Dibblee, 1961b). Westward and southwestward dipping Pelona-type schist in the easternmost San Gabriel Mountains, overlain by the Vincent thrust and its crystal-

line allochthon (Ehlig, 1968, 1975) represent part of an antiform truncated by the Punchbowl fault (Dibblee, 1970b). Similarly, the Pelona-type schist in the Orocopia Mountains is exposed in the core of a broad antiform with the Orocopia thrust and its crystalline allochthon exposed on both flanks (Crowell, 1962, 1975). The northeastern flank of the antiform is truncated by the Clemens Well fault, the southwestern flank is largely covered by Plio-Pleistocene terrestrial accumulations in the Mecca Hills sliced by several high-angle faults associated with the right-lateral Hidden Springs fault. A narrow, discontinuous antiform extends southeastward through the southern Chocolate Mountains (Dillon, 1975) the Picacho-Peter Kane area (Haxel, 1977), and into southwestern Arizona as far as the Middle Mountains (Haxel and Dillon, 1978). The structure is a complexly faulted anticlinorium that began to form by at least mid-Tertiary, because the folded thrust is overlapped in places by lower Miocene volcanics and terrestrial deposits.

In the Chocolate Mountains, Pelona-type schist and the Vincent-Chocolate Mountain thrust are depositionally overlain by the Quechon volcanics (Haxel and Dillon, 1978), which range in age from lower Oligocene (~ 35 m.y.) to lower Miocene (~ 22 m.y.) (Crowe, 1978; Crowe et al., 1979). A similar overlap situation appears to exist in the Soledad Basin on the south flank of the Sierra Pelona, where Vasquez formation rests on Pelona schist (Jahns and Muehlberger, 1954; Muehlberger, 1958; Jahns, 1973). If present at all, however, clasts of Pelona-type schist are extremely rare in terrestrial sediments associated with volcanics.

From a regional perspective, with the known occurrences of Pelona-type schist restricted to the area of the Transverse Ranges and Mojave

Desert, the tectonic setting of the schist is enigmatic. If the concept of a single regional allochthon thrust over a substrate of Pelona-type schist is correct, then the tectonic interpretation for the origin of the schist depends crucially on whether the overriding allochthon moved northeastward or southwestward. In my opinion, although arguments can be presented on both sides, the answer to that question has not been resolved. Northeastward vergence for the allochthon requires a pre-thrust paleogeology with continental crust outboard of Pelona-type schist, which may lead to models, such as those proposed by Haxel and Dillon (1978), in which the protolith accumulates in an ensimatic(?) intracontinental basin caused by either back-arc spreading (Dillon and Haxel, 1975) or oblique rifting associated with a proto-San Andreas fault (Haxel and Dillon, 1977), both of which rift blocks of continental crust to create basins for sedimentary accumulation of the protolith. More complicated models can be devised in which a block of continental crust is tectonically emplaced outboard of the protolith for the Pelona-type schist after its accumulation, then thrust northeastward over the schist.

All of these models are rendered suspect by the apparent present continuity between some of the crystalline rocks which were supposedly rifted or translated then thrust northeastward as an allochthon, and those crystalline rocks that remained fixed as part of the unrifted continent. A further problem exists in that even an approximate trace for the northeastern limit of the allochthon has not been identified in the Mojave Desert (Haxel and Dillon, 1978). The models are also suspect because no sedimentologic or stratigraphic evidence presented in the literature corroborates deposition of the protolith for Pelona-type

schist in an intracontinental basin. If such a basin formed by oblique rifting, then there must have been conglomeratic facies at the margins, as seen today for instance, in the Salton trough, and yet none has been found.

If the basin formed by back-arc spreading in the Late Cretaceous (cf. Dillon and Haxel, 1975; Haxel and Dillon, 1978) in a fashion analogous to that proposed for a fossil marginal basin in the southern Andes (Dalziel et al., 1974), then one might expect to find lithologic features akin to those found in the analog. In the southern Andes, the graywackes, volcanics, and cherts that would correspond to a protolith for the Pelona-type schist overlie an oceanic basement consisting of pillow basalts, sheeted diabase dikes, and gabbros which cross-cut the continental rocks at the margins of the back-arc basin. No remnants of a simatic basement are found associated with Pelona-type schist, nor are young diabasic or gabbroic rocks found cross-cutting the continental crystalline rocks marginal to the proposed basin. Finally, in the southern Andes, the volcanic arc that supplied volcanics and detritus to fill the back-arc basin was built on the continental block which was rifting seaward during basin formation. The young batholith emplaced beneath this volcanic arc is analogous to the Late Cretaceous granodiorite to quartz monzonitic batholith of the Mojave Desert and Transverse Ranges. It appears to be impossible to postulate an allochthon such that its palinspastic reconstruction will restore all of the known and probable Late Cretaceous plutons of the Transverse Ranges and Mojave Desert into an analogous continental block outboard of the Pelona-type schist without disrupting pre-batholithic bedrock patterns.

Southwestward vergence permits a variety of tectonic interpreta-

tions that begin with offshore sedimentary accretion of the protolith for Pelona-type schist. Prior to its involvement in regional thrusting, perhaps along a convergent continental margin, the protolith may have been approximately in situ off the coast of a pre-San Andreas California, or it may be an exotic terrane tectonically introduced along some pre-thrusting strike-slip fault, now concealed beneath the upper plate of the Vincent-Chocolate Mountain thrust. If the Pelona-type schist is indigenous, then its protolith may correlate with the protoliths of the Franciscan formation and Catalina schist, which contain similar pre-metamorphic lithologies and occur in similar tectonic settings (Crowell, 1968; Ehlig, 1968; Yeats, 1968; cf. Platt, 1975). The primary differences would lie in the degree of metamorphism (blueschist vs. greenschist) and perhaps in its timing, since K-Ar mineral and whole rock dates on metamorphic Franciscan rocks range from 150 to 70 m.y. (Suppe and Armstrong, 1972).

TECTONIC SYNTHESIS

Eastern Transverse Ranges

The observations and arguments discussed in the previous sections of this chapter can be incorporated within a hypothetical tectonic framework that links the left-lateral faults in the Eastern Transverse Ranges, the zone of cataclasis and brecciation in the Little San Bernardino Mountains, and the Vincent-Chocolate Mountain thrust with its structurally subjacent Pelona-type schist.

At the southern limit of the Eastern Transverse Ranges, the pre-batholithic structures plunge northward (see Chapter IV). If this northward plunge is maintained to the south, then successively deeper structural levels should be encountered southward at the earth's surface. Thus, widespread Pelona-type schist in the Orocochia and Chocolate Mountains beneath a regional thrust fault (Vincent-Chocolate Mountain thrust) may be interpreted to represent one such deeper structural level, which should then conversely project northward beneath the Eastern Transverse Ranges. This interpretation implies that the structure controlling the plunge was formed after the emplacement of a crystalline allochthon above Pelona-type schist. Some structural link between the two provinces is indicated by the direct superposition of San Gabriel terrane rocks above Pelona-type schist on the Vincent-Chocolate Mountain (Orocochia) thrust in both the western Orocochia Mountains (Crowell, 1962; Crowell and Walker, 1962) and the San Gabriel Mountains (Ehlig, 1958, 1968, 1975; Crowell, 1962; Crowell and Walker, 1962), with no intervening rocks of the Joshua Tree terrane. Tectonic elision of this sort is consistent with the interpretation of a low-angle crystalline allochthon being emplaced over an autochthon (?) of Pelona-

type schist.

Where observed in the Chocolate Mountains and eastern San Gabriel Mountains, the emplacement of an allochthonous crystalline slab has produced a tectonic stratification that consists of Pelona-type schist overlain by mylonite immediately above the Vincent-Chocolate Mountain thrust. The mylonite grades upward through progressively less cataclastic rocks eventually to undeformed Mesozoic plutonic rocks intrusive into pre-batholithic gneisses. The thrusting event must have occurred between 70-90 m.y. ago and 20-25 m.y. ago, and probably occurred at least 50-60 m.y. ago. The post-batholithic cataclastic foliation extensively developed in the Little San Bernardino and southern San Bernardino Mountains and sporadically developed in the east-central Orocochia Mountains is inferred to indicate proximity to the mylonite zone of the Vincent-Chocolate Mountain thrust.

A regionally continuous, post-batholithic antiform is proposed to extend along the southwestern flank of the Eastern Transverse Ranges from the southern San Bernardino Mountains through the Little San Bernardino Mountains into the east-central Orocochia Mountains, where it is structurally truncated. The antiform probably extends still farther northwestward through the San Bernardino Mountains. Foliation attitudes on the southwestern flank of the antiform are generally steeper than those on the northwestern flank, suggesting a southwestward component of vergence for the structure. Given the inferred projection of Pelona-type schist beneath the southern Eastern Transverse Ranges, and given the tectonically stratified package associated with emplacement of the crystalline allochthon above the schist, it follows that the antiform of cataclastically foliated and brecciated crystalline rocks

in the Little San Bernardino and eastern Orocopia Mountains must be cored in the subsurface by mylonite and Pelona-type schist.

Some tectonic activity along the present axis of the fold may have started as early as the time of deposition of the marine Eocene Maniobra formation (~ 40-45 m.y.) in the central Orocopia Mountains, inasmuch as the presence of very large boulders (see Crowell and Susuki, 1959) of locally-derived Cretaceous(?) monzogranite indicates considerable relief at the Eocene shoreline. Further tectonic activity certainly was in progress during the deposition of the Oligo-Miocene Diligencia formation (~ 20-25 m.y.), with its abundant coarse clastic debris. The Diligencia formation is folded in a synclinal trough along the southwest flank of the southeast projection of the Little San Bernardino Mountains antiform across the Chiriaco fault in the eastern Orocopia Mountains, so that the folding event appears to be synchronous with and/or younger than the deposition of that unit. It is the timing and location of this last tectonic episode that is incorporated into the regional antiform. The synformally folded Tertiary sedimentary rocks are truncated by the Clemens Well fault.

The pattern of left-lateral faulting in the Eastern Transverse Ranges has brittlely disrupted the crystalline rocks of those ranges along discrete fault zones up to 80 kilometers long. The nature of the faulting suggests that they formed in a brittle crystalline slab with a mechanical response independent from the response of a less brittle tectonic substrate. This substrate is inferred to be Pelona-type schist. If the maximum depth of seismic activity is taken to be the base of the brittle crystalline slab, and if the discontinuity in mechanical response is postulated to occur as a reactivated zone at

or near the Vincent-Chocolate Mountain thrust, then the subhorizontal plane defined by the maximum hypocenters of earthquakes at 12 to 15 kilometers beneath the Eastern Transverse Ranges can be inferred to reflect the subsurface position of the Vincent-Chocolate Mountain thrust. This depth corresponds roughly to the 6.2/6.7 km/sec seismic velocity boundary proposed by Hadley and Kanamori (1977, fig. 3) east of the San Andreas fault.

In transecting the lip of the escarpment from the Little San Bernardino Mountains into the Salton trough, the left-lateral faults tend to die out westward, losing their definition in the fracturing and brecciation that has affected the cataclastic zone. The left-lateral faults do, however, offset the antiform that has folded the cataclastic foliation. Although some of the fracturing and brecciation probably developed during the buckling of the crystalline slab, it also seems likely that some of it has occurred coevally with more recent movement along the left-lateral faults as a mechanism for diffusing and absorbing their displacement. Some such difference in mechanical response is required by the transition in structural style from the Eastern Transverse Ranges regime of discrete left-lateral faults into the Little San Bernardino Mountains zone of pervasive cataclasis and brecciation. It is inferred that this structural transition was triggered along the axis of the antiform where differential mechanical response across some zone such as a reactivated thrust would be obstructed by folding of that zone across the steep limb of the antiform.

San Andreas Fault

It was argued above that the regional antiform along the southwest flank of the Eastern Transverse Ranges has a core of Pelona-type schist. Conversely, it has been observed that every major exposure of Pelona-type schist lies in the core of an antiformal fold flanked by mylonite and cataclastic crystalline rocks. It is postulated here that all of the antiformal occurrences of Pelona-type schist, together with the crystalline rock antiform bounding the Eastern Transverse Ranges, once formed a nearly continuous structural feature that was subsequently disrupted along Cenozoic strike-slip faults. This feature consisted of at least three antiforms in a nose-to-nose en echelon array. If this hypothesis is valid, then the nearly aligned axes of the antiforms at the thrust contact define a linear feature that must intersect any disrupting fault at a point. Such piercing points can be used to constrain palinspastic reconstruction of the disrupting faults.

The present distribution of fragments of the proposed series of antiforms is shown in Plate VI-A. Restoration of displacement along the San Andreas fault using only the piercing point criterion yields the distribution shown in Plate VI-B. It shows that the San Andreas must have sliced obliquely across the antiformal array to displace the Sierra Pelona and eastern San Gabriel Mountains from positions originally aligned with the western Orocopia and northern Chocolate Mountains. Fault slices between the Punchbowl and San Andreas faults in the north-eastern San Gabriel Mountains and between the San Andreas-Mill Creek and Banning faults from the Crafton Hills through San Geronio Pass are fitted to make the antiform as complete as possible. It must be acknowledged, however, that this cavalier treatment glosses over com-

plexities in structural boundaries of these slices.

The offset along the San Andreas fault indicated by this reconstruction is 220 kilometers. Predictably, in light of earlier discussion, this offset using a structural criterion related to the occurrences of Pelona-type schist is consistent with offset estimates based on lithologic match-ups of Pelona-type schist (Hill and Dibblee, 1953; Crowell, 1962; Ehlig, 1968; Haxel and Dillon, 1978). The results of this exercise also corroborate offset estimates based on correlation of pre-batholithic rocks associated with anorthosite in the San Gabriel and Orocopia Mountains (Crowell, 1962; Crowell and Walker, 1962). Precisely this antiformal match-up for the Sierra Pelona and Orocopia Mountains is shown by Bohannon (1975, fig. 3) with a displacement of 210 kilometers. The displacement arrived at by reconstructing the antiformal axis is identical to that reached by matching the San Francisquito, Fenner, and Clemens Well faults, as proposed in part by Dibblee (1968) and more completely by Ehlig (1977, personal comm.). The displacement is somewhat less than the 250 kilometers derived from reconstruction of an inferred Miocene drainage system (Ehlig and Ehlert, 1972; Ehlig et al., 1975; Ehlig, 1976).

Plate VI-B shows that this palinspastic reconstruction has aligned nearly all of the exposures of Pelona-type schist into two nearly continuous en echelon antiforms, but it has not aligned the antiform within the crystalline rocks of the Eastern Transverse Ranges. Movement along the San Gabriel fault has been restored to approximately align the Pelona-type schist of Mt. Pinos with the western end of the Sierra Pelona. A displacement of about 55 to 65 kilometers is indicated. This figure is equivalent to the previously proposed value of 60 kilometers

(Crowell, 1952; Carman, 1964; Ehlig et al., 1975).

In order to achieve alignment of the Pelona-type schist composite antiform with the Eastern Transverse Range antiform, it is necessary to restore movement along a right-lateral fault segmentally composed of the San Francisquito, Fenner, and Clemens Well faults as well as a buried continuation of that structure that is inferred to run between the northern Chocolate and southern Chuckwalla Mountains and south of the Little Chuckwalla Mountains. A palinspastic movement of 80-90 kilometers is required to complete the reconstruction of a continuous antiformal array.

Smith (1977) hypothesized that the Clemens Well fault was the southern segment of a major mid-Tertiary right-lateral fault that had offset the crystalline rocks of the La Panza Range from those of the Thermal Canyon area of the southernmost Little San Bernardino Mountains. To the north, this fault zone comprised the San Juan and Chimeneas faults east of the La Panza Range and is represented by a shear zone (St. Francis) in the westernmost Sierra Pelona; to the south, it hypothetically merges with the present San Andreas fault. Smith's proposed displacement for the San Juan - St. Francis fault zone is 170-175 kilometers. The palinspastic reconstructions of Smith (1977, fig. 5a,b) prior to movement along this structure are not compatible with the basement rock geology of southern California. Based on the Cretaceous batholithic trends discussed in Chapter V, it is proposed herein that his crystalline rock criteria are compatible with a smaller displacement. The bedrock patterns of southern California also require that the southern extension of the fault diverge from the present San Andreas fault as shown in Plate VI-C.

Inasmuch as this set of palinspastic reconstructions (Plate VI-A to C) has been based solely on realigning the piercing points defined by the axes of a proposed en echelon array of post-batholithic antiforms, its validity can be tested by the compatibility of the palinspastically juxtaposed pre-batholithic and batholithic bedrock patterns. Plate VI-C shows that the reconstructions result in an excellent match-up of pre-batholithic lithologic and structural trends. The San Gabriel terrane rocks of the San Gabriel Mountains and the Frazier Mountain-Alamo Mountain area are preserved in the synform related to the post-batholithic antiform. Under these conditions, it is possible to accommodate the displacement discussed above for the combined San Francisquito-Fenner-Clemens Well northwest into the Coast Ranges along the San Juan-Chimeneas-Blue Rock fault as proposed by Smith (1977; cf. Bohannon, 1975, fig. 3).

Mojave Desert-Transverse Ranges

The orientations of the reconstructed antiforms and synforms indicate a northeast to northnortheast axis of maximum principal stress. Because this axis is coincident with that inferred for the conjugate fault system, it is plausible that the two deformations are related.

Regional uplift within a northeast-southwest compressional regime may account for the spatial distribution of the two provinces shown in Figure 6-1. The crystalline rocks of the Eastern Transverse Ranges and western Mojave Desert (Province II), virtually devoid of Tertiary cover, seem to represent a broad upwarp asymmetrically (perhaps monoclinally) culminating in the antiforms cored with Pelona-type schist. Those regions with extensive accumulations of terrestrial Tertiary volcanic and sedimentary rocks would then represent flanking downwarps.

If the evolution presented earlier for the conjugate strike-slip fault system is correct, then at an early stage in their development the right-lateral faults probably had a north-northeast to north orientation and the left-lateral faults had an east-northeast to northeast orientation. As deformation progressed, the conjugate faults were rotated as they absorbed greater amounts of shearing movement. It is proposed that the east-northeast to northeast orientation of the left-lateral faults in the Soledad Basin and San Gabriel Mountains (Jahns and Muehlberger, 1954; Muehlberger, 1950; Oakeshott, 1958; Carter and Silver, 1972; Jahns, 1973; Powell and Silver, 1979) represents a domain of this early-stage fracture set that was shielded from continued development by translation along the San Andreas fault (see Plate VI-A to C). These structures were active during and slightly after the time of deposition of the Oligo-Miocene Vasquez Formation. Most of the movement had ceased by the time of deposition of the Mio-Pliocene Mint Canyon Formation.

In this model, the timing of the inception of the San Andreas fault system is controlled by the age of the antiformal folding event. The antiformal feature appears to be covered by the upper Miocene Mint Canyon Formation (~ 10-15 m.y. ago) at the west end of the Sierra Pelona, but at least the lower portion of that unit is also folded along the same synformal axis as the older Vasquez Formation (Oligo-Miocene) (Jahns, 1973). Within the context of the proposed model, it appears that reactivation of the antiform during continuing deformation within the Transverse Ranges may be required. In any case, at least part of the Mint Canyon Formation overlaps the west end of the San Francisquito fault, which requires that the antiform, as an integral feature, must

have been developed and been offset along the San Francisquito-Fenner-Clemens Well branch of the San Andreas system by the time of the overlapping deposition. On the basis of vertebrate fauna, the restricted Mint Canyon Formation of Jahns (1940) has been subdivided into a Barstovian lower part and a Clarendonian upper part (Durham et al., 1954). In the Cenozoic time scale of Berggren (1969), the Barstovian-Clarendonian boundary is placed at the boundary between middle and upper Miocene at 10 m.y. ago. Because ~60 km of offset are proposed along the San Francisquito-Fenner-Clemens Well fault branch, the interval of movement would span 1 m.y. at a rate of 6 cm/yr, or 10 m.y. at 6 mm/yr. Because the youngest volcanic age yet found in any of the Oligo-Miocene formations (Quechon, Diligencia, Vasquez) is about 20 m.y., it is possible within the known timing constraints to fold the crystalline rocks and Oligo-Miocene sedimentary/volcanic units, offset them along the San Francisquito-Fenner-Clemens Well fault, and overlap the fold and fault with upper Mint Canyon rocks. At the faster rate, it would be possible to complete the offset between the times of deposition of the lower and upper parts of the Mint Canyon Formation.

Southern California

This section is intended to explore aspects and implications of the tectonic models discussed above within yet a broader tectonic context of southern California geology, to test whether they may be plausibly incorporated within the framework of a Cenozoic continental margin. The ideas are largely conjectural, developed in an attempt to carry previous lines of argument to some sort of logical conclusion from a regional perspective. This section also represents an attempt to relate the Cenozoic geologic history of southern California to events recorded in the magnetic signature and fracture zone pattern on the floor of the northeast Pacific Ocean. The insights derived from this exercise provide constructive feedback which seems to strengthen some of the earlier interpretations. From the arguments presented earlier, the following sequence of structural relationships is assumed to pertain and must be fit into any regional tectonic framework:

1. The rocks of the western Mojave Desert and the Transverse Ranges comprise a regional crystalline allochthon that has overridden a tectonic substrate of Pelona-type schist. The tectonic vergence is inferred to have been westward or southwestward, based on lithologic affinities between crystalline rocks of the allochthon and those still attached to autochthonous North American craton.

2. This allochthon was folded in a regional northwest-trending array of en echelon antiforms that anticipated the future trace of the San Andreas fault system. Either the location of the antiformal array controlled the subsequent location of the San Andreas, or both structures were sequential crustal responses to a deeper-seated controlling

feature. Flanking synforms may have served as basins of accumulation for Tertiary sedimentary and volcanic rocks.

3. The San Andreas fault system broke in an anastomosing pattern along and subparallel to the axes of the antiforms.

4. The left- and right-lateral faults of the Mojave Desert and Transverse Ranges form a conjugate fracture set within the allochthonous crystalline rocks above Pelona-type schist. At least in part, movement along these structures is coincident with movement along the San Andreas system; in part, however, their activity may pre-date development of the San Andreas fault. The conjugate fracture set apparently formed within a regional stress field in which the maximum principal stress axis is oriented approximately northeast and the minimum axis northwest.

If the lithologic and structural features involved in this sequence of events are a tectonically related package, then it is necessary to consider the areal extent of these features and the way in which the package is linked to bounding regions. For the purposes of the discussion that ensues, the following geologic relationships are deemed plausible but not proven:

1. Pelona-type schist and Franciscan formation are assumed to have been derived from a common protolith. This assumption has neither been conclusively demonstrated nor conclusively refuted, but it is a necessary condition for the proposed model.

2. The Cretaceous batholithic rocks originally occurred as a single, continuous belt which may have varied in width. In general, the belt was characterized by more basic rocks to the west and more felsic rocks to the east.

3. The tectonic setting of the batholithic rocks in the Mojave Desert and Transverse Ranges is fundamentally different than their setting in the Sierra Nevada and Peninsular Ranges. Aspects of this difference can be seen physiographically (Figure 1-1), geologically, and geophysically across rather abrupt transitions. East of the San Andreas fault these transitions occur at the Garlock fault to the north and the lineament along the Gila River to the south. West of the San Andreas fault the southern boundary occurs between the Peninsular Ranges and San Gabriel Mountains and the northern boundary presumably exists at some unrecognized place within or immediately north of the Salinian block.

Both the Sierra Nevada and Peninsular Ranges consist of continuous uplifted crustal blocks of Mesozoic batholithic rocks overlapped seaward by accumulations of uppermost Cretaceous and Tertiary marine sedimentary rocks. Somewhere beneath(?) the nonconformity flanking both ranges, a boundary must exist between the batholithic rocks and rocks of the Franciscan terranes that lie outboard of the batholiths. Because the Franciscan contains fossils that are as old as Jurassic and yet is not intruded by batholithic rocks, it seems likely that the boundary is tectonic. The Sierra Nevada and the Peninsular Ranges both yield geophysical indications (seismic or gravimetric) of deep (~ 50 km) crustal roots (Eaton, 1966; Gastil et al., 1975). The eastern boundary of both the southern Sierra Nevada and the Peninsular Ranges is marked by great continuous Quaternary scarp systems with thousands of feet of topographic and structural relief.

None of these features can be traced continuously through the Mojave Desert or the Transverse Ranges between the boundaries discussed above.

There is no continuous mountain range of batholithic rock, no geophysical root, and no through-going east-facing scarp with normal displacement. The belt of batholithic rocks and the shorelines for overlapping Cretaceous and Tertiary marine sedimentary rocks are structurally disrupted. In contrast, the boundary between the batholithic rocks and Pelona-type schist in the Mojave Desert and the rootless Transverse Ranges is a regional low-angle structure. The Cenozoic structural patterns characteristic of this crystalline allochthon (discussed above) have not developed in the Sierra Nevada-Great Basin nor in Peninsular Ranges-Gulf of California provinces.

Whatever mechanism is postulated to account for the difference in tectonic style between the Mojave Desert-Transverse Range block and the Sierra Nevada to the north or the Peninsular Ranges to the south must have been operating during and/or before the late Mesozoic-early Cenozoic emplacement of the crystalline allochthon over Pelona-type schist. Magnetic anomaly patterns on the ocean floor have been interpreted to indicate that this interval of time was characterized by convergence between the North America and Farallon plates. Because Mesozoic batholithic rocks are present in the Mojave Desert and Transverse Ranges as well as in the Sierra Nevada and Peninsular Ranges, it seems likely that development of a distinct tectonic style for the Mojave Desert and Transverse Ranges occurred after the last interval of batholithic emplacement between about 70 and 90 m.y. ago.

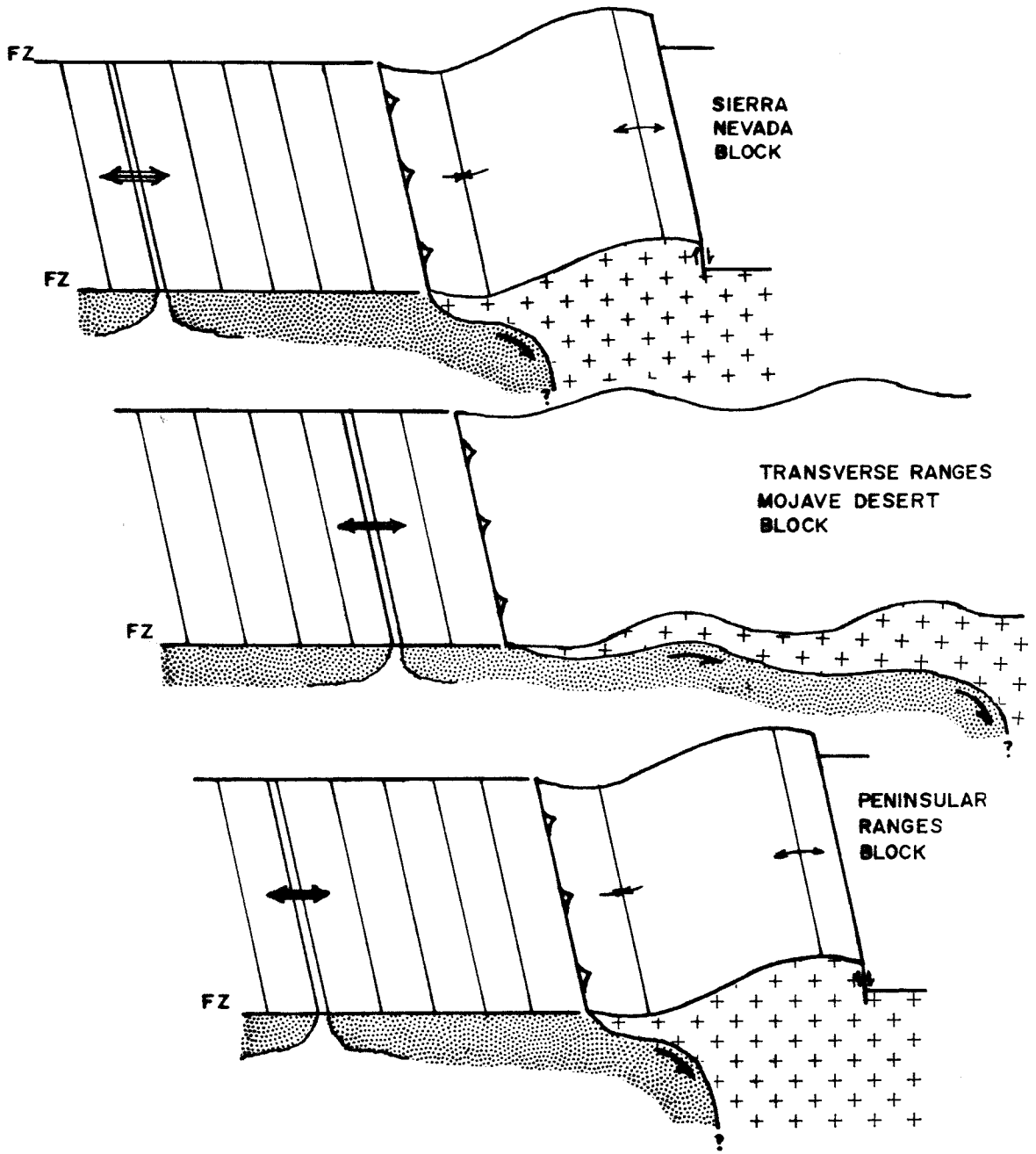
Within the context of a late Mesozoic-early Cenozoic convergent plate margin, a relatively simple tectonic model can be proposed to establish a base configuration of adjoining crustal blocks that may

then respond differently to subsequent deformations. The model initially consists of a convergent plate margin with oceanic crust subducting beneath continental crust in late Cretaceous time resulting in the emplacement of the Cordilleran batholiths. By the beginning of the Cenozoic era, fracture zones on the ocean floor are postulated to have been aligned with the northern and southern limits of two continental crustal blocks separately incorporating the Sierra Nevada and Peninsular Ranges batholiths. The fracture zones at the southern limit of the Sierra Nevada batholith and the northern limit of the Peninsular Ranges batholith delineated an intermediate crustal block that during the Cenozoic era would be deformed into the present Transverse Ranges and Mojave Desert (Figure 6-3).

In latest Cretaceous time (ca. 90-70 m.y.), conditions of convergence were favorable for voluminous magma production on a batholithic scale. However, by about 65-60 m.y. ago some factor had affected the nature of the convergence enough to cause a cessation of coastal magmatism. Perhaps the spreading rate was slowing, or perhaps the angle of subduction was decreasing as progressively hotter oceanic crust reached the trench from an encroaching spreading axis. Accumulation of a sedimentary (+ volcanic) protolith for the offshore Franciscan formation indicate depositional ages that range from late Jurassic through Eocene (Bailey et al., 1964).

At about 55 to 60 m.y., the fracture-bounded segment of oceanic crust offshore from the precursor to the Mojave Desert-Transverse Ranges crustal block began to subduct at a shallower angle than adjacent segments subducting beneath the Sierra Nevada block to the north and the Peninsular Ranges block to the south. The cause for such a difference

Figure 6-3. Model for the early Cenozoic generation of Transverse Ranges-Mojave Desert crustal block as a tectonic block distinct from the Sierra Nevada and Peninsular Ranges blocks. The block probably began to develop about the time of anomalies 21-23 (ca. 53-59 m.y. ago). North is toward the top of the page. See text for discussion.



in the angle of subduction is not clear, although modern analogs do occur along the Andean subduction zone on the west coast of South America (Barazangi and Isacks, 1976; Isacks and Barazangi, 1977). Cobbing, Pitcher, and Taylor (1977; Pitcher, 1978) suggest that the compositional segmentation of the Coastal batholith of Peru on a scale of 200 to 900 km is a continental manifestation of this lateral segmentation of the subducting slab.) As a segmented ridge axis approaches the continent, the oceanic crust formed in segments between fracture zones where the ridge axis is nearest the continent will be hotter than the crust formed in adjacent segments where the ridge axis is farther from the continent. It seems plausible that the hotter (less dense) the oceanic crust arriving at the trench, the less steeply it would subduct. Thus the angle of subduction for a leading, hotter segment would be less than those of adjoining segments with older, cooler crust at the trench (Figure 6-3).

It is proposed that the Mojave Desert-Transverse Ranges block was shallowly underthrust by a relatively young, hot segment of oceanic crust, whereas the Sierra Nevada and Peninsular Ranges were underthrust at steeper angles by older, cooler oceanic segments. The shallowly dipping subduction zone beneath the Mojave Desert-Transverse Ranges block must have either sheared off the batholithic root or uplifted it, or some combination of the two. Uplift of deep crustal levels, followed by erosion (prior to San Andreas movement) might explain the Cretaceous (?) granulites exposed in the Salinian block (see Compton, 1960, 1966). Shearing off the batholithic root would superpose allochthonous crystalline rocks above the protolith for the Pelona-type schist. If this thrusting occurred soon enough after emplacement of the Cretaceous

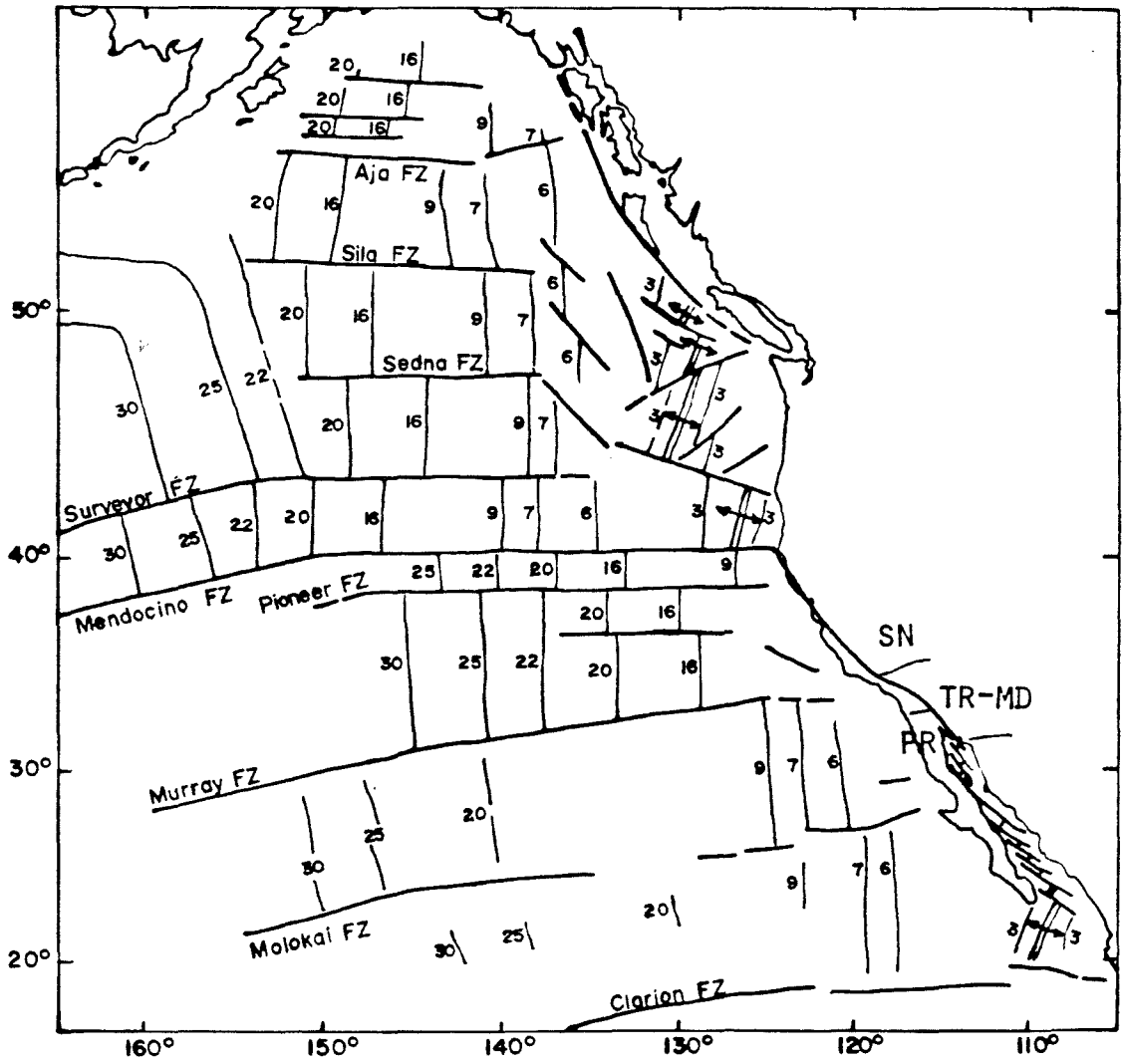
batholithic rocks, then heat conducted from the overriding slab could have contributed to the inverted thermal gradient in addition to the shear heating proposed by Graham and England (1976).

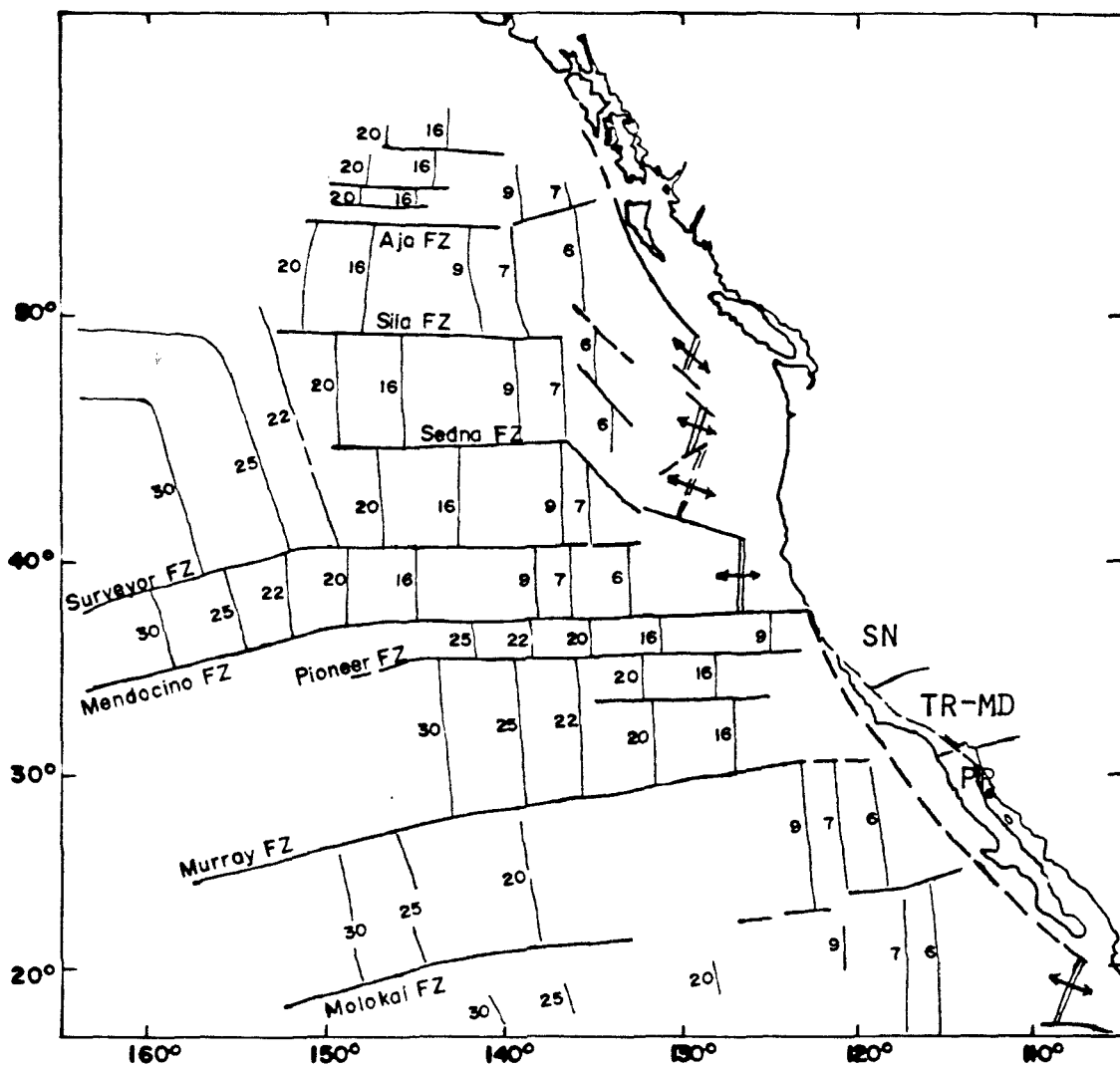
If this model is valid, then it must match the pattern of magnetic anomalies and transform faults on the Pacific floor insofar as they can be inferred to mirror the pattern of the since-subducted Farallon plate. The fracture zone pattern of the northeastern Pacific floor (Atwater, 1970; Hilde et al., 1977) shows two inter-fracture segments with the anomaly configuration described above (Figure 6-4A). One segment lies between Mendocino (or Pioneer) and Murray fracture zones, the other lies between the Sedna and Surveyor fracture zones. The distance between the latter pair is precisely the distance between the Garlock faults and the lineament along the Gila River (3.5° of latitude).

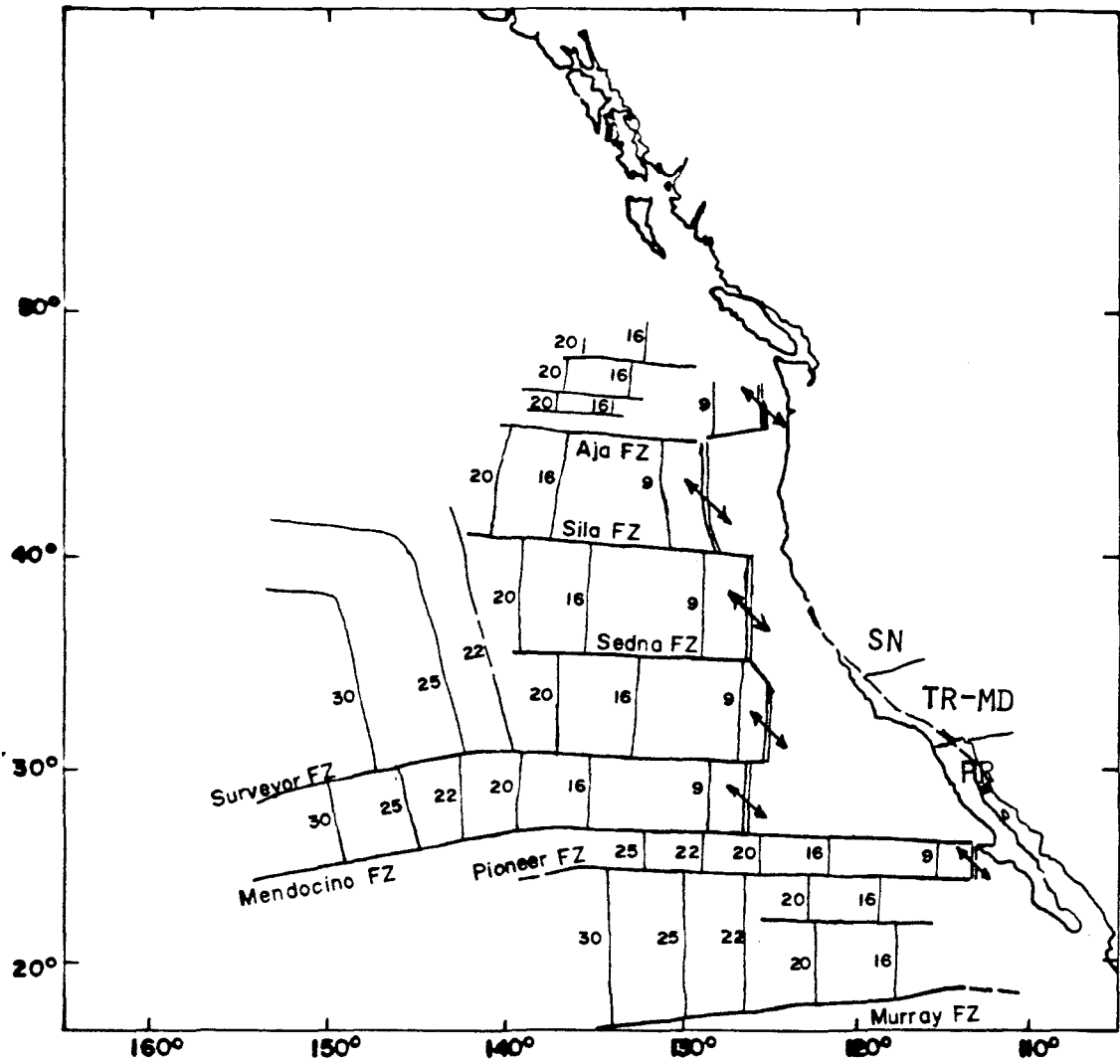
The Cretaceous episode of coastal magmatism appears to have ended within the interval of 70 to 60 m.y. ago (anomalies 25 to 30, using the anomaly time scale of Heirtzler et al., 1968; cf. Sclater et al., 1974; Tarling and Mitchell, 1976; Berggren et al., 1978; Ness et al., 1980) (Figure 6-4E). Between about 30 m.y. ago and the time of anomalies 21-23 (ca. 53-59 m.y. ago), the magnetic anomaly and fracture zone patterns of the Pacific plate indicate nearly east-west (present latitudes) spreading between the Pacific and Farallon plates (Figure 6-4D). In order for the model discussed above to work, the motion of the Farallon plate relative to North America during this interval must have been roughly east to eastnortheast, the orientation of the Garlock fault and Gila lineament (cf., e.g., Atwater, 1970; Coney, 1978). The timing and orientation of these fracture zones permit their use as bounding structures for the proposed relatively shallow subducting slab beneath the Transverse Ranges-Mojave

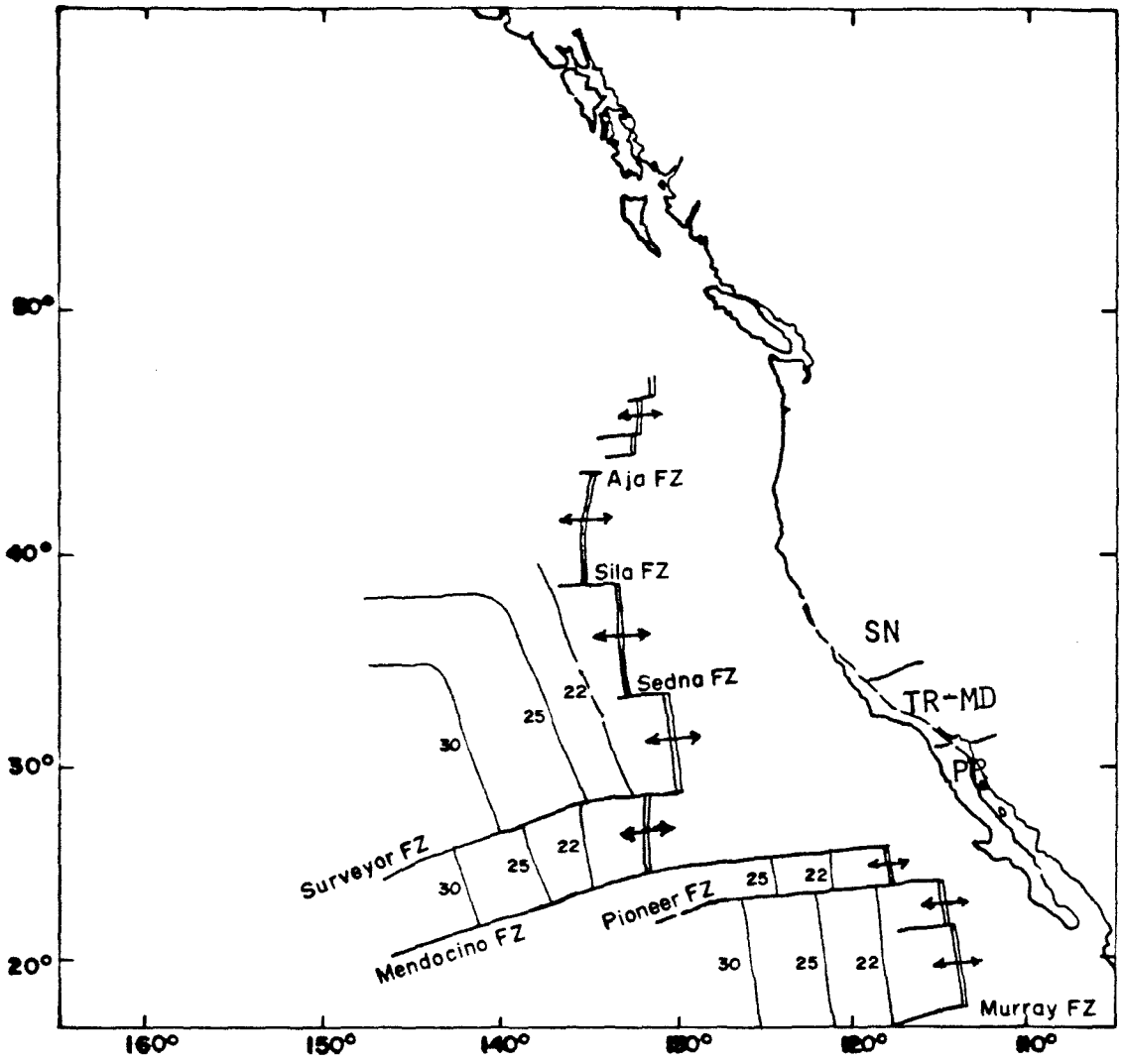
Figure 6-4. Restoration of magnetic anomaly and fracture zone patterns of the northeastern Pacific Ocean floor relative to North America that is proposed to align the Sedna and Surveyor fracture zones with the Garlock fault and Gila River lineament, respectively. Present latitude and longitude are maintained throughout the sequence of diagrams. Magnetic anomaly and fracture zone patterns are modified from Atwater (1970, fig. 1) and Hilde et al. (1977, fig. 19). See text for discussion. The sequence of diagrams records anomaly and fracture zone patterns at the times of successively older anomalies (from Heirtzler et al., 1968; Sclater et al., 1974; Tarling and Mitchell, 1976; Ness et al., 1980):

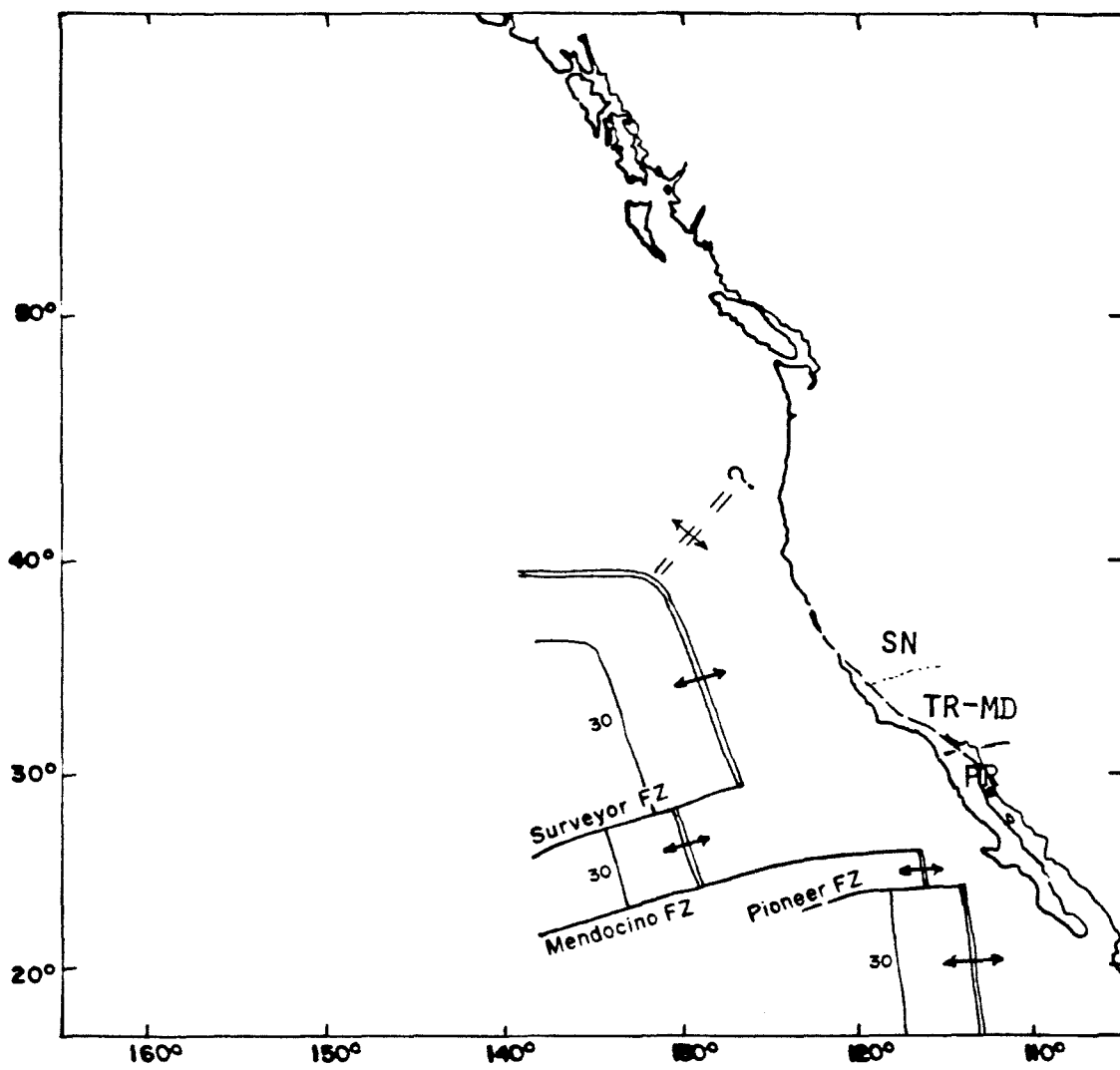
	<u>H1968</u>	<u>S1974</u>	<u>TM1976</u>	<u>N1980</u>
A. Present				
B. Anomaly 3 (ca. 4.5 m.y.	4.5 m.y.	4.5 m.y.	4.5 m.y.	4.5 m.y. ago)
C. Anomaly 7 (ca. 27 m.y.	26 m.y.	25.5 m.y.	25 m.y. ago)	
D. Anomaly 20 (ca. 49 m.y.	46.5 m.y.	41 m.y.	44.5 m.y. ago)	
E. Anomaly 25 (ca. 63 m.y.	59 m.y.	53 m.y.	58 m.y. ago).	











Desert crustal block (Figure 6-3). This timing also corresponds to that of the minimum angles of subduction proposed by Coney and Reynolds (1977) and Keith (1978) in models based on relating the eastward migration of arc magmatism in southwestern North America (see Lipman et al., 1971; Anderson and Silver, 1974; Silver et al., 1975) to the intersection of a subducting slab with specific depths at which magma is generated.

After the shallow underthrusting of Pelona-type schist beneath the continental crust of the Mojave Desert-Transverse Ranges, the stage was set for the impending change in plate interaction as the Farallon plate was consumed and the San Andreas fault system initiated. The northwesterly strike-slip translation commenced 32 m.y. ago (anomaly 10) at the earliest (Atwater, 1970), when the ridge axis south of the Pioneer fracture zone and then one between the Pioneer and Mendocino fracture zones intersected the North America plate. The positioning of the Sedna and Surveyor fracture zones opposite the Transverse Ranges-Mojave Desert block is consistent with the about 1200 kilometers of right-lateral displacement along the Mendocino transform fault--accommodated by about 300 kilometers of displacement along the San Andreas fault and about 900 kilometers of displacement along an offshore fault system required along the coast of Baja California and California (Atwater's (1970) model of constant motion between the Pacific and North America plates) (Figures 6-4A,B).

A ridge segment north of the Aja fracture zone must have reached the North America plate at about the time of anomalies 7 and 8, as can be seen in the anomaly pattern shown by Hilde et al., (1977, fig. 19). When this double linking of the North America and Pacific plates was accomplished at the time of anomalies 8 and 7 (27-29 m.y. ago), the

translational interaction between these two plates affected the spreading direction between the Pacific and Farallon plates (Figure 6-4C). This effect can be seen in the record remaining on the Pacific plate: every major fracture zone other than the Pioneer appears to bend abruptly southeastward at anomalies 7-8 (Figure 6-4; cf. Atwater, 1970, fig. 1; Hilde et al., 1977, fig. 19). If transform faults are formed parallel to the direction of spreading, then that direction must have changed 27-29 m.y. ago. However, because the younger anomalies remain parallel to those that predate anomaly 8, the spreading must have been oblique rather than perpendicular to the ridge axis. At anomalies 3 to 5 (5-9 m.y. ago), the ridge axis began to rotate, perhaps an adjustment to align the ridge axis normal to the spreading direction (Figure 6-4B). Such a pattern is consistent with the patterns of experimental (cooling wax) and natural (cooling lava lake) analogs to plate interactions (Oldenburg and Brune, 1972; Duffield, 1972). There appears to be promise in pursuing these lines of thought concerning the interactions among the North America, Pacific, and Farallon plates after 27-29 m.y. (anomalies 7-8) with regard to oroclinal bending and extension within the Basin and Range province, but this will not be done here.

It is proposed here that, as the regional stress system changed in the transition from convergence between the Farallon and North America plates to strike-slip translation between the Pacific and North America plates, the great keeled batholiths were rotated clockwise by right-lateral couples associated with the new northwest-oriented fracture zones, whereas the rootless Mojave Desert-Transverse Ranges block responded as an easily deformable "soft" zone between the left-lateral couple of the two rigid, rotating batholithic blocks as well as to the

right-lateral shear imposed by the newly oriented northwest-trending fracture zones (Plate VIIA-G).

One major implication of this model is that the Mojave Desert-Transverse Ranges crustal block must make structural adjustments in response to two crustal tectonic regimes:

1. The clockwise rotation of the batholithic crustal blocks bounding the province to the north and south imposes a left-lateral couple on the intervening block;

2. The right-lateral translational movement of the North American continent past the Pacific plate is ultimately responsible for the clockwise rotation of the batholithic blocks, and in addition imposes a right-lateral shear across the Mojave Desert-Transverse Ranges block. The interaction of these two couples through time has led to the deformational complexity of the region. The deformational pattern produced by each couple is progressively distorted by the influence of the other. The net effect, however, seems to be a northeast-southwest compressional axis that has tended to produce folding and thrusting within a northwest-southeast zone perpendicular to the compressional axis (Plate VII).

The initial response to this regional stress field is inferred to have been the development of a throughgoing northwest-trending antiform or an echelon antiformal array diagonally across the Mojave Desert-Transverse Ranges block (Plate VIC; Plate VIIA). The regional fold array is now represented by the fragmented fold segments cored by Pelona-type schist. Accumulation of mid-Tertiary terrestrial sediments and volcanics seems to have been localized in the synforms flanking this antiform. During or following the growth of this fold, the conjugate

fracture set began to form, possibly represented now in their early orientation by the east northeast- to northeast-oriented left-lateral faults of Soledad Basin, subsequently isolated from further development by translation along the San Andreas fault system.

As translation continued along the plate boundary, the Mojave Desert-Transverse Ranges block broke subparallel to the antiform along successive strands of the San Andreas fault system, with intervening or coeval episodes of counterclockwise (left-lateral) rotation. As old strands of the San Andreas fault system were rotated, new strands tended to break across the preceding strands near pivot points in the Transverse Ranges-Mojave Desert crustal block, resulting in west-to-east younging of faults north of the pivotal region and east-to-west younging south of it. These relationships are portrayed in the series of generalized palinspastic reconstructions shown in Plate VIIA to G. During this time interval, the Mojave Desert and Eastern Transverse Ranges, both fixed to North America, were rotated in the left-lateral couple, continuing the northeast-southwest compression that resulted in rotation and increased displacement on the conjugate fracture system of these regions. Increasing northwestward translation of the Peninsular Ranges block and clockwise rotation of both batholithic blocks has yielded increasing compression in the zone of convergence between the two batholithic blocks. With increasing compression this zone has been marked by late Cenozoic folding along east-west to westnorthwest axes and eventually to north-south thrusting as the minimum principal stress axis rotated from westnorthwest to vertical. Eventually, however, translation along the San Andreas fault must prevail to move the two batholithic blocks past one another. Structurally, most of the Neogene compressional features of southern California, including

thrust faults and folds, lie within and subparallel to the northwest-southeast normal to this axis of maximum principal stress (see Jennings, 1977).

A stress regime for southern California has been experimentally modelled by Lowell (1972) as a clay layer above two tin plates. The clay was deformed by moving the tin plates right-laterally while sliding one plate beneath the other. The sequence and style of deformational events produced in the model is very similar to the geologically inferred tectonic evolution described above for southern California. First, en echelon anticlines formed parallel to the long axis of the strain ellipsoid. While these folds continued to grow, a conjugate fracture system developed with its acute angle nearly bisected by the axis of compression. Finally, a zone of uplift with thrust margins developed above the right-lateral shear. However, a through-going right-lateral break did not develop parallel to the underlying shear zone, presumably because the right-lateral model deformation was stopped before such a structure was produced. Physiographically, the highest elevations in southern California follow the eastern flanks of the batholithic blocks of the Sierra Nevada and the Peninsular Ranges, but in the intervening block the maximum elevations roughly coincide with the zone of compression, in a pattern analogous to the upwarp of Lowell's clay model (see Figure 1-1).

Seismically, the distribution of epicenters in southern California vaguely reflects the zigzag pattern of the physiography (cf. Fuis et al., 1977, pl. 10). The correlation is more striking for epicenters of earthquakes with magnitude $M > 6.0$ (see Allen et al., 1965, fig. 5, with the addition of the San Fernando earthquake (1971) located in the western San Gabriel Mountains, earthquakes at Borrego Mountain (1968) and

Calexico (1979) located on the eastern margin of the Peninsular Ranges, and the Mammoth Lakes earthquake (1980) located on the east flank of the Sierra Nevada). Similarly, the strain release map of southern California (Allen et al., 1965, fig. 6) mimics the physiography.

On the basis of teleseisms from an earthquake in the Java trench recorded by the southern California seismograph network, Hadley and Kanamori (1977) have delimited a belt of early arrival times that trends east along the western and central Transverse Ranges then across the San Andreas fault into the northwestern Mojave Desert. In this anomalous belt residual differences between actual and calculated arrival times are sharply reduced from values in the surrounding region. From the magnitude of the reduction, Hadley and Kanamori infer an anomalous velocity zone within the upper mantle. By combining this information with the results of a reversed seismic refraction profile along the Transverse Ranges, they postulate that the anomalous velocity zone consists of an elongate prism of high velocity mantle material ($V_p = 8.0$ km/sec) inserted within lower velocity material (7.8 km/sec). The top of the prism is at a depth of 40 kilometers beneath the axis of the belt of early arrival times, but the flanks drop off steeply to depths of at least 100 kilometers.

Because the incidence of the teleseisms is nearly vertical (4°), Hadley and Kanamori conclude that the anomalous velocity zone in the mantle lies directly beneath its surface expression. Because the trend of the velocity anomaly at the surface crosses the San Andreas fault at a high angle with little or no offset, it follows that the mantle anomaly itself is not offset by the San Andreas fault. Hadley and Kanamori argue that the mantle anomaly is older than the San Andreas fault and is probably related to a landward extension of the Murray fracture zone.

The observation that the mantle anomaly is not disrupted along the San Andreas fault implies that the mantle expression of the plate boundary is not linked to the crustal break, but rather must pass around one end of the anomaly. They propose that the plate boundary in the mantle truncates the east end of the anomaly. Hadley and Kanamori also propose that the San Andreas fault is offset from this mantle location by horizontal shearing along the crust-mantle interface at a depth of about 30 kilometers.

Within the context of the tectonic model presented above, interpretation of the mantle velocity anomaly is ambiguous. Horizontal displacement of the San Andreas fault at the crust-mantle boundary is not obviously reflected in the surface geology. Right-lateral shear along a mantle plate boundary beneath the overlying crust of the central Mojave Desert would provide a driving mechanism for producing the conjugate strike-slip faults of the region, but there is not similar surface evidence that the mantle plate boundary extends north across the Garlock fault beneath the southern Sierra Nevada as required in their interpretation. In fact, the geological and geophysical contrasts between the Mojave Desert and Sierra Nevada seem to preclude a simple projection. Furthermore, the system of right lateral faults in the Mojave Desert appears to trend southeastward through the Colorado Desert rather than converging on the San Andreas fault toward the south.

In the interpretation of Hadley and Kanamori, the mantle anomaly is offset by a mantle expression of the San Andreas fault beneath the Mojave Desert. In the palinspastic reconstruction of the San Andreas fault system presented here, the offset segment of the mantle anomaly should occur beneath the Gila River lineament. The station coverage shown by

Hadley and Kanamori is not sufficient to test the prediction.

An alternative interpretation of the mantle velocity anomaly emerges from the tectonic model presented above. Plate VII shows that, as the Sierra Nevada and Peninsular Ranges batholithic crustal blocks are rotated clockwise and moved toward one another by right-lateral translation along the San Andreas fault system, the crust of the Transverse Ranges and Mojave Desert is complexly deformed. The two batholithic blocks, however, with their deep crustal roots are relatively undeformed as they converge. The locations of the batholiths with respect to the surface expression of the mantle anomaly are shown in Plate VIIG. It is apparent that the mantle may be jammed between the batholithic roots. The anomaly may be produced by a combination of upward squeezing of the mantle and velocity contrasts between the batholithic roots and the mantle material beneath the Mojave Desert and Transverse Ranges. The anomaly contours of Hadley and Kanamori (1977) overlap southward from the Transverse Ranges into the Peninsular Ranges (Plate VIIG). This overlap may be the result of southward projection of the anomaly by teleseisms arriving along a great circle route from Java with an incidence angle of a few degrees. In this interpretation, the mantle anomaly is not offset by the San Andreas fault, but rather is forming beneath it contemporaneously with translation along the fault and convergence of the two thick batholithic crustal blocks. It is possible that structurally high mantle beneath the Transverse Ranges-Mojave Desert block impedes the rate of right-lateral displacement along the San Andreas fault, which would result in clockwise rotation of the Sierra Nevada and Peninsular Ranges blocks, thereby imposing a left-lateral couple on the Transverse Ranges-Mojave Desert crustal block.

VII. CONCLUSIONS

The essential accomplishment contained within this study is the comprehensive geologic map (Plate I) of the crystalline basement complex of the southern Eastern Transverse Ranges. The region mapped comprises about 3000 km² in the Chuckwalla, Orocopia, Eagle, Cottonwood, Hexie, Little San Bernardino, and Pinto Mountains of Riverside County, California. The field study has led to the definition of regional stratigraphic units within the crystalline complex and to the discovery of several previously unrecognized stratigraphic and structural features and relationships that permit, for the first time, the construction of a coherent model for the geologic evolution of the basement complex. The stratigraphic, metamorphic, and structural patterns established in the mapping constrain palinspastic reconstructions of regional tectonic features that have disrupted those patterns.

The rocks of the crystalline complex that are older than the Jurassic(?) and Cretaceous(?) batholiths comprise two lithologically distinct terranes of regional extent. These terranes are superposed along a previously unrecognized thrust system of comparable extent (Red Cloud thrust). The terranes are called the Joshua Tree and San Gabriel terranes for the regions of southern California in which their lithologies were initially characterized. Most of the individual lithologies of both terranes had been observed and characterized to varying degrees prior to the start of this study. For the Joshua Tree terrane, the elements included the Pinto gneiss (Miller, 1938), the quartzite of the Eagle and Pinto Mountains (Harder, 1912; Hadley, 1945; Hope, 1966, 1969; Dubois and Brummett, 1968), and the granite gneiss of the Eagle Mountains (Hope, 1966), although the Pinto gneiss was not differentiated from the Hexie and Augustine gneisses and the granite gneiss was not mapped as a

separate unit. For the San Gabriel terrane, most of the lithologies initially had been defined in the San Gabriel Mountains, including the anorthosite-gabbro (Miller, 1934; Higgs, 1954; Oakeshott, 1958; Silver et al., 1963; Silver, 1971; Carter and Silver, 1972; Carter, 1980b), syenite-mangerite-jotunite (Silver et al., 1963; Silver and Carter, 1965; Silver, 1971; Carter and Silver, 1972; Carter, 1980b), and retrograded granulite (Mendenhall) gneiss (Oakeshott, 1958; Silver et al., 1963; Silver and Carter, 1965; Carter, 1980b). All of these lithologies had also been recognized in the Eastern Transverse Ranges in the Orocochia Mountains (Crowell and Walker, 1962; Silver, 1971) and the Soledad gneiss and syenite-mangerite-jotunite in the Chuckwalla and Little Chuckwalla Mountains (Silver, 1971). In addition, the Soledad gneiss lithology had also been mapped (without specific correlation) in the Hexie Mountains (Hope, 1966, 1969), although the Hexie, Augustine, and Pinto gneisses around it had not been differentiated.

During the course of this study, the structurally lower of the two terranes (Joshua Tree terrane) has been characterized for the first time as a stratigraphically coherent group of crystalline rocks. This synthesis hinged upon the recognition of certain key stratigraphic relationships, including the nonconformity at the base of the quartzite and the interfingering of quartzite with pelitic granofels and schist. The Joshua Tree terrane consists of a basement of Precambrian granite (> 1650 m.y. old, L. Silver, personal comm.) capped by a paleo-weathered zone and overlain nonconformably by orthoquartzite that interfingers westward with pelitic and feldspathic granofelses. The quartzite contains near-basal quartz/quartzite clast conglomerates, and has well-preserved cross-bedding that appears upright wherever it has been observed.

Pelitic and feldspathic granofelses crop out to the west of the quartzite exposures in four lithologically different belts that trend north-northwest throughout the area mapped. These lithologic belts are interpreted to have been derived from stratigraphically interfingering sedimentary protoliths deposited in a basin offshore from a quartzose beach-sand protolith. In proximity to the early Red Cloud thrust, this whole stratigraphic package was pervasively deformed to granite gneiss, stretched pebble conglomerates, lineated quartzites, and schist.

An analysis of the metamorphic imprint on the metasedimentary rocks of the Joshua Tree terrane has provided useful tectonic as well as petrologic information. A northeast-trending pattern of metamorphic isograds was orthogonally superimposed on the northnorthwest-trending protoliths of the Pinto gneiss. A central zone of andalusite, located in the southern Little San Bernardino and Hexie, and northern Eagle Mountains, is flanked to the northwest and southeast by sillimanite zones. Coincident with this symmetrical distribution of aluminosilicates is an asymmetrical distribution of other pelitic mineral zones, with prograde cordierite-aluminosilicate-biotite- and K-feldspar-aluminosilicate-bearing assemblages to the northwest in the northern Little San Bernardino and Pinto Mountains, staurolite-bearing assemblages in a narrow zone in the southern Little San Bernardino-Hexie and northern Eagle Mountains, and retrograde chlorite-muscovite-bearing assemblages in the southernmost Little San Bernardino, Cottonwood, southern Eagle, Orocopia, and Chuckwalla Mountains. One occurrence of chloritoid-sillimanite in the central Eagle Mountains is apparently also retrograde. The isograds involving the Fe-Mg-Al silicates must intersect the andalusite-sillimanite isograd. The crossing isograds are interpreted to result from a temporal increase

in P_{H_2O} relative to P_T from south to north through the field area. Comparison of the pelitic assemblages with experimental studies suggests peak conditions of $P_T \approx 3.5$ to 4 kb, $T \approx 525$ to 625°C. From the pattern of retrograde assemblages, P_{H_2O} is inferred to have been regionally less than P_T during the early stages of metamorphism, then to have approached equality with P_T during the later stages. The timing of the early stages of metamorphism must have pre-dated the thrusting event because the prograde mineral assemblages become deformed within the thrust-related fabric. In addition, the Hexie gneiss (sillimanite-garnet-biotite-bearing assemblages) of the San Gabriel terrane is thrust over the andalusite zone within the Pinto gneiss. The retrograde stage of the metamorphism, however, may have overlapped in time with the emplacement of the San Gabriel terrane allochthon. Talc-chlorite-clinoamphibole and cordierite-orthoamphibole-chlorite \pm garnet assemblages occur in one stratigraphic zone within one of the pelitic granofels of the Pinto gneiss. One sample of cordierite-orthoamphibole granofels contains ferro-aluminous enclaves of corundum + spinel (hercynite?) + staurolite armored within cordierite.

In this study, the known occurrences of the syenite-mangerite-jotunite and retrograded granulite lithologies as well as the newly differentiated Hexie gneiss lithology of the allochthonous San Gabriel terrane have been extended to include all of the Eastern Transverse Ranges south of the Pinto Mountains. The lithologies of the San Gabriel terrane in the Eastern Transverse Ranges are modeled as a three-part lower crustal section, with upper-amphibolite grade pelitic (Hexie) gneiss intruded by granodioritic to monzogranitic (Soledad) augen gneiss at the highest level, retrograded granulite (Augustine) gneiss at an intermediate level, and syenite-mangerite-jotunite at the lowest level

exposed within the Eastern Transverse Ranges. The Hexie gneiss is derived from a metasedimentary protolith that has been regionally metamorphosed to uppermost amphibolite grade gneiss characterized by sillimanite-garnet-biotite-bearing assemblages. Deformed sheets of Soledad granodioritic augen gneiss were originally intrusive into the Hexie gneiss. The Augustine gneiss appears to be intrusive into the Hexie and Soledad gneisses and is characterized by calcic hornblende-plagioclase-sphene-bearing assemblages that could not have been derived exclusively from melting or mobilization of the pelitic Hexie gneiss lithologies. Syenite-mangerite-jotunite intrudes the Augustine gneiss, but has not been found in contact with Hexie-Soledad gneiss.

The stratigraphic relationships discussed above were resolved concurrently with the unraveling of the Red Cloud thrust system, such that each incremental advance in understanding of the stratigraphy helped clarify the structure, and vice versa. Within this context, the Red Cloud thrust is inferred to consist of three or four sequential structural events:

- 1) early thrusting that probably moved parallel to the eastnortheast mineral lineations recorded in both plates;
- 2) regional folding of the initial thrust surface around northnortheast-trending axes;
- 3) later thrusting that broke with some component of westward movement across a fold in the older thrust surface to produce a stacking of crystalline thrust plates of the two terranes;
- 4) continued or renewed folding of both thrust faults with eventual overturning toward the southwest.

It is consistent with all observations to date to link these structural events into the culmination of a regional tectonic episode that resulted in the westward-vergent allochthonous emplacement of the San Gabriel terrane over Joshua Tree terrane. The absolute age of the development of composite thrust system is loosely bracketed between the age of the emplacement of the syenite-mangerite-jotunite (1195 m.y. ago, L. Silver, personal comm.) and the intrusion of the monzogranite of the older Mesozoic batholithic suite (165 m.y. ago, L. Silver, personal comm.).

The pre-batholithic (i.e., pre-Jurassic(?)) terranes and the westward-vergent thrust system that joined them are considered to be lithologically and tectonically exotic with respect to pre-batholithic rocks exposed to the north and east of the field area in the San Bernardino Mountains and southern Mojave and Colorado Deserts. The bounding discontinuity has apparently been obliterated by intrusion of both suites of Mesozoic batholithic rocks.

The Mesozoic plutonic rocks appear to comprise two batholithic suites, both of which have intruded the Joshua Tree and San Gabriel terranes and the Red Cloud thrust system. Three plutonic lithologies have been mapped within each batholithic suite: the oldest lithology of the younger suite intrudes the youngest lithology of the older suite. Generally, each lithology occurs in distinct plutons aligned in belts that trend northwest-southeast through the field area in the Eastern Transverse Ranges south of the Pinto Mountain fault. The older suite, lying to the northeast, appears to have an alkalic character; the younger suite appears calc-alkaline. The older suite consists of biotite- and K-feldspar-bearing gabbro-diorites intruded by low-quartz monzogranites. The younger suite includes hornblende-biotite-sphene granodiorite intruded

by porphyritic monzogranites, intruded in turn by nonporphyritic monzogranite.

Within and bounding the Eastern Transverse Ranges, post-batholithic tectonic events have resulted in disruption of the bedrock patterns that had developed by the end of the Mesozoic history. The Eastern Transverse Ranges south of the Pinto Mountain fault are defined by several east-west Cenozoic left-lateral strike-slip faults that have a cumulative westward displacement from south to north of about 50 kilometers (see Hope, 1966, 1969; Dibblee, 1968b; Powell, 1975; Powell and Silver, 1979). Movement along these faults has apparently ceased in the south where they are not active seismically and where Quaternary depositional and down-cutting events have occurred since the most recent fault movement, whereas to the north, the left-lateral faults break all but the youngest alluvium and have associated seismicity (Fuis et al., 1977). The left-lateral faults are interpreted to represent part of a conjugate fault set with complementary right-lateral faults that are active in the southern Mojave Desert and inferred to be present beneath alluvium in the valleys of the Colorado Desert east of the southern Eastern Transverse Ranges. This conjugate system is perceived to extend farther to the southeast than that considered in the models of Garfunkel (1974) or Cummings (1976).

Along the western boundary of the Eastern Transverse Ranges in the Little San Bernardino Mountains, the crystalline rocks have been pervasively cataclasized by an event that post-dates intrusion of the Cretaceous(?) plutonic rocks. It is hypothesized that the cataclasis is a fabric related to the Vincent-Orocopia-Chocolate Mountains thrust which is transitional upward from mylonite at the thrust through cataclastic crystalline rocks into uncataclasized rock (see Ehlig, 1958; Crowell,

1962; Haxel and Dillon, 1978). The cataclastic foliation is folded about an antiformal axis that traverses the length of the Little San Bernardino Mountains (see Hope, 1966, 1969; Dibblee, 1967e). The antiform is inferred to be cored in the subsurface with Pelona-type schist; except for the level of exposure, this antiform is thought to be analogous to those antiforms in which Pelona-type schist is exposed in the core (Ehlig, 1958; Muehlberger and Hill, 1958; Crowell, 1962; Dillon, 1975; Haxel, 1977; Haxel and Dillon, 1978).

If it is hypothesized that, prior to any movement along the San Andreas fault system in southern California, all of the antiformal exposures of Pelona-type schist along the San Andreas once formed a continuous antiformal feature that was then disrupted during the development of the San Andreas system, then the antiformal axes can be used as piercing points to palinspastically reconstruct displacement along the strands of the San Andreas system (see Bohannon, 1975). Reconstruction of a single antiformal feature is possible with restoration of 220 km of right-lateral movement on the present San Andreas fault and about 80 km of right-lateral displacement along a fragmented older San Andreas strand that consisted of the San Francisquito, Fenner, and Clemens Well faults and a buried extension of this fault beneath the alluvial fill of the valley between the Chocolate and southern Chuckwalla Mountains.

REFERENCES

- Albee, A. L., 1965, A petrogenetic grid for the Fe-Mg silicates of pelitic schists: *Am. Jour. Sci.*, v. 263, p. 512-536.
- _____, 1968, Metamorphic zones in northern Vermont, *in* Zen, E-an and others, eds., *Studies in Appalachian geology: northern and maritime*: John Wiley & Sons, Inc., New York, ch. 25, p. 329-341.
- _____, 1972, Metamorphism of pelitic schists: reaction relations of chloritoid and staurolite: *Geol. Soc. Am. Bull.*, v. 83, p. 3249-3268.
- _____ and Chodos, A. A., 1969, Minor element content of coexistent Al_2SiO_5 polymorphs: *Am. Jour. Sci.*, v. 267, p. 310-316.
- Albritton, C. C., Jr. and Smith, J. F., Jr., 1956, The Texas lineament: *20th Internat. Geol. Cong.*, v. 5, pt. 2, p. 501-518.
- Alexandrov, E. A., 1973, Precambrian iron-formations of the Soviet Union: *Econ. Geol.*, v. 68, p. 1035-1062.
- Allen, C. R., 1957, San Andreas fault zone in San Gorgonio Pass, southern California: *Geol. Soc. Am. Bull.*, v. 68, p. 315-350.
- _____, St. Armand, P., Richter, C. F., and Nordquist, J. M., 1965, Relationship between seismicity and geologic structure in the southern California region: *Bull. Seism. Soc. Am.*, v. 55, p. 753-797.
- Akella, J. and Winkler, H. G. F., 1966, Orthorhombic amphiboles in some metamorphic reactions: *Contr. Miner. Petrol.*, v. 12, p. 1-12.
- Althaus, E., 1966, Der Stabilitätsbereich des Pyrophyllits unter dem Einfluss von Sauren. I. Mitteilung, Experimentelle Untersuchungen: *Contr. Miner. Petrol.*, v. 13, p. 31-50.
- _____, 1967, The triple point andalusite-sillimanite-kyanite: *Contr. Miner. Petrol.*, v. 16, p. 29-44.
- _____, 1969, Das System $Al_2O_3-SiO_2-H_2O$. Experimentelle Untersuchungen und Folgerungen für die Petrogenese der metamorphen Gesteine, Teil I und II: *Neues Jahrb. Miner. Abh.*, v. 111, p. 74-143.
- _____, Karotke, E., Nitsch, K. H., and Winkler, H. G. F., 1970, An experimental re-examination of the upper stability limit of muscovite plus quartz: *Neues Jahrb. Miner. Monatsh.* v. 7, p. 325-326.
- Anderson, P. A. M. and Kleppa, O. J., 1969, The thermochemistry of the kyanite-sillimanite equilibrium: *Am. Jour. Sci.*, v. 267, p. 285-290.
- Anderson, T. H., Eells, J. H., and Silver, L. T., 1979, Precambrian and Paleozoic rocks of the Caborca region, Sonora, Mexico, *in* Anderson, T. H. and Roldan-Quintana, J., eds., *Geology of northern Sonora: guidebook--field trip #27*, 1979 Annual Meeting *Geol. Soc. Am.*: Inst. Geol., U.N.A.M., Hermosillo, Sonora, Mexico and Univ.

Pittsburgh, Pittsburgh, p. 1-22.

_____ and Silver, L. T., 1970, Reconnaissance survey of Precambrian rocks, northwestern Sonora, Mexico [abs.]: Geol. Soc. Am., Abs. with Prog., v. 2, n. 7, p. 484.

_____ and _____, 1971, Preliminary history for Precambrian rocks, Bamori Region, Sonora, Mexico [abs.]: Geol. Soc. Am., Abs. with Prog., v. 3, n. 3, p. 72-73.

_____ and _____, 1974, Late Cretaceous plutonism in Sonora, Mexico and its relationship to circum-Pacific magmatism [abs.]: Geol. Soc. Am., Abs. with Prog., v. 6, p. 484.

_____ and _____, 1979, The role of the Mojave-Sonora megashear in the tectonic evolution of northern Sonora, in Anderson, T. H. and Roldan-Quintana, J., eds., Geology of northern Sonora: guidebook--field trip #27, 1979 Annual Meeting Geol. Soc. Am.: Inst. Geol., U.N.A.M., Hermosillo, Sonora, Mexico and Univ. Pittsburgh, Pittsburgh, p. 59-68.

Armstrong, R. L. and Suppe, J., 1973, Potassium-argon geochronometry of Mesozoic igneous rocks in Nevada, Utah, and southern California: Geol. Soc. Am. Bull., v. 84, p. 1375-1392.

Atwater, T. 1970, Implications of plate tectonics for the Cenozoic tectonic evolution of western North America: Geol. Soc. Am. Bull., v. 81, p. 3513-3536.

Badgley, P. C., 1965, Structural and tectonic principles: Harper & Row, Inc., New York, 521 p.

Bailey, E. H., Irwin, W. P., and Jones, D. L., 1964, Franciscan and related rocks, and their significance in the geology of western California: Calif. Div. Mines Geol., Bull. 183, 177 p.

Barazangi, M. and Isacks, B. L., 1976, Spatial distribution of earthquakes and subduction of the Nazca plate beneath South America: Geology, v. 4, p. 686-692.

Bateman, P. C. and Dodge, F. C. W., 1970, Variations of major chemical constituents across the central Sierra Nevada batholith: Geol. Soc. Am. Bull., v. 81, p. 409-420.

Bayley, R. W. and James, H. L., 1973, Precambrian iron-formations of the United States: Econ. Geol., v. 68, p. 934-959.

Berggren, W. A., 1969, Cenozoic chronostratigraphy, planktonic and foraminiferal zonation and the radiometric time scale: Nature, v. 224, p. 1072-1075.

_____, McKenna, M. C., Hardenbol, J., and Obradovich, J. D., 1978, Revised Paleogene polarity time scale: Jour. Geol., v. 86, p. 67-81.

- Biehler, S., Kovach, R. L., and Allen, C. R., 1964, Geophysical framework of northern end of Gulf of California structural province, in Marine geology of the Gulf of California--a symposium: Am. Assoc. Petrol. Geol. Memoir 3, p. 126-143.
- Bird, G. W. and Fawcett, J. J., 1973, Stability relations of Mg-chlorite-muscovite and quartz between 5 and 10 Kb water pressure: Jour. Petrol., v. 14, p. 415-428.
- Bishop, C. C., compiler, 1964, Geologic map of California, Needles sheet: Calif. Div. Mines Geol., scale 1:250,000.
- Bjørlykke, K., 1975, Mineralogical and chemical changes during weathering of acid and basic rocks in Uganda: Norsk Geol. Tidsskrift, v. 55, p. 81-89.
- Bohannon, R. G., 1975, Mid-Tertiary conglomerates and their bearing on Transverse Range tectonics, southern California, in Crowell, J. C., ed., San Andreas fault in southern California, a guide to San Andreas fault from Mexico to Carrizo Plain: Calif. Div. Mines Geol., Spec. Rept. 118, p. 99-110.
- Bouchez, J-L. and Pécher, A., 1976, Plasticité du quartz sens de cisaillement dans des quartzites du Grand Chevauchement Central himalayen: Bull. Soc. géol. France, p. 1377-1385.
- Broderick, T. M., 1919, Detail stratigraphy of the Biwabik iron-bearing formation, East Mesabi district, Minnesota: Econ. Geol., v. 14, p. 441-451.
- Brøgger, W. C., 1934, On several Archean rocks from the south coast of Norway, II. The south Norwegian hyperites and their metamorphism: Vidensk.-Selsk. Skrifter Oslo I, Math Naturv. Kl. Bd. I, fide Sørbye, 1964, Tilley, 1935.
- Brown, G. C. and Fyfe, W. S., 1971, Kyanite-andalusite equilibrium: Contr. Miner. Petrol., v. 33, p. 227-231.
- Buddington, A. F., 1939, Adirondack igneous rocks and their metamorphism: Geol. Soc. Am. Mem. 7, 354 p.
- Bugge, J. A. W., 1943, Geological and petrographical investigations in the Kongsberg-Bamble formation: Norges Geol. Undersøkelse, n. 160, 150 p., fide Sørbye, 1964, Grant, 1968.
- Burchfiel, B. C. and Davis, G. A., 1972, Structural framework and evolution of the southern part of the Cordilleran orogen, western United States: Am. Jour. Sci., v. 272, p. 97-118.
- Burke, D. B. and Clark, M. M., 1978, Late Quaternary activity along the Garlock fault at Koehn Lake, Fremont Valley, California [abs.]: Trans. Am. Geophys. Union (EOS), v. 59, p. 1126.

- Burnell, J. R. and Rutherford, M. J., 1979, The terminal equilibrium of chlorite in the system $K_2O-MgO-FeO-Al_2O_3-SiO_2-H_2O$ [abs.]: *Trans. Am. Geophys. Union (EØS)*, v. 60, p. 423.
- Butler, J. R., 1964, Contact metamorphism along the base of the Stillwater Complex, Montana [abs.]: *Geol. Soc. Am. Spec. Paper, Annual Meeting Prog.*, 1964, p. 24.
- Cameron, S., Guth, P. L., and Burchfiel, B. C., 1979, The early Mesozoic Cave Mountain sequence: its implications for Mesozoic tectonics [abs.]: *Geol. Soc. Am., Abs. with Prog.*, v. 11, n. 7, p. 397.
- Carman, M. F., Jr., 1964, Geology of the Lockwood Valley area, Kern and Ventura Counties, California: *Calif. Div. Mines Geol., Spec. Rept.* 81, 62 p.
- Carter, B., 1970, Structure of the San Gabriel anorthosite massif, California [abs.]: *Trans. Am. Geophys. Union (EØS)*, v. 51, p. 446.
- _____, 1971, Quaternary displacement on the Garlock fault, California [abs.]: *Trans. Am. Geophys. Union (EØS)*, v. 52, p. 350.
- _____, 1980a, Possible Pliocene inception of lateral displacement on the Garlock fault, California [abs.]: *Geol. Soc. Am., Abs. with Prog.*, v. 12, n. 3, p. 101.
- _____, 1980b, Structure and petrology of the San Gabriel anorthosite-syenite body, Los Angeles County, California: Unpub. Ph.D. thesis, Calif. Inst. Technology, 393 p.
- _____ and Silver, L. T., 1972, Structure and petrology of the San Gabriel anorthosite-syenite body, California: 24th Int. Geol. Congress, Sec. 2, p. 303-311.
- Chapman, C. A., 1939, Geology of the Mascoma quadrangle, New Hampshire: *Geol. Soc. Am. Bull.*, v. 50, p. 127-180.
- Chatterjee, N. D., 1972, The upper stability limit of the assemblage paragonite + quartz and its natural occurrences: *Contr. Miner. Petrol.*, v. 34, p. 288-303.
- _____, and Johannes, W., 1974, Thermal stability and standard thermodynamic properties of synthetic $2M_1$ -muscovite, $KAl_2[AlSi_3O_{10}(OH)_2]$: *Contr. Miner. Petrol.*, v. 48, p. 89-114.
- Chernosky, J. V., Jr., 1974, The upper stability of clinocllore at low pressure and the free energy of formation of Mg-cordierite: *Am. Miner.*, v. 59, p. 496-507.
- _____, 1975, The stability of the assemblage clinocllore + quartz at low pressure [abs.]: *Trans. Am. Geophys. Union (EØS)*, v. 56, p. 466.

- Chernosky, J. V., Jr., 1976, The stability of anthophyllite--a reevaluation based on new experimental data: *Am. Miner.*, v. 61, p. 1145-1155.
- _____, and Autio, L. K., 1979, The stability of anthophyllite in the presence of quartz: *Am. Miner.*, v. 64, p. 294-303.
- Chinner, G. A. and Fox, J. S., 1974, The origin of cordierite-anthophyllite rocks in the Land's End aureole: *Geol. Mag.*, v. 111, p. 397-408.
- _____, Smith, J. V., and Knowles, C. R., 1969, Transition metal contents of Al₂SiO₅ polymorphs: *Am. Jour. Sci.*, v. 259, p. 641-650.
- Christie, J. M., 1963, The Moine Thrust zone in the Assynt region, north-west Scotland: *Univ. Calif. Publ. Geol. Sci.*, v. 40, p. 345-439.
- Clark, M. M., 1973, Map showing recently active breaks along the Garlock and associated faults, California: U.S. Geol. Surv. Misc. Geol. Inv. Map I-741, scale 1:24,000.
- _____, and Lajoie, K. R., 1974, Holocene behavior of the Garlock fault [abs.]: *Geol. Soc. Am., Abs. with Prog.*, v. 6, n. 3, p. 156-157.
- Cloos, E., 1955, Experimental analysis of fracture patterns: *Geol. Soc. Am. Bull.*, v. 66, p. 241-256.
- Cobbing, E. J. and Pitcher, W. S., 1972, The Coastal batholith of Peru: *Jour. Geol. Soc. London*, v. 128, p. 421-460.
- _____, _____, and Taylor, W. P., 1977, Segments and super-units in the Coastal batholith of Peru: *Jour. Geol.*, v. 85, p. 625-631.
- Compton, R. R., 1966, Granitic and metamorphic rocks of the Salinian block, California Coast Ranges, in Bailey, E. H., ed., *Geology of northern California*: Calif. Div. Mines Geol., Bull. 190, p. 277-287.
- _____, 1960, Charnockitic rocks of Santa Lucia Range, California: *Am. Jour. Sci.*, v. 258, p. 609-636.
- Coney, P. J., 1978, Mesozoic-Cenozoic Cordilleran plate tectonics, in Smith, R. B. and Eaton, G. P., eds., *Cenozoic tectonics and regional geophysics of the western Cordillera*: *Geol. Soc. Am., Memoir 152*, p. 33-50.
- _____, and Reynolds, S. J., 1977, Cordilleran Benioff zones: *Nature*, v. 170, p. 403-406.
- Conrad, R. L. and Davis, T. E., 1977, Rb/Sr geochronology of cataclastic rocks of the Vincent thrust, San Gabriel Mountains, southern California [abs.]: *Geol. Soc. Am., Abs. with Prog.*, v. 9, n. 4, p. 403-404.
- Crowe, B. M., 1973, Tertiary volcanism east of the San Andreas fault, southeastern California, in Kovach, R. L. and Nur, A., eds., *Proceed-*

ings of the conference on tectonic problems of the San Andreas fault system: Stanford Univ. Publ. Geol. Sci., v. 13, p. 334-338.

Crowe, B. M., 1978, Cenozoic volcanic geology and age of inception of Basin-Range faulting in the southeasternmost Chocolate Mountains, California: Geol. Soc. Am. Bull., v. 89, p. 251-264.

_____, Crowell, J. C., and Kruppenacher, D., 1979, Regional stratigraphy, K/Ar ages, and tectonic implications of Cenozoic volcanic rocks, southeastern California: Am. Jour. Sci., v. 279, p. 186-216.

Crowell, J. C., 1952, Probable large lateral displacement on the San Gabriel fault, southern California: Am. Assoc. Petrol. Geol. Bull., v. 36, p. 2026-2035.

_____, 1962, Displacement along the San Andreas fault, California: Geol. Soc. Am., Spec. Paper 71, 61 p.

_____, 1974, The Orocochia thrust, southeastern California [abs.]: Geol. Soc. Am., Abs. with Prog., v. 6, p. 159.

_____, 1975, The San Andreas fault in southern California, in Crowell, J. C., ed., San Andreas fault in southern California: Calif. Div. Mines Geol., Spec. Report 118, p. 7-27.

_____ and Susuki, T., 1959, Eocene stratigraphy and paleontology, Orocochia Mountains, southeastern California: Geol. Soc. Am. Bull., v. 70, p. 581-592.

_____ and Walker, J. W. R., 1962, Anorthosite and related rocks along the San Andreas fault, southern California: Univ. Calif. Publ. Geol. Sci., v. 40, p. 219-287.

Cummings, D., 1976, Theory of plasticity applied to faulting, Mojave Desert, southern California: Geol. Soc. Am. Bull., v. 87, p. 720-724.

Dalziel, I. W. D., de Wit, M. J., and Palmer, K. F., 1974, Fossil marginal basin in the southern Andes: Nature, v. 250, p. 291-294.

Davis, G. A. and Burchfiel, B. C., 1973, Garlock fault: an intracontinental transform structure, southern California: Geol. Soc. Am. Bull., v. 84, p. 1407-1422.

Day, H. W., 1976, A working model of some equilibria in the system alumina-silica-water: Am. Jour. Sci., v. 276, p. 1274-1284

Deer, W. A., Howie, R. A., and Zussman, J., 1966, An introduction to the rock-forming minerals: Longman Group Ltd., London, 528 p.

Dibblee, T. W., Jr., 1954, Geology of the Imperial Valley region, California, in Jahns, R. H., ed., Geology of Southern California: Calif. Div. Mines, Bull. 170, ch. II, p. 21-28.

- Dibblee, T. W., Jr., 1961a, Evidence of strike-slip movement on northwest-trending faults in Mojave Desert, California: U.S. Geol. Surv. Prof. Paper 424B, p. B197-B199.
- _____, 1961b, Geologic map of the Bouquet Reservoir quadrangle, Los Angeles County, California: U.S. Geol. Surv. Miner. Inv. Field Studies Map MF-79, scale 1:62,500.
- _____, 1964a, Geologic map of the Lucerne Valley quadrangle, San Bernardino County, California: U.S. Geol. Surv. Misc. Geol. Inv. Map I-426, scale 1:62,500.
- _____, 1964b, Geologic map of the Ord Mountains quadrangle, San Bernardino County, California: U.S. Geol. Surv. Misc. Geol. Inv. Map I-427, scale 1:62,500.
- _____, 1964c, Geologic map of the Rodman Mountains quadrangle, San Bernardino County, California: U.S. Geol. Surv. Misc. Geol. Inv. Map I-430, scale 1:62,500.
- _____, 1964d, Geologic map of the San Gorgonio Mountain quadrangle, San Bernardino and Riverside Counties, California: U.S. Geol. Surv. Misc. Geol. Inv. Map I-431, scale 1:62,500.
- _____, 1966, Geologic map of the Lavic quadrangle, San Bernardino County, California: U.S. Geol. Surv. Misc. Geol. Inv. Map I-472, scale 1:62,500.
- _____, 1967a, Areal geology of the Mojave Desert, California: U.S. Geol. Surv. Prof. Paper 522, 153 p.
- _____, 1967b, Geologic map of the Deadman Lake quadrangle, San Bernardino County, California: U.S. Geol. Surv. Misc. Geol. Inv. Map I-488, scale 1:62,500.
- _____, 1967c, Geologic map of the Emerson Lake quadrangle, San Bernardino County, California: U.S. Geol. Surv. Misc. Inv. Map I-490, scale 1:62,500.
- _____, 1967d, Geologic map of the Joshua Tree quadrangle, San Bernardino and Riverside Counties, California: U.S. Geol. Surv. Misc. Inv. Map I-516, scale 1:62,500.
- _____, 1967e, Geologic map of the Ludlow quadrangle, San Bernardino County, California: U.S. Geol. Surv. Misc. Inv. Map I-477, scale 1:62,500.
- _____, 1967f, Geologic map of the Morongo Valley quadrangle, San Bernardino and Riverside Counties, California: U.S. Geol. Surv. Misc. Inv. Map I-517, scale 1:62,500.
- _____, 1967g, Geologic map of the Old Woman Springs quadrangle, San Bernardino County, California: U.S. Geol. Surv. Misc. Geol. Inv. I-518, scale 1:62,500.

- Dibblee, T. W., Jr., 1968a, Displacements on San Andreas fault system in San Gabriel, San Bernardino, and San Jacinto Mountains, southern California, in Dickinson, W. R. and Grantz, A., eds., Proceedings of the conference on geologic problems of the San Andreas fault system: Stanford Univ. Pubs. Geol. Sci., v. 11, p. 260-278.
- _____, 1968b, Evidence of major lateral displacement on the Pinto Mountain fault, southern California [abs.]: Geol. Soc. Am., Abs. for 1967, Spec. Paper 115, p. 322.
- _____, 1968c, Geologic map of the Twentynine Palms quadrangle, San Bernardino and Riverside Counties, California: U.S. Geol. Surv. Misc. Geol. Inv. Map I-561, scale 1:62,500.
- _____, 1970a, Geologic map of the Daggett quadrangle, San Bernardino County, California: U.S. Geol. Surv. Misc. Geol. Inv. Map I-592, scale 1:62,500.
- _____, 1970b, Regional geologic map of San Andreas and related faults in eastern San Gabriel Mountains, San Bernardino Mountains, western San Jacinto Mountains and vicinity, Los Angeles, San Bernardino, and Riverside Counties, California: U.S. Geol. Surv. open-file map, scale 1:125,000.
- _____, 1971, A great Middle Tertiary buttress unconformity in the Newberry Mountains, Mojave Desert, California, and its paleogeologic implications [abs.]: Geol. Soc. Am., Abs. with Prog., v. 3, n. 2, p. 110.
- _____, 1975, Late Quaternary uplift of the San Bernardino Mountains on the San Andreas and related faults, in Crowell, J. C., ed., San Andreas fault in southern California, a guide to San Andreas fault from Mexico to Carrizo plain: Calif. Div. Mines Geol., Spec. Rept. 118, p. 127-135.
- _____ and Bassett, A. M., 1966a, Geologic map of the Cady Mountains quadrangle, San Bernardino County, California: U.S. Geol. Surv. Misc. Geol. Inv. Map I-467, scale 1:62,500.
- _____ and _____, 1966b, Geologic map of the Newberry quadrangle, San Bernardino County, California: U.S. Geol. Surv. Misc. Geol. Inv. Map I-461, scale 1:62,500.
- Dillon, J. T., 1975, Geology of the Chocolate and Cargo Muchacho Mountains, southeasternmost California: Unpub. Ph.D. thesis, University of California, Santa Barbara, 405 p.
- _____ and Haxel, G., 1975, The Chocolate Mountain-Orocopia-Vincent thrust system as a tectonic element of late Mesozoic California [abs.]: Geol. Soc. Am., Abs. with Prog., v. 7, n. 3, p. 311-312.
- Dubois, R. L. and Brummett, R. W., 1968, Geology of the Eagle Mountain Mine area, in Ridge, J. D., ed., Ore deposits of the United States, 1933-1967, v. 2: AIMME, Inc., New York, ch. 76, p. 1592-1606.

- Duffield, W. A., 1972, Kilauea Volcano provides a model for plate tectonics: *Geotimes*, v. 17 (Apr.), p. 19-21.
- Durham, J. W., Jahns, R. H., and Savage, D. E., 1954, Marine-nonmarine relationships in the Cenozoic section of California, in Jahns, R. H., ed., *Geology of southern California*: Calif. Div. Mines, Bull. 170, ch. 3, p. 59-71.
- Eaton, J. P., 1966, Crustal structure in northern and central California from seismic evidence, in Bailey, E. H., ed., *Geology of northern California*: Calif. Div. Mines Geol., Bull. 190, p. 419-426.
- Ehlert, K. W. and Ehlig, P. L., 1977, The "polka-dot" granite and the rate of displacement on the San Andreas fault in southern California [abs.]: *Geol. Soc. Am., Abs. with Prog.*, v. 9, n. 4, p. 415-416.
- Ehlig, P. L., 1958, *Geology of the Mount Baldy region of the San Gabriel Mountains, California*: Unpub. Ph.D. thesis, Univ. Calif., Los Angeles, 195 p.
- _____, 1968, Causes of distribution of Pelona, Rand, and Orocochia schists along the San Andreas and Garlock faults, in Dickinson, W. R. and Grantz, A., eds., *Proceedings of conference on geologic problems of San Andreas fault system*: Stanford Univ. Publ. Geol. Sci., v. 11, p. 294-305.
- _____, 1975, Basement rocks of the San Gabriel Mountains, south of the San Andreas fault, southern California, in Crowell, J. C., ed., *San Andreas fault in southern California, a guide to San Andreas fault from Mexico to Carrizo Plain*: Calif. Div. Mines Geol., Spec. Rept. 118, p. 177-186.
- _____, 1976, Magnitude and timing of displacement on San Andreas fault in southern California and its palinspastic implications [abs.]: *Am. Assoc. Petrol. Geol. Bull.*, v. 60, p. 668.
- _____ and Ehlert, K. W., 1972, Offset of Miocene Mint Canyon formation from volcanic source along the San Andreas fault, southern California [abs.]: *Geol. Soc. Am., Abs. with Prog.*, v. 4, n. 3, p. 154.
- _____, _____, and Crowe, B. M., 1975, Offset of the upper Miocene Caliente and Mint Canyon formations along the San Gabriel and San Andreas faults, in Crowell, J. C., ed., *San Andreas fault in southern California, a guide to San Andreas fault from Mexico to Carrizo Plain*: Calif. Div. Mines Geol., Spec. Rept. 118, p. 83-92.
- Eskola, P., 1914, On the petrology of the Orijärvi region in southwestern Finland: *Bull. Comm. Géol. Finlande*, v. 40, p. 1-277.
- _____, 1915, On the relations between the chemical and mineralogical composition in the metamorphic rocks of the Orijärvi region [English summary]: *Bull. Comm. Géol. Finlande*, n. 44, p. 109-145.
- _____, 1952, On the granulites of Lapland: *Am. Jour. Sci.*, Bowen Volume,

- pt. 1, p. 133-171.
- Evans, B. W., 1965, Application of a reaction-rate method to the breakdown equilibria of muscovite and muscovite plus quartz: *Am. Jour. Sci.*, v. 263, p. 647-667.
- Evans, J. R., 1964, Xenotime mineralization in the southern Music Valley area, Riverside County, California: *Calif. Div. Mines Geol., Spec. Report 79*, 23 p.
- Evernden, J. F. and Kistler, R. W., 1970, Chronology of emplacement of Mesozoic batholithic complexes in California and western Nevada: *U.S. Geol. Surv. Prof. Paper 623*, 42 p.
- Fawcett, J. J. and Yoder, H. S., 1966, Phase relationships of chlorite in the system $MgO-Al_2O_3-SiO_2-H_2O$: *Am. Miner.*, v. 51, p. 353-380.
- Fleming, P. D. and Fawcett, J. J., 1976, Upper stability of chlorite + quartz in the system $MgO-FeO-Al_2O_3-SiO_2-H_2O$ at 2 kbar water pressure: *Am. Miner.*, v. 61, p. 1175-1193.
- Floyd, P. A., 1965, Metasomatic hornfels of the Land's End aureole at Tater-du, Cornwall: *Jour. Petrol.*, v. 6, p. 223-245.
- Froese, E., 1969, Metamorphic rocks from the Coronation Mine and surrounding area, in Byers, A. R., ed., *Symposium on the geology of Coronation Mine, Saskatchewan*: *Geol. Surv. Can. Paper 68-5*, p. 55-77.
- Frost, B. R., 1979, Metamorphism of iron-formation: parageneses in the system $Fe-Si-C-O-H$: *Econ. Geol.*, v. 74, p. 775-785.
- Fuis, G. S., Friedman, M. E., and Hileman, J. A., 1977, Preliminary catalog of earthquakes in southern California, July 1974 - September, 1976: *U.S. Geol. Surv. and Seismo. Lab., Calif. Inst. Tech., Pasadena, Calif., Open-file Rept. 77-181*, 107 p.
- Fyfe, W. S. and Hollander, M. A., 1964, Equilibrium dehydration of diaspore at low temperatures: *Am. Jour. Sci.*, v. 262, p. 709-712.
- Ganguly, J., 1968, Analysis of the stabilities of chloritoid and staurolite and some equilibria in the system $FeO-Al_2O_3-SiO_2-H_2O-O_2$: *Am. Jour. Sci.*, v. 266, p. 277-298.
- _____, 1969, Chloritoid stability and related parageneses: Theory, experiments, and applications: *Am. Jour. Sci.*, v. 267, p. 910-944.
- _____, 1972, Staurolite stability and related parageneses: Theory, experiments and applications: *Jour. Petrol.*, v. 13, p. 335-365.
- _____ and Newton, R.C., 1968, Thermal stability of chloritoid at high pressure and relatively high oxygen fugacity: *Jour. Petrol.*, v. 9, p. 444-466.
- Garfunkel, Z., 1974, Model for the late Cenozoic tectonic history of the

- Mojave Desert, California, and for its relation to adjacent regions: Geol. Soc. Am. Bull., v. 85, p. 1931-1944.
- Gastil, R. G., Phillips, R. P., and Allison, E. C., 1975, Reconnaissance geology of the State of Baja California: Geol. Soc. Am. Memoir 140, 170 p.
- Geijer, P., 1916, Årsbok Sveriges Geol. Unders., v. 10, n. 1, fide Tilley, 1935.
- _____, 1923, Kungl. Kommerskoll. Beskriv. Mineralfyndig., n. 1, fide Tilley, 1935.
- Graham, C. M., 1975, Inverted metamorphic zonation and mineralogy of the Pelona schist, Sierra Pelona, Transverse Ranges [abs.]: Geol. Soc. Am., Abs. with Prog., v. 7, n. 3, p. 321-322.
- _____, and England, P. C., 1976, Thermal regimes and regional metamorphism in the vicinity of overthrust faults--an example of shear heating and inverted metamorphic zonation from southern California: Earth Planet. Sci. Lett., v. 31, p. 142-152.
- Grant, J. A., 1968, Partial melting of common rocks as a possible source of cordierite-anthophyllite bearing assemblages: Am. Jour. Sci., v. 266, p. 908-931.
- Greenwood, H. J., 1961, The system $\text{NaAlSi}_2\text{O}_6\text{-H}_2\text{O-argon}$: total pressure and water pressure in metamorphism: Jour. Geophys. Res., v. 66, p. 3923-3946.
- _____, 1963, The synthesis and stability of anthophyllite: Jour. Petrol., v. 4, p. 317-351.
- _____, 1967, Mineral equilibria in the system $\text{MgO-SiO}_2\text{-H}_2\text{O-CO}_2$, in Abelson, P. H., ed., Researches in Geochemistry, v. 2: John Wiley & Sons, Inc., New York, p. 542-567.
- _____, 1971, Anthophyllite: corrections and comments on stability: Am. Jour. Sci., v. 270, p. 151-154.
- _____, 1976, Metamorphism at moderate temperatures and pressures, in Bailey, D. K. and MacDonald, R., eds., The evolution of the crystalline rocks: Academic Press, Inc., London, ch. 2, p. 187-259.
- Grieve, R. A. F. and Fawcett, J. J., 1974, The stability of chloritoid below 10 kb $\text{P}_{\text{H}_2\text{O}}$: Jour. Petrol., v. 15, p. 113-139.
- Guillou, R. B., 1953, Geology of the Johnston grade area, San Bernardino County, California: Calif. Div. Mines, Spec. Report 31, 18 p.
- Haas, H., 1972, Diaspore-corundum equilibria determined by epitaxis of diaspore on corundum: Am. Miner., v. 57, p. 1375-1385.

- Haas, H. and Holdaway, M. J., 1973, Equilibrium in the system $Al_2O_3-SiO_2-H_2O$ involving the stability limits of pyrophyllite and thermodynamic data of pyrophyllite: *Am. Jour. Sci.*, v. 273, p. 449-464.
- Hadley, D. and Kanamori, H., 1977, Seismic structure of the Transverse Ranges, California: *Geol. Soc. Am. Bull.*, v. 88, p. 1469-1478.
- Hadley, J. B., 1945, Iron-ore deposits in the eastern part of the Eagle Mountains, Riverside County, California: *Calif. Div. Mines Bull.* 129, pt. A, 24 p.
- Hall, A. L. and du Toit, A. L., 1923, On the section across the floor of the Bushveld Complex at the Hartebeestpoort Dam, west of Pretoria: *Trans. Geol. Soc. So. Africa*, v. 26, p. 69-97.
- Hamilton, W., 1964, Geologic map of the Big Maria Mountains NE quadrangle, Riverside County, California and Yuma County, Arizona: *U.S. Geol. Surv. Geol. Quad. Maps of the U.S.*, GQ-350, scale 1:24,000.
- _____, 1969, Mesozoic California and the underflow of the Pacific mantle: *Geol. Soc. Am. Bull.*, v. 80, p. 2409-2430.
- _____ and Myers, W. B., 1966, Cenozoic tectonics of the western United States: *Rev. Geophys.*, v. 4, p. 509-549.
- Hansen, E., 1967, Methods of deducing slip-line orientations from the geometry of folds: *Carnegie Inst. Washington Yrbk.* 65, p. 387-405/
- Harder, E. C., 1912, Iron-ore deposits of the Eagle Mountains, California: *U.S. Geol. Surv. Bull.* 503, 81 p.
- Harrison, J. B., 1933, The katamorphism of igneous rocks under humid tropical conditions: *Imper. Bur. Soil Sci., Rothamsted Experimental Sta.*, Harpenden, England.
- Harvill, L. L., 1969, Deformational history of the Pelona schist, northwestern Los Angeles County, California: *Unpub. Ph.D. thesis, Univ. Calif. Los Angeles*, 117 p.
- Haxel, G. B., 1977, The Orocochia schist and the Chocolate Mountain thrust, Picacho-Peter Kane Mountain area, southeasternmost California: *Unpub. Ph.D. thesis, Univ. of California, Santa Barbara*, 277 p.
- _____ and Dillon, J., 1977, The Pelona and Orocochia schists and the proto-San Andreas fault of southern California [abs.]: *Geol. Soc. Am., Abs. with Prog.*, v. 9, n. 4, p. 423-433.
- _____ and _____, 1978, The Pelona-Orocochia schist and Vincent-Chocolate Mountain thrust system, southern California, *in* Howell, D. G. and McDougall, K. A., eds., *Mesozoic paleogeography of the western United States, Pacific Coast Paleogeography Symposium 2: Pacific Section, Soc. Econ. Paleon. Miner.*, Los Angeles, p. 453-469.

- Hays, W. H., 1957, Geology of the central Mecca Hills, Riverside County, California: Unpub. Ph.D. thesis, Yale Univ., New Haven, Conn. 324 p.
- Heirtzler, J. R., Dickson, G. O., Herron, E. M., Pitman, W. C., III, and Le Pichon, X., 1968, Marine magnetic anomalies, geomagnetic field reversals, and motions of the ocean floor and continents: *Jour. Geophys. Res.*, v.73, p. 2119-2136.
- Helgeson, H. C., Delaney, J. M., Nesbitt, H. W., and Bird, D. K., 1978, Summary and critique of the thermodynamic properties of rock-forming minerals: *Am. Jour. Sci.*, v. 278, p. 1-229.
- Hemley, J. J., 1967, Stability relations of pyrophyllite, andalusite and quartz at elevated pressures and temperatures [abs.]: *Am. Geophys. Union Trans.*, p. 224.
- _____, Montoya, J. W., Shaw, D. R., and Luce, R. W., 1977, Mineral equilibria in the MgO-SiO₂-H₂O system: II. Talc-antigorite-forsterite-anthophyllite-enstatite stability relations: *Am. Jour. Sci.*, v. 277, p. 353-383.
- _____ and Jones, W. R., 1964, Chemical aspects of hydrothermal alteration with emphasis on hydrogen metasomatism: *Econ. Geol.*, v. 59, p. 538-569.
- Hess, P. C., 1969, The metamorphic paragenesis of cordierite in pelitic rocks: *Contr. Miner. Petrol.*, v. 24, p. 191-207.
- Hewett, D. F., 1954, General geology of the Mojave Desert region, California, in Jahns, R. H., ed., *Geology of southern California*: Calif. Div. Mines Bull. 170, ch. 2, p. 5-20.
- _____, 1955, Structural features of the Mojave Desert region: *Geol. Soc. Am. Spec. Paper* 62, p. 377-390.
- Higgs, D. V., 1954, Anorthosite and related rocks of the western San Gabriel Mountains, southern California: *Calif. Univ., Publ. Geol. Sci.*, v. 30, p. 171-222.
- Hilde, T. W. C., Isezaki, N., and Wageman, J. M., 1977, Mesozoic sea-floor spreading in the North Pacific, in Sutton, G. H., Manghani, M. H., Moberly, R., and McAfee, E. U., eds., *The geophysics of the Pacific Ocean basin and its margin (The Woollard Volume)*: *Am. Geophys. Union, Geophys. Monograph* 19, p. 205-226.
- Hill, M. L., 1954, Tectonics of faulting in southern California, in Jahns, R. H., ed., *Geology of southern California*: Calif. Div. Mines Bull. 170, ch. 4, p. 13.
- _____ and Dibblee, T. W., Jr., 1953, San Andreas, Garlock, and Big Pine faults, California: *Geol. Soc. Am. Bull.*, v.64, p. 443-458.
- Hill, R. T., 1928, Southern California geology and Los Angeles earthquakes: Los Angeles, The Southern California Academy of Sciences, 232 p.

- Hirschberg, A. and Winkler, H. G. F., 1968, Stabilitätsbezeichnungen zwischen Chlorit, Cordierit und Almandin bei der Metamorphose: *Contr. Miner. Petrol.*, v. 18, p. 17-42.
- Hobbs, B. E., Means, W. D., and Williams, P. F., 1976, *An outline of structural geology*: John Wiley & Sons, Inc., New York, 571 p.
- Hødal, J., 1945, Rocks of the anorthosite kindred of Vossestrand, Norway: *Norsk Geol. Tidsskr.*, v. 24, p. 129-243.
- Holdaway, M. J., 1971, Stability of andalusite and the aluminum silicate phase diagram: *Am. Jour. Sci.*, v. 271, p. 97-131.
- Holtedahl, O., 1960, *Geology of Norway*: Norges Geol. Undersøkelse Nr. 208, 540 p.
- Hope, R. A., 1966, *Geology and structural setting of the Eastern Transverse Ranges, southern California*: Unpub. Ph.D. thesis, Univ. Calif., Los Angeles, 201 p.
- _____, 1969, The Blue Cut fault, southeastern California: *U.S. Geol. Surv. Prof. Paper 650-D*, p. D116-D121.
- Hoppin, R. A., 1954, *Geology of the Palen Mountains gypsum deposit, Riverside County, California*: Calif. Div. Mines, Spec. Report 36, 25 p.
- Hoschek, G., 1967, Untersuchungen zum Stabilitätsbereich von Chloritoid und Staurolith: *Contr. Miner. Petrol.*, v. 14, p. 123-162.
- _____, 1969, The stability of staurolite and chloritoid and their significance in metamorphism of pelitic rocks: *Contr. Miner. Petrol.*, v. 22, p. 208-232.
- Hossack, J. R., 1968, Pebble deformation and thrusting in the Bygdin area (southern Norway): *Tectonophys.*, v. 5, p. 315-339.
- Hsu, K. J., 1955, *Granulites and mylonites of the region about Cucamonga and San Antonio Canyons, San Gabriel Mountains, California*: Univ. Calif. Publ. Geol. Sci., v. 30, p. 223-351.
- Hsu, L. C., 1968, Selected phase relationships in the system Al-Mn-Fe-Si-O-H: a model for garnet equilibria: *Jour. Petrol.*, v. 9, p. 40-83.
- _____ and Burnham, C. W., 1969, Phase relationships in the system $\text{Fe}_3\text{Al}_2\text{Si}_3\text{O}_{12}$ - $\text{Mg}_3\text{Al}_2\text{Si}_3\text{O}_{12}$ - H_2O at 2.0 kilobars: *Geol. Soc. Am. Bull.*, v. 80, p. 2393-2408.
- Hulin, C. D., 1925, *Geology and ore deposits of the Randsburg quadrangle, California*: Calif. State Mining Bur., Bull. 95, 152 p.
- Isacks, B. L. and Barazangi, M., 1977, Geometry of Benioff zones: lateral segmentation and downwards bending of the subducted lithosphere, in

- Talwani, M. and Pitman, W. C., III, eds., Island arcs, deep sea trenches, and back-arc basins, Maurice Ewing Ser., v. 1, Am. Geophys. Union, Washington, D.C., p. 99-114.
- Jahns, R. H., 1940, Stratigraphy of the easternmost Ventura basin, California, with a description of a new lower Miocene mammalian fauna from the Tick Canyon formation: Carnegie Inst. Washington, Bull. 574, p. 147-194.
- Jahns, R. H., 1954, Investigations and problems of southern California geology, in Jahns, R. H., ed., Geology of southern California: Calif. Div. Mines, Bull. 170, ch. 1, p. 5- 29.
- _____, 1973, Tectonic evolution of the Transverse Ranges province as related to the San Andreas fault system, in Kovach, R. L. and Nur, A., eds., Proceedings of the conference on tectonic problems of the San Andreas fault system: Stanford Univ. Publ. Geol. Sci., v. 13, p. 149-170f.
- _____ and Muehlberger, W. R., 1954, Geology of the Soledad Basin, Los Angeles County, California: Map Sheet 6 (scale 1" = 1 mi.), in Jahns, R. H., ed., Geology of southern California: Calif. Div. Mines Geol., Bull. 170.
- James, R. S., Grieve, R. A. F., and Pauk, L., 1978, The petrology of cordierite-anthophyllite gneisses and associated mafic and pelitic gneisses at Manitouwadge, Ontario: Am. Jour. Sci., v. 278, p. 41-63.
- James, R. S., Turnock, A. C., and Fawcett, J. J., 1976, Stability and phase relations of iron chlorite below 8.5 kb P_{H_2O} : Contr. Miner. Petrol., v. 56, p. 1-25.
- Jennings, C. W., compiler, 1967, Geologic map of California, Salton Sea sheet: Calif. Div. Mines Geol., scale 1:250,000.
- _____, compiler, 1977, Geologic map of California: Calif. Div. Mines Geol., Geol. Data Map No. 2, scale 1:750,000.
- Johannes, W., 1967, Zur Bildung und Stabilität von Forsterite, Talk, Serpentin, Quarz und Magnesit im System $MgO-SiO_2-H_2O-CO_2$: Contr. Miner. Petrol., v. 15, p. 233-250.
- _____, 1969, An experimental investigation of the system $MgO-SiO_2-H_2O-CO_2$: Am. Jour. Sci., v. 267, p. 1083-1104.
- Kanamori, H. and Hadley, D., 1975, Crustal structure and temporal velocity change in southern California: Pure Appl. Geophys., v. 113, p. 257-280.
- Keith, S. B., 1978, Paleosubduction geometries inferred from Cretaceous and Tertiary magmatic patterns in southwestern North America: Geology, v. 6, n. 9, p. 516-521.
- Keller, W. D., 1955, The principles of chemical weathering: Lucas Bros. Publ., Columbia, Mo., 88 p.

- Kerrick, D. M., 1968, Experiments on the upper stability limit of pyrophyllite at 1.8 kilobars and 3.9 kilobars water pressure: *Am. Jour. Sci.*, v. 266, p. 204-214.
- _____, 1972, Experimental determination of muscovite + quartz stability with $P_{H_2O} < P_{total}$: *Am. Jour. Sci.*, v. 272, p. 946-958.
- Kerrick, D. M., 1974, Review of metamorphic mixed-volatile (H_2O-CO_2) equilibria: *Am. Miner.*, v. 59, p. 729-762.
- Kulke, H. and Schreyer, W., 1973, Kyanite-talc schist from Sar E Sang, Afghanistan: *Earth Planet. Sci. Letters*, v. 18, p. 324-328.
- Kvale, A., 1953, Linear structures and their relation to movement in the Caledonides of Scandinavia and Scotland: *Geol. Soc. London, Quart. Jour.*, v. 109, p. 51-73.
- Labotka, T. C., 1978, Geology of the Telescope Peak quadrangle, California and late Mesozoic regional metamorphism, Death Valley area, California: Unpub. Ph.D. thesis, Calif. Inst. Tech., Pasadena, Calif., 352 p.
- Lal, R. K. and Moorhouse, W. W., 1969, Cordierite-gedrite rocks and associated gneisses of Fishtail Lake, Harcourt Township, Ontario: *Can. Jour. Earth Sci.*, v. 6, p. 145-165.
- Lipman, P. W., Prostka, H. J., and Christiansen, R. L., 1971, Evolving subduction zones in the western United States, as interpreted from igneous rocks: *Science*, v. 174, p. 821-825.
- Lowell, J. D., 1972, Spitsbergen Tertiary orogenic belt and the Spitsbergen fracture zone: *Geol. Soc. Am. Bull.*, v. 83, p. 3091-3102.
- Luth, W. C., Jahns, R. H., and Tuttle, O. F., 1964, The granite system at pressures of 4 to 10 kilobars: *Jour. Geophys. Res.*, v. 69, p. 759-773.
- MacLellan, D. D., 1936, The geology of the East Coachella Tunnel of the Metropolitan Water District of southern California: Unpub. Ph.D. thesis, Calif. Inst. Tech., Pasadena, Calif., 90 p.
- McCulloh, T. H., 1952, Geology of the southern half of the Lane Mountain quadrangle, California: Unpub. Ph.D. thesis, Univ. Calif. Los Angeles, 180 p.
- _____, 1954, Problems of the metamorphic and igneous rocks of the Mojave Desert, California, in Jahns, R. H., ed., *Geology of southern California*: Calif. Div. Mines., Bull. 170, ch. 7, p. 13-24.
- McIntyre, D. B., 1951, The tectonics of the area between Grantown and Tomin-toul (mid-Strathspey): *Geol. Soc. London, Quart. Jour.*, v. 107, p. 1-22.
- McKee, E. D. and Sterrett, T. S., 1961, Laboratory experiments on form and structure of longshore bars and beaches, in Peterson, J. A. and Osmond, J. C., eds., *Geometry of sandstone bodies*: *Am. Assoc. Petrol. Geol.*,

Tulsa, Okla., p. 13-28.

- McOnie, A. W., Fawcett, J. J., and James, R. S., 1975, The stability of intermediate chlorites of clinocllore-daphnite series at 2 kbar P_{H_2O} : *Am. Miner.*, v. 60, p. 1047-1062.
- Merifield, P. M. and Lamar, D. L., 1975, Faults on Skylab imagery of the Salton Trough area, southern California: *Calif. Earth Sci. Corp. Tech. Report 75-1*, 23 p.
- Merrill, R. B., Robertson, J. K., and Wyllie, P. J., 1970, Melting reactions in the system $NaAlSi_3O_8$ - $KAlSi_3O_8$ - SiO_2 - H_2O to 20 kilobars compared with results for other feldspar-quartz- H_2O and rock H_2O systems: *Jour. Geol.*, v. 78, p. 558-569.
- Michael, E. D., 1966, Large lateral displacement on Garlock fault, California, as measured from offset fault system: *Geol. Soc. Am. Bull.*, v. 77, p. 111-113.
- Miller, E. L., 1977, Geology of the Victorville region, California: Unpub. Ph.D. thesis, Rice Univ., Houston, Texas, 226 p.
- _____, 1979, Eugeoclinal, miogeoclinal and cratonal rocks in the Mojave Desert region, California: Poster session presented at Penrose Conference, Elko, Nevada, Sept. 1979.
- _____, Burchfiel, B. C., and Carr, M. D., 1979, Enigmatic metasedimentary rocks of the western Mojave Desert, California, and their relationship to Cordilleran miogeocline and platform rocks: *Geol. Soc. Am., Abs. with Prog.*, v. 11, n. 3, p. 92.
- _____ and Carr, M. D., 1978, Recognition of Aztec equivalent sandstones and associated mid-Mesozoic metasedimentary deposits within the Mesozoic magmatic arc in the southwestern Mojave Desert, southern California, in Howell, D. G. and McDougall, K. A., eds., *Mesozoic paleogeography of the western United States: Pacific Sect., Soc. Econ. Paleon. Miner., Pacific Coast Paleogeography Symposium 2*, p. 283-290.
- Miller, F. K., 1970, Geologic map of the Quartzsite quadrangle, Yuma County, Arizona: *U.S. Geol. Surv. Geol. Quad. Maps of the U.S.*, GQ-841, scale 1:62,500.
- _____ and Morton, D. M., 1977, Comparison of granitic intrusions in the Pelona and Orocochia schists, southern California: *U.S. Geol. Surv. Jour. Research*, v. 5, p. 643-649.
- _____ and _____, 1980, Potassium-argon geochronology of the Eastern Transverse Ranges and southern Mojave Desert, southern California: *U.S. Geol. Surv. Prof. Paper 1152*, 30 p.
- Miller, W. J., 1934, Geology of the western San Gabriel Mountains of California: *Calif. Univ., Los Angeles, Publ. Math. Phys. Sci.*, v. 1, p. 1-114.

- Miller, W. J., 1938, Pre-cambrian and associated rocks near Twenty-nine Palms, California: Geol. Soc. Am. Bull., v. 49, p. 417-446.
- _____, 1944, Geology of Palm Springs-Blythe strip, Riverside County, California: Calif. Jour. Mines, v. 40, p. 11-72.
- _____, 1946, Crystalline rocks of southern California: Geol. Soc. Am. Bull., v. 57, p. 457-542.
- Morse, S. A., 1968, Feldspars: Ann. Rept. Geophys. Lab., Carnegie Inst. Yrbk. 67, p. 120-126.
- Morton, D. M., 1975, Synopsis of the geology of the eastern San Gabriel Mountains, in Crowell, J. C., ed., San Andreas fault in southern California: Calif. Div. Mines Geol., Spec. Report 118, p. 170-176.
- Muehlberger, W. R., 1958, Geology of northern Soledad Basin, Los Angeles County, California: Am. Assoc. Petrol. Geol. Bull., v. 42, p. 1812-1844.
- Muehlberger, W. R. and Hill, H. S., 1958, Geology of the central Sierra Pelona, Los Angeles County, California: Am. Jour. Sci., v. 256, p. 630-643.
- Murray, K., Bell, J., and Crowe, B., 1976, Stratigraphy and structure of the Orocochia, Chocolate and Cargo Muchacho Mountains, southeastern California: Sundersert Nuclear Plant Early Site Review Report, Appendix 2.5L, Amendment 10, Fugro, Inc., Long Beach, California, 29 p.
- Navrotsky, A., Newton, R. C., and Kleppa, O. J., 1973, Sillimanite-disordering enthalpy by calorimetry: Geochim. et Cosmochim. Acta, v. 37, p. 2497-2508.
- Ness, G., Levi, S., and Couch, R., 1980, Marine magnetic anomaly timescales for the Cenozoic and Late Cretaceous: a précis, critique, and synthesis: Rev. Geophys. Space Phys., v. 18, p. 753-770.
- Newton, R. C., 1966a, Kyanite-sillimanite equilibrium at 750°C: Science, v. 151, p. 1222-1225.
- _____, 1966b, Kyanite-andalusite equilibrium from 700 to 800°C: Science, v. 153, p. 170-172.
- _____, 1966c, Some calc-silicate equilibrium relations: Am. Jour. Sci., v. 264, p. 204-222.
- Nicolas, A. and Poirier, J. P., 1976, Crystalline plasticity and flow in metamorphic rocks: Wiley & Sons, Interscience, London, 444 p.
- Nitsch, K.-H. and Storre, B., 1972, Zur Stabilität von Margarit in H₂O-CO₂ Gasgemischen: Fortschr. Miner., v. 50, Beiheft 1, p. 71-73.
- Oakeshott, G. B., 1958, Geology and mineral deposits of the San Fernando

- quadrangle, Los Angeles County, California: Calif. Div. Mines Bull. 172, p. 1-147.
- Oldenburg, D. W. and Brune, J. N., 1972, Ridge transform fault spreading pattern in freezing wax: *Science*, v. 178, p. 301-304.
- Okrusch, M. and Evans, B. W., 1970, Minor element relationships in coexisting andalusite and sillimanite: *Lithos*, v. 3, p. 261-268.
- Peach, B. N., Horne, J., Gunn, W., Clough, C. T., Hinxman, L. W., and Teall, J. J. H., 1907, The geological structure of the north-west Highlands of Scotland: *Geol. Surv. Gt. Brit. Memoir*, 668 p.
- Pelka, G. J., 1973, Geology of the McCoy and Palen Mountains, southeastern California: Unpub. Ph.D. thesis, Univ. Calif. Santa Barbara, 162 p.
- Perkins, D., III, Essene, E. J., Westrum, E. F., Jr., and Wall, V. J., 1979, New thermodynamic data for diaspore and their application to the system $Al_2O_3-SiO_2-H_2O$: *Am. Miner.*, v. 64, p. 1080-1090.
- Pettijohn, F. J., 1975, *Sedimentary rocks* (3rd ed.): Harper & Row, Publ., Inc., New York, 628 p.
- Philpotts, A. R., 1966, Origin of anorthosite-mangerite rocks in southern Quebec: *Jour. Petrol.*, v. 7, p. 1-64.
- Pitcher, W. S., 1978, The anatomy of a batholith: *Jour. Geol. Soc. London*, v. 135, p. 157-182.
- Piwinskii, A. J., 1968, Experimental studies of igneous rock series, central Sierra Nevada Batholith, California: *Jour. Geol.*, v. 76, p. 548-570.
- Platt, J. P., 1975, Metamorphic and deformational processes in the Franciscan complex, California--some insights from the Catalina schist terrane: *Geol. Soc. Am. Bull.*, v. 86, p. 1337-1347.
- Powell, R. E., 1975, The Chiriaco fault: a left-lateral strike-slip fault in the eastern Transverse Ranges, Riverside County, California [abs.]: *Geol. Soc. Am., Abs. with Prog.*, v. 7, n. 3, p. 362.
- _____ and Silver, L. T., 1979, Geologic analysis of ASTP photographs of parts of southern California, in El-Baz, F. and Warner, D. M., eds., Apollo-Soyuz test project, summary science report: Volume II, Earth observations and photography: NASA SP-412, National Aeronautics and Space Administration, Washington, D.C., p. 9-27.
- Proctor, R. J., 1968, Geology of the Desert Hot Springs-Upper Coachella Valley, Salton Sea, and vicinity: *Calif. Div. Mines Geol., Spec. Report* 94, 50 p.
- Pruss, D. E., Olcott, G. W., and Oesterling, W. A., 1959, Areal geology of a portion of the Little San Bernardino Mountains, Riverside and San Bernardino Counties, California [abs.]: *Geol. Soc. Am. Bull.*, v. 70,

- n. 12, pt. 2, p. 1741.
- Raisz, E., 1962, Principles of Cartography: McGraw-Hill Book Company, Inc., New York, 315 p.
- Reed, B. L. and Hemley, J. J., 1966, Occurrence of pyrophyllite in the Kekiktuk Conglomerate, Brooks Range, northeastern Alaska: U.S. Geol. Surv. Prof. Paper 550-C, p. C162-C166.
- Reineck, H. E. and Singh, I. B., 1975, Depositional sedimentary environments: Springer-Verlag, Berlin, 439 p.
- Reynolds, D., 1947, Hercynian Fe-Mg metasomatism in Cornwall: Geol. Mag., v. 84, p. 33-50.
- Rich, M., 1971, Fusulinids from central Mojave Desert and adjoining area, California: Jour. Paleon., v. 45, p. 1022-1027.
- Rich, M., 1977, Pennsylvanian paleogeographic patterns in the western United States; in Howell, D. G. and McDougall, K. A., eds., Mesozoic paleogeography of the western United States: Pacific Sect., Soc. Econ. Paleon. Miner., Pacific Coast Paleogeography Symposium 2, p. 277-282.
- Richardson, S. W., 1968, Staurolite stability in a part of the system Fe-Al-Si-O-H: Jour. Petrol., v. 9, p. 468-488.
- _____, Gilbert, M. C., and Bell, P. M., 1969, Experimental determination of kyanite-andalusite and andalusite-sillimanite equilibria; the aluminum silicate triple point: Am. Jour. Sci., v. 267, p. 259-272.
- Richmond, J. F., 1960, Geology of the San Bernardino Mountains north of Big Bear Lake, California: Calif. Div. Mines, Spec. Report 65, 68 p.
- Robinson, P. and Jaffe, H. W., 1969, Aluminous enclaves in gedrite-cordierite gneiss from southwestern New Hampshire: Am. Jour. Sci., v. 267, p. 389-421.
- Rogers, J. J. W., 1961, Igneous and metamorphic rocks of the western part of Joshua Tree National Monument, Riverside and San Bernardino Counties, California: Calif. Div. Mines Geol., Spec. Report 68, 26 p.
- Rogers, T. H., compiler, 1966, Santa Ana sheet: Calif. Div. Mines Geol., Geologic Atlas of California, scale 1:250,000.
- _____, compiler, 1969, San Bernardino sheet: Calif. Div. Mines Geol., Geologic Atlas of California, scale 1:250,000.
- Rosen-Spence, A. de, 1969, Genèse des roches à cordiérite-anthophyllite des gisements cupro-zincifères de la région de Rouyn-Noranda, Québec, Canada: Can. Jour. Earth Sci., v. 6, p. 1339-1345.
- Rotstein, Y., Combs, J., and Biehler, S., 1976, Gravity investigation in the southeastern Mojave Desert, California: Geol. Soc. Am. Bull., v. 87,

p. 981-993.

- Ruxton, B. P. and Berry, L., 1957, Weathering of granite and associated erosional features in Hong Kong: *Geol. Soc. Am. Bull.*, v. 68, p. 1263-1292.
- Schreyer, W., 1976, Experimental metamorphic petrology at low pressures and high temperatures, in Bailey, D. K. and MacDonald, R., eds., *The evolution of the crystalline rocks*: Academic Press, Inc., London, ch. 3, p. 261-331.
- _____, Ohnmacht, W., and Mannchen, J., 1972, Carbonate-orthopyroxenites (sagvandites) from Troms, northern Norway: *Lithos*, v. 5, p. 345-364.
- _____ and Seifert, F., 1969, Compatibility relations of the aluminum silicates in the systems $MgO-Al_2O_3-SiO_2-H_2O$ and $K_2O-MgO-Al_2O_3-SiO_2-H_2O$ at high pressures: *Am. Jour. Sci.*, v. 267, p. 371-388.
- Sclater, J. G., Jarrard, R. D., McGowran, B., and Gartner, S., Jr., 1974, Comparison of the magnetic and biostratigraphic time scales since the Late Cretaceous, in *Initial reports of the Deep Sea Drilling Project*, v. 22: U.S. Government Printing Office, Washington, D. C., p. 381-386, fide Berggren et al., 1978; Ness et al., 1980.
- Seifert, F., 1970a, Low-temperature compatibility relations of cordierite in haplopetites of the system $K_2O-MgO-Al_2O_3-SiO_2-H_2O$: *Jour. Petrol.*, v. 11, p. 73-99.
- _____, 1970b, Das petrogenetische P_{H_2O} -T-Netz des Systems $MgO-Al_2O_3-SiO_2-H_2O$ im Druck-Temperatur-Bereich 0-7 kb., 400-1,250°C: Habilitationsschrift, Ruhr-Universität Bochum, fide Schreyer, 1976.
- _____, 1973, Stability of the assemblage cordierite-corundum in the system $MgO-Al_2O_3-SiO_2-H_2O$: *Contr. Miner. Petrol.*, v. 41, p. 171-177.
- _____ and Schreyer, W., 1970, Lower temperature stability of Mg cordierite in the range 1-7 kilobars water pressure. A redetermination: *Contr. Miner. Petrol.*, v. 27, p. 225-238.
- Shlemon, R. J. and Purcell, C. W., 1976, Geomorphic reconnaissance southeastern Mojave Desert, California and Arizona: Sundesert Nuclear Plant Early Site Review Report, Appendix 2.5M, Amendment 10, Fugro, Inc. Long Beach, California, 28 p.
- Shklanka, R., 1963, Repeated metamorphism and deformation of evaporite-bearing sediments, Little Maria Mountains, California: Unpub. Ph.D. thesis, Stanford Univ., Stanford, Calif.
- Silver, L. T., 1968, Pre-Cretaceous basement rocks and their bearing on large-scale displacements in the San Andreas fault system [abs.], in Dickinson, W. R. and Grantz, A., eds., *Proceedings of conference of geologic problems of San Andreas fault system*: Stanford Univ., Publ. Geol.

Sci., v. 11, p. 279.

- _____, 1969, Precambrian batholiths of Arizona [abs.]: Geol. Soc. Am., Abs. for 1968, Spec. Paper 121, p. 558-559.
- _____, 1971, Problems of crystalline rocks of the Transverse Ranges [abs.]: Geol. Soc. Am., Abs. with Prog., v. 3, n. 2, p. 193-194.
- _____, Anderson, C. A., Crittenden, M., and Robertson, J. M., 1977a, Chronostratigraphic elements of the Precambrian rocks of the southwestern and far western United States [abs.]: Geol. Soc. Am., Abs. with Prog., v. 9, p. 1176.
- _____, and Anderson, T. H., 1974, Possible left-lateral early to middle Mesozoic disruption of the southwestern North American craton margin [abs.]: Geol. Soc. Am., Abs. with Prog., v. 6, n. 7, p. 955-956.
- _____, _____, Conway, C. M., Murray, J. D., and Powell, R. E., 1977b, Geological features of southwestern North America, in Skylab explores the Earth: NASA SP-380, National Aeronautics and Space Administration, Washington, D.C., p. 89-135.
- _____ and Carter, B. A., 1965, Precambrian syenites of northern Los Angeles County [abs.]: Geol. Soc. Am., Spec. Paper 87, p. 228-229.
- _____, Early, T. O., and Anderson, T. H., 1975, Petrological, geochemical, and geochronological asymmetries of the Peninsular Ranges batholith [abs.]: Geol. Soc. Am., Abs. with Prog., v. 7, p. 375-376
- _____, McKinney, C. R., Deutsch, S., and Bolinger, J., 1960, Precambrian age determinations of some crystalline rocks of the San Gabriel Mountains of southern California: Jour. Geophys. Res., v. 65, p. 2522-2523.
- _____, _____, _____, _____, 1963, Precambrian age determination in the western San Gabriel Mountains, California: Jour. Geol., v. 71, p. 196-214.
- _____, _____, and Wright, L. A., 1962, Some Precambrian ages in the Panamint Range, Death Valley, California [abs.]: Geol. Soc. Am., Abs. for 1961, Spec. Paper 68, p. 55.
- Smith, D. P., 1977, San Juan-St. Francis fault--hypothesized major middle Tertiary right-lateral fault in central and southern California: Calif. Div. Mines Geol., Spec. Report 129, p. 41-50.
- Smith, G. I., 1962, Large lateral displacement on Garlock fault, California, as measured from offset dike swarm: Am. Assoc. Petrol. Geol. Bull., v. 46, p. 85-104.
- Smith, G. I. and Ketner, K. B., 1970, Lateral displacement on the Garlock fault, southeastern California, suggested by offset sections of similar metasedimentary rocks: U.S. Geol. Surv. Prof. Paper 700-D, p. D1-D9.

- Sørbye, R. C., 1964, Anthophyllite-cordierite gneisses in the basal rock complex of the Hagesund peninsula, western Norway: *Norsk, Geol. Tidsskr.*, v. 44, p. 323-340.
- Stewart, J. H. and Poole, F. G., 1975, Extension of the Cordilleran miogeosynclinal belt to the San Andreas fault, southern California: *Geol. Soc. Am. Bull.*, v. 86, p. 205-212.
- Stoddard, E. F., 1979, Zinc-rich hercynite in high-grade metamorphic rocks: a product of the dehydration of staurolite: *Am. Miner.*, v. 64, p. 736-741.
- _____ and Miller, C. F., 1979, Phase petrology of cordierite-amphibole rocks, Old Woman-Piute Range, southeastern California [abs.]: *Geol. Soc. Am., Abs. with Prog.*, v. 11, p. 130.
- Storre, B. and Nitsch, K.-H., 1974, Zur Stabilität von Margarit im System $\text{CaO-Al}_2\text{O}_3\text{-SiO}_2\text{-H}_2\text{O}$: *Contr. Miner. Petrol.*, v. 43, p. 1-24.
- Streckeisen, A. L., 1967, Classification and nomenclature of igneous rocks: *Neues Jahrb. Miner. Abh.*, v. 107, p. 144-214.
- Strens, R. G. J., 1968, Stability of Al_2SiO_5 solid solutions: *Miner. Mag.*, v. 36, p. 839-849.
- Suppe, J. and Armstrong, R. L., 1972, Potassium-argon dating of Franciscan metamorphic rocks: *Am. Jour. Sci.*, v. 272, p. 217-233.
- Tarling, D. H. and Mitchell, J. G., 1976, Revised Cenozoic polarity time scale: *Geology*, v. 4, p. 133-136.
- Thompson, A. B., 1970a, A note on the kaolinite-pyrophyllite equilibrium: *Am. Jour. Sci.*, v. 268, p. 454-458.
- _____, 1970b, Laumontite equilibria and the zeolite facies: *Am. Jour. Sci.*, v. 269, p. 267-275.
- _____, 1971a, Analcite-albite equilibria at low temperatures: *Am. Jour. Sci.*, v. 271, p. 72-92.
- _____, 1971b, P-CO_2 in low-grade metamorphism; zeolite, carbonate; clay mineral, prehnite relations in the system $\text{CaO-Al}_2\text{O}_3\text{-SiO}_2\text{-CO}_2\text{-H}_2\text{O}$: *Contr. Miner. Petrol.*, v. 33, p. 145-161.
- _____, 1976, Mineral reactions in pelitic rocks: I. Prediction of P-T-X(Fe-Mg) phase relations. II. Calculation of some P-T-X(Fe-Mg) phase relations: *Am. Jour. Sci.*, v. 276, p. 401-454.
- Thompson, J. B., Jr., 1955, The thermodynamic basis for the mineral facies concept: *Am. Jour. Sci.*, v. 253, p. 65-103.
- _____, 1957, The graphical analysis of mineral assemblages in pelitic

schists: *Am. Miner.*, v. 42, p. 842-858.

_____ and Norton, S. A., 1968, Paleozoic regional metamorphism in New England and adjacent areas, in Zen, E-an and others, eds., *Studies of Appalachian geology: northern and maritime*: John Wiley & Sons, New York, ch. 24, p. 319-326.

Thompson, W. O., 1937, Original structures of beaches, bars, and dunes: *Geol. Soc. Am. Bull.*, v. 48, p. 723-752.

Tilley, C. E., 1925, Petrographical notes on some chloritoid rocks: *Geol. Mag.*, v. 62, p. 309-318.

_____, 1935, Metasomatism associated with the greenstone-hornfelses of Kenidjack and Botallack, Cornwall: *Miner. Mag.*, v. 24, p. 181-202.

_____, 1937, Anthophyllite-cordierite granulites of the Lizard: *Geol. Mag.*, v. 74, p. 300-309.

_____, and Flett, J. S., 1929, Hornfelses from Kenidjack, Cornwall: *Great Britain Geol. Surv. Summ. Prog.*, pt. II, p. 24-41, *fide* Tilley, 1935, Grant, 1968, Chinner and Fox, 1974.

Touminen, H. V. and Mikkola, T., 1950, Metamorphic Mg-Fe enrichment in the Orijärvi area as related to folding: *Finlande Comm. Géol. Bull.*, no. 150, p. 67-92.

Turner, F. J., 1968, *Metamorphic petrology: Mineralogical and field aspects*: New York, McGraw-Hill, Inc., 403 p.

Tuttle, O. F. and Bowen, N. L., 1958, Origin of granite in the light of experimental studies: *Geol. Soc. Am. Mem.* 74, 153 p.

Vallance, T. G., 1967, Mafic rock alteration and isochemical redevelopment of some cordierite-anthophyllite rocks: *Jour. Petrol.*, v. 8, p. 84-96.

Vargo, J. M., 1972, Structural geology of a portion of the eastern Rand Mountains, Kern and San Bernardino Counties: Unpub. M.A. thesis, Univ. Southern California, Los Angeles, 117 p.

Vaughan, D., 1963, The crystallization ranges of the Spruce Pine and Harding Pegmatites: Unpub. M.S. thesis, Pennsylvania State Univ., *fide* Piwinski, 1968, p. 567.

Vaughan, F. E., 1922, Geology of San Bernardino Mountains, north of San Gorgonio Pass: *Univ. Calif., Dept. Geol. Sci. Bull.*, v. 13, p. 319-411.

Velde, B., 1973, Phase equilibria in the system $MgO-Al_2O_3-SiO_2-H_2O$: chlorites and associated minerals: *Miner. Mag.*, v. 39, p. 297-312.

Velde, B. and Kornprobst, J., 1969, Stabilité des silicates d'alumine hydrates: *Contr. Miner. Petrol.*, v. 21, p. 63-74.

- Waard, D. de, 1967, Absolute P-T conditions of granulite-facies metamorphism in the Adirondacks: Koninkl. Nederl. Akad. Wetenschap., Proc. Ser. B, v. 70, p. 400-410.
- _____, 1969, The anorthosite problem: the problem of the anorthosite-charnockite suite of rocks: in Isachsen, Y. W., ed., Origin of anorthosite and related rocks, New York State Museum and Science Service Mem. 18, p. 71-91.
- Ware, G. C., Jr., 1958, The geology of a portion of the Mecca Hills, Riverside County, California: Unpub. M.A. thesis, Univ. Calif., Los Angeles, 60 p.
- Weill, D. F., 1966, Stability relations in the Al_2O_3 - SiO_2 system calculated from solubilities in the Al_2O_3 - SiO_2 - Na_3AlF_6 system: Geochim. et Cosmochim. Acta, v. 30, p. 223-237.
- White, D. A., 1954, The stratigraphy and structure of the Mesabi Range, Minnesota: Minn. Geol. Surv. Bull., v. 38, 92 p.
- Winkler, H. G. F., 1976, Petrogenesis of metamorphic rocks, 4th ed.: Springer-Verlag, New York, 334 p.
- Wood, D. S., 1973, Patterns and magnitudes of natural strain in rocks: Roy. Soc. London, Philos. Trans., Ser. A, v. 274, p. 373-382.
- Woodford, A. O. and Harriss, T. F., 1928, Geology of Blackhawk Canyon, San Bernardino Mountains, California: Univ. Calif., Dept. Geol. Sci. Bull., v. 17, p. 265-304.
- Wright, L., 1976, Late Cenozoic fault patterns and stress fields in the Great Basin and westward displacement of the Sierra Nevada block: Geology, v. 4, n. 8, p. 489-494.
- Yardley, B. W. D., 1980, Metamorphism and orogeny in the Irish Dalradian: Jour. Geol. Soc. London, v. 137, p. 303-309.
- Yeats, R. S., 1968, Rifting and rafting in the southern California borderland, in Dickinson, W. R. and Grantz, A., eds., Proceedings of conference on geologic problems of San Andreas fault system: Stanford Univ. Publ. Geol. Sci., v. 11, p. 307-320.
- _____, 1980, Quaternary flake tectonics of the California Transverse Ranges [abs.]: Geol. Soc. Am., Abs. with Prog., v. 12, n. 3, p. 160.
- Zen, E-an, 1969, The stability relations of the polymorphs of aluminum silicate: a survey and some comments: Am. Jour. Sci., v. 267, p. 297-309.
- Zwart, H. J., 1962, On the determination of polymetamorphic mineral associations, and its application to the Bosost area (central Pyrenees): Geol. Rundsch., v. 52, p. 38-64.

APPENDIX

PLATE II

LEGEND

FOR THE GEOLOGIC MAP (PLATE I)
AND STRUCTURE SECTIONS (PLATE III)

QUATERNARY

- Qal Undifferentiated alluvium; may include some Pliocene alluvium in Pinto Basin and on the south flank of the Chuckwalla Mountains.
- Qg Undifferentiated high gravels.

QUATERNARY - CENOZOIC

- QTr Rhyolite.
- QTb Basalt.
- QTs Clastic sediments beneath basalt.

CENOZOIC

- Tmd Miocene Diligencia formation: only the lowermost unit is shown on Plate I; it is very coarse terrestrial megabreccia to megaconglomerate with abundant large boulders from the crystalline basement complex; the matrix is indurated and arkosic; rare clasts of limestone are derived from the underlying Maniobra formation.
- Tmvs Unnamed Tertiary volcanics (basalt/andesite) and terrestrial sedimentary rocks in the southern Chuckwalla and Little Chuckwalla Mountains, probably correlative with the Diligencia formation. The sedimentary rocks include red arkosic sandstones, rare white sandstone, conglomerates, megaconglomerates, and debris flows. The volcanics include basaltic to andesitic flows and pyroclastic units.
- Tem Eocene Maniobra formation: basal, well-indurated megaconglomerate overlaps the crystalline basement of the eastern Orocopia Mountains; most of the formation is white to yellowish white sandstone interbedded with yellowish brown shale and scattered boulder conglomerates. The sandstones and shales are characterized by isolated large boulders of locally-derived crystalline rock. Rare, thin, gray to grayish brown, fossiliferous marine limestone is present.

CENOZOIC - MESOZOIC

- KTq1 Quartz latite that occurs principally in a dike swarm along the east flanks of the Chuckwalla and Eagle Mountains, although it also occurs elsewhere in isolated dikes: light- to medium-gray, with phenocrysts of quartz, K-feldspar, and plagioclase in a siliceous aphanitic groundmass that constitutes 80 to 85% of the rock; the dikes take on a deep patina of desert varnish.
- KTt Trachyte that occurs in a dike swarm on the east flank of the Chuckwalla Mountains: creamy to pinkish white K-feldspar phenocrysts (2-3 mm to 2 cm) set in a very dark gray, aphanitic groundmass that makes up 75-80% of the rock; small phenocrysts of hornblende, biotite, and rare quartz also occur.
- KTd Propylitized dacite dike that supports Alligator Ridge in the northern Chuckwalla Mountains; it is also found in the southeastern corner of the Eagle Mountains: light mottled greenish gray rock with phenocrysts (1-3 mm) of plagioclase, K-feldspar, quartz, biotite, and rare amphibole and garnet; propylitization has produced abundant secondary chlorite, sericite, calcite, and epidote.
- KTf Undifferentiated felsitic dikes; may include older dikes as well.
- KTm Undifferentiated mafic to intermediate dikes, including basalt, andesite, and diabase; may include older dikes as well.
- KTlg Light-colored, apparently uncataclasized granitic rocks in the southern Little San Bernardino Mountains.

MESOZOIC

CRETACEOUS(?)

- Kmg Medium- to very coarse-grained, nonporphyritic biotite monzogranite; pinkish gray, white-weathering leucocratic rock that weathers into tors of joint-controlled granite boulders that characteristically disintegrate to guss; quartz is abundant, typically forming 25 to 35% of the rock; in the Orocopia Mountains, the unit grades from a biotite monzogranite to muscovite granite.
- Kmgp Porphyritic monzogranite map unit that incorporates two textural units that display consistent sequencing relationships through the Chuckwalla, Orocopia, and Little San Bernardino Mountains:

- 1) The older unit is coarse- to very coarse-grained porphyritic biotite monzogranite with 2- to 8-cm, zoned, Carlsbad-twinned phenocrysts of K-feldspar; the K-feldspar is usually light flesh-colored pink, but at a few localities it has a lavender cast similar to that of the Jurassic(?) monzogranite;

rapakivi overgrowths of plagioclase are locally present; biotite is the typical mafic mineral, but hornblende may be present; quartz is usually abundant.

2) The younger unit is finer-grained porphyritic biotite monzogranite characterized by scattered pea-sized (.5 to 1.5 cm) phenocrysts of K-feldspar; the porphyritic rock grades into fine-grained equigranular monzogranite that contains local concentrations of dark bluish gray spherical clots of biotite, quartz, and muscovite commonly surrounded by white zones from which all the mafics have been leached; the clots are generally 2-5 cm in diameter ("polka-dots" of Ehlert and Ehlig (1977), who report relict cordierite in some clots).

Kgd Hornblende-biotite-sphene granodiorite: medium-grained with stubby to acicular hornblende and euhedral biotite, where undeformed; in the eastern Chuckwalla Mountains, a pervasive lineation overprints the northern third of one pluton of this lithology.

Kt Hornblende-biotite-sphene tonalite found in the southern Little San Bernardino Mountains.

CRETACEOUS(?) - JURASSIC(?)

JKi Undifferentiated Mesozoic plutonic rocks; especially in the central Pinto Mountains, where their mapping is not complete, the map unit may contain older intrusive rocks as well.

JURASSIC(?)

Jg Fine-grained, light-colored granitic rock with pea-sized phenocrysts of quartz in a fine-grained matrix of quartz and feldspar.

Jmg Coarse- to very coarse-grained nonporphyritic monzogranite; K-feldspar has a lavender cast.

Jmgs Coarse- to very coarse-grained hornblende-biotite porphyritic monzogranite characterized by 1- to 4-cm euhedral, tabular phenocrysts of K-feldspar with a distinct lavender cast; the rock generally takes a deeper desert varnish than the Cretaceous(?) monzogranites; secondary chlorite, epidote, and carbonate are ubiquitous and abundant, and impart a greenish cast to the rock; quartz content ranges approximately from 10 to 25%, so that, strictly, some of the unit is monzonite.

Jbi Gabbro-diorites: map unit for mafic lithologies of variable composition and texture including gabbro, diorite, and monzodiorite. Most of the mafic rocks can be classified in two textural categories: one characterized by stubby equant to tabular hornblende crystals, the other by prismatic to acicular hornblende crystals.

Both categories contain rocks that range in color index from about 50 to >95: where its color index is relatively low, the stubby hornblende unit has a spotted, leopard-skin appearance; where the color index is high, these rocks are hornblendites. In these latter rocks, clinopyroxene and olivine can be found poikilitically enclosed within the hornblende. Mafic-rich gabbros with acicular hornblende sporadically show an igneous layering defined by planes of otherwise randomly oriented hornblende crystals. Biotite is common in most of the mafic rocks. Small modal abundances of K-feldspar and quartz are almost always present. Sphene and secondary epidote and chlorite are ubiquitous.

PALEOZOIC(?) - MESOZOIC(?)

- md/mdp Equigranular and porphyritic monzodiorite in the Munsen Canyon area of the southwestern Eagle Mountains: leucocratic feldspathic rock with 5 to 10% quartz; porphyritic phase in places consists of abundant phenocrysts of gray K-feldspar with very little matrix; mafic minerals include hornblende and clinopyroxene as well as biotite.
- lg Foliated leucocratic granitic rocks of uncertain age intrusive into Pinto gneiss.

PALEOZOIC(?) - PRECAMBRIAN(?)

Joshua Tree Terrane (j): Pinto gneiss (jp)

- jp1d Iron Chief dolomite: very coarse-grained, recrystallized dolomite marble with grains up to 1 cm across; white to light gray, grayish orange (10YR7/4) to buff weathering; thin to thick-bedded to massive; scattered layers are rich in dark-brown weathering nodules, pods, and lenses that were probably derived from chert; layers of very coarse-grained white calcite marble (< 10 ft) occur sporadically, as do ferriferous layers of hematite-dolomite.
- jp Granofelses: the map unit comprises four lithosomes within the Pinto gneiss:

1) Black Eagle pelitic granofels/schist: predominantly pelitic and ferriferous pelitic granofels where undeformed; schist in proximity to the early Red Cloud thrust. Pelitic rocks consist of quartz + muscovite + aluminosilicate ± K-feldspar. Ferriferous pelitic rocks are varicolored, mottled in red, purple, lavender, blue, gray, and white; a phyllitic sheen is common on foliation surfaces; the rock contains quartz + aluminosilicate + biotite/chlorite + muscovite ± K-feldspar ± plagioclase + hematite (up to 25-30%); in places the unit is exclusively quartz + hematite. At least one thin layer of calcite marble (containing clinopyroxene + forsterite) occurs within the unit.

2) Baumonk Mill pelitic granofels: light bluish gray, vitreous granofels composed of quartz (~ 50 to 60%), sericite, and books of reddish brown biotite, commonly bleached.

3) Music Valley gneiss: feldspathic gneiss with discontinuous segregations (up to 1 cm thick) of light-colored quartzo-feldspathic layers and dark-colored biotite-rich layers; the unit consists of subequal amounts of quartz, plagioclase, and biotite.

4) Lost Horse pelitic granofels: dark bluish gray, vitreous granofels that is extremely tough when fresh; medium-grained, compositionally laminated, composed of quartz + cordierite + aluminosilicate + biotite ± garnet ± relict staurolite; retrograde muscovite and chlorite are present in southern exposures. Near its contact with the Music Valley gneiss, the unit contains thin layers of ferromagnesian granofels and schist characterized by cordierite + orthoamphibole + biotite ± chlorite ± garnet ± clinoamphibole ± quartz and talc + chlorite + clinoamphibole + biotite + quartz assemblages.

jpq Pinto Mountain quartzite: the map unit comprises three lithologies:

1) Cross-bedded quartzite: coarse- to very coarse-grained, vitreous, mottled light to dark gray to bluish gray; medium-bedded to massive with low-angle sets of tangential planar cross-laminations; thin black laminae (< 1 mm) of opaque minerals occur sporadically; compositionally mature (> 95% quartz) with abundant white aluminosilicate, locally with abundant viridine that imparts a green color to the rock.

2) Conglomerate: occurs in layers and lenses up to 10 ft thick interbedded near the base of the cross-bedded quartzite. Clasts, constituting 75 to 85% of the rock, consist of roughly equidimensional pebbles and cobbles of very coarse-grained white quartz/quartzite (85-95%), tabular clasts of fine-grained black specular hematite-rich quartzite (5-15%), and rare fine-grained jasper. The matrix is similar to the cross-bedded quartzite. Hematite imparts a characteristic rusty brown stain to the rock. Deformation in the Eagle Mountains has stretched the pebbles as much as 10:2:1.

3) Vitreous white quartzite: very coarse-grained (up to 1 cm) white quartzite; recrystallized grains have sutured boundaries; massive with bedding obscure or obliterated; white to light gray, in places stained brownish to light red-brownish white; compositionally supermature, commonly with 98-99+% quartz; thin seams of reddish black hematite + aluminosilicate + quartz occur sporadically; the rock is a ledge-former and is intensely jointed.

PRECAMBRIAN

San Gabriel Terrane (s):

P€smj Syenite-mangerite-jotunite: rusty-brown weathering rock, extensively fractured; consists predominantly of two textural varieties:

1) Medium-grained, light brown, sugary-textured, feldspathic, equigranular rock with varying abundance of mafic clots composed of fine-grained aggregates of biotite, hornblende, and quartz; bluish gray quartz is locally abundant, but is generally less than 5% of the rock.

2) Darker-colored, more mafic-rich rock, with cream-colored to slightly brownish gray; within a given hand specimen, the rock is roughly equigranular, but the grain size varies from 1-3 mm to 5-10mm; mafic clots consist of fine-grained aggregates of biotite, hornblende, quartz, and relict pyroxene.

A third textural variety of the unit is a very coarse-grained, leucocratic, porphyritic rock that ranges in composition from tonalite to granite; it occurs in scattered isolated domains of uncertain sequencing relationships within the unit.

P€sga Augustine gneiss: heterogeneous mixture of mafic and felsic gneisses at least locally intrusive into the Hexie and Soledad gneisses; felsic and mafic layers are commonly interlayered on a scale of 1-10 ft; compositionally, the gneisses range from tonalite to granite. The gneisses are retrograded granulites with corona-textured replacement of pyroxene(?) by clots of uralite, biotite, and quartz, relict mesoperthite, antiperthite and garnet. Felsic gneisses are characteristically coarse- to very coarse-grained with a blotchy texture produced by aggregates of equant, blocky quartz and feldspar, and by garnet porphyroblasts and biotite aggregates pseudomorphous after garnet and/or pyroxene(?). Layered segregations at all scales pinch and swell and have short lateral continuity, imparting a wispy character to the rock. The mafic rocks vary texturally from amphibolitic to granoblastic. Quartz is ubiquitous.

P€ss Soledad granodiorite/augen gneiss: where undeformed, e.g., at localities in the southern Chuckwalla and northern Hexie Mountains, the unit has a porphyritic igneous texture with randomly oriented phenocrysts of white K-feldspar in a dark, medium-grained matrix of quartz, biotite, and feldspar; the phenocrysts commonly exhibit a rapakivi texture, with overgrowths of plagioclase. Where deformed, the rock contains pink to white tabular megacrysts of K-feldspar oriented in a foliation; with increasing deformation, the megacrysts take on eye-shapes; locally the gneiss is transformed to mylonite; deformed quartzo-feldspathic veins are common in the gneiss. The rock is granodioritic to monzogranitic.

P€sh Hexie gneiss: pelitic gneiss characterized by mineral assemblages containing quartz + biotite + plagioclase ± sillimanite ± garnet ± K-feldspar. Muscovite ± chlorite may be present as retrograde minerals. Typically, the gneiss is medium- to coarse-grained, dark-colored with multiple generations of ptymatically folded quartzo-feldspathic veins.

Joshua Tree Terrane (j):

P€jg/jgg Joshua Tree granite/granite gneiss: where undeformed in the Pinto Mountains, the rock is porphyritic leuco-granite with phenocrysts of white to gray K-feldspar and greenish-white plagioclase, spheroidal quartz phenocrysts (< 1 cm), and less than 10% biotite, typically in recrystallized clots. The granite has been deformed to a leucocratic augen gneiss in the Eagle and Chuckwalla Mountains. The granite is capped by a aluminous unit (aluminosilicate + muscovite + quartz) characterized by large quartz grains. The unit is inferred to represent a metamorphosed paleo-weathered zone. In the Eagle and Chuckwalla Mountains, this unit has been deformed into pelitic schist with quartz augen.

SYMBOLS

 22 Bedding: strike and dip

 53 Deformational foliation: strike and dip

 60 Cumulate(?) layering: strike and dip

 18 Mineral lineation

 32 Fold-axis lineation

 47 Contact, with dip

 70 Fault, with dip

 Early Red Cloud thrust

 Later Red Cloud thrust

 KTq1

 KTf

 KTt

 KTm

 KTd

Contacts are solid where visible in the field, dashed where uncertain, dotted where concealed, queried where extrapolated or where interpolated over a long distance.

PLATE VI
(In pocket)PALINSPASTIC RECONSTRUCTION OF THE SAN ANDREAS FAULT SYSTEM
IN SOUTHERN CALIFORNIA

Explanation. The reconstruction is based on the assumption that several antiformal features distributed along the present San Andreas fault system once formed a nearly continuous feature that has been disrupted by that fault system. Each of antiforms is cored or inferred to be cored by Pelona-type schist that is overthrust by a crystalline slab with mylonite at the thrust passing upward through cataclasized crystalline rocks into unaffected rocks. The intersections of the axes of these folds with strands of the San Andreas fault system are used as piercing points to constrain the reconstruction. The restoration reassembles the lithologies of the San Gabriel terrane in a pattern that is consistent with the Cenozoic antiformal folding of its layered crustal section. The restoration also predicts that some of the pre-batholithic rocks in the southeastern San Gabriel Mountains may be part of the Joshua Tree terrane exposed where the pre-batholithic fold associated with the Red Cloud thrust system has been refolded across the Cenozoic antiform.

A. Present distribution of crystalline rocks within the Transverse Ranges (cf. Geologic Map of California, scale 1:750,000, Jennings, 1977; see also Plate I, Figures 1-1, 1-2A, 6-1).

B. Paleogeology of the Transverse Ranges crystalline rocks after restoration of 220 km of right-lateral displacement along the San

San Andreas fault, about 60 km of right-lateral displacement along the San Gabriel fault north of its juncture with the Sierra Madre fault, with that displacement split between those two faults south of the juncture, and about 20 km of displacement along the San Jacinto fault. In addition, left-lateral displacement has been restored along the Pinto Mountain fault (16 km), Blue Cut fault (5 km), Chiriaco fault (11 km), and Salton Creek-Aztec Mines Wash fault (8 km)

C. Paleogeology of the Transverse Ranges crystalline rocks after restoration of about 90 km of right-lateral displacement along an inferred fault strand that incorporates the San Francisquito, Fenner, and Clemens Well faults.

PLATE VII
(In pocket)EVOLUTION OF THE SAN ANDREAS FAULT SYSTEM
IN SOUTHERN CALIFORNIA

Explanation. The model is based on reconstruction of lithologic patterns and structural features within the crystalline basement complex of the Transverse Ranges. Progressive strands of the fault system are represented as the effects of an alternating sequence of counterclockwise rotation and right-lateral translation. The counterclockwise rotation is produced by clockwise rotation of the two batholithic blocks; the right-lateral translation is related to the movement of the Pacific plate relative to North America. In actuality, the two are active simultaneously resulting in a maximum principal stress axis oriented approximately northeast-southwest. See text (Chapter VI) for further discussion and references.

A. Formation of a regional antiform cored by Pelona-type schist at ca. 15-30 m.y. The antiform probably consists of an array of three en echelon segments rather than the continuous feature shown. If drawn, these segments would terminate at the bends located at (O) and (LSB) in the diagram. (SS?), not labeled in the diagram, represents the Sierra de Salinas as possibly part of the antiformal feature.

B. Disruption of the antiform by displacement along the proposed right-lateral San Francisquito-Fenner-Clemens Well fault, ca. 20 to 10 m.y. ago. Movement on this strand had ceased by the time of deposition of the upper Miocene Mint Canyon formation (ca. 15 to 10 m.y. ago).

- C. Inception of the San Gabriel-San Andreas fault strand of the San Andreas system, followed by about 60 km of right-lateral displacement, ca. 10 to 2 m.y. ago.
- D. Counterclockwise rotation (left-lateral bending) of the San Gabriel-San Andreas fault strand, ca. 10 m.y. ago to the present. Possible inception of the Garlock fault, followed by about 60 km of left-lateral displacement ca. 5 m.y. ago to the present.
- E. Inception of the present San Andreas fault, followed by 220 km of right-lateral displacement, ca. 2 m.y. ago to the present.
- F. Counterclockwise rotation (left-lateral bending) of the San Andreas fault strand, ca. 2 m.y. ago to the present.
- G. Present configuration of the San Andreas fault and the Sierra Nevada and Peninsular Ranges batholiths. The teleseism P-delay contours (in seconds) of Hadley and Kanamori (1977) are also shown: solid and dashed lines represent the contours drawn by Hadley and Kanamori; dotted lines have been added here to close the contours around their data from stations on the Channel Islands. The Transverse Ranges, marked by hachures, diagonally transect the modified P-delay anomaly. The mantle structure proposed by Hadley and Kanamori is inferred to represent material squeezed up between the crustal roots of the converging batholithic blocks. This upwelling might impede movement along the San Andreas fault through the Transverse Ranges-Mojave Desert block which could result in the regional counterclockwise rotation.